DEPOSITIONAL ENVIRONMENTS AND TIMING OF FORMATION OF THE LILESVILLE GRAVELS, ANSON COUNTY, NC

by

Matthew Robert Yankech

A thesis submitted to the faculty of
The University of North Carolina at Charlotte
In partial fulfillment of the requirements
for the degree of Master of Science in
Earth Sciences

Charlotte

2022

Approved by:

_____
Dr. John A Diemer

_____
Dr. Andy Bobyarchick

_____
Dr. Martha Cary Eppes

©2022
Matthew Robert Yankech
ALL RIGHTS RESERVED

ABSTRACT

MATTHEW ROBERT YANKECH. Depositional Environments and Timing of Formation of the Lilesville Gravels, Anson County, NC (Under the direction of DR. JOHN DIEMER).

Near Lilesville, North Carolina, on the western margin of the Fall Zone, there occur upland gravels containing unusually coarse-grained, imbricated pebbles and cobbles. These upland Lilesville gravels form an extensive plateau capping the hilltops at an elevation of ~135 meters above sea level (~100 meters above the current Pee Dee River). They unconformably overlie weathered Lilesville granite and locally cap Cretaceous sediments belonging to the Middendorf Formation. The origin and age of the Lilesville gravels and other upland gravel deposits have been debated for decades.

This study was performed at the BV Hedrick Gravel and Sand quarry. Due to the quarry actively being mined, observation of outcrops in several locations with orientations at various trends are described. In these outcrops the Lilesville gravels contain the following facies: 1) massive to poorly bedded gravel; 2) trough cross-bedded gravel; 3) trough cross-bedded sand; 4) horizontally laminated sand; 5) massive sand; 6) ripple cross laminated sand, 7) laminated sand, silt and clay; and 8) organic rich silt and clay. Architectural elements include channel forms, point bars with lateral accretion surfaces, and crevasse splay complexes.

The Lilesville gravels are assigned to the Neogene based on pollen, plant macrofossils and phytoliths derived from the organic rich (lignite) facies. The age of the Lilesville gravels may be further constrained to the mid-to-late Miocene (7-10 million years old), based on their elevation above the current position of the Pee Dee River. Soil profiles from quarry high walls suggest multiple periods of post-Miocene soil formation, indicating times of stable conditions alternating with periods of deposition by the ancient Pee Dee River.

Lithofacies analysis and facies architectural elements suggest that the Lilesville gravels are the product of braided fluvial systems and record an interval of erosion followed by

aggradation by the southerly-flowing ancestral Pee Dee River system as it migrated back and forth across the landscape. The deposition of the Lilesville gravels indicates that a combination of processes were involved in their formation: a “Miocene Rejuvenation” leading to epeirogenic uplift in the source area and a transition to a wetter paleoclimate during the late Miocene, creating the external conditions to mobilize large quantities of coarse-grained sediment.

ACKNOWLEDGMENTS

First and foremost, I want to pay my special regards to my graduate advisor Dr. John Diemer for the immeasurable amount of guidance and patience provided during my master's studies and thesis. I would also like to thank committee members Dr. Andy Bobyarchick and Dr. Martha Cary Eppes for contributing their knowledge, technical support, and suggestions to this project. I thank Rufus McLean for sharing with me his knowledge of the Lilesville Gravels. I also thank Dr. Fred Rich from Georgia Southern University and Dr. Ethan Hyland from the Department of Marine, Earth and Atmospheric Sciences at NC State University for their expertise and assistance with this project. I want to thank Dr. Valerie Reynolds for providing encouragement and technical support in the petrology lab. I also extend my gratitude to BV Hedrick Gravel and Sand for granting access to their property. I want to thank my friends and colleagues Steve Rachide and Jacob Parra for assistance both in the lab and in the field, along with all other colleagues who lent a helping hand throughout the course of this project. I also want to thank the faculty and staff of the Department of Geography and Earth Sciences at the University of North Carolina at Charlotte who provided guidance and assistance throughout the course of my academic endeavors.

TABLE OF CONTENTS

LIST OF TABLES ix

LIST OF FIGURES x

LIST OF ABBREVIATIONS xiii

CHAPTER 1: INTRODUCTION 1

1.1 Introduction to the Lilesville Gravels 1

1.2 Goals/Importance of Study 5

CHAPTER 2: CENOZOIC GEOLOGIC HISTORY OF EASTERN NORTH AMERICA 6

2.1 Allogenic Controls 6

2.2 Regional Cenozoic Tectonics and Sedimentation 7

2.3 Neogene Climate 9

2.4 Other Upland Gravel Deposits of the Piedmont Region of North America 10

CHAPTER 3: FIELD AREA: BV HEDRICK SAND AND GRAVEL QUARRY 13

3.1 Site Location 13

3.2 Geologic Setting 14

3.3 Modern Pee Dee River 16

3.4 Modern Climate in the Field Area 17

CHAPTER 4: METHODS 18

4.1 Sedimentologic Logs 18

4.2 Cross-sections 18

4.3 Digital Image Photomosaics 18

4.4 Paleoflow Analysis 19

4.5 Grain Size Analysis 19

4.6 Mineralogy 20

4.7 Age Estimation 20

4.8 Soil Analysis 21

CHAPTER 5: DATA/RESULTS 23

5.1 Facies Overview and Facies Architecture 23

5.1.1 Gravely Facies 23

5.1.2 Sandy Facies 24

5.1.3 Fine Grained Facies 25

5.1.4 Lignite Facies 26

5.1.5 Macroscale Architectural Elements 27

5.2 Composite Facies Log for Field Area 31

5.3 Highwall Exposures Adjacent to Ponds 32

5.3.1 Sedimentological Logs at Site 1 of the Ponds Location 32

5.3.2 Facies Architecture along the Ponds 38

5.3.3 Imbrication Data 45

5.3.4 Mineralogy 46

5.3.5 Grain Size Data 47

5.3.6 Soil Profile Data 48

5.4 Location at Lignite Pit - Overview 51

5.4.1 Sedimentological Log at Lignite Pit 52

5.4.2 Facies Architecture at Lignite Pit 52

5.4.3 Organic Digestion and Grain Size Analysis Data 53

5.4.4 Pollen Data 54

5.4.5 Phytolith and Plant Macrofossil Data 55

5.5 Location at Sump Pit - Overview 60

5.5.1 Sedimentological Log at Sump Pit 60

5.5.2 Facies Architecture at Sump Pit 65

5.5.3 Organic Digestion and Grain Size Data 67

5.6 Location at Sump Pit 2 Overview 67

5.6.1 Sedimentological Log at Sump Pit 2 68

5.6.2 Soil Profile Data 68

5.7 HQ-G Sample Grain Size Analysis 72

5.8 Facies Architecture of Other Remotely Viewed Outcrops 72

CHAPTER 6: INTERPRETATION 76

6.1 Facies Associations and Depositional Models 76

6.2 Paleocurrents 81

6.3 Provenance 82

6.4 Soil Characteristics 84

6.5 Age Estimation 89

6.6 Controls for the Deposition of the Lilesville gravels 90

CHAPTER 7: CONCLUSIONS 92

REFERENCES 94

APPENDIX A: GRAIN SIZE ANALYSIS OF HQ-P1 SAMPLES (PONDS) 100

APPENDIX B: GRAIN SIZE ANALYSIS OF HQ-L SAPMLES (LIGNITE PIT) 113

APPENDIX C: GRAIN SIZE ANALYSIS OF HQ-SP SAMPLES (SUMP PIT) 143

APPENDIX D: GRAIN SIZE ANALYSIS OF HQ-G SAMLES 158

APPENDIX E: IMBRICATION DATA FOR SITES 1, 2 AND 3 166

APPENDIX F: HEAVY MINERAL SEPARATION GRAIN COUNTS 169

APPENDIX G: SOIL FIELD DESCRIPTIONS 170

APPENDIX H: EXTRACTABLE IRON ANALYSIS 171

APPENDIX I: XRF ANALYSIS FOR SOIL PROFILES 172

APPENDIX J: DOCUMENTED PLANT MACRO AND MICRO FOSSILS 173

LIST OF TABLES

TABLE 5.1: Heavy mineral weight percentages 47

TABLE 5.2: Heavy mineral non opaque heavy mineral percentages 47

TABLE 5.3: Organic digestion results for HQ-L samples 54

TABLE 5.4: Organic digestion results of HQ-SP samples 67

TABLE 5.5: Grain size analysis of HQ-G samples 72

LIST OF FIGURES

FIGURE 1.1: Map of major litho-tectonic features of North Carolina 1

FIGURE 1.2: Geologic map of the vicinity of the study area from Brown et al. (1985) 2

FIGURE 1.3: Geologic map of the study area from Brown et al. (1985) 2

FIGURE 1.4: Generalized map of lignite deposits of eastern North America 3

FIGURE 2.1: Graph of terrigenous siliciclastic sediment flux into the Atlantic 9

FIGURE 3.1: Satellite view of the BV Hedrick field area 13

FIGURE 3.2: Topographic profile of the Lilesville Gravels and Pee Dee River 14

FIGURE 3.3: Geologic map of field area from Owen 16

FIGURE 5.1: Photos of gravely facies 24

FIGURE 5.2: Photos of sandy facies 25

FIGURE 5.3: Photos of fine-grained facies 26

FIGURE 5.4: Photo of lignite facies 27

FIGURE 5.5: Channel form in outcrop along ponds 28

FIGURE 5.6: Crevasse splay architecture in outcrop along ponds 29

FIGURE 5.7: Channel form in outcrop near Sump Pit 2 30

FIGURE 5.8: Composite facies log 31

FIGURE 5.9: Generalized map of field area with site names 32

FIGURE 5.10: Sedimentologic log at Pond 1 33

FIGURE 5.11: Photo of units 4-9 at Pond 1 35

FIGURE 5.12: Photo of units 9-14 at Pond 1 37

FIGURE 5.13: Panorama of outcrop at Pond 1 39

FIGURE 5.14: Panorama of outcrop at Pond 2 40

FIGURE 5.15: Panorama of outcrop at Pond 3 41

FIGURE 5.16: Panorama of outcrop at Pond 4 42

FIGURE 5.17: Panorama of outcrop farthest north pond 43

FIGURE 5.18: Sedimentologic logs from sites 1-15 44

FIGURE 5.19: Rose diagrams of imbrication study 45

FIGURE 5.20: Photo of upper portion of soil profile at Pond 1 48

FIGURE 5.21: Photo of middle portion of soil profile at Pond 1 49

FIGURE 5.22: Photo of lower portion of soil profile at Pond 1 49

FIGURE 5.23: Fed depth profile at Pond 1 50

FIGURE 5.24: Plot of depletion/enrichment factors 51

FIGURE 5.25: Sedimentological log at the Lignite Pit 52

FIGURE 5.26: Panorama of outcrop at the Lignite Pit 53

FIGURE 5.27: Percentages of pollen types found in the Lilesville Lignite 54

FIGURE 5.28: Microscopic photos of angiosperm tree phytoliths 55

FIGURE 5.29: Microscopic photos of conifer phytoliths 56

FIGURE 5.30: Microscopic photos of wetland grass phytoliths 56

FIGURE 5.31: Photos of Pinus macrofossils 57

FIGURE 5.32: Photos of Fagaceae macrofossil 58

FIGURE 5.33: Photo of Fabaceae macrofossil 59

FIGURE 5.34: Photo of Poales macrofossil 59

FIGURE 5.35 Sedimentological log at the Sump Pit 60

FIGURE 5.36: Photo of units 1-4 at the Sump Pit 61

FIGURE 5.37: Photo of units 5-7 at the Sump Pit 62

FIGURE 5.38: Photos of units 7-12 at the Sump Pit 63

FIGURE 5.39: Photos of units 13-16 at the Sump Pit 64

FIGURE 5.40: Panorama of outcrop at the Sump Pit 66

FIGURE 5.41: Sedimentological log at Sump Pit 2 68

FIGURE 5.42: Photo of soil profile at Sump Pit 2 69

FIGURE 5.43: Fed depth profile for soil pit HQB at Sump Pit 2 70

FIGURE 5.44: Generalized map of field area showing HQ-G sample locations 71

FIGURE 5.45: Cumulative weight percent graphs for HQ-G samples 72

FIGURE 5.46: Map of field area showing location of temporary outcrops 73

FIGURE 5.47: Panorama of outcrop near the backside of the Lignite Pit 74

FIGURE 5.48: Panorama of outcrop near HQ-G sample locations 75

FIGURE 6.1: Depositional model for facies association 1 (FA1) 78

FIGURE 6.2: Depositional model for facies association 2 (FA2) 80

FIGURE 6.3: Depositional model for facies association 3 (FA3) 81

FIGURE 6.4: Diagram showing imbrication process 82

FIGURE 6.5: Geologic map of North Carolina with trace of the Pee Dee River 83

FIGURE 6.6: Photo of Soil profile at Pond 1 with fragipan 85

FIGURE 6.7: Photo of soil profile at Sump Pit 2 showing plinthite 86

FIGURE 6.8: Close up photo of fragipan characteristics 87

FIGURE 6.9: Plot of depletion/enrichment factors with facies associations 88

FIGURE 6.10: Ternary diagram of age relationships between proportions of pollen types 90

LIST OF ABBREVIATIONS

FA1	Facies association 1
FA2	Facies association 2
FA3	Facies association 3
Fl	Laminated sand silt and clay facies
Fo	Fragmented plant material in a matrix of silt and clay facies
Gm	Massive to crudely bedded gravel facies
Gt	Trough cross-bedded gravel facies
MAP	Mean annual precipitation
MAT	Mean annual temperature
MCO	Miocene Climatic Optimum
Sh	Horizontally laminated sand
Sm	Massive sand
Sr	Cross laminated sand
St	Trough cross-stratified sand
St+h	Trough cross-stratified and horizontally laminated sand
Sto	Trough cross-stratified sand with plant fragments

CHAPTER 1: INTRODUCTION

1.1 Introduction to the Lilesville Gravels

Unusually coarse gravel and sand deposits of Cenozoic age occur on interfluves situated between through-going rivers that cross the Fall Line of North and South Carolina. An example of these upland gravel deposits occurs near Lilesville, North Carolina, where they mantle an upland plateau and have been mapped as Tertiary in age on the North Carolina State Geologic map (Figure 1.1; Brown et al., 1985). In Lilesville, these enigmatic quartz-rich upland gravels lie unconformably on the Pennsylvanian-aged Lilesville Pluton and Late Proterozoic to Cambrian-aged metamudstones, gneisses, and schists, as well as on finer-grained Cretaceous siliciclastic sedimentary strata of the Middendorf Formation (Figure 1.2). The nonconformity separating the Lilesville gravels from the Lilesville Pluton represents about 300 million years, whereas the disconformity separating the Lilesville gravels from the Middendorf Formation represents about 100 million years (Brown et al., 1985; Owens, 1989) (Figure 1.2 and 1.3). The origin and age of the Lilesville gravels have remained a topic of debate for more than a century.

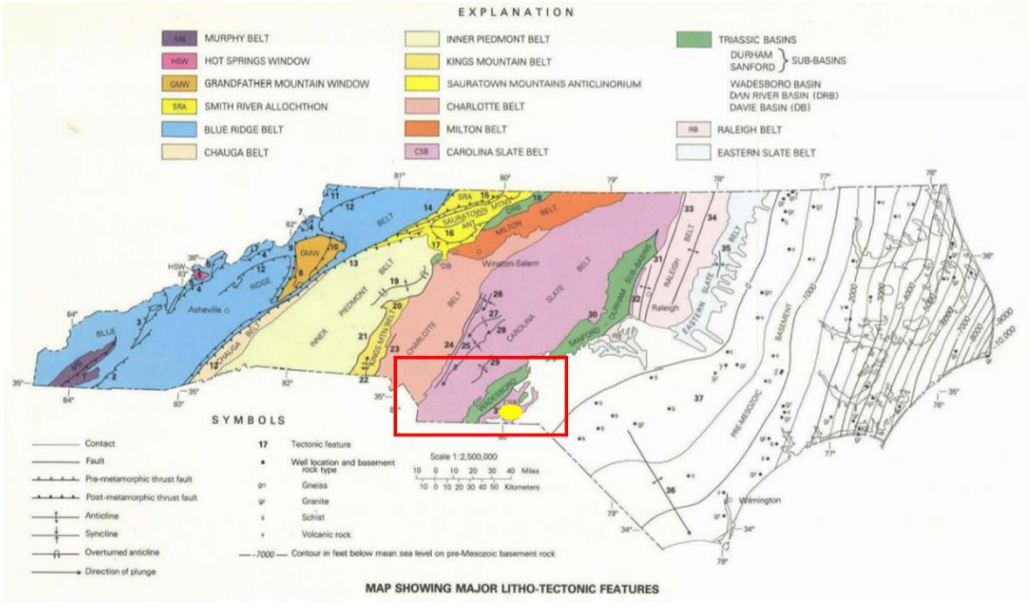

Figure 1.1. Map of major litho-tectonic features (or 'belts') of North Carolina. Yellow dot is the approximate location of the BV Hedrick Sand and Gravel Quarry. Red box is the region represented by Figure 1.2 (modified from Brown et al. 1985. Geologic Map of North Carolina, Raleigh: NC Geological Survey).

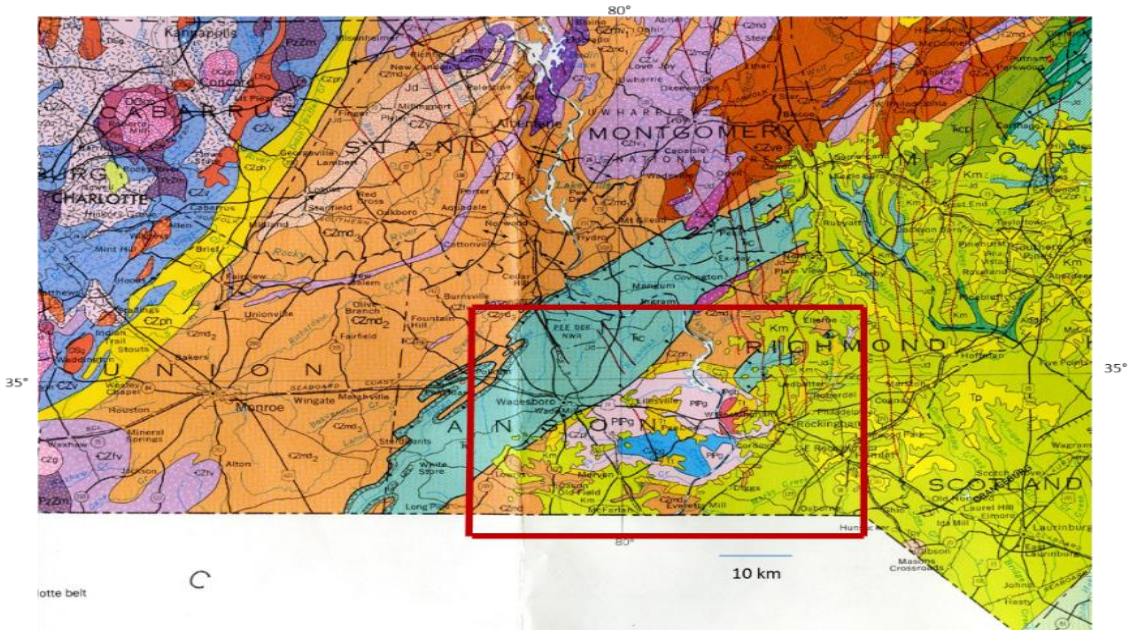

Figure 1.2. Geologic map in the vicinity of the study area (from Brown et al. 1985. Geologic Map of North Carolina, Raleigh: NC Geologic Survey). Area on Figure 1.3 outlined by rectangle.

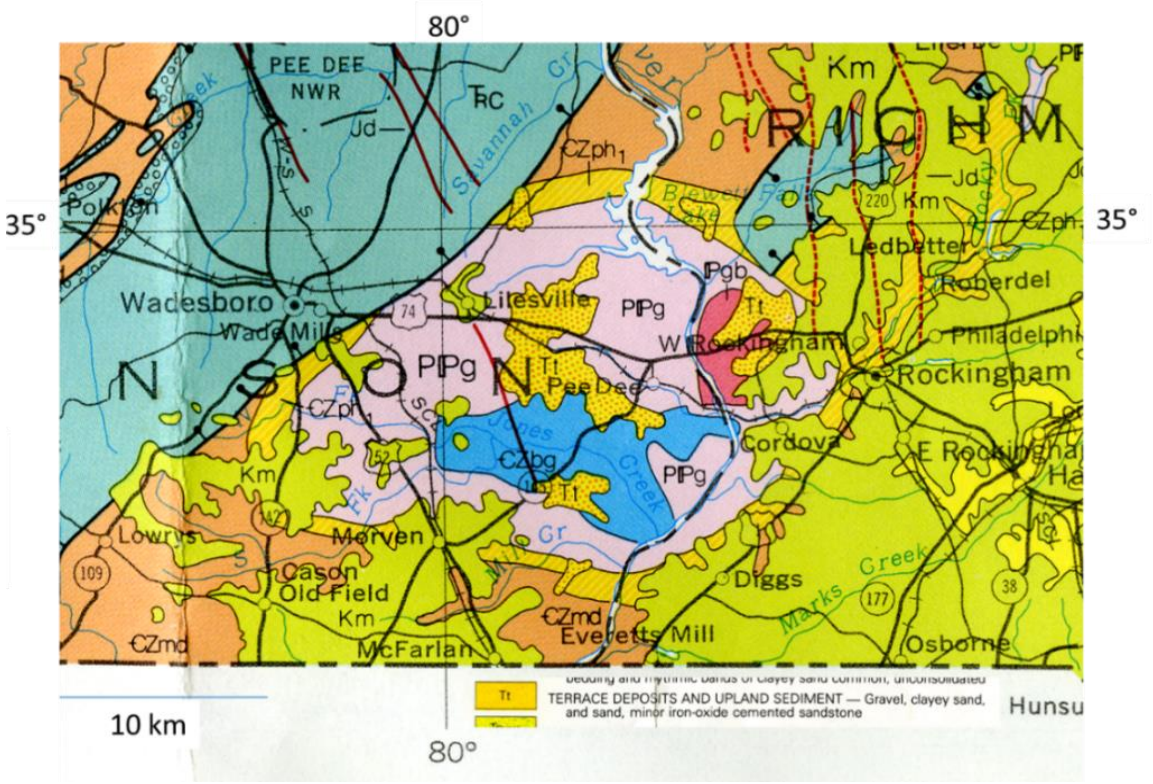

Figure 1.3. Geologic map of study area (from Brown et al. 1985). The Lilesville pluton (PPg) intrudes Late Proterozoic mudstones (CZmd) and is capped by a pendant composed of biotite gneiss (CZbg). The pluton was exposed, weathered, eroded and overlain by the Cretaceous Middendorf Formation (Km), and Tertiary terrace deposits and upland sediments (Tt). (From Brown et al. 1985. Geologic Map of North Carolina, Raleigh: NC Geologic Survey).

Some previous workers have assigned similar upland gravels to Eocene marine deposits (Emmons 1852, Kerr 1875), the post-middle Eocene fluvial Citronelle Fm (Cooley 1970), the Miocene Citronelle Fm (Conley 1962), the Late Miocene (Daniels 1966), the Pliocene fluvial Brandywine Fm (Cooke 1936), or the Pliocene Duplin Fm (Owens 1989), among others. Recent work by McLean (2013) has documented braided stream deposits within the upland gravels exposed in the nearby Bonsal Quarry, also near Lilesville, NC. McLean interpreted the Lilesville gravels at the Bonsal Quarry as strath terrace deposits formed by the ancestral Pee Dee River and assigned them an inferred age of Late Miocene (~10 million years ago) based on regional incision rates inferred for the Piedmont of North Carolina (Mills 2000). He also identified lower elevation, and presumably younger terraces along the Pee Dee River valley (McLean 2013).

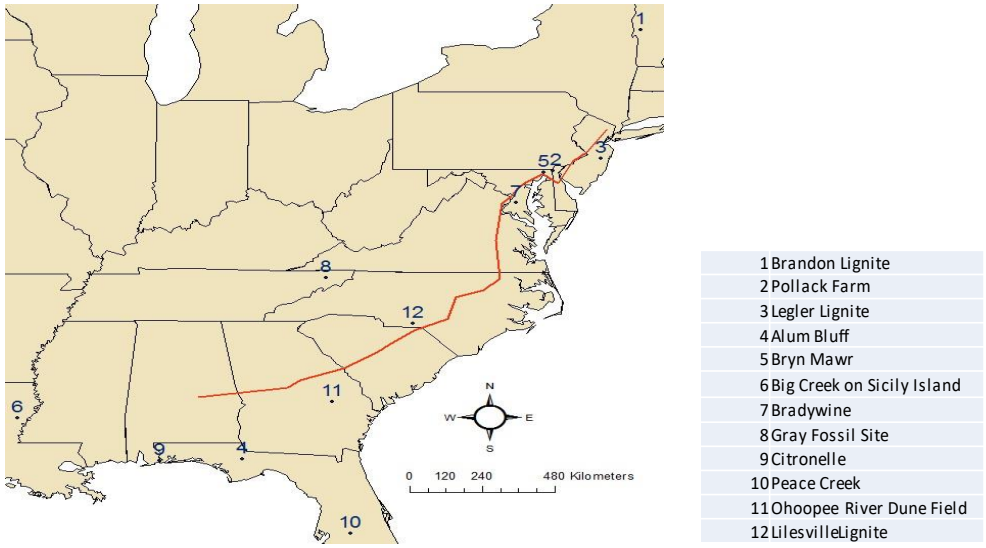

Figure 1.4. Generalized map of lignite deposits of eastern North America and locations of field area (Lilesville Lignite, point 12) along the fall zone which separates the Piedmont from the Coastal Plain provinces. The numbered points represent lignite deposits. Note the geographical gap the Lilesville Lignite occupies between the other study locations. (Modified from Baumgartner, 2014)

The origin of the upland plateau, mantled by the Lilesville gravels, is puzzling. The eastern margin of North America has long been viewed as a passive tectonic margin that has been receiving sediment since the opening of the Atlantic Ocean in the Jurassic (200 million years ago), resulting in the Coastal Plain and continental shelf clastic wedge. The sediments in the clastic wedge are generally fine-grained (sands, silts and clays) and they thicken eastward from the Fall Zone to several thousand meters thick beneath the present continental shelf. The sediments were likely sourced from clay-rich saprolitic material derived from weathering and erosion of the Paleozoic crystalline source rock of the Piedmont and Blue Ridge geologic provinces. This eroded material was then transported southeastward by river systems, many with headwaters at the continental divide in the Blue Ridge. Today, most of the sediments being transported by these rivers are sands and fine to medium gravels and the rivers are classified as meandering systems with abundant fine material as suspended load (Leigh et al., 2004). Leigh et al., (2004) note that sediment size has not changed in modern Piedmont rivers since the late Pleistocene. Furthermore, Baldwin et al., (2006) argued that the amount of sediment being delivered to Winyah Bay by the Pee Dee River today is much less than what was being deposited during the Pliocene and Pleistocene. Large amounts of suspended sediment (such as clays, silts and fine sands) are still transported by the Pee Dee River, but in smaller volumes than what was transported during the Pleistocene (Patchineelam et al., 1999). Thus, it is noteworthy that the Lilesville gravels represent a pulse of significantly coarser sediment than what is currently being transported by the active nearby Pee Dee River.

It is likely that changes in allogenic controls on sedimentation such as tectonics, climate and/or eustacy played a role in the deposition of the upland Lilesville gravels and nearby lower-elevation terrace deposits (cf. Nystrom et al., 1991; Pazzaglia et al., 1997). The pulse of coarser grain size of the Lilesville gravels could be due to (1) an interval of increased slope due to topographic rejuvenation from tectonic uplift, (2) an interval of increased discharge due to a wetter climate, (3) localized deposition at the site due to a raised base level caused by a relatively

short-lived sea level highstand (Leeder 2011), or some combination of those three allogenic controls.

1.2 Goals/Importance of Study

Many studies have been undertaken throughout the Piedmont of eastern North America, an area stretching from Maryland on the north to Alabama on the south and from the Blue Ridge on the west to the Fall Zone in the east (Hack, 1955; Kite, 1982; Owens and Minard, 1924; Pazzaglia and Gardner, 1993; Stanford et al., 2002; among others). Less attention, however, has been focused on sediments deposited by fluvial systems in the Piedmont physiographic region of North Carolina, especially fluvial sediments of Neogene age (McLean, 2013).

A potentially interesting sedimentary record exists in these upland gravel deposits. The work presented here describes the sedimentology and stratigraphy of the Lilesville gravels which could potentially constrain their origin and age and thereby increase our understanding of the tectonic, paleoclimatic and/or eustatic controls acting along the eastern margin of the US at the time of their deposition. Such a study could contribute to our understanding of the origin of widespread upland gravel and terrace deposits throughout the Fall Zone of the eastern US.

CHAPTER 2: CENOZOIC GEOLOGIC HISTORY OF EASTERN NORTH AMERICA

2.1 Allogenic Controls

Tectonic uplift can play a major role in the creation and preservation of fluvial terraces because of its ability to produce relief in a landscape. Tectonic uplift can cause vertical incision of the river valley as shown in Tornqvst's (1994) study on the Rhine River, Netherlands. If a river incises vertically down into the substrate it can lose its connection to its adjacent floodplain. The abandoned floodplain could then become a terrace surface, or terrace tread. While studying the Yellow River in China, Pan et al. (2009) found that the rate of incision was most likely related to the rate of uplift. This tells us that uplift can be an important driving factor of river incision and terrace formation.

At times of little to no vertical incision, lateral migration of channels accompanied by lateral erosion can take place. Laterally migrating river channels cut into the channel banks while at the same time producing an extensive basal erosion surface and depositing point bars on the inner banks of single-thread meandering streams. Lateral migration of multi-thread channels can also produce lateral accretion deposits on mid channel bars in braided streams. The lateral accretion of the bars can potentially narrow parts of the river channels, however, at the same time, lateral erosion of the cut banks can maintain the channels with cross-sectional areas adjusted to discharge. The migration of the channels and their talwegs can therefore produce widespread basal erosion surfaces overlain by bar deposits and associated floodplain deposits (Maddy, 2001). Should vertical incision resume, the surfaces of the floodplains can be abandoned to form terrace treads. These observations suggest there are multiple factors that need to be considered when reconstructing the development and preservation of terraces.

An intricate relationship exists between tectonics and climate change as the controlling factors of a fluvial system (Zhang et al. 2016). Wegman et al. (2002) observed that changes in sediment flux into a river was due to hillslope instability and climatic variation in Clear River

Basin in the state of Washington. Commonly, climatic variation controls the extent of glaciers which has implications for the fluctuation in eustatic sea level. From this relationship, correlations between evidence preserved in fluvial systems and transgressive/regressive periods in Earth history can be made in order to reconstruct global climatic conditions. It is worth noting that the direct influence of glaciers in the Piedmont of North Carolina is lacking, as the extent of the glacial maximum around 18,000 years ago did not reach this far south (Thelin and Pike, 1991). However, the low stand in sea level at the Last Glacial Maximum likely exposed much of the present day-continental shelf due to the lower base level. That lower base level was approximately 150 meters lower than present day sea level. A lower base level can cause knickpoints to form which can incise channels as the knickpoints migrate headward. As incision occurs, former floodplains along the incising channel can be abandoned thereby forming treads of fluvial terraces.

2.2 Regional Cenozoic Tectonics and Sedimentation

A question arises, what tectonic mechanisms are possible driving factors for the influx of coarser-grained sediments and the eventual abandonment of ancestral Pee Dee River floodplains? Various theories have been postulated including: 1) epiorogenic uplift due to migration of portions of the subducted Farallon plate underneath the North American continental plate (Gallen et al., 2011; Gallen et al., 2013; Gallen and Wegmann 2015) inducing a ‘Miocene Rejuvenation’, or 2) the creation of a peripheral bulge due to westward-directed mantle movement responding to the continual addition and thickening of clastic wedge sediments to form the Coastal Plain and continental shelf stretching the length of much of eastern North America (Pazzaglia and Gardner, 1994) . The peripheral bulge arguably played a role in creating large scale scarp features (such as the Fall Zone and Blue Ridge Escarpment) in a seemingly tectonically dormant landscape. Since the break-up of Pangaea in the Jurassic, and the subsequent formation of the Atlantic Ocean, the eastern margin of the United States is generally believed to have experienced a state of continual transfer of sediment, where sediments were eroded from the Appalachian crystalline rocks in the

highlands and then transported across the Piedmont and deposited on the Coastal Plain and continental shelf as a clastic wedge prograding eastward into the Atlantic Ocean basin.

Contrary to a commonly accepted history of steady erosion with a decaying and leveling landscape, some areas along the Appalachian Mountains have seen an increase in relief in topography. For example, the Cullasaja River Basin in the southern Appalachians Mountains around the Tennessee and North Carolina border has been a site of active knickpoint propagation attributed to Late Miocene uplift (Gallen et al., 2013). The Cullasaja basin terrain has experienced an increase in relief of greater than 150% since the Miocene (Gallen et al., 2013; Gallen and Wegmann 2015). The estimate for the increase in relief was derived from observing the propagation of knickpoints migrating upriver in the Cullasaja River basin. Paleo-relief was estimated by creating equilibrium longitudinal river profiles of 8 relict channel reaches based on erosion rates and elevations of ridge lines. This shows a 163% +/- 24% increase in relief since the highest knickpoint entered the mouth of the Cullasaja River. Mechanisms that could cause knickpoint formation include tectonic uplift and base level fluctuations. Schumm (1993) showed that change in sea level is an unlikely mechanism in inland watersheds because river adjustments to the change in base level do not propagate past the lower reaches of rivers, as exemplified by the Mississippi River. Base level change associated with stream capture has been discussed by Gallen (2013).

Furthermore, analysis of erosion rates indicates that the eastern region of North America has been tectonically active. Work performed by Hack (1982) suggests that uplift was tectonically driven, rather than being caused by isostatic rebound of the continental crust while the Appalachian Mountains were being eroded. Hack's reasoning is supported by Ahnert's (1970) study of denudation compared to relief of an area. Ahnert showed that in a setting where isostacy is the dominant mechanism for uplifted terrains, those terrains would have a reduction to 10% of its original relief over a period of about 30 million years. Currently, the mean relief of the Blue Ridge is about 300 meters. If isostacy was solely responsible for Cenozoic uplift, via Hack's

calculation, the Blue Ridge province of the Appalachians would have had improbable relief of 30,000 meters in the late Paleocene. Therefore, it is likely that isostatic rebound was not a driving factor but rather tectonic uplift via topographic rejuvenation was involved in creating the relief we see in the Blue Ridge.

Sedimentary and stratigraphic evidence also indicate that regional tectonism is a driver for landscape evolution along the eastern margin of the United States. Poag and Sevon (1989) analyzed the sediments comprising the clastic wedge of the Atlantic Ocean and found a pulse of increased sedimentation in the middle Miocene (Figure 2.1). Terrigenous sediment rates in the mid-Atlantic basins during the middle Miocene increased by a factor of 20, which is significantly higher than any other post-rift depositional period (Poag and Sevon, 1989; Pazzaglia and Brandon 1996).

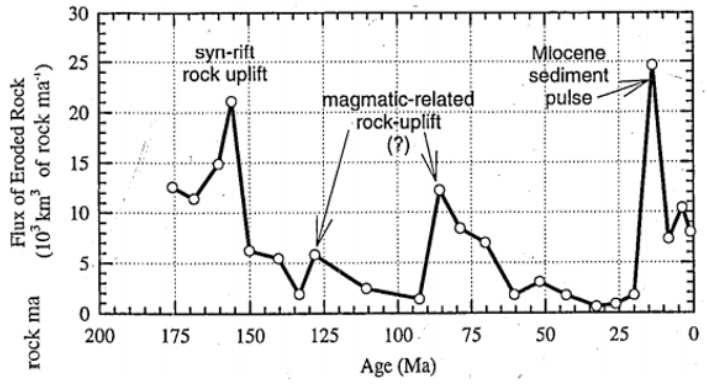

Figure 2.1. Graph showing terrigenous siliciclastic sediment flux from New England and central Appalachians into offshore basins in the middle Atlantic. Modified by Pazzaglia and Brandon, 1996, from data compiled by Poag and Sevon, 1989.

2.3 Neogene Climate

The late Miocene climate of North Carolina shares similarities to today where the mean annual temperature (MAT) and mean annual precipitation (MAP) are 17-18 degrees Celsius and 1,340-1,560 millimeters, respectively (Baumgartner, 2014). A major event known as the Miocene Climatic Optimum (MCO), which took place in the early Miocene, was a time when average temperatures were 6-8 degrees warmer than the average temperature in modern times (Lawrence

et al., 2021). This would have been a climate with higher rates of chemical weathering and erosion and transport of sediment (Cleaves, 1989). When analyzing pollen and plant fragments from lignite deposits similar to the Lilesville Lignite, Baumgartner (2014) showed that in the beginning and middle of the Miocene the climate would have been warmer and slightly wetter. The climate would have become more similar to today towards the end of the Miocene (see Figure 1.4 for the distribution of similar lignite deposits in eastern North America). An important finding by Baumgartner (2014) was that, although there was an overall cooling trend that lasted from the beginning of the Miocene and into the Pliocene, there were no indication of impactful changes in precipitation. This overall cooling trend continued into the Pliocene.

2.4 Other Upland Gravel Deposits of the Piedmont Region of North America

Similar age (Tertiary) upland gravel deposits along the Fall Zone of eastern North America have been extensively studied and documented (Schlee, 1967; Reinhardt et al., 1984; Isphording et al., 1987; Rachele, 1976; Pazzaglia, 1993; McCartan et al., 1990; Pazzaglia et al., 1996; McLean, 2013; Nystrom et al., 1991; among others). Variability in both the ages and the interpreted modes of deposition is intriguing, which is reasonable when considering the geographic extent along the Piedmont and Atlantic coastline where gravels occur. Nystrom et al. (1991) described upland gravel deposits as widespread, heterogeneous, and easily identifiable fluvial sediments that cap highlands between interfluves. Nystrom et al. (1991) assigned a middle Miocene age to these upland deposits (Citronelle Formation) that extend from northern Georgia to central South Carolina. What is particularly interesting about these upland deposits of the Citronelle Formation is that they are truncated by the Orangeburg Scarp, an erosional feature produced by wave action of a transgressive ocean during a Pliocene highstand, helping to establish a minimum age for the upland unit. In North Carolina, similar upland deposits exist and have been described by McLean (2013) during a previous investigation of the Lilesville gravels. Lithologies documented by McLean (2013) include clays, silts, silty-sands, cross-bedded sands, cross-bedded gravels, and clast-supported gravel and cobble conglomerates.

A study by Pazzaglia (1996) showed that the Bryn Mawr Formation, in Cecil County Maryland, is Late Miocene in age. Discovery of a plant-rich lignite aided in the age determination based in part on comparisons to well-dated chronostratigraphic units. The lithology of the Bryn Mawr Formation consists of a quartzose, sandy gravel deposited in a braided alluvial plain setting with the most extensive gravel deposits at the head of the Chesapeake Bay, Maryland (Pazzaglia, 1993). Pazzaglia was able to use fossil pollen data, consisting of oak (*Quercus*), hickory (*Carya*), pine (*Pinus*), holly (*Ilex*), birch (*Betula*), and exotic taxa such as *Pterocarya*, *Sciadopitys*, *Cupuliferoidaepollenites* species and *Engelhardia*-type in order to assign ages to the sediments of the Bryn Mawr Formation based on biostratigraphic correlations.

Work performed on the Cohansey Formation located in New Jersey by Rachele (1976) documented an organic lignite-rich deposit (the Legler Lignite) situated above cross-bedded sands and beneath clays and more cross-bedded sands and gravels. Analysis of fossil pollen from this site indicated a slightly more humid climate with higher winter temperatures than the current warm-temperate climate. The paleoclimate would have been generally similar to that of present-day North Carolina south into Georgia and extending west into Texas, where the most similar climate would be found along the coast of Georgia. The paleoenvironment where the Legler Lignite was deposited likely represented the transition from warm early Miocene conditions to a progressively cooler Pliocene-type climate. It is interesting to note that the flora of the Legler Lignite is similar to the flora of the Lilesville Lignite, along with sharing similar fluvial sedimentary features. However, the Legler Lignite was believed to be associated with marine or beach deposits (Owens and Minard, 1960; Markewicz, 1958; Widmer, 1964) suggesting that the Legler Lignite was in an environment that shared some combination of fluvial and coastal influences. Based on the stratigraphic column produced by Rachele (1976), the Cohansey Formation likely formed initially in a beach depositional environment. The Legler Lignite then recorded the change to a depositional setting dominated by fluvial processes, probably as the result of progradation of the shoreline. The fine-grained nature of the Legler Lignite indicates that

it may have formed in a swamp or pond within a dense forest near the main branch of the fluvial system.

A late Tertiary floral assemblage contained within the Brandywine Formation, near Washington D.C., helps to constrain the age of those deposits to late Miocene (6-10 million years) (McCartan et al., 1990). The Brandywine Formation is believed to have been deposited in a braided stream system with facies including interbedded and poorly sorted sands and gravels, and lenses of both trough cross-stratified and planar-bedded sands. The fossil flora were found in a clay deposit, and the presence of clay suggests a low energy environment with some connection to the main channel. The clay possibly was deposited in depressions on a flood plain during high stands of the water such as occurs during flood events. Pollen types extracted from the clay deposit are 54% trees, 18% shrubs, 14% aquatic plants, 8% vines, and 6% terrestrial herbs. An absence of grass pollen indicates lack of open space for grasses to proliferate. This distribution of vegetation, dominated by deciduous species (74%), indicates a temperate climate, similar to the current climate in the southeastern U.S. The flora of the Brandywine Formation is similar to that of the Legler Lignite. However, the Legler Lignite contains some warmer-adapted flora (thermophilic varieties) indicating that the Brandywine Formation cannot be older than the Legler Lignite.

CHAPTER 3: FIELD AREA: BV HEDRICK SAND AND GRAVEL QUARRY

3.1 Site Location

The BV Hedrick Gravel and Sand Company operates a quarry, located south of US Highway 74 in Lilesville, North Carolina (Figure 3.1), which exhibits stunning exposures of the Lilesville gravels and the Lilesville lignite.

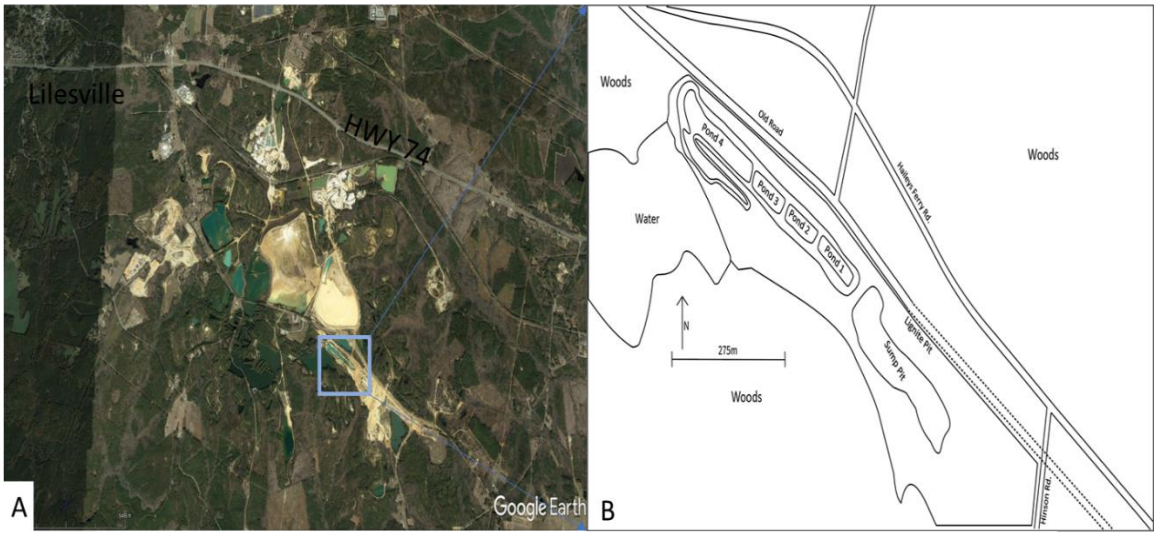

Figure 3.1. A: Satellite view of the BV Hedrick Quarry (blue box is outline of zoomed-in area). B: Generalized map of the BV Hedrick field area with locations and features indicated.

The exposures of the Lilesville gravels are the product of mining that has been occurring in this area for over a century. The quarry operation mines these quartzite-rich gravels for landscaping, construction, metallurgy, and water filtration; along with various types of sands used for golf courses, baseball and softball fields, and concrete aggregate mixtures.

The BV Hedrick Gravel and Sand Company's quarry is about 5.68 kilometers to the west of the current Pee Dee River channel (Figure 3.2). The quarry is situated on top of the highest elevation, that occurs locally, and it is in the oldest surviving terrace created by the Pee Dee River. The quarry is about 100 meters above the modern channel. The modern Pee Dee River has cut down to its current elevation after a series of incisions into underlying sediments and/or bedrock (Figure 3.2). The incisions are recorded by terrace deposits along the Pee Dee River.

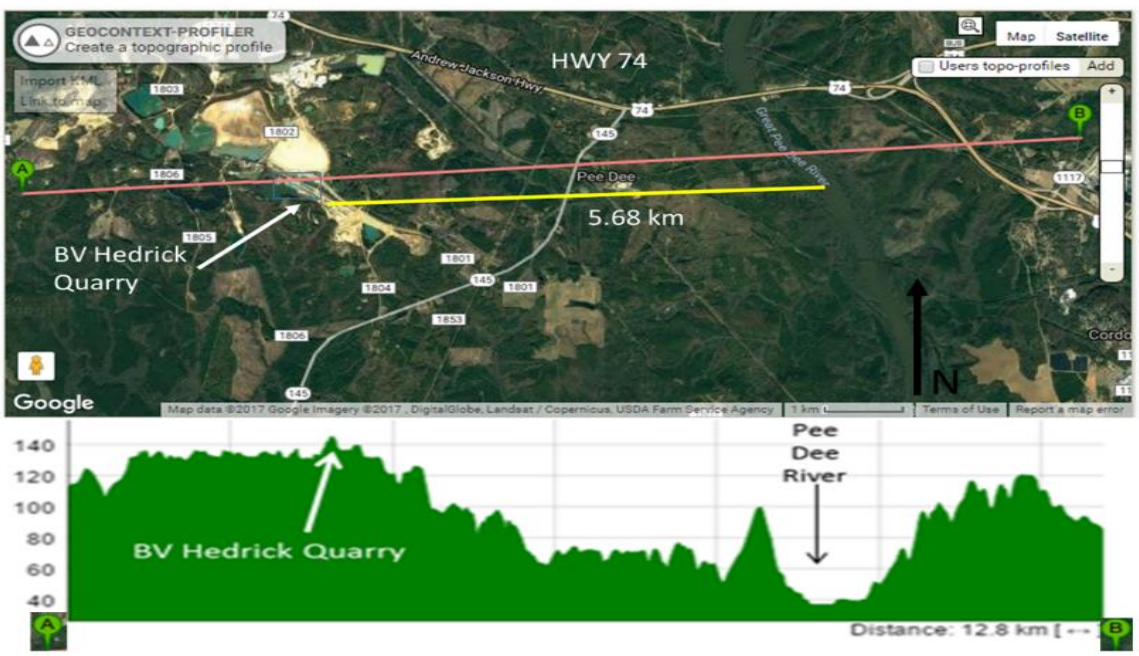

Figure 3.2. Topographic profile for the Lilesville gravels situated on the highest terrace at the BV Hedrick Quarry (about 135 meters asl). The quarry lies about 5.68 kilometers to the west of the current Pee Dee River channel (about 35 meters above sea level).

3.2 Geologic setting

The North American continent has been subjected to multiple mountain building events (Taconic Orogeny, 472 million years ago; Acadian Orogeny, about 390 million years ago; and Alleghenian Orogeny, about 300 million years ago) which contributed to the creation of the Appalachian Mountain Range. The first two of these orogenies accreted island arcs that existed in the Iapetus and Rheic Oceans onto the North American landmass. As the Iapetus and Rheic ocean crust was being subducted under North America these accreted arcs added metamorphic and igneous rock. The Alleghenian Orogeny was the final phase in creating Pangaea, the most recent super continent that was created about 330 million years ago when all of Earth's landmasses had collided into each other. Since the break-up of Pangaea, around 200 million years ago, the eastern margin of North America has been considered a passive margin with no active tectonism and only continual loading of sediments and subsequent subsidence of the continental crust. As the Atlantic Ocean continued to spread, the newly formed basin received terrestrial sediments that

were continually eroded from the high relief, mountainous landscape and deposited as a clastic wedge prograding out towards the center of the basin.

Today, the eastern margin of North America is divided into three distinct physiographic provinces including the 1) Blue Ridge, 2) Piedmont, and 3) Coastal Plain (Figure 1.1). The Piedmont and Coastal Plain provinces are separated by a feature known as the Fall Zone, where the last rapids before the sea are located, and where the rivers exhibit a noticeable drop in elevation. To the east of the Fall Zone there are unconsolidated sands and to the west of the Fall Zone there are highlands consisting of crystalline rocks draped locally by sediments. As the Pee Dee River flows in a southerly to southeasterly direction, it traverses these various terrains that comprise the geology of eastern North America (see Figure 1.2, Figure 1.3, and Figure 3.3), cutting down into bedrock composed of crystalline and sedimentary rocks and transporting that sediment to the coast. A geologic map by Owens (1989) shows other upland gravels (Tug) located on the flanks of the Pee Dee River occupying strath terraces at varying elevations and composed of a range of rock types (see Figure 3.3). McLean (2013) mapped the upland gravels (Tug) as three distinct sets of terrace deposits going from oldest to youngest as the Pee Dee River is approached. The oldest terrace, to the west of the Pee Dee River, is about 100 meters above the current Pee Dee River elevation and is where the BV Hedrick Quarry is located. The middle-aged terrace lies southeast across the Pee Dee River and is about 80 meters above the current Pee Dee River. Moving south along the Pee Dee River the youngest terrace sits at about 60 meters above the current elevation of the Pee Dee River (Figure 3.3).

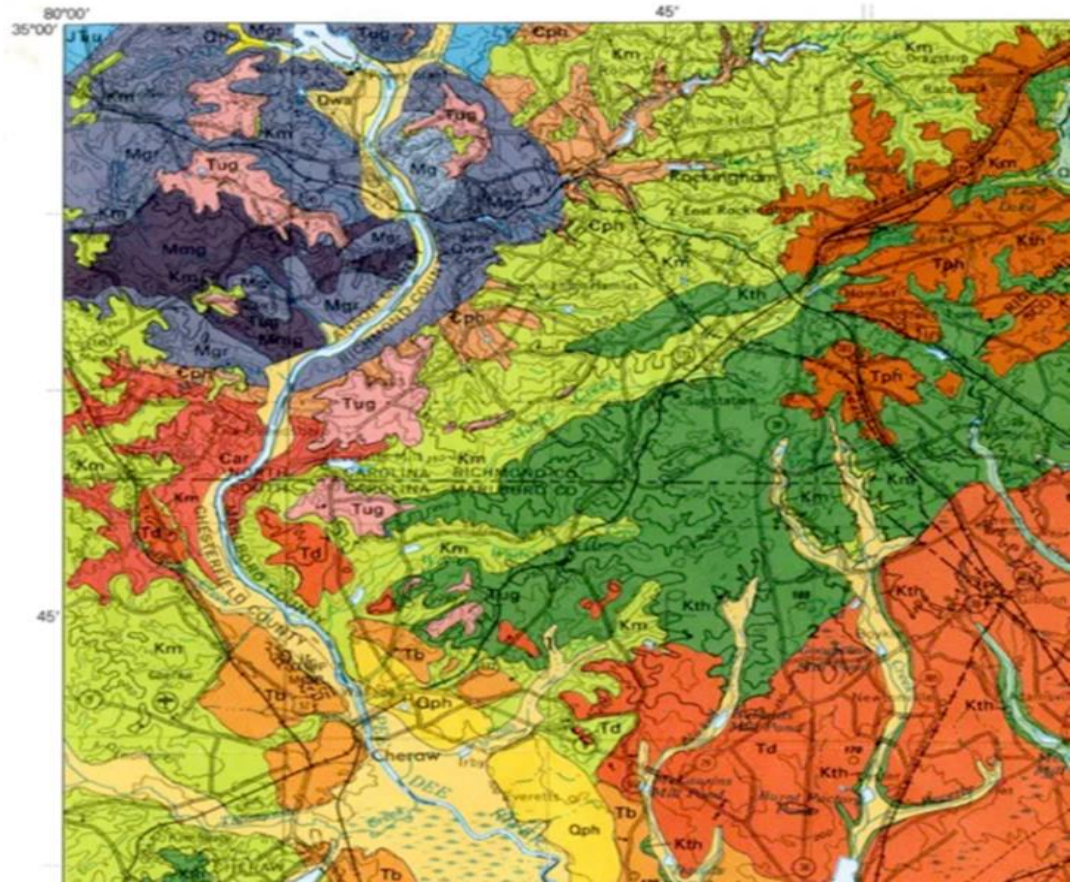

Figure 3.3: Geologic map of field area by Owens (1989) which shows the extent of the Lilesville granite pluton (Mgr) and its associated gabbro (Mg) and biotite gneiss (Mmg) intruded into phyllites (Cph) and argillites (Car) of the Carolina Slate Belt. The upland gravels (Tug) (pink) lie on top of Middendorf Formation (Km).

3.3 Modern Pee Dee River

The Pee Dee River, also known as the Great Pee Dee River, begins at the confluence of the Yadkin and Uwharrie rivers. The Yadkin River drains the eastern slope of the Blue Ridge escarpment with its headwaters near Blowing Rock, North Carolina, while the Uwharrie River has its headwaters in northwestern Randolph County near High Point, NC. The Pee Dee River flows in a southerly to southeasterly direction for about 373 kilometers eventually emptying into the Atlantic Ocean in Winyah Bay in South Carolina. The modern Pee Dee River provides water, electricity and recreation for local residents. Hydroelectric dams have greatly altered the river which now has reduced capacity to transport sediment to the coast. Most of the sediment in

transport is in the form of suspended load (Patchineelam et al., 1999). This means that the Pee Dee River no longer provides enough sediment to beaches and barrier islands where about 80% of fine-grained sediment does not reach open waters but rather is deposited in Winyah Bay (Patchineelam et al., 1999). Baldwin et al. (2006) attributes this to a shift in the source of sediment where the Pee Dee River, up until the late Pleistocene, was sourcing most of its sediment from the Blue Ridge whereas today the Pee Dee River is sourcing most of its sediment from existing coastal plain deposits.

3.4 Modern Climate in the Field Area

North Carolina currently has an overall warm temperate climate with a mean annual temperature ranging from 15-18 degrees Celsius and a mean annual precipitation ranging from 1,116-1,340 millimeters (Baumgartner, 2014). Based on 2018 US Climate Data version 2.3, the average annual high temperature in Anson County, North Carolina is 22.4 degrees Celsius with an annual average low temperature of 9.3 degrees Celsius. Mean annual precipitation (rainfall and snowfall combined) is 1233 millimeters. The average high temperature in January is 11 degrees Celsius and the average low temperature is -1.6 degrees Celsius. The average high temperature in July is 32.4 degrees Celsius and the average low temperature is 20.3 degrees Celsius.

CHAPTER 4: METHODS

4.1 Sedimentologic Logs

The BV Hedrick Sand and Gravel Quarry is an active quarry. As a result, at the margins of excavated pits, there are highwalls of exposed Lilesville gravel. These highwalls provide a cross-sectional view of the Lilesville gravels. To document the internal character of the Lilesville gravels, panoramic photographs were taken and sedimentologic logs were created at numerous locations along the highwalls in order to record the lithofacies using standard logging techniques (Coe, 2010; Tucker, 1988). The thicknesses and grains sizes of distinctive lithofacies were described by using a tape measure, grain size comparator, hand lens and camera (see below in 4.3). The sedimentologic logs were spaced at appropriate intervals along the outcrops to permit correlation of lithofacies from one sedimentologic log to the next.

4.2 Cross-sections

Once the sedimentologic logs were constructed, and lithofacies assigned to the various units in the logs, then cross-sections were made to document the architecture of those lithofacies. Features such as basal erosion surfaces, channel forms, pinch-outs of lithofacies, and presence of through-going marker beds were noted and portrayed on the cross-sections. These cross-sections comprise both line drawings with no vertical exaggeration and annotated photomosaics.

4.3 Digital Image Photomosaics

A Canon Rebel T3i DSLR camera with a Canon Zoom Lens EF 24-105mm lens was used to produce high quality digital photographs of outcrop exposures. The photographs were then stitched together using Canon software PhotoStitch version 3.1. The single photos and stitched images were then used in the lab as well as the field to document fluvial architecture, bedforms and sedimentary structures such as lateral accretion surfaces, crevasse splays, channel forms, ripples, etc. Adobe Illustrator was subsequently used in order to create facies overlays. These facies overlays permit the correlation of distinctive units from one sedimentologic log to the next

and build facies associations for the field area. Since the B.V. Hedrick Sand and Gravel Quarry is an operating quarry, new exposures were created throughout the study interval. Those new exposures were in effect serial sections that allowed various perspectives of the lithofacies architecture to develop over time. The serial sections allowed the testing of hypotheses concerning the geometry of the outcrops based on an initial inspection of an outcrop. Conversely, previous exposures were also covered up or destroyed by mining operations. Therefore, these photos record time-lapse views of the depositional structures present in upland gravels of the Piedmont of North Carolina.

4.4 Paleoflow Analysis

Observation of clast size, composition and orientation were recorded at several sites in order to determine the paleoflow of the ancestral fluvial systems responsible for depositing the Lilesville gravels. At each location at least 40 cobbles were selected, and the lengths of the a, b, and c axes were measured, as were the dip direction and the dip angle. In many cases, the clasts were clearly imbricated where the clasts dipped towards an up-current direction. The compositions (predominantly quartzite and minor vein quartz) were also recorded along with the thickness, if present, of a weathering rind for each of the measured clast samples at each location.

4.5 Grain Size Analysis

Grain size analyses were performed both in the field and in the lab. Field based measurements were conducted by use of a 5-gallon bucket, a column of sieves, and a scale for mass. The phi sizes analyzed include -6, -5, -4, -3, -2 and -1. Any sediment that was smaller than -1 phi (less than 2 millimeters in diameter) sieve was brought back to the lab and analyzed using a Beckman Coulter LS 13 320 Laser Diffraction System equipped with an Autoprep station and Aqueous Liquid Module (ALM). This equipment is capable of measuring particles from the 2000um (coarse sand) to .017um (very fine clays). Therefore, it was necessary to sieve all bulk samples down to the less than 2-millimeter fraction before using the laser diffraction system. Approximate percentages of clasts larger than 2 millimeters were recorded in the field. Samples

were also prepared by using a dispersing agent, which is a solution composed of deionized water, sodium pyrophosphate, and sodium bicarbonate, in order to properly disperse the clay component of the sample. Removal of any organic matter from samples was also accomplished by organic digestion with a hydrogen peroxide solution and sodium phosphate solution (deflocculant). Graphic mean grain size, inclusive graphic standard deviation, inclusive graphic skewness, and inclusive graphic kurtosis were then calculated for each of the detailed grainsize samples.

4.6 Mineralogy

Heavy mineral separation was performed to separate out heavy minerals present in samples to be more easily identifiable. This method helps in describing the provenance of sediment that was transported and deposited by the ancestral Pee Dee River system. Samples were split until a small enough amount was remaining. The split samples were then weighed and put into a vial with deflocculation solution composed of deionized water, sodium pyrophosphate, and sodium bicarbonate. The samples were then placed on a shaker table for 15 minutes so the sediment could properly separate. The samples were then put through a separatory funnel with a series of coffee filters and a solution of sodium polytungstate. The density of the sodium polytungstate was measured with a hydrometer and adjusted to achieve a density of 2.94 g/cm3. Once all the solution had passed through the coffee filters the remaining heavy mineral sediment was thoroughly rinsed and the sample was placed in a drier oven overnight. The samples were then weighed once more and placed on glass slides with epoxy to be analyzed with a petrographic microscope. The heavy minerals in each sample were identified and point-counted by use of the petrographic microscope.

4.7 Age Estimation

One method for calculating the age of the upland gravels is to use a regional incision rate curve (Mills 2000). Mills found that by plotting the ages of terraces relative to their heights above the modern river level, the age increases approximately by the square of the height above modern river level. By using this approach, the age of the Lilesville gravels can be estimated using its

elevation relative to the modern Pee Dee River. The difference in elevations will be compared to a regional incision rate curve developed for the Piedmont of the eastern United States (Mills 2000).

The age of Lilesville gravels can also be estimated by biostratigraphic correlation of pollen and plant macrofossils derived from the Lilesville Lignite, contained within the gravels (Diemer et al. 2017; Yankech et al. 2018). Samples were sent to Georgia Southern University for pollen analysis by Dr. Fred Rich. The pollen assemblages helped with the environmental reconstructions and the age dating of the deposit. The lignite layer contained within the Lilesville gravels has the potential to further constrain the age of the Lilesville gravels by comparison with the macroflora found at other fossil-bearing localities in eastern North America. Lignite samples have been examined by Dr. Ethan Hyland in the Department of Marine, Earth and Atmospheric Sciences at NC State University. Comparing the lignite and pollen assemblages from the Lilesville Lignite to lignite and pollen assemblages at other locations along the east coast of North America (Figure 1.4) further constrains the age of the Lilesville gravels.

4.8 Soil Analysis

Two soil profiles were analyzed in the quarry. The first is located at Pond 1 (see Figure 3.1) located in the northern portion of the field area. The second is located near the Sump Pit 2 location (see Figure 3.1). Soil horizons were described using Birkeland (1999, Appendix A) which includes soil characteristics such as color, texture, structure, and consistency, among others. Samples were collected from each horizon identified to perform laboratory analysis. An iron activity ratio was obtained (Fe_h/Fe_d) by extracting various species of iron from the soil sample where Fe_h (hydroxylamine extractable iron, crystalline or 'background' iron)/Fe_d (dithionite extractable iron, pedogenic iron) of each buried soil horizon, and the modern soil horizon (McKeague and Day, 1996). In addition, characteristic features in soils, such as presence of plinthites and reticulate and vertical tubule mottling, aid in reconstructing the past paleoclimate and paleoenvironment. Depletion/enrichment factors were produced using x-ray fluorescence

(XRF) on each soil profile sample in order to create a depletion/enrichment profile for the elements silicon, aluminum, iron, and titanium (method outlined by Taylor and Blum, 1995). This profile indicates the elemental constituents present in the soils along with where pedogenesis has translocated various elements either increasing or decreasing the elemental concentration in each soil horizon.

CHAPTER 5: DATA/RESULTS

5.1 Facies Overview and Facies Architecture

Throughout the field area 8 facies were consistently found including: massive or crudely bedded gravel (Gm), trough cross-bedded gravel (Gt), trough cross-bedded sands (St), horizontally laminated sands (Sh), massive sand (Sm), ripple cross laminated sands (Sr), laminated sand, silt and clay (Fl) and lignite facies composed of organic-rich silt and clay (Fo). The variations of these facies were described following Miall's classification of fluvial facies.

5.1.1 Gravely Facies

Two types of gravel facies that are found throughout the field area are the massive to crudely bedded gravel (Gm) facies and the trough cross-bedded gravel (Gt) facies. The two facies commonly grade one into the other over short (meter scale) vertical and horizontal distances. The Gm facies consistently occurs at the bases of outcrops along the highwalls that parallel the settling ponds (see Figure 3.1) and generally thickens to the northwest. The Gm facies occurs in layers ranging from 4 to 8 meters in thickness. The Gm facies consists of clast-supported quartz pebble conglomerates with a medium-grained sand to silt matrix. The gravels generally range in size from 4 centimeters up to 11 centimeters and appear massive to poorly sorted. Imbrication of clasts is present locally and the imbrication typically dips to the northwest (Figure 5.1A). In the highwall on the northeast side of ponds 1 to 4, discrete sandy-to-silty lenses that are up to 40 centimeters thick are interbedded within the Gm facies. The sandy-to-silty lenses can extend for a few meters, up to ten meters, before pinching out. Cross bedding and mud rip-up clasts are present within these finer-grained lenses. Documented mud rip-up clasts are around 2 centimeters in diameter (Figures 5.1B and C).

The trough cross-bedded gravel (Gt) facies is present throughout the field area and it is well exposed in the Lignite Pit, Sump Pit, and Sump Pit 2 locations (see Figure 3.1). The Gt facies occurs as cross-bedded fining-upward sequences, 50 centimeters to 1.5 meter in thickness

where the basal portions of the cross bed sets comprise coarse gravels which grade up to sandy gravels in the upper portions of the cross bed sets.

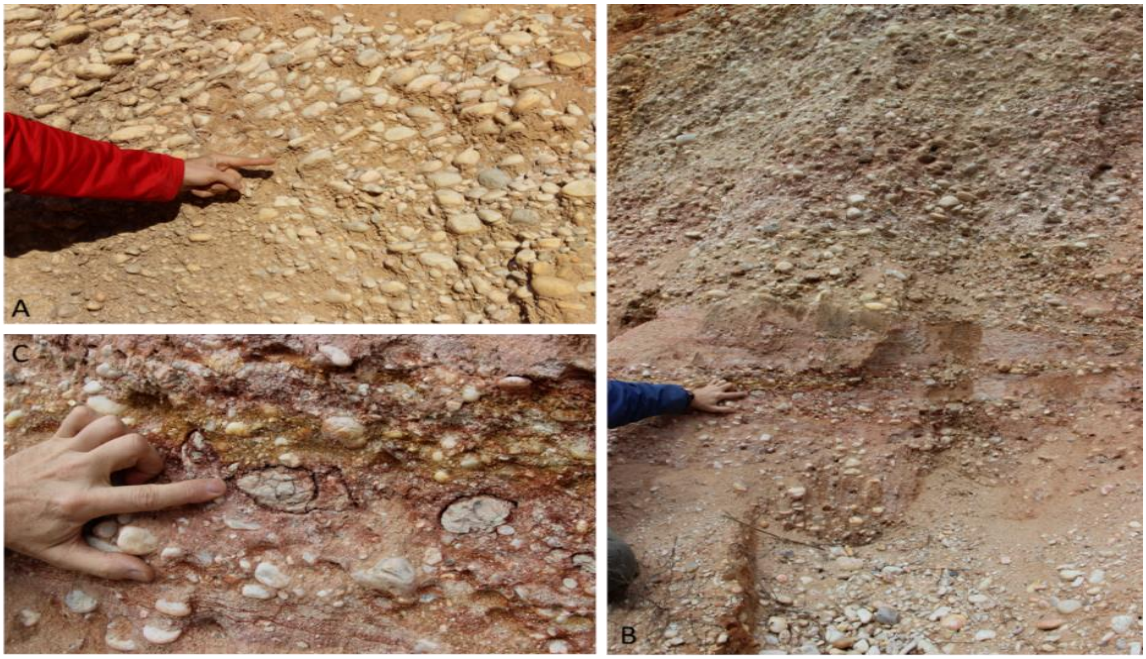

Figure 5.1. A – Imbrication of gravels to cobbles contained within facies Gm. B – Silty-sandy lens within facies Gm containing mud rip-up clasts. C – Close up photograph of mud rip-up clasts in B.

5.1.2 Sandy Facies

Sandy facies present in the field area include trough cross-stratified sand (St), horizontally laminated sand (Sh), cross laminated sand (Sr), and massive sand (Sm) (Figure 5.2). The cross-stratified sand facies (St) consists predominantly of medium grained, well-rounded, spherical, and moderately to well sorted trough cross stratified quartz sand. Locally there can be pebbles ranging in size up to 1 centimeter but these are generally sparse and occur mainly on lag surfaces. This facies can have well developed, tubular, and vertical mottling. Locally the St facies can also have organic material draping the toe sets of trough cross bedding. Facies Sh is similar in grain size and composition to St but can have increased grainsize ranging from medium to coarse sand. The laminations in Sh range in thickness from millimeters up to a few centimeters. The Sr facies is a fine grained cross-laminated sand that locally contains preserved ripple forms that

appear to be draped by clays and silts. The cross-laminations are mostly less than a few millimeters thick but sets of cross-laminations can range up to a few centimeters in thickness.

There are two types of massive sand (Sm) facies which occur. One is a white marker bed up to 40 centimeters thick that is widespread and laterally continuous throughout the field area. The second type of massive sand (Sm) facies occurs locally as a clay-rich sand and caps the field area everywhere that it has not been removed or covered up by mining spoils. Grain size distribution of this unit ranges from fine-to-medium grained sands where the grains are typically well rounded, spherical and composed of quartz sand.

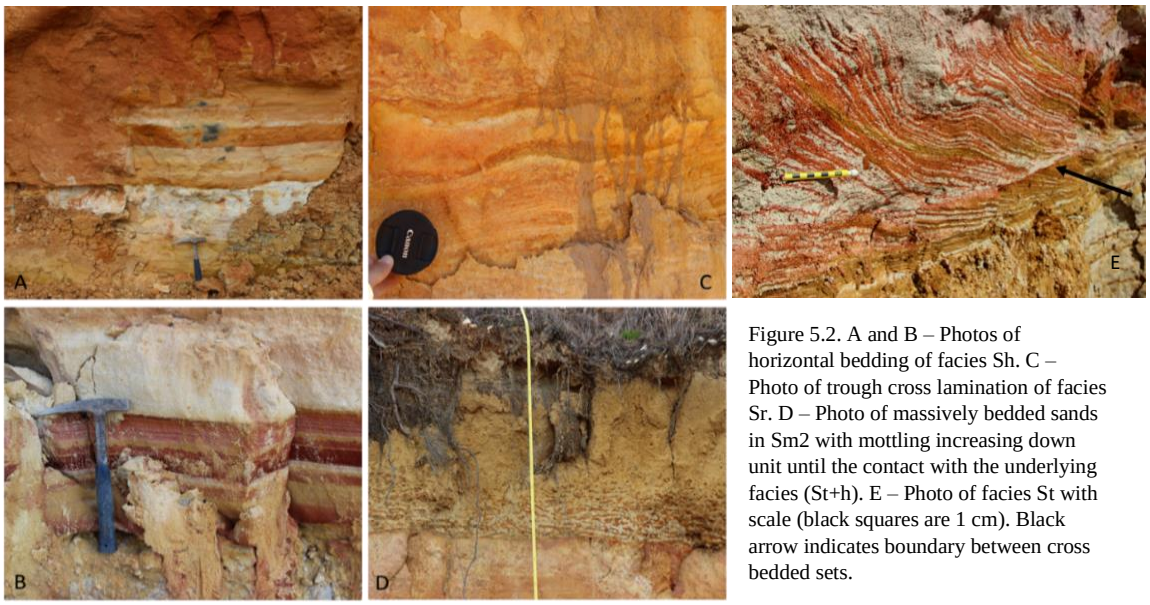

Figure 5.2. A and B – Photos of horizontal bedding of facies Sh. C – Photo of trough cross lamination of facies Sr. D – Photo of massively bedded sands in Sm2 with mottling increasing down unit until the contact with the underlying facies (St+h). E – Photo of facies St with scale (black squares are 1 cm). Black arrow indicates boundary between cross bedded sets.

5.1.3 Fine-Grained Facies

One fine grained facies is present in the field area and is designated Fl (laminated sand, silt and clay). This facies can have prominent to faint laminations and also locally appear massive. Color can vary from light to dark grey, light tan, beige, and red (Figure 5.3). This facies can have small amounts of gravelly material usually on a basal erosion surface. This facies also has a tendency to form recessed layers visible at outcrop scale where the outcrop face has been exposed to weathering and erosion for an extended period of time. Newly cut outcrops do not exhibit this recessed morphology.

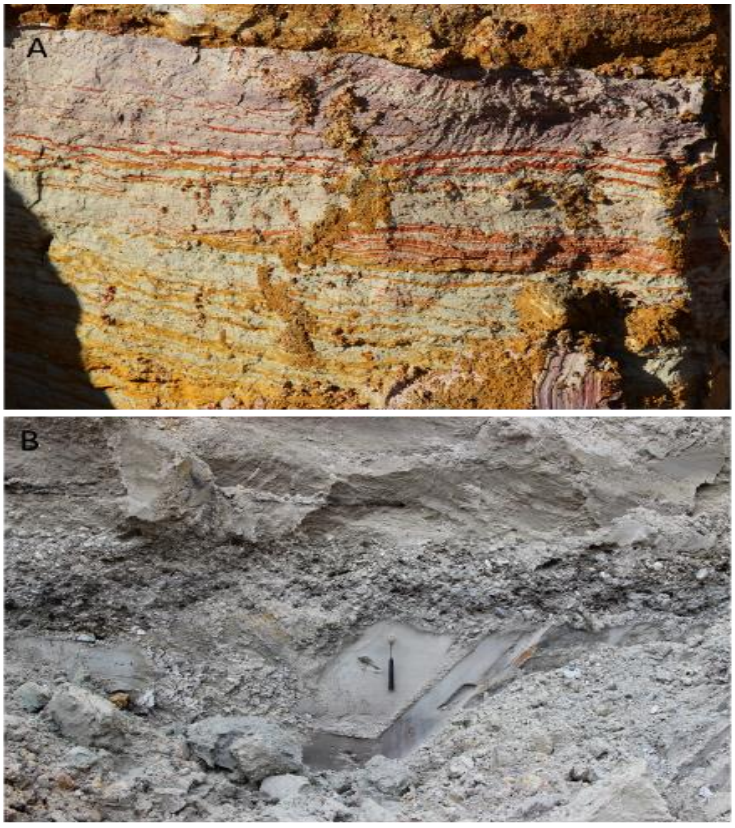

Figure 5.3. A – Photo of alternating clays, silts and fine sands containing horizontal and cross laminations of facies Fl. B – Photo of the massive structure of facies Fl (under the position of the rock hammer) however very faint laminations were noted at the base of the unit.

5.1.4 Lignite Facies

A distinctive facies of particular importance to this study is present in the field area and is designated Fo (fragmented plant material in a matrix of silt and clay) and also is referred to as lignite. This facies appears to have a massive appearance in general but can have laminations locally. The color ranges from dark gray to black. The lignite facies consists of plant fragments ranging from millimeters to centimeters in scale, and locally up to a decimeter in size. The clays and silts coarsen upward and are commonly capped by silts grading up into fine to medium grained sands. The sands are cross-bedded where foreset laminae comprise both fine sand and silt (Figure 5.4).

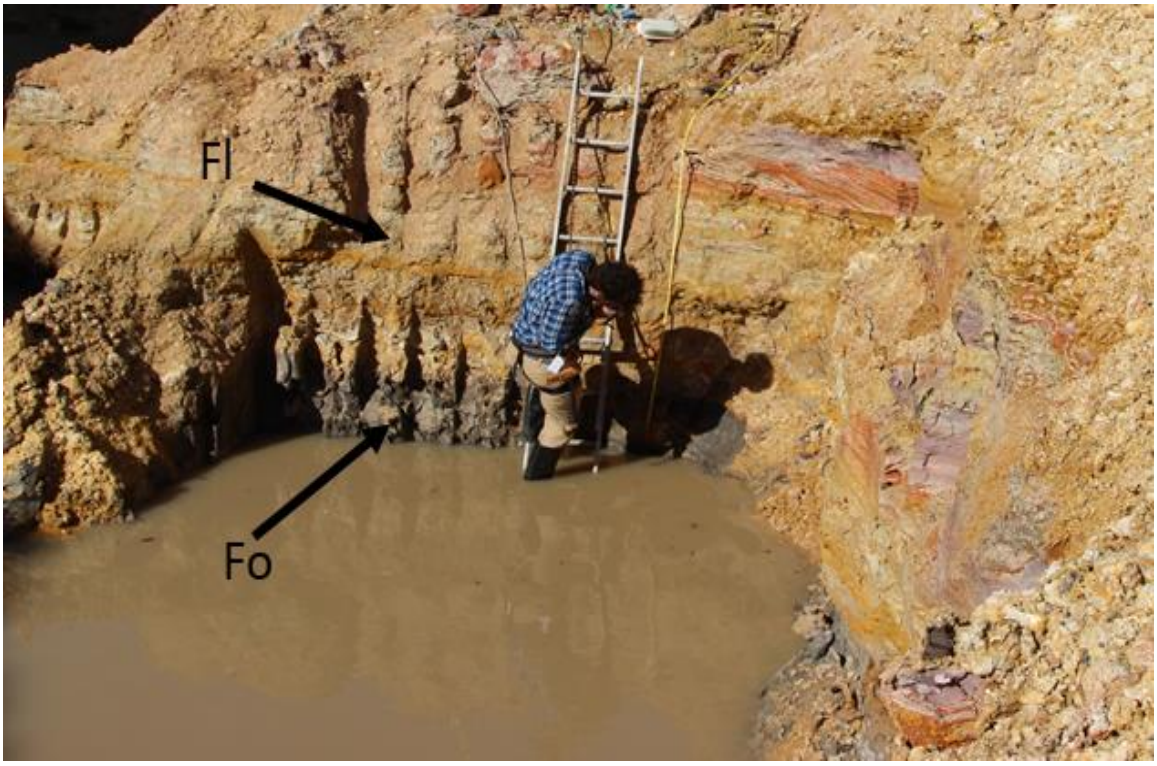

Figure 5.4. Photo showing facies Fo (at the water level of a settling pond) at the Lignite Pit location. Note the horizontal and cross laminated facies Fl directly above the organic clay and silt facies Fo.

5.1.5 Macroscale Architectural Elements

Large scale sedimentary architecture is important in interpreting the depositional environment of a fluvial system because it can indicate the sedimentary processes which deposited the sediment (Mirzai et al., 2017). In order to characterize large scale sedimentary architecture, boundaries between architectural elements are used. Such boundaries may include erosional surfaces, paleosols, and lag surfaces and they can be used to delineate geometric shapes which can be interpreted (Miall, 1985). The main types of large scale sedimentary architectural elements observed in the field area consist of large-scale channel forms (Figure 5.5 and Figure 5.6), lateral accretion deposits (Figure 5.6) and smaller crevasse channels and associated splays (Figure 5.7).

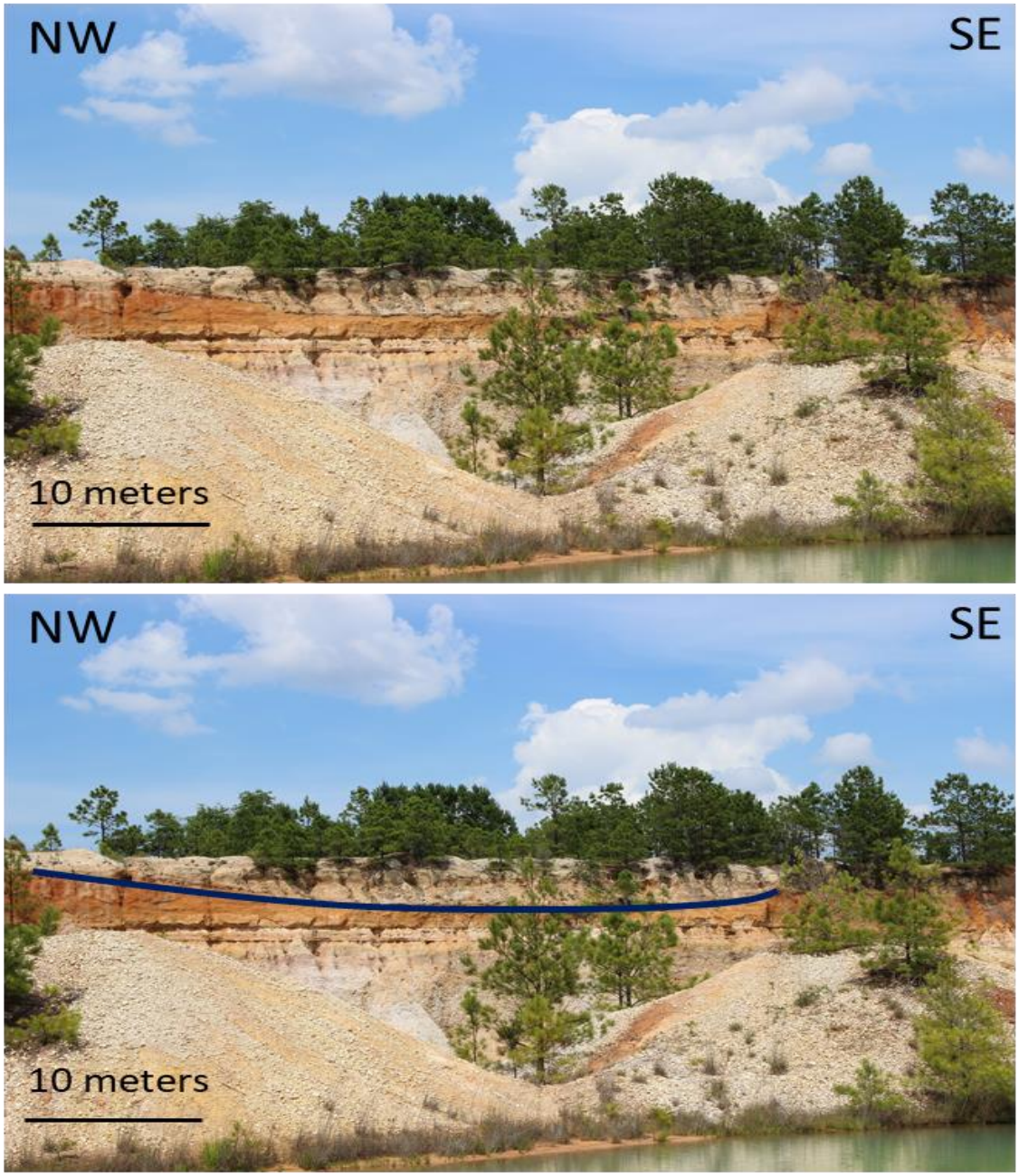

Figure 5.5. Uninterpreted (top) and interpreted (bottom) photo of a channel form observed from an oblique angle (due to obstructions) and at unknown distance to the outcrop at the Ponds Location along pond 3. The estimated width of the channel is 38 meters. Note that the scale bar is relative to the outcrop, not the material in the foreground.

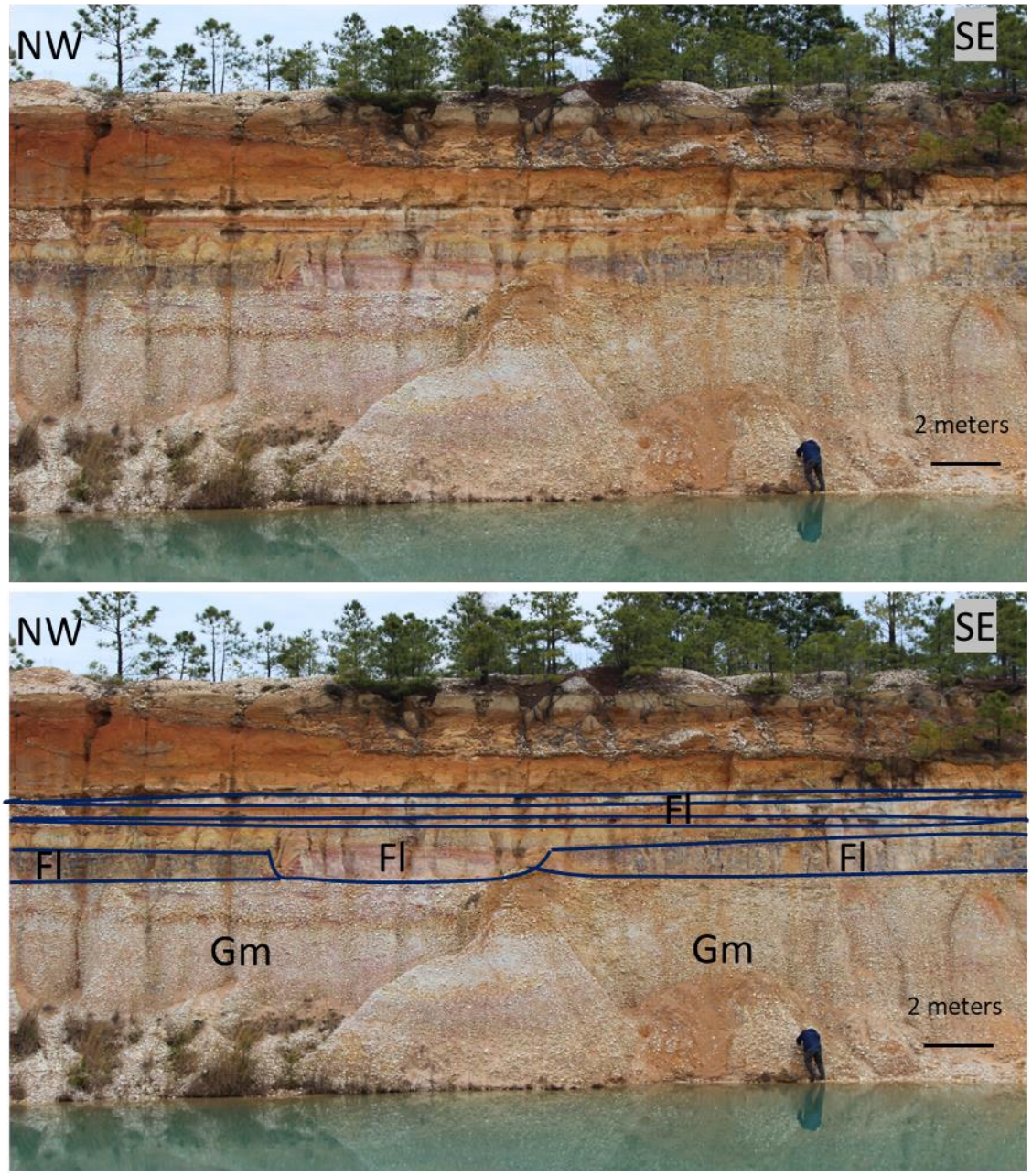

Figure 5.6. Uninterpreted (top) and interpreted (bottom) photos showing crevasse complex features such as splays and a channel form (located near the center of the photo) of facies Fl directly above facies Gm at Pond 3 along the outcrop in the Ponds locations.

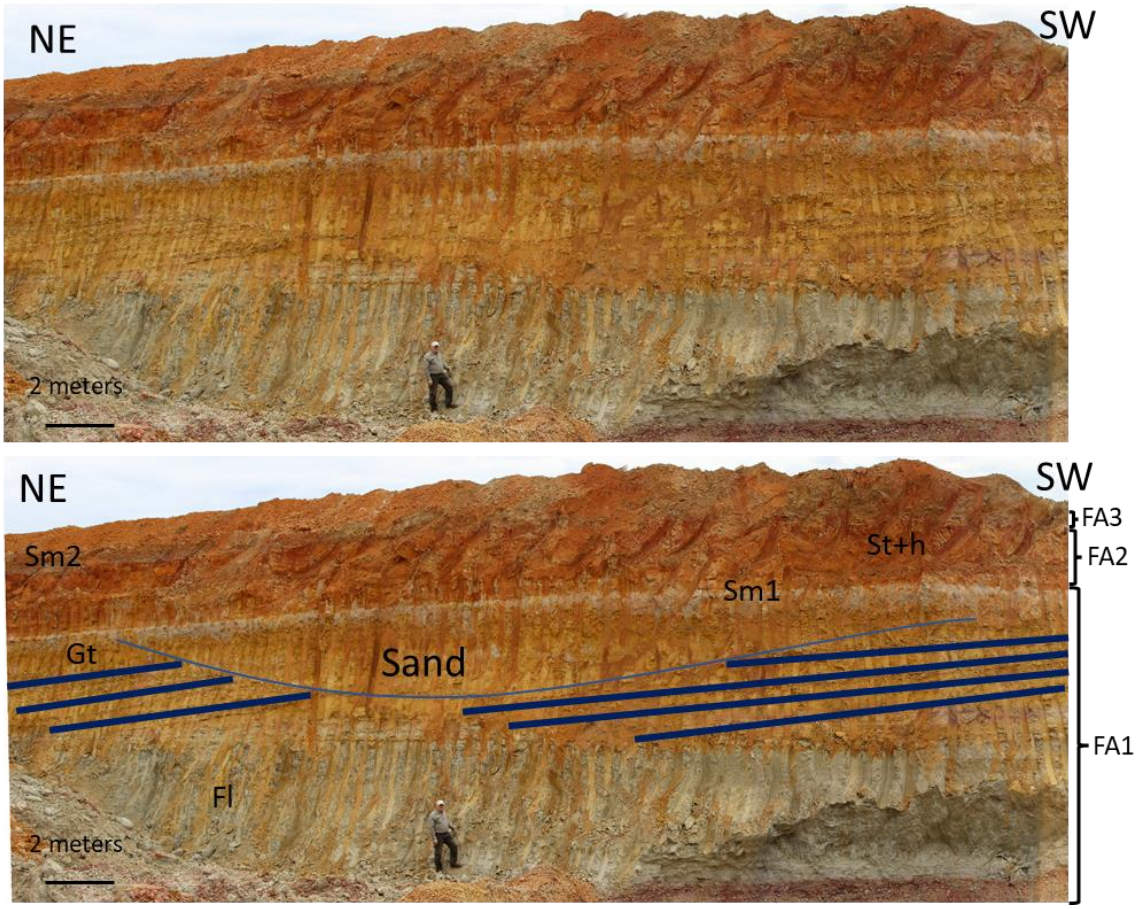

Figure 5.7. Uninterpreted (top) and interpreted (bottom) photos of a channel form incised into an earlier point bar deposit with lateral accretion surfaces near the Sump Pit 2 location. The channel is estimated to be 20 meters in width and 2 meters in height and indicates a flow direction that is due southeast. The earlier point bar migrated due northeast. The interpreted photo shows facies associations on the right-hand side. Facies are indicated on the photo. The channel form underlined in blue, occupying the center of the photo, could not be sampled but it consisted of sand.

5.2 Composite Facies Log for Field Area

Sedimentologic logs were measured throughout the field area and will be discussed in detail in following sections. Taken together, it is possible to construct an idealized, composite log containing the 8 lithofacies (Figure 5.8). Thus, the Lilesville gravels are comprised of a wide range of grain sizes and lithofacies that were deposited in stacked fining upwards sequences.

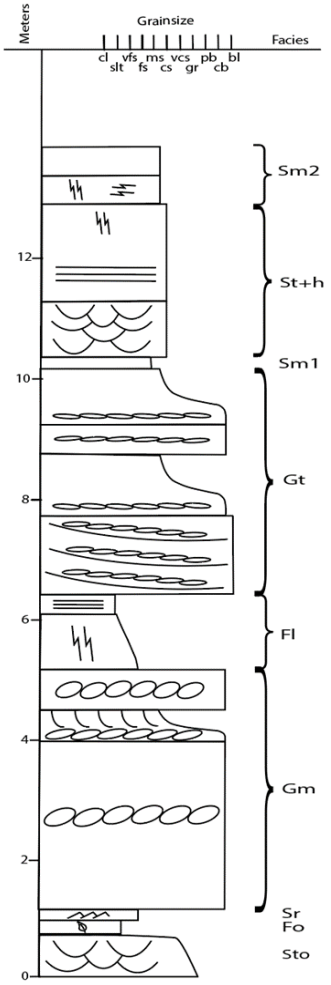

Figure 5.8. Idealized log created by merging the 8 lithofacies seen in the field area which include: Gm, Gt, St, Sm, Sh, Sr, Fl and Fo. Note that some variations of facies is present in this log in order to show stratigraphic significance such as Sto (at the base) and was observed at the 'Sump Pit' location. Sm1 is the white marker layer that is visible throughout the entire field area and is always beneath facies St+h. Facies St+h is always overlain by facies Sm2.

5.3 Highwall Exposures Adjacent to Ponds

The Lilesville gravels are well-exposed in the highwall adjacent to a set of ponds in the northern portion of the quarry. That highwall trends continuously for about 480 meters from southeast to northwest (Figure 5.9). The highwall is parallel to a series of settling ponds and adjacent to the edge of the old road right-of-way. At the southeastern end of Pond 1 (see site location on Figure 5.9) a detailed sedimentological log was described, and samples were taken for grainsize analysis. A soil profile was described for that site as well (see Figure 5.9). Imbrication data were collected from the facies Gm near Pond 1, site 4, and Pond 4, sites 14 and 15 (see Figure 5.9).

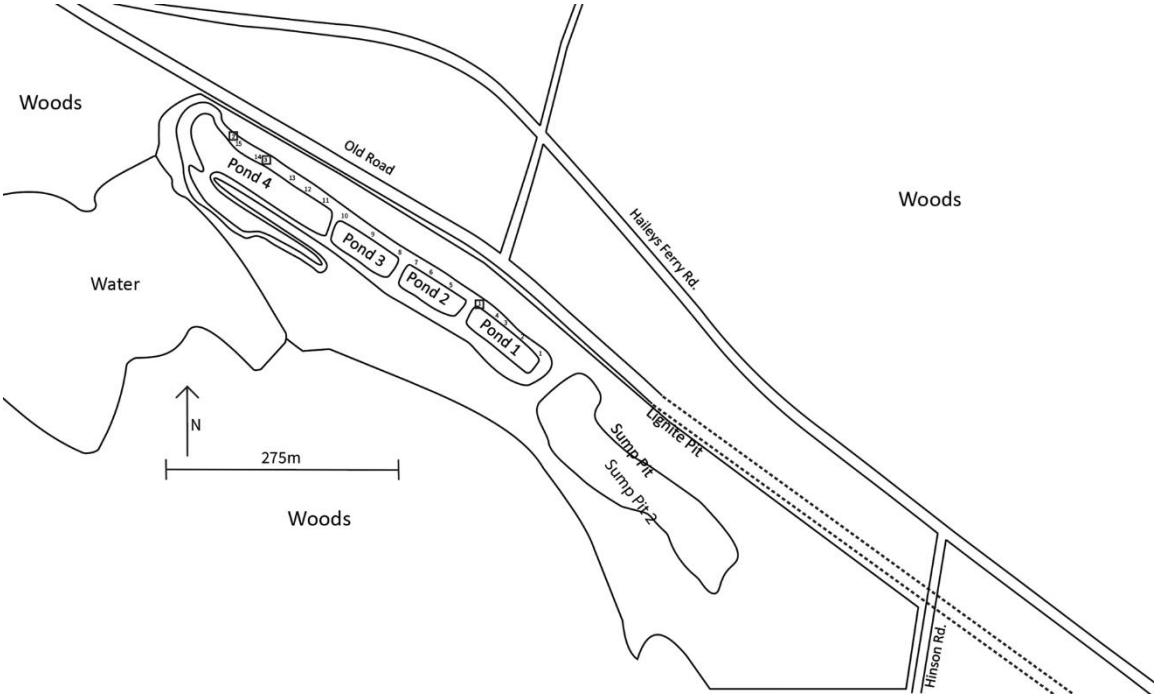

Figure 5.9. Generalized map of the Ponds, Lignite Pit, Sump Pit and Sump Pit 2 locations. Numbers 1-15 indicate sites where sedimentary logs were measured. The numbers outlined by square boxes are locations where imbrication, clast mineralogy and weathering rind data were collected.

5.3.1 Sedimentological Log at Site 1 of the Ponds Location

In these exposures, the Lilesville gravels are about 12 meters thick and composed of up to 8 lithofacies. At site 1 of the Pond 1 location a detailed sedimentological log was described (Figure 5.10) which contains 5 of these lithofacies. 14 more sedimentary logs were constructed by remotely viewing the outcrops along the east side of each of the ponds from south to north (see

Figure 5.9 for log sites 1-15). Units were then delineated to show the laterally continuous facies Sm1 marker bed and to show variations in facies Gm (Figure 5.18). These logs were used to construct facies overlays for panoramas of the outcrop (Figures 5.13, 5.14, 5.15, 5.16, 5.17, 5.18).

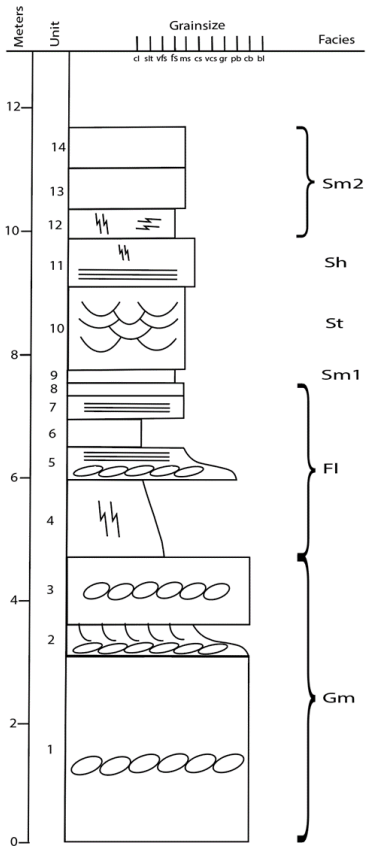

Figure 5.10. Sedimentological Log for site 1 along the outcrop at the Ponds location showing unit lithologies and associated facies.

At the base of the outcrop a massive gravel occurs (Figure 5.10). Facies Gm contains units 1, 2, and 3 which are composed of framework-supported quartz cobble conglomerates with interbedded medium to coarse cross-bedded sand lenses. The cobbles are white (N9.5 to 10YR 8.5/1), well-rounded, low sphericity, commonly imbricated, and usually range in length from around 4 centimeters to 10 centimeters. Larger clasts measuring up to 32 centimeters in length can be found locally in facies Gm. The cross-stratified sand lens is 40 centimeters thick and consists of medium to coarse grained, light reddish brown (2.5YR 6/4) quartz sand with mud rip-up clasts interbedded with clast supported gravels up to 15 cm thick (Figure 5.1B and 5.1C). The total thickness of facies Gm is about 4.5 meters starting from the water level surface in the

southeast of the outcrop at the first pond location and generally increases moving in a northwest direction along the ponds to a thickness of about 8 meters at the farthest north location.

The sandy silty facies (Fl) consists of units 4, 5, 6, 7, and 8 in Figures 5.10 and 5.11. Facies Fl overlies the basal gravel conglomerate along the ponds and each of these units seems to pinch in and out and appear at different positions for the length of the outcrop (Figure 5.7). Unit 4 is a 145-centimeter-thick silty fine sand that grades upwards into a very fine sandy silt. For most of the entire outcrop, this unit is a distinctive lavender color (5R 5/3) with dark red (5R 3/6) and white (2.5Y 8/1) mottling. Unit 5 is 65 centimeters thick and is composed of a cobble conglomerate grading into a fine-medium grained sand towards the top of the unit. The basal cobbles are 7 centimeters in length and are typically white (5YR 9/1). A 20-centimeter-thick dark grey pebbly sand is located in the middle of the unit. The upper portion of the unit is fine to medium grained yellowish red (5YR 5/6) sand with millimeter scale laminations in the upper 30 centimeters. Unit 6 is a 45-centimeter massive silt that outcrops as a recessive layer with a clay rich matrix and mottling (Figure 5.11). The unit is mostly white (N8.5) and the mottling is yellow (10YR 8/6) to yellowish red (5YR 5/8). Unit 7 is a 35-centimeter medium grained, quartz arenite sand layer with centimeter-scale horizontal bedding. Color varies from pink (7.5YR 8/4) to pale brown (7.5YR 7/6). Unit 8 is a 30-centimeter fine to medium grained, massive, poorly sorted sand layer. The color ranges from yellow (10YR 8/6) to very pale brown (10YR 8/4). This unit is not as well lithified as others and as a result it is a slope forming layer. Some granule-sized clasts are present at various locations in the lower part of the unit. The presence of units 5-8 is variable throughout the length of the pond outcrop moving from the southeast to the northwest.

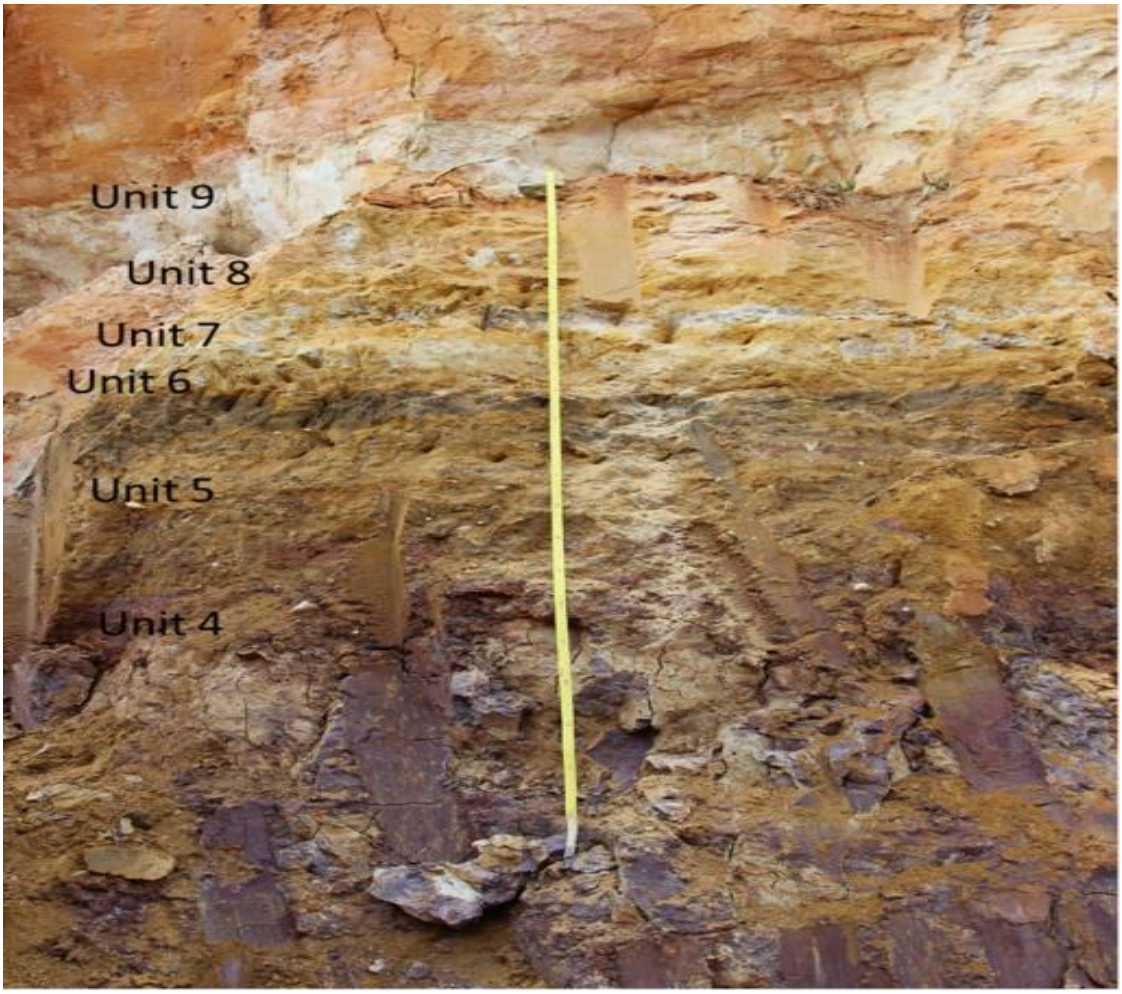

Figure 5.11. Photo of outcrop at Pond 1, site 1, showing units 4-9.

Facies Sm1 (white massive sand) consists of unit 9 and it is a 25-centimeter thick, fine-medium grained white (10YR 9.5/1) sand layer. This unit has some zones that have a concentrated clay matrix as well as some zones where the sand is very loose, spilling out and cascading down the outcrop very easily. This is a recessive layer that is poorly cemented and eroded back into the quarry wall. This layer is laterally extensive and consistent in thickness on the order of decimeters at all locations in the quarry unless it has been removed by mining operations. This unit is an important 'marker bed' present throughout the quarry exposures.

Sandy facies St (trough cross-bedded sand) and Sh (horizontally bedded sand) include units 10 and 11. Unit 10 is a 110-centimeter, medium grained sand layer (Figure 5.12). Grains are

sub-rounded to sub-angular and the unit is primarily light red (5R 7/6) in color. Cross-bedding occurs in sets that are 30-40 centimeters thick and cross-bed sets dip to the south indicating a southerly flow direction. Occasional sub-vertical white (10YR 9/1) mottles that are 5–8 centimeters in diameter and up to 1 meter in length are present. Unit 11 is a 70-centimeter, medium- to coarse-grained sand layer dominated by vertical mottling. The mottles are 5-8 centimeters in diameter and up to 70 centimeters in length. Mottles are filled with brownish yellow (10YR 6/6) sand, and surrounded by red (2.5YR 4/8) sands. Where mottles are not present, thin horizontal laminations and cross bedding similar to Unit 10 can be seen. Throughout the field area these sandy facies always occur above facies Sm1 however the nature of the next facies overlying Sm1, whether trough cross-beds or horizontal beds, can vary. At Pond 1, site 1, trough cross-bedding (unit 10) directly overlies facies Sm1 (unit 9).

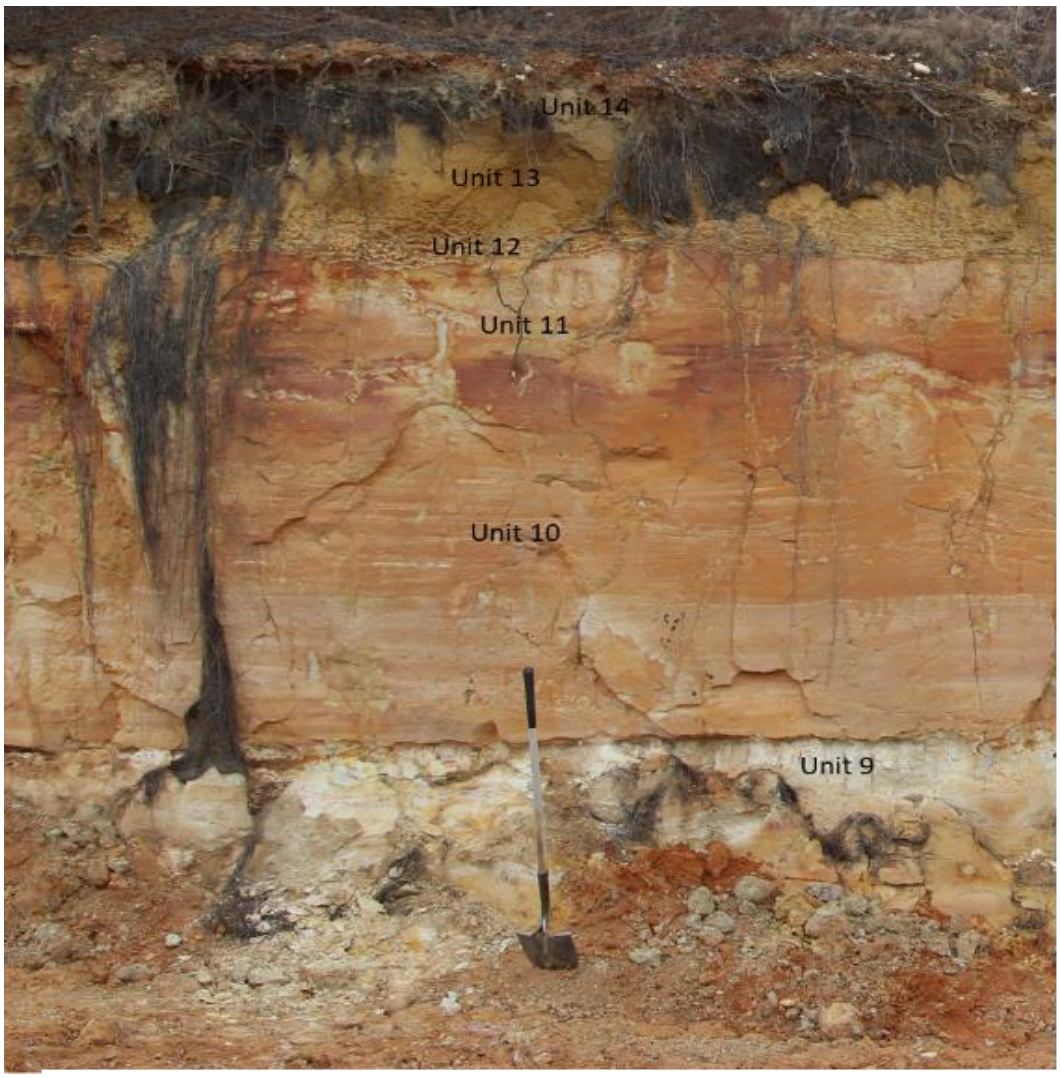

Figure 5.12. Photo of outcrop at Pond 1, site 1, showing units 9-14. Note the distinctive flat, sharp boundary between unit 9 and unit 10 as well as the distinctive undulating boundary between unit 11 and unit 12.

Facies Sm2 consists of units 12-14 and is comprised of brownish-yellow to tan, fine to medium grained, moderately to well-sorted sands (Figure 5.12). Mottling is most extensive in unit 12, diminishing in abundance moving up-section into unit 13 and not present in unit 14. Unit 12 is a 50-centimeter-thick fine- to medium-grained massive sand layer. This unit has abundant reticulated mottling filled with brownish yellow (10YR 6/6) sand. The mottles are 1-5 centimeters in diameter and a decimeter or so in length. The sand surrounding the mottles is oxidized red (2.5YR 5/8). Unit 13 is a 70-100 centimeter, fine- to medium-grained, massive, brownish yellow (10YR 6/6) sand layer. The sands are quartz-dominated with moderately-well

rounded and occasional sub-angular grains. Mottling is largely absent from this unit, as are observable sedimentary structures. Unit 14 is 50 centimeters thick and is composed of a fine- to medium-grained, massive, light tan (10YR 6/6) sand layer. The sands are quartz-dominated with moderately well-rounded and occasional sub-angular grains. Mottling is absent from this unit, as are observable sedimentary structures.

Capping the outcrop is a layer of spoils of various thickness and composition, a product of mining operations.

5.3.2 Facies Architecture along the Ponds Location

The construction of panoramic images of quarry exposures yields valuable information about the facies architecture of the Lilesville gravels at the B V Hedrick Gravel and Sand quarry field site. These panoramas can be used to trace the boundaries between, and geometries of, different facies throughout the exposures. The highwall exposure on the east side of the ponds in the quarry provides an example of the facies architecture of this depositional system.

In these panoramas (Figures 5.13 to 5.17), facies Gm (highlighted in green) extends along the base of the entire exposure thickening to the northwest. Facies Fl (highlighted in red) can be seen to thicken and thin along the length of the highwall outcrop adjacent to all 4 ponds (Figures 5.13 to 5.17). Those units are overlain or cut out by facies Sm1, a distinctive white colored recessive ‘marker bed’ found throughout the quarry. The thickness of the ‘marker bed’ is generally uniform however it can thin and thicken by a few to several centimeters in some areas. The ‘marker bed’ is overlain by the sandy facies St+h (highlighted in yellow) which also extends the full length of the panorama with a consistent thickness (Figures 5.13 to 5.17). The top of the outcrop is capped by facies Sm2 (highlighted in pink) which maintains somewhat uniform thickness for the full length of this panorama but some portions of it may have been removed due to mining operations (Figures 5.13 to 5.17). The top of the profile comprises a laterally discontinuous layer of spoils material.

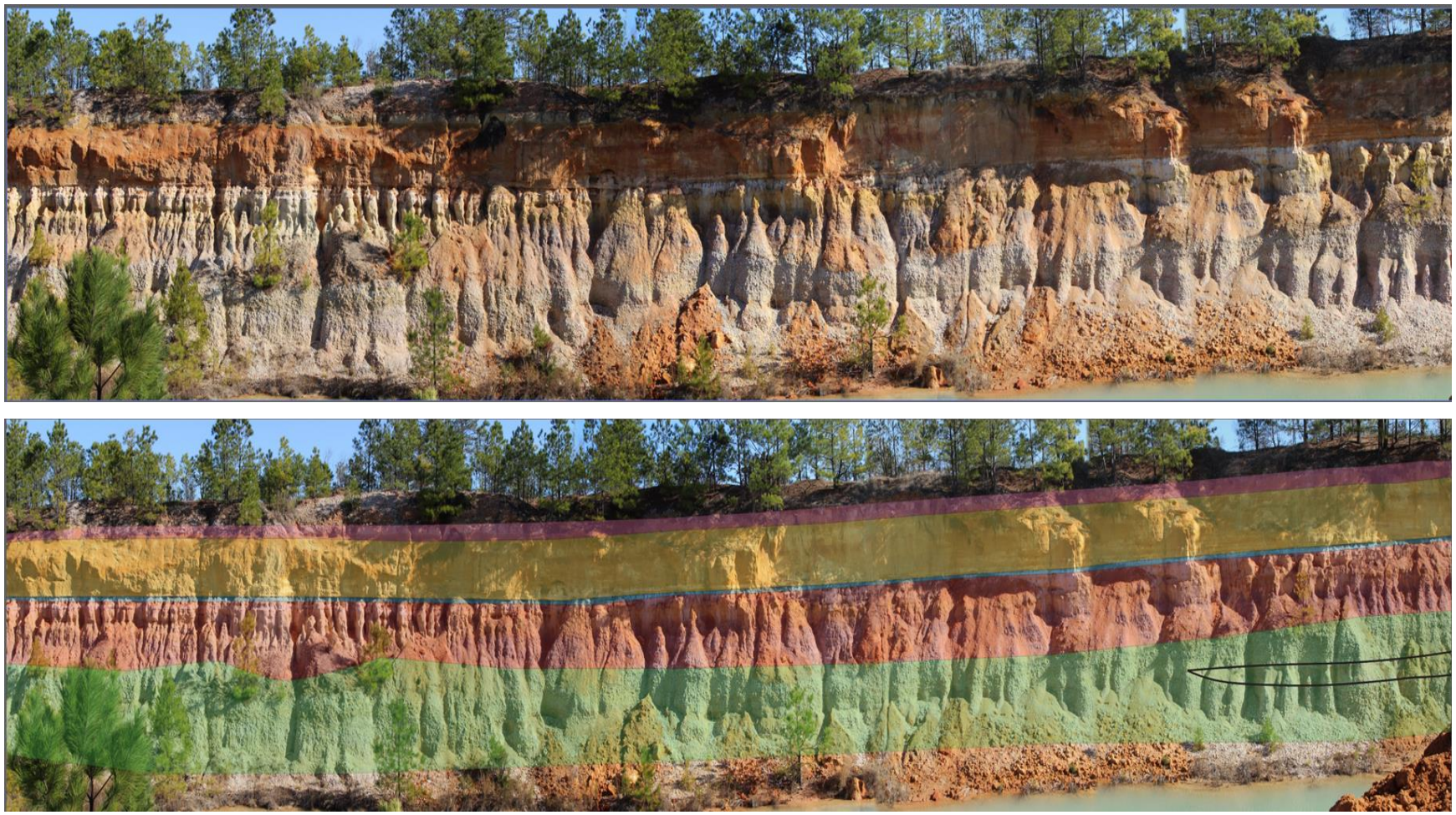

Figure 5.13. Uninterpreted (top) and interpreted (bottom) panoramas of the outcrop along the Pond 1 location. Facies Gm (green), Fl (red), Sm1 (blue), St+h (yellow) and Sm2 (pink). There is a channel form where facies Fl cut into Gm in the middle left of the panorama as well as the lateral continuity of facies Sm1 and St+h. Note the sandy lens interbedded in facies Gm outlined in black.

Figure 5.14. Uninterpreted (top) and interpreted (bottom) panoramas of the outcrop along the Pond 2 location. Facies Gm (green), Fl (red), Sm1 (blue), St+h (yellow) and Sm2 (pink). Facies Gm is seen to be interbedded with facies Fl with variable thickness.

Figure 5.15. Uninterpreted (top) and interpreted (bottom) panoramas of the outcrop along the Pond 3 location. Facies Gm (green), Fl (red), Sm1 (blue), St+h (yellow) and Sm2 (pink). Facies Gm and facies Fl are interbedded for the entire length of the outcrop and continue into Pond 4.

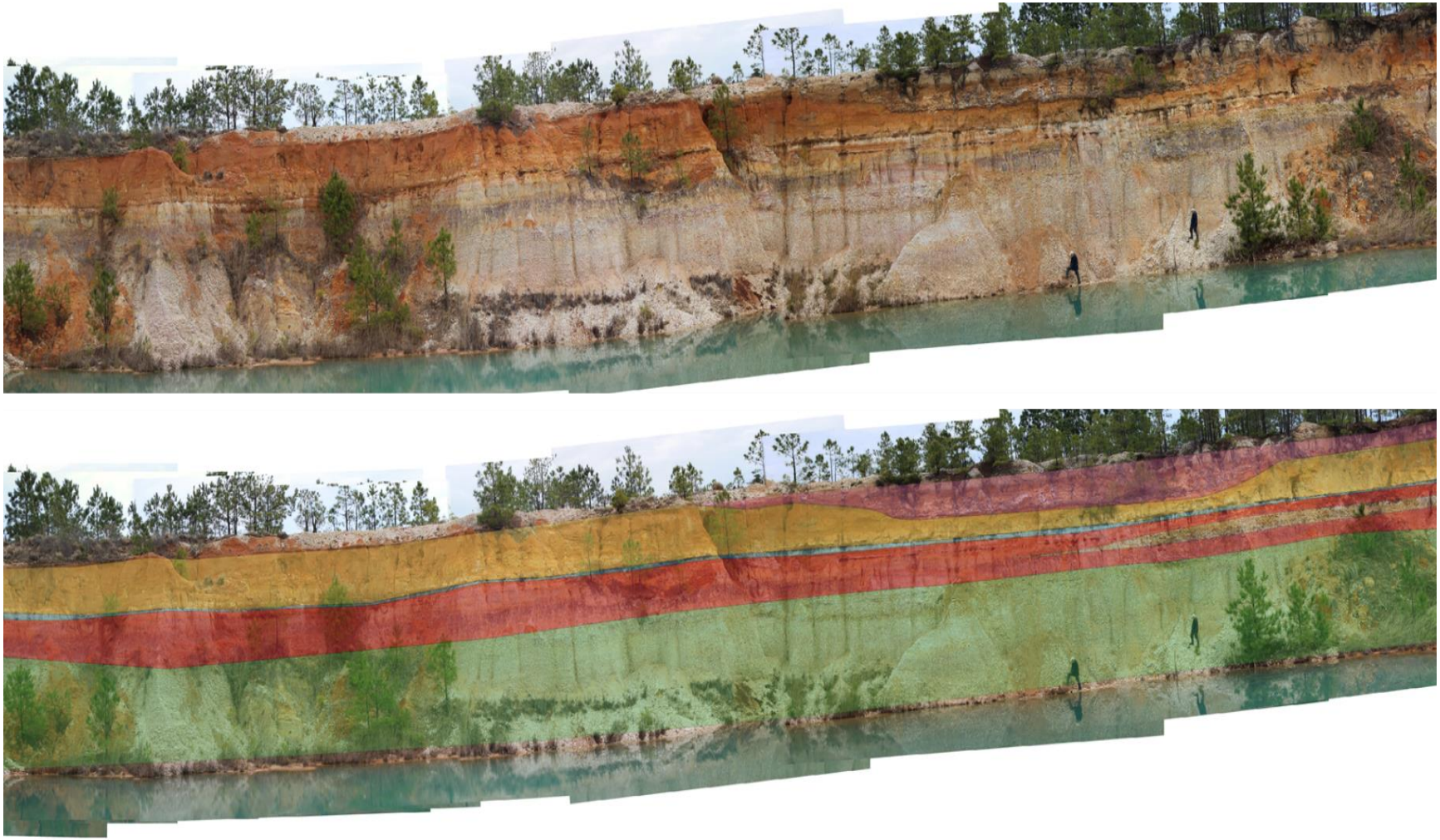

Figure 5.16. Uninterpreted (top) and interpreted (bottom) panoramas of the outcrop along the Pond 4 location. Facies Gm (green), Fl (red), Sm1 (blue), St+h (yellow) and Sm2 (pink). Facies Gm pinches out of facies Fl in the beginning third of the panorama. A channel form can be seen cutting into facies St+h consisting of what is believed to be facies Sm2 (close observation was not possible).

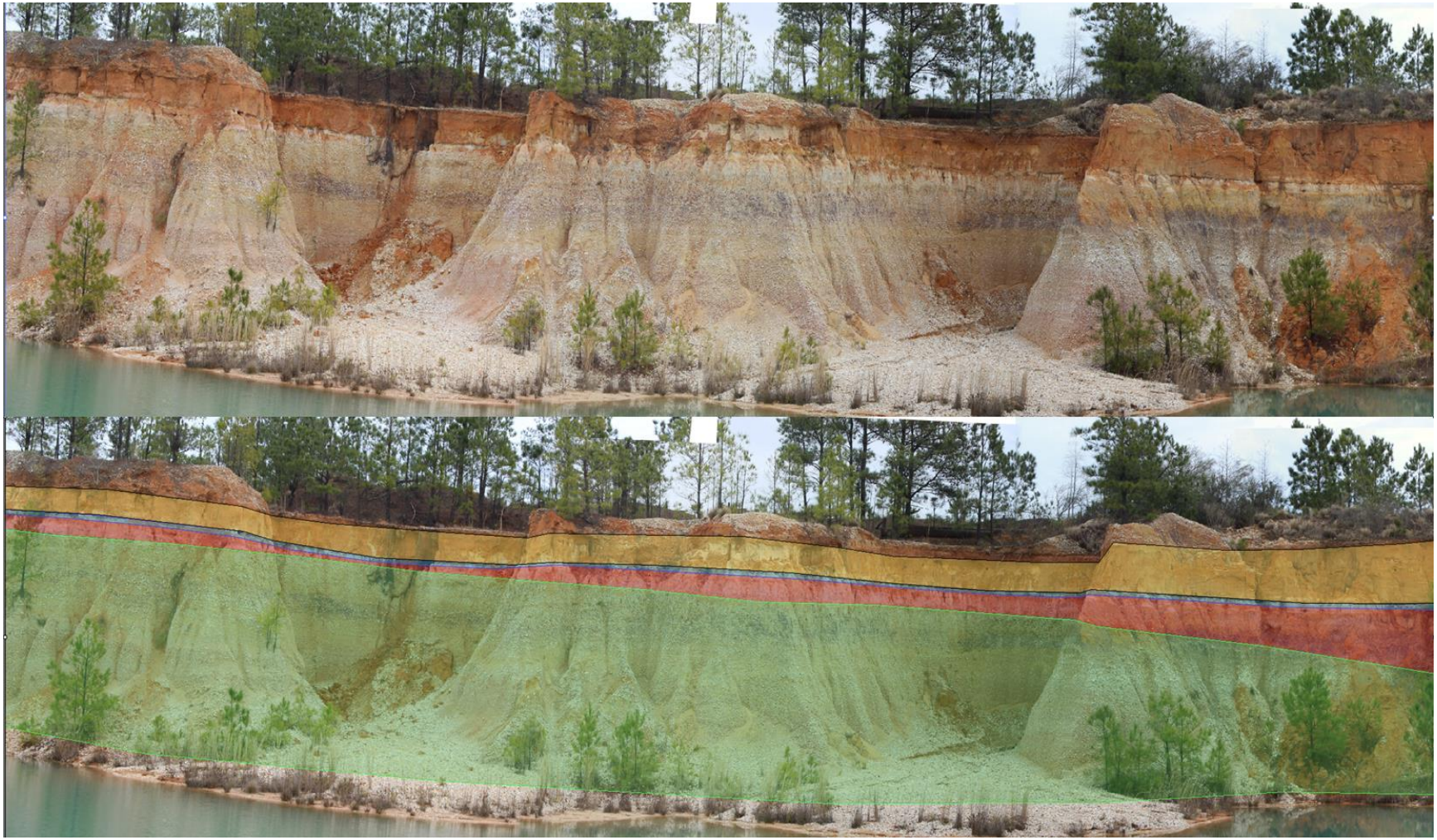

Figure 5.17. Uninterpreted (top) and interpreted (bottom) panoramas of the farthest north reach of the outcrop in the Ponds location. Facies Gm (green), Fl (red), Sm1 (blue), St+h (yellow) and Sm2 (pink). Facies Gm reaches its thickest moving north while facies Fl thins over the length of this entire outcrop. The curvature for all facies towards the north end of the panorama is due to variation in the distance to the outcrop.

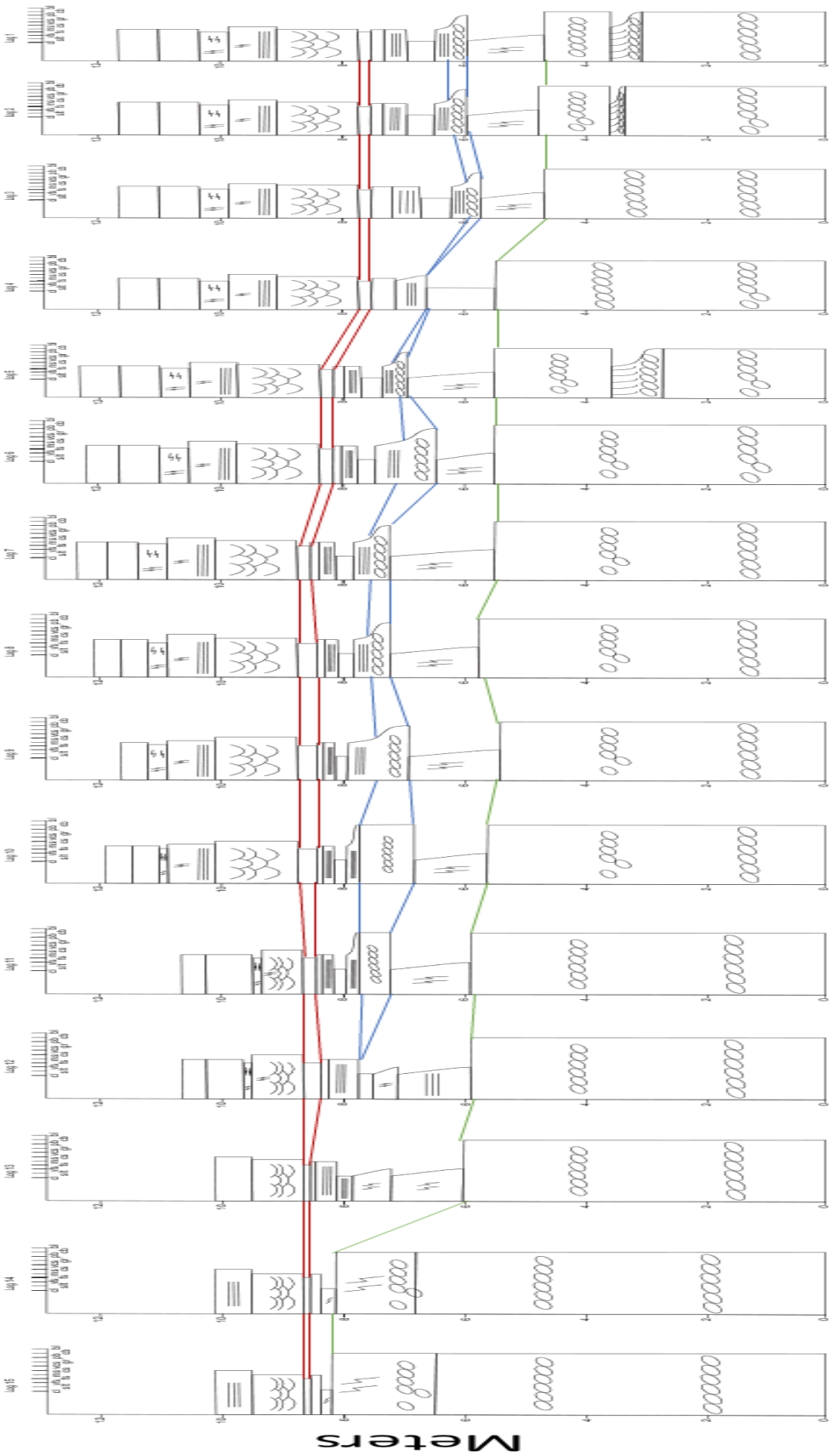

Figure 5.18: Facies Logs along the highwall at the Ponds locations. Red Lines indicate upper and lower boundaries for the laterally extensive white layer. The blue lines indicate upper and lower boundaries for a gravely lens that is present from log one and pinches out by log 4. Then reappearing at the site 5 position and continuing until the site 11 position. The green line shows the boundary for the gravely facies that thickens moving to the northwest from site 1 to site 15.

5.3.3 Imbrication data

Imbricated clasts were abundant primarily at the Pond locations (Figure 5.9) as well as in other gravely deposits in other locations in the field area. Imbrication, composition, and weathering rind thickness measurements were collected from three locations along the ponds (see Figure 5.9 for imbrication locations). Clasts were taken from the massive to crudely bedded gravelly (Gm) facies. Rose diagrams were then created which show flow direction as well as dip magnitude and dip direction (Figure 5.19). In general, the flow direction trends to the southeast. At Location 1, a few clasts were measured that had dips opposite to the prevailing flow direction. The average dip magnitude for the three locations combined is 26.4°. The data sheets for imbrication data appear in Appendix E.

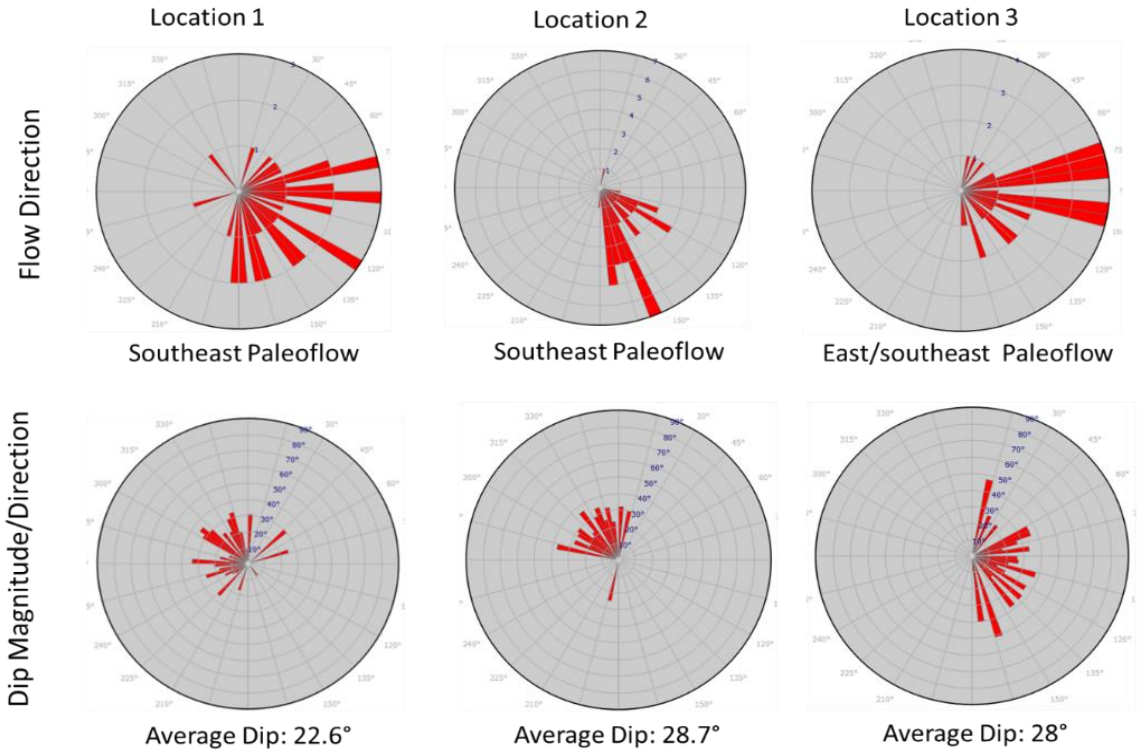

Figure 5.19. Rose diagrams showing Paleoflow from imbrication measurements.

5.3.4 Mineralogy

Mineralogy of each clast was recorded while measuring imbrication (Appendix E). The dominant mineral in the field area is quartz, most of which being quartzite (92%) and minor vein quartz (8%).

Heavy minerals were separated and weighed, and the masses recorded for each of the samples collected from the Pond 1 location at site 1 and shown in Table 5.1. The heavy mineral fraction of the samples was epoxied to slides and viewed under a petrographic microscope to determine the heavy mineral composition and percentages of each sample. Minerals were identified following the method outlined by Lindholm (1987) and include properties such as: 1) whether the mineral is isotropic or anisotropic, 2) pleochroism, 3) birefringence, 4) extinction angle, 5) color, and 6) cleavage. Minerals identified include opaque minerals as well as several non-opaque minerals such as zircon, rutile, kyanite, tourmaline, sillimanite, monzonite, and any unknown non opaque minerals were noted as well (Table 5.2). Specific grain count data are located in Appendix G.

The gravely facies (samples HQ-P1- units 1, 2 and 3, for locations of unit numbers see Figure 5.10) are similar in mineral composition with a large proportion of opaque minerals followed by zircon. HQ-P1- unit 2 is a sandy lens within the gravely facies and has a higher percentage of non-opaques. The fine facies (samples HQ-P1- units 4, 5, 6, 7 and 8) are similar with higher proportions of opaque minerals than zircon. The percentage of rutile increases compared to the gravely facies samples. Heavy minerals in facies Sm1 (sample HQ-P1- unit 9) have a distribution similar to the gravely facies as well as the fine facies, however, no kyanite was observed. The percentage of rutile in sample HQ-P1- unit 9 is the highest of all the samples at 10%. The trough cross bedded sand (St) facies (sample HQ-P1- unit 10) is consistent with previous samples. HQ-P1- unit 11, sandy facies Sh, has the lowest proportion of opaque minerals at 48%. Zircon and tourmaline are highest in this unit at 21% and 11%, respectively. Samples

HQ-P1-units 12 and 13 are very similar to each other and don't show any major differences in heavy mineral percentages and composition from previous samples.

A few general trends are noticeable: 1) The percentage of heavy minerals are generally higher in the gravely facies (HQ-P1- units 1, 2 and 3) and fine facies (HQ-P1- units 4, 5, 6, 7 and 8) (see Table 5.1 and Figure 5.10); 2) Zircon, rutile and tourmaline are present in all facies (see Table 5.2); 3) Beginning at facies Sm1 (HQ-P1- unit 9) the proportion of opaque minerals are lower than in facies Fl and Gm (see Table 5.2).

Location at Pond 1				
Sample	Starting mass (g)	After seperation mass (g)	% Heavies	Facies
HQ-P1-1	0.93	0.03	2.81	Gm
HQ-P1-2	0.95	0.03	3.17	St
HQ-P1-3	1.14	0.02	1.45	Gm
HQ-P1-4	5.21	0.03	0.56	Fl
HQ-P1-5	1.02	0.01	0.86	Fl
HQ-P1-6	6.07	0.01	0.12	Fl
HQ-P1-7	6.80	0.02	0.36	Fl
HQ-P1-8	7.66	0.03	0.42	Fl
HQ-P1-9	8.07	0.02	0.19	Sm1
HQ-P1-10	6.67	0.01	0.09	St
HQ-P1-11	6.45	0.00	0.07	Sh
HQ-P1-12	6.54	0.01	0.18	Sm2
HQ-P1-13	6.78	0.02	0.32	Sm2

Table 5.1. Results of heavy mineral separation for samples at site 1, Pond 1. See Figure 5.10 for locations of unit samples.

Sample	% Opaque	% Zircon	% Kyanite	% Rutile	% Tourmaline	% Sillimenite	% Monazite	% Unknown	% Non Opaques
HQ-P1-1	91.94	2.84	1.42	1.90	1.90	0.00	0.00	0.00	8.06
HQ-P1-2	83.21	9.38	1.23	1.98	2.22	0.99	0.99	0.00	16.79
HQ-P1-3	87.84	6.08	0.00	1.35	2.03	0.00	2.03	0.68	12.16
HQ-P1-4	94.74	2.63	0.00	1.58	0.53	0.00	0.53	0.00	5.26
HQ-P1-5	88.98	5.51	0.85	3.39	0.85	0.00	0.42	0.00	11.02
HQ-P1-6	81.31	6.07	2.91	6.80	1.46	1.46	0.00	0.00	18.69
HQ-P1-7	92.59	1.59	0.79	2.91	1.32	0.00	0.79	0.00	7.41
HQ-P1-8	90.00	0.48	1.43	5.71	0.95	0.48	0.95	0.00	10.00
HQ-P1-9	83.65	4.09	0.00	10.06	2.20	0.00	0.00	0.00	16.35
HQ-P1-10	84.51	1.88	1.41	6.57	3.29	1.41	0.47	0.47	15.49
HQ-P1-11	48.48	21.21	8.08	8.08	11.11	2.02	0.00	1.01	51.52
HQ-P1-12	76.80	8.17	1.63	7.52	4.25	1.63	0.00	0.00	23.20
HQ-P1-13	79.77	7.62	2.35	4.99	4.11	0.59	0.59	0.00	20.23

Table 5.2. Results of petrographic microscope analysis of opaque and non-opaque minerals for samples at site 1, Pond 1

5.3.5 Grain Size data

The grain sizes calculated from the samples collected at the site 1 location include the finer than 2-millimeter fraction (phi size -1). This means that the grainsize data describes the matrix of the samples collected for the Gm facies. A more thorough analysis of the Gm and Gt facies was conducted where measurements were taken in the field for the coarser than 2-

millimeter fraction. That data will be discussed later in the results with the 'HQ-G' data set. The results of the grainsize analysis studies can be seen in Appendix A and includes grainsize distribution graphs as well as grainsize statistics.

5.3.6 Soil Profile Data

Five generations of soils were identified in the outcrop at Pond 1, site 1 (Figure 5.9). The soil descriptions for the entire profile are listed in Appendix H. The five soil units consist of HQA-2 (Figure 5.20), HQA-5 (Figure 5.20 and 5.21), HQA-6 (Figure 5.21), HQA-7 (Figure 5.21), and HQA-9 (Figure 5.22). HQA-1 is at the top of the profile, which is a layer of spoils produced by mining operations and does not exhibit in situ soil features.

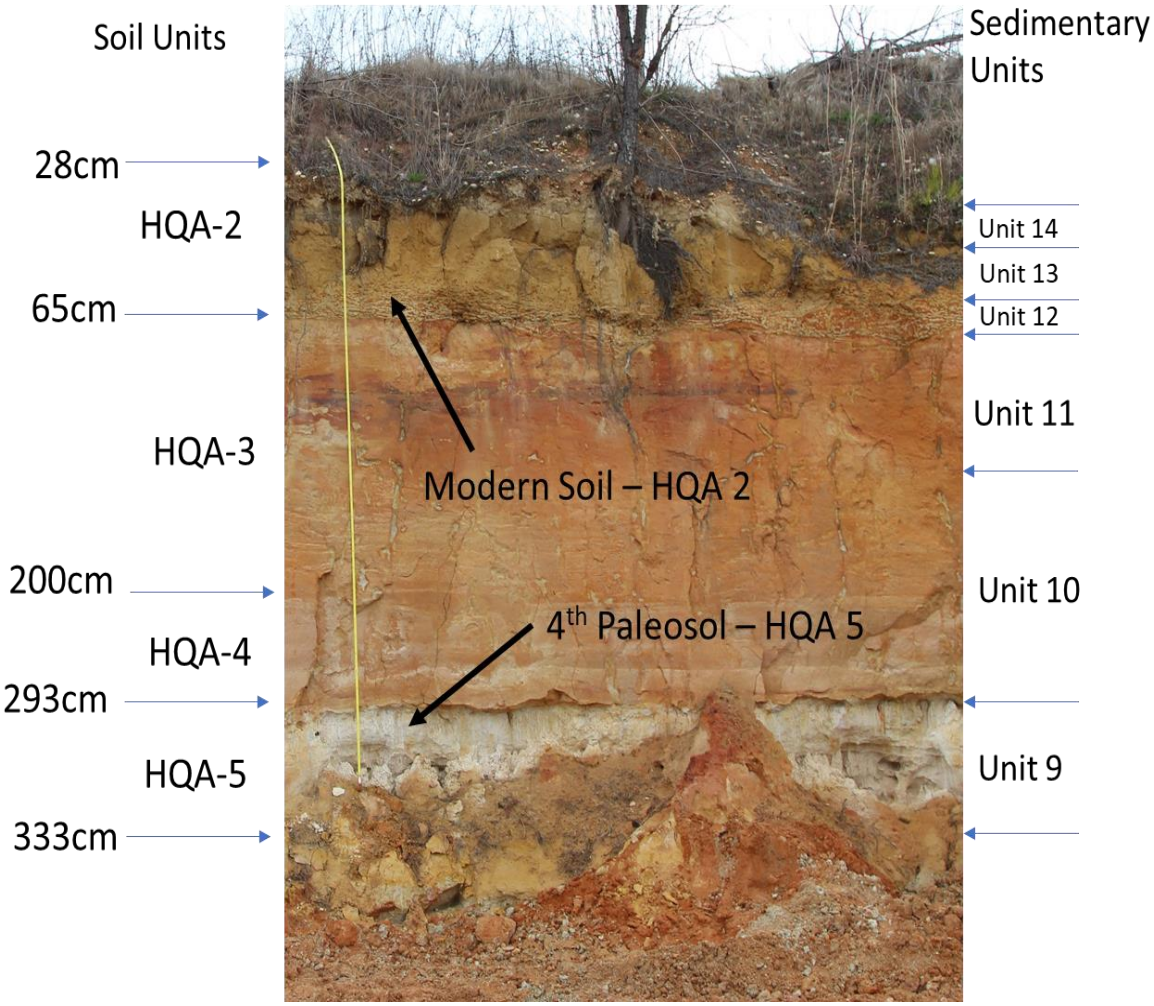

Figure 5.20. Outcrop photo at Pond 1 showing soil profile and paleosol HQA-5 and the modern soil HQA-2. Arrows indicate approximate depths of units. See Figures 5.10 and 5.12 for explanation of sedimentary units on right side of photograph.

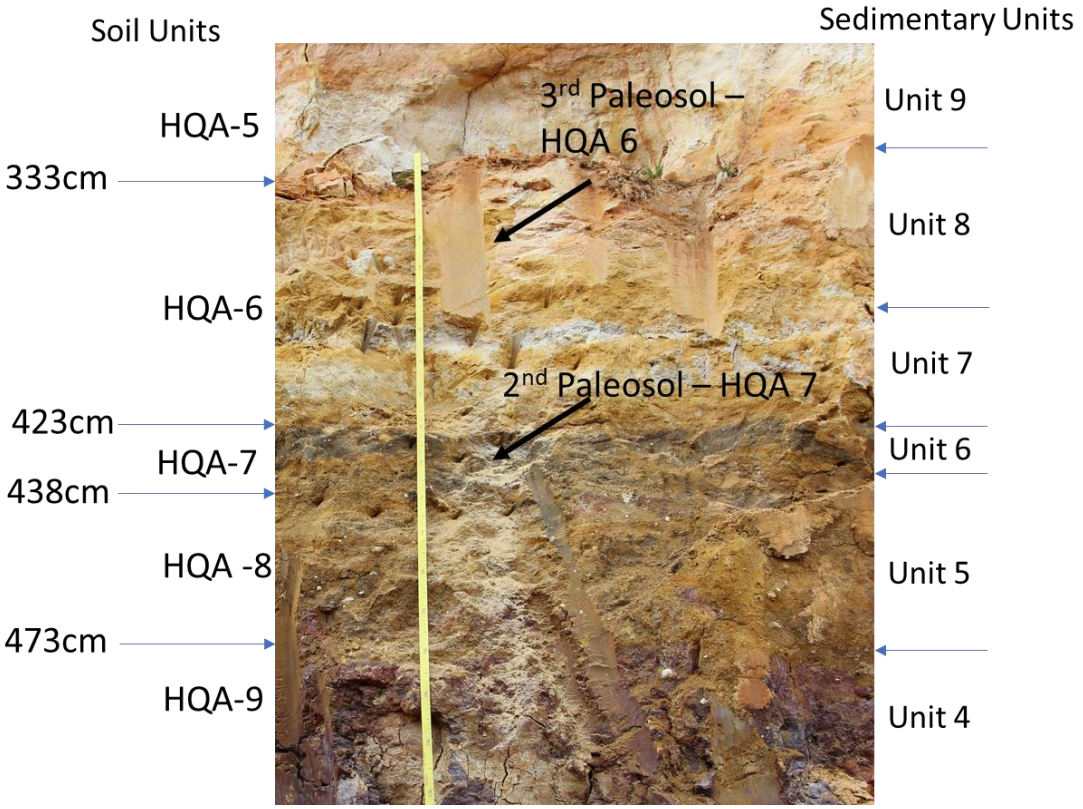

Figure 5.21. Photo of outcrop at Pond 1 showing soil profile and paleosols HQA-6 and HQA-7. Arrows indicate approximate depths of units. See Figure 5.10 and 5.11 for explanation of sedimentary units.

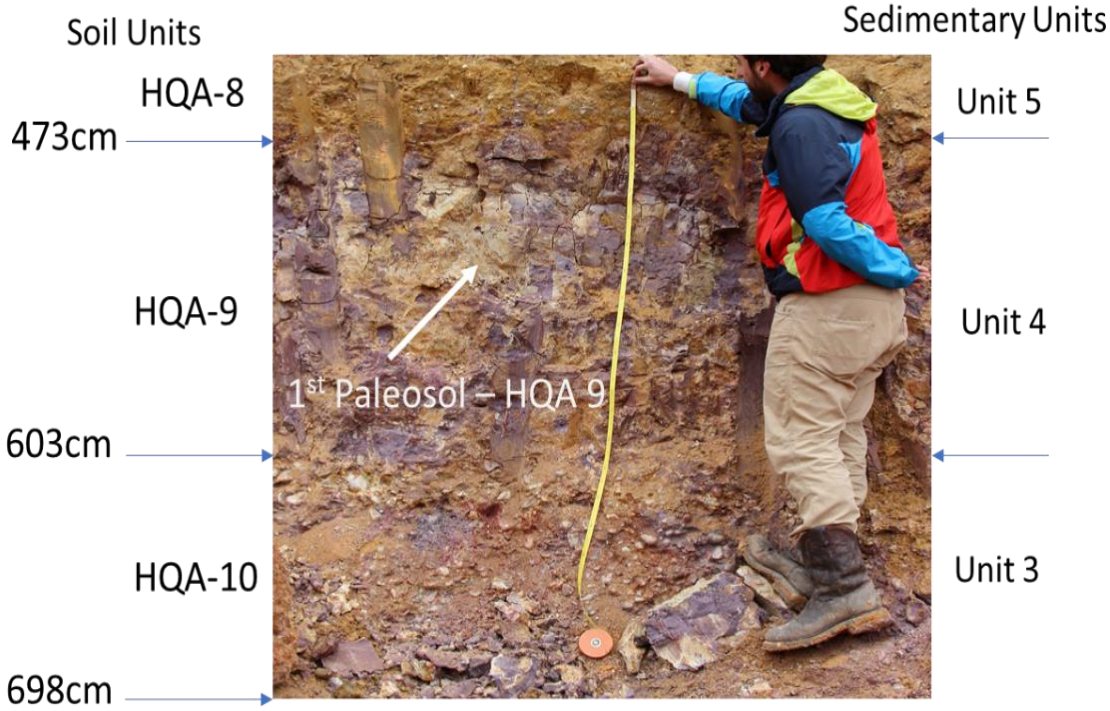

Figure 5.22. Photo of outcrop at Pond 1 showing soil profile and paleosol HQA-9. Arrows indicate approximate depths of units. See Figures 5.10 and 5.11 for explanation of sedimentary units.

Percentages of extractable iron values for Fe_h and Fe_d and the iron activity ratio were calculated for all samples taken from the soil profile and are listed in Appendix I. Higher Fe_d weight percentages are present in three of the soils described in the field including HQA-9, HQA-7, and HQA-2 (Figure 5.23). HQA-5 shows a relatively low weight percent of Fe_d.

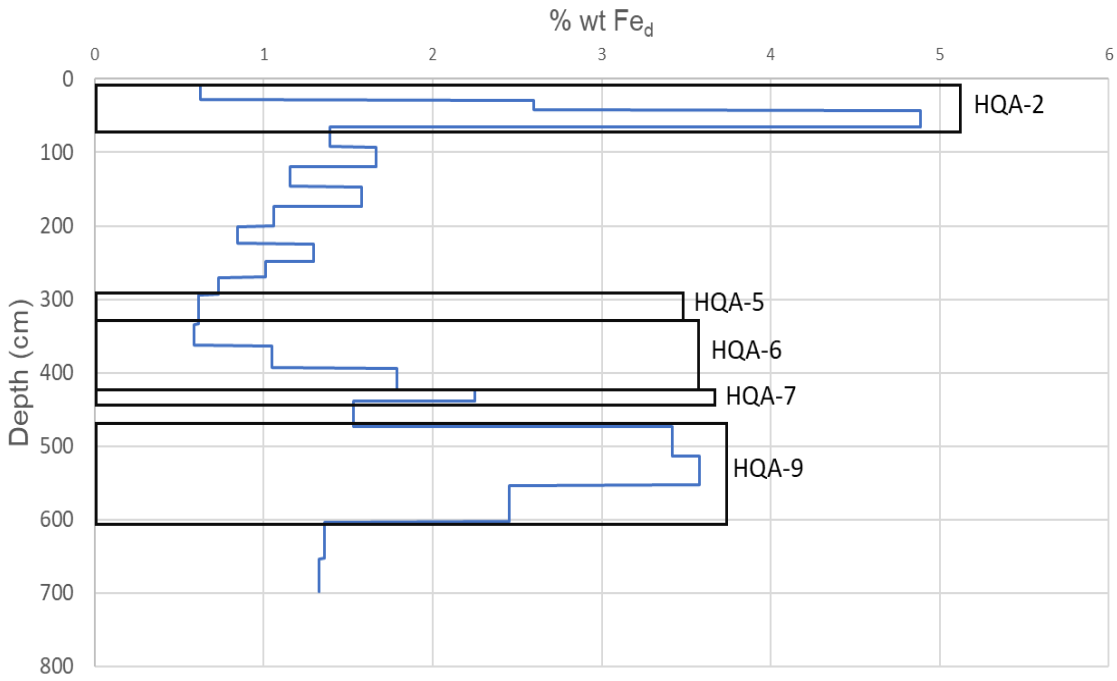

Figure 5.23. Depth profile of Fe_d at Pond 1, site 1. Boxes outline soils identified in the field.

Elemental compositions of silicon, aluminum, iron, and titanium were produced from XRF analysis for all of the HQA samples. Elemental compositions were used to produce depletion/enrichment curves for each of the elements (Figure 5.24) using sample HQA-10-2 as the parent material. This method assumes titanium is an immovable element so all others can be compared to it. Soils HQA-2 and HQA-9 increase in iron with depth especially B horizons in HQA-2 and HQA-9. Soils HQA-5 and HQA-6 become depleted in iron. The percent of aluminum decreases in HQA-2, HQA-5, and HQA-6. In HQA-9 the percentage of aluminum remains constant through the horizons. Silicon decreases in HQA-2, HQA-5, HQA-6, and HQA-9. HQA-7 (described as a buried A horizon) does not have a change in elemental percentages with iron,

aluminum and silicon. Overall, there is an enrichment of iron, aluminum and silicon that occurs from 65 centimeters to 293 centimeters.

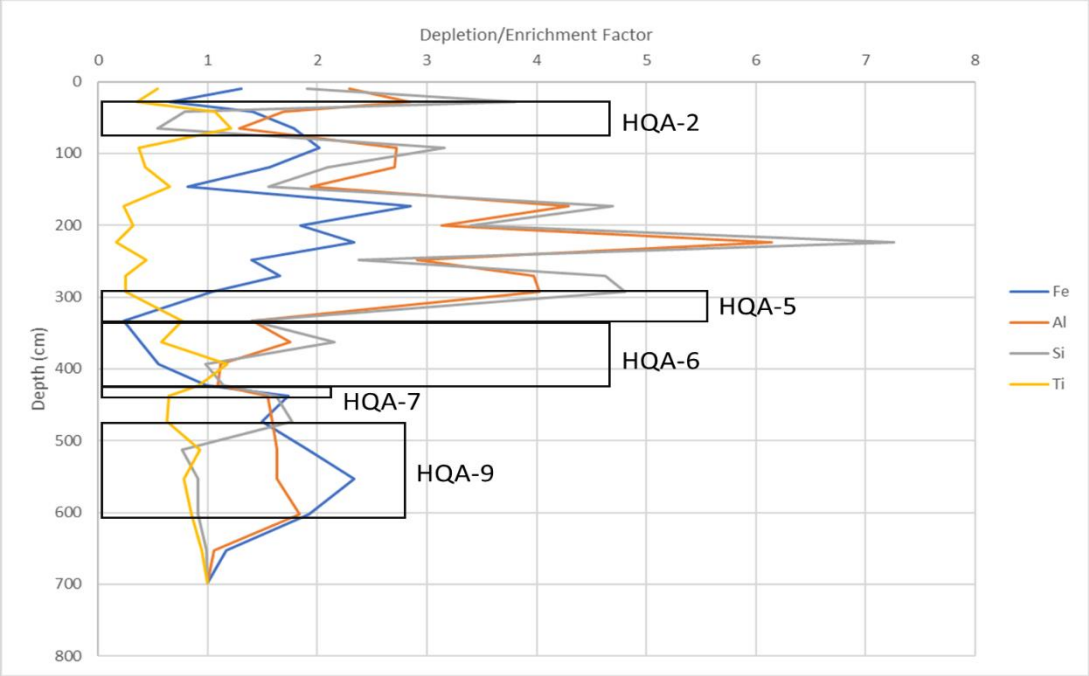

Figure 5.24. Depletion/enrichment factors for elements iron (Fe), aluminum (Al) and silicon (Si) at Pond 1, site 1. The titanium curve represents the titanium ratio, not the depletion/enrichment factor (because titanium is considered immobile). Black boxes outline soil horizons.

5.4 Lignite Pit Location - Overview

The lignite pit was unearthed during mining operations and prompted much interest in this location. Organic matter, including plant micro- and macro-fossils, found within the lignite could yield information to help infer the age of the Lilesville gravels. The Lignite Pit location, containing the Lilesville Lignite, is in the southeastern part of the field area, just south and east of the Ponds locations (Figure 5.9). A remotely constructed sedimentological log was created for the entire lignite outcrop along with detailed sampling for grainsize analysis of a 2 meter interval beginning at the water surface contact with the lignite and upward into the overlying silts and sands. Samples collected from the lignite unit were sent to Dr. Frederick Rich at Georgia Southern University to be analyzed for pollen content.

5.4.1 Sedimentological Log at the Lignite Pit

The outcrop exposed at the Lignite Pit is about 12 meters in height from water level to the top of the highwall and it was recorded remotely (Figure 5.25).

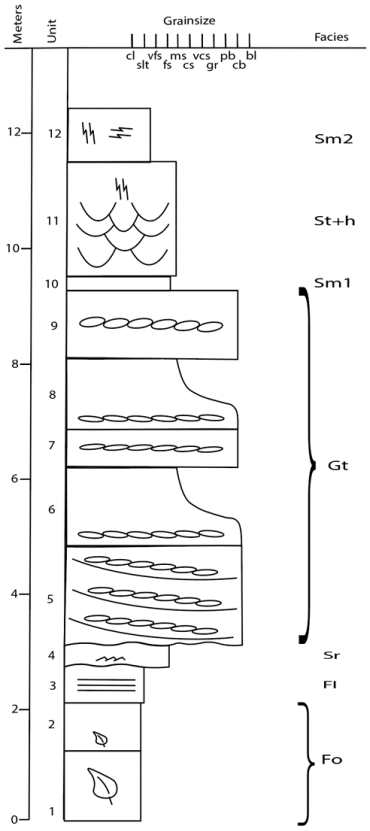

Figure 5.25. Sedimentological log for outcrop at the Lignite Pit.

5.4.2 Facies Architecture at the Lignite Pit

A panorama with facies overlays was created from the outcrop at the Lignite Pit location (Figure 5.26). Here, the lignite facies (Fo) is located at the base of the outcrop and is overlain by the fine sand, silt, and clay facies (Fl). Above facies Fl is the trough cross-bedded gravel (Gt) facies. The widespread white massive sand facies (Sm1) truncates facies Gt and is present for segments of the outcrop where it has not been removed by mining operations. The trough cross bedded sand and horizontal laminated facies (St+h) cap the exposure and are only present in the upper right portion of the photo.

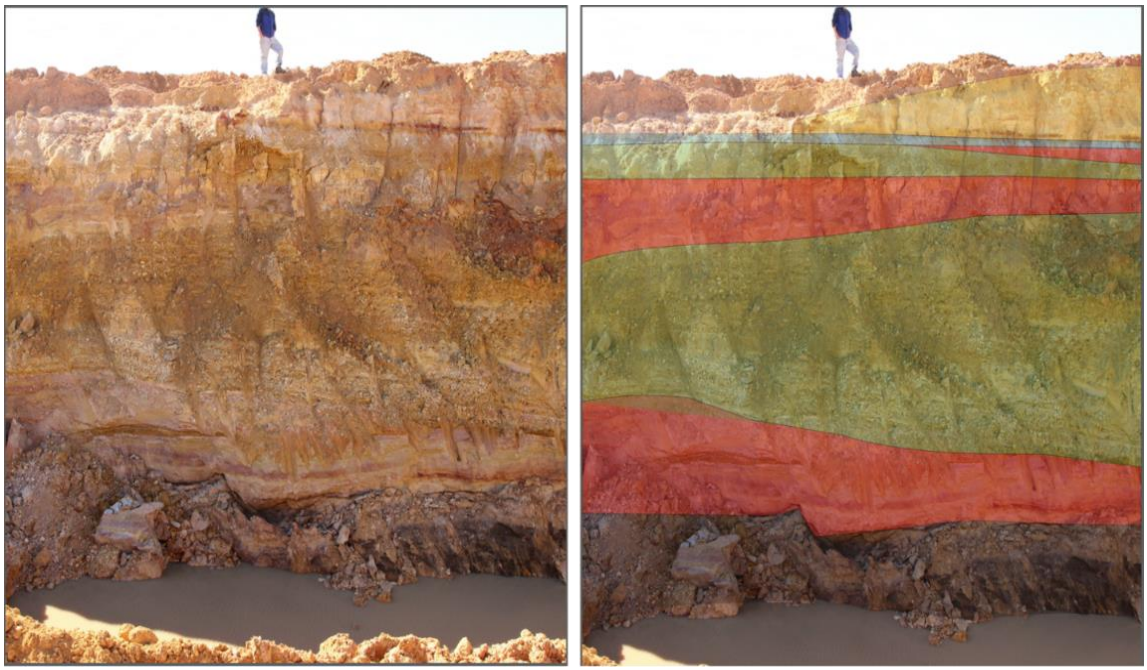

Figure 5.26. Uninterpreted (left) and interpreted (right) photos of the Lignite Pit location. The Lilesville Lignite is at the bottom of the outcrop and is partially covered by water. The interpreted photo shows facies Fo (black) overlain by Fl (red). Coarsening upward there is facies Gt which is interbedded with facies Fl and eventually cut out by facies Sm1 (blue). A small portion of sandy facies St+h (yellow) is present, although it was mostly missing due to mining.

5.4.3 Organic Digestion and Grain Size Analysis Data for the Lignite Pit

Samples for grain size analysis starting at the grey-dark grey lignite deposit (unit 2 of Figure 5.25) and extending up into the laminated sands (unit 3) were collected in 5-centimeter intervals from 0 to 1 meter. On the date of collecting these samples previous rains filled the lignite pond covering up the lower part of the dark lignite deposit (unit 1 of Figure 5.25) however one sample was obtained from under the water level (HQ-L-29). Samples at 10-centimeter intervals were collected from 1 to 1.7 meters. Finally, two 15-cm samples from 1.7 to 1.85 meters and 1.85 to 2 meters were collected. These grainsize data can be seen in Appendix B.

Samples containing organic material, such as plant micro- and macro-fossils, underwent organic digestion to remove that organic material. This ensures that only lithic material would be analyzed by the laser diffraction analysis, yielding more accurate measurements of grainsize distributions. The proportion of nonorganic to organic material was recorded (Table 5.3).

Proportions of organic material range from 31.3% to 50.9% with an average of 42.6%. The results in the form of grainsize distribution graphs are in Appendix B.

Location at Lignite Pit			
Sample	Mass (g) before digestion	Mass (g) after digestion	% Organic
HQ-L-1	1.12	0.46	40.93
HQ-L-2	1.55	0.64	41.38
HQ-L-3	0.75	0.35	46.82
HQ-L-4	1.43	0.58	40.65
HQ-L-5	1.01	0.38	37.35
HQ-L-6	0.97	0.30	31.28
HQ-L-7	1.02	0.42	41.49
HQ-L-8	1.31	0.66	50.15
HQ-L-9	1.14	0.53	46.10
HQ-L-10	0.88	0.37	41.99
HQ-L-29	1.57	0.80	50.87

Table 5.3. Results of organic digestion for Lignite Pit samples (HQ-L).

5.4.4 Pollen Data

Three sets of samples were analyzed for pollen assemblages by Dr. Frederick Rich. The major pollen and spore taxa that were found in the Lilesville Lignite include cypress (*Taxodium*) (18.2%), pine (*Pinus*) (17.1%), oak (*Quercus*) (15.4%), hickory/pecan (*Carya*) (13.5%), alder (*Alnus*) (5.3%), and genera-form including *Tricolpites* (5.7%), *Tricolporopollenites* (4.3%), among others. A detailed list of pollen and spore taxa can be found in Figure 5.27.

Total number of pollen/spores of different taxa, and relative abundances expressed as *per cent* from samples #1, 2, and 3.

Taxon	%, #1	%, #2	%, #3	Mean	common name
Alnus	2.5	6.8	6.6	5.3	alder
Betula	.55	––	––	.18	birch
Carya	18.3	11.8	10.4	13.5	hickory/pecan
Castanea	––	1.1	.29	.46	chestnut
Corylus	*1.1*	1.4	1.1	1.2	hazel
Ericaceae	.83	––	.58	.47	heath/heather
Ilex	1.4	.56	1.4	1.12	holly
Itea	1.7	––	––	.57	sweet spire
Liquidambar	1.7	.28	.29	.76	sweetgum
Myrica	.27	.28	.58	1.13	bayberry/wax myrtle
Nuphar	––	.84	.29	.38	water lilly
Nyssa	.55	.56	.29	.47	tupelo
Ostrya/Carpinus	.55	––	––	.18	hophornbeam/hornbeam
Ovoidites	.27	––	––	.09	freshwater algae
Pinus	22.4	10.4	18.4	17.1	pine
Quercus	11.6	17.5	17.0	15.4	oak
Taxodium	9.7	23.7	21.3	18.2	cypress
Tsuga	.27	––	––	.09	hemlock
Ulmus	.55	.84	.86	.75	elm
Indeterminate	1.1	13.8	10.7	8.5	
Form genera					
Inaperturate	1.1	––	2.0	1.03	
Nothofagidites	.27	.28	2.3	.95	beech
Tricolpites	5.8	7.0	4.3	5.7	pollen w/ 3 apertures
Tricolporopollenites	8.9	2.8	1.2	4.3	

Figure 5.27. Percentages of pollen types found in the Lilesville Lignite (from Diemer et al. 2017; Yankech et al. 2018).

5.4.5 Phytolith and Plant Macrofossil Data

Photos of processed and cleaned slides of phytoliths and hand specimens of plant macrofossils were produced by Dr. Ethan Hyland of NC State University and morphotypes were identified. Phytoliths identified in the samples include angiosperm trees (Fagales?) (Figure 5.28), conifers (Pinopsida) (Figure 5.29) and wetland grasses (Oryzeae?) (Figure 5.30).

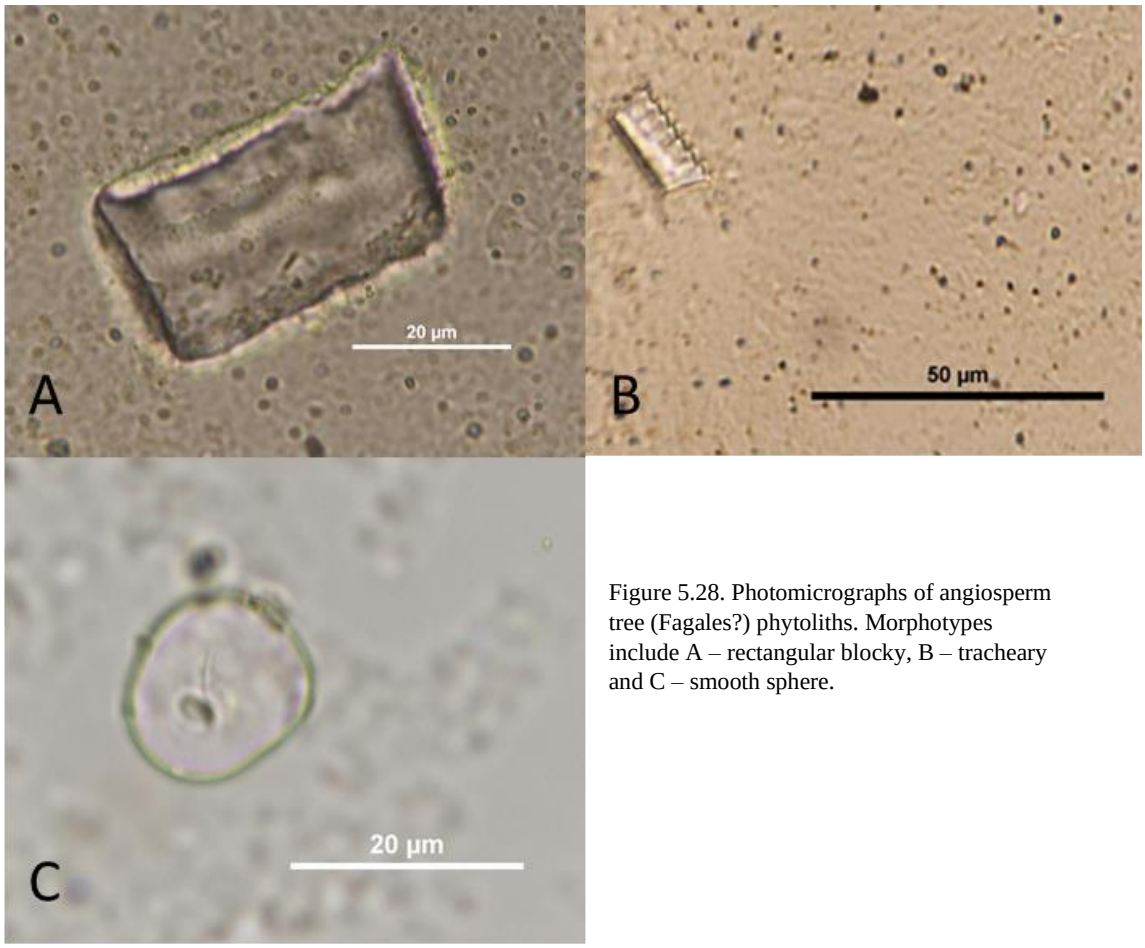

Figure 5.28. Photomicrographs of angiosperm tree (Fagales?) phytoliths. Morphotypes include A – rectangular blocky, B – tracheary and C – smooth sphere.

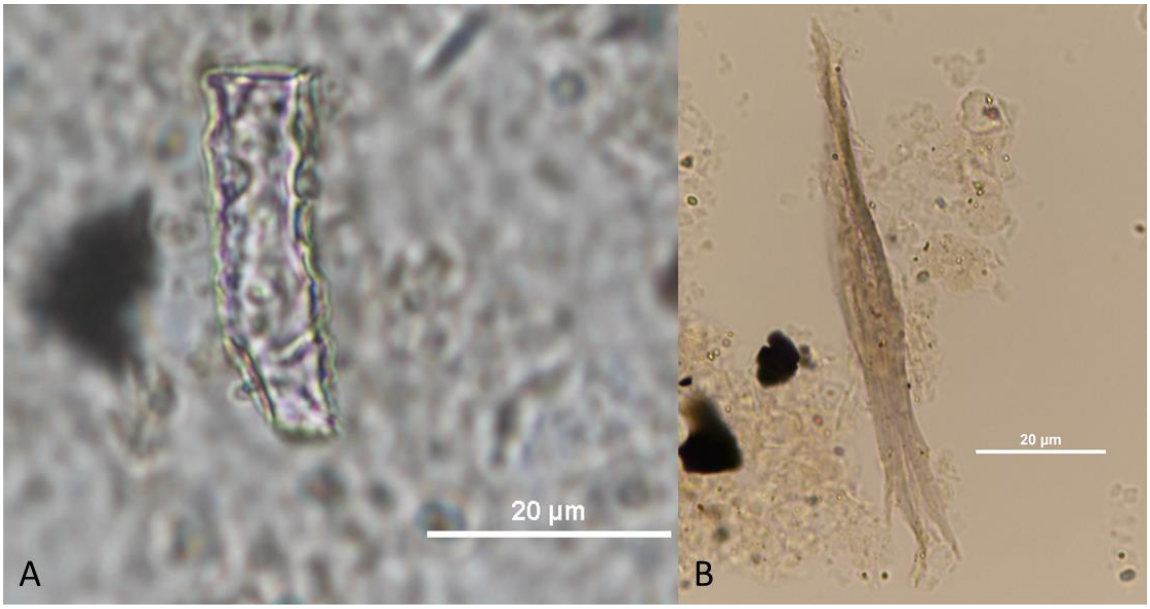

Figure 5.29. Photomicrographs of conifer (Pinopsida) phytoliths. Morphotypes include A – spiney elongate and B – trichome.

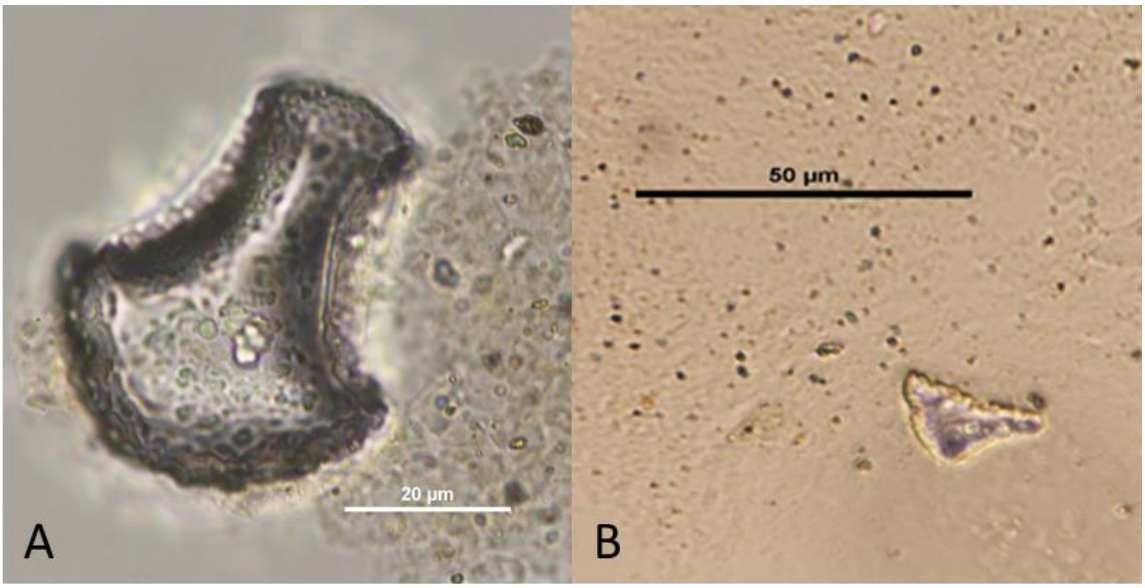

Figure 5.30. Photomicrographs of wetland grass (Oryzeae?) phytoliths. Morphotypes include A – flabellate elongate and B –triangular blocky.

Plant macrofossils were identified to their genus and include Pinus (Figure 5.31), Fagaceae (Quercus?) (Figure 5.32A), Fagaceae (Fagus?) (Figure 5.32B), Fabaceae (Figure 5.33) and Poales (Typhaceae? or Poaceae?) (Figure 5.34).

Figure 5.31. Photos of plant fossils from the genus Pinus.

Figure 5.32. Photos of plant fossils from the genus Fagaceae. A – Quercus? And B – Fagus?

Figure 5.33. Photo of plant fossils from the genus Fabaceae.

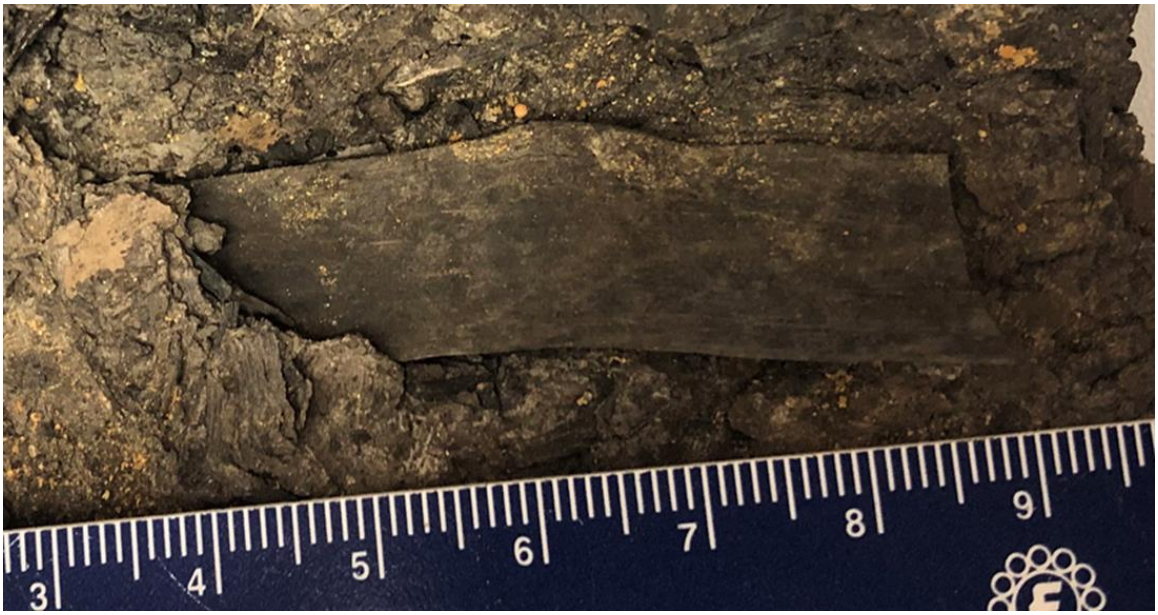

Figure 5.34. Photo of plant fossils from the genus Poales (Typhaceae? or Poaceae?).

5.5 Location at Sump Pit - Overview

A large pit, named the Sump Pit, was excavated to the west of the Lignite Pit location (Figure 5.9). The Sump pit exposes stratigraphy not seen at any other location in the field area. Most importantly, this location reveals gravely material both underneath and above the Lilesville Lignite. A detailed sedimentological log of these deposits was created along with grainsize analysis data for each unit described.

5.5.1 Sedimentological Log at Sump Pit

In these exposures, the Lilesville gravels are about 14.5 meters thick and composed of the same 8 lithofacies described elsewhere in the field area. A detailed sedimentological log shows 7 of the 8 lithofacies (Figure 5.35).

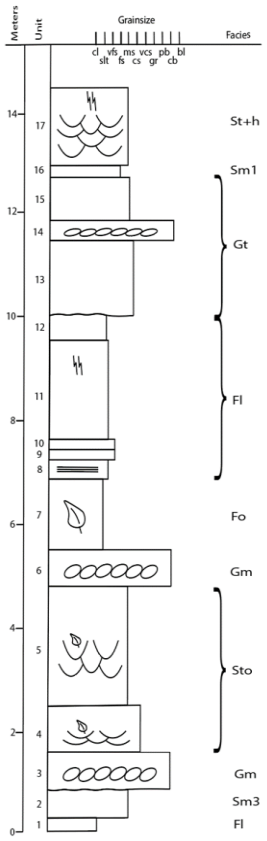

Figure 5.35. Sedimentological log at the Sump Pit location.

Here the exposures are about 14.5 meters in height. Unit 1 (see Figure 5.35) is part of facies Fl and is the basal unit of the outcrop consisting of a 30-cm thick, medium to dark grey, highly compacted clay with medium-sized quartz sand and abundant mica. The unit is mostly massive but has some faint laminations. The compacted clay is hard and difficult to force the pick end of a rock hammer into it in order to obtain a sample to examine by hand (Figure 5.36).

Unit 2 (Figure 5.35) is a variation of facies Sm, a 70-cm massive, coarse quartz arenite with enough clay in the matrix to make it sticky. There is, however, indistinct horizontal bedding visible towards the bottom of the otherwise massive unit (Figure 5.36).

Unit 3 (Figure 5.35) is a clast-supported cobble conglomerate associated with facies Gm. The thickness of the unit varies from 50 to 90 cm due to the wavy erosive basal boundary with unit 2. The upper contact of the unit with unit 4 is flat (Figure 5.36).

Figure 5.36. Photo of Sump Pit outcrop showing units 1-4. See Figure 5.28 for explanation of units.

Units 4 and 5 (Figure 5.35) are associated with facies St and called facies subtype Sto (trough cross stratified sands with plant fragments). Unit 4 is 120 cm thick and composed of

pebbly trough cross-bedded coarse- to very coarse-quartz sands with rounded quartz pebbles. The cross beds are about 90 cm in length and about 10 cm thick, and dip to the southeast. Lenses of plant material occur at minor basal erosion surfaces within this unit (Figure 5.37). Unit 5 is a 230 cm trough cross-stratified coarse quartz arenite sand with pebble clasts on lag surfaces and plant material draping toe sets of cross-bedding (Figure 5.37). The cross beds are 20 to 60 cm thick with a southeasterly dip direction. Shown in Figure 5.30 is an example of plant material draping cross-beds that is about 3 m in length and 5 cm thick.

Unit 6 (Figure 5.35) is a 50 cm clast-supported gravel deposit associated with facies Gm (Figure 5.37).

Unit 7 (Figure 5.35) is a 150 cm dark grey to black, silty to very fine sand with abundant plant fragments. Based on this unit's stratigraphic position, it likely correlates with the lignite deposit and facies Fo described previously at the Lignite Pit location (Figure 5.37).

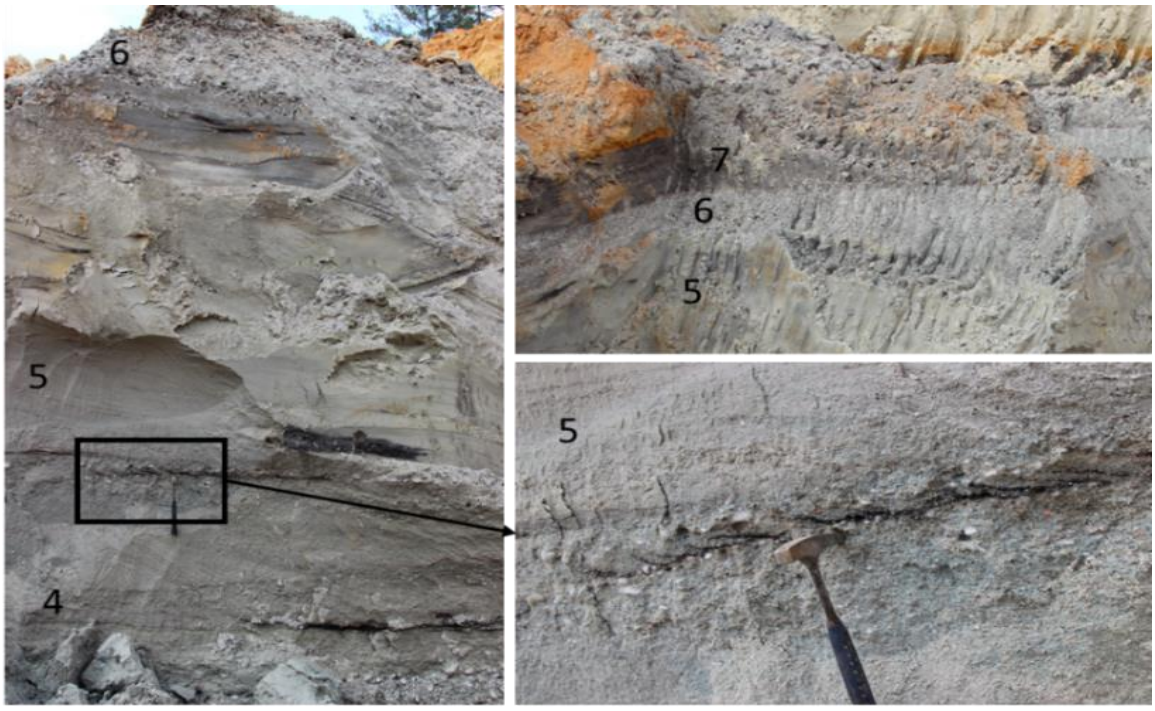

Figure 5.37. Photos of Sump Pit outcrop showing units 5-7. See Figure 5.28 for explanation of units.

Units 8, 9, 10, 11, and 12 (Figure 5.35) are associated with facies Fl and shown in Figure 5.38. Unit 8 is a 30 cm cross-laminated, light brown to brown/orange, fine sand. Laminations are

highlighted by oxidation of iron that becomes less visible up-section. Unit 9 is a 25 cm light greyish white, fine sand that fines up-section into units 10 and 11. Unit 10 is also 25 cm thick and is similar in color to unit 9 but is much more friable. Unit 11 is 200 cm pale green to light greyish white, predominantly silt with fine grained sand and contains large, up to 1 meter long, orange mottles. Unit 12 is a 50 cm light brown/yellow, silty clay with red/purple mottles due to oxidation where the top 5 cm is purple in color (Figure 5.38).

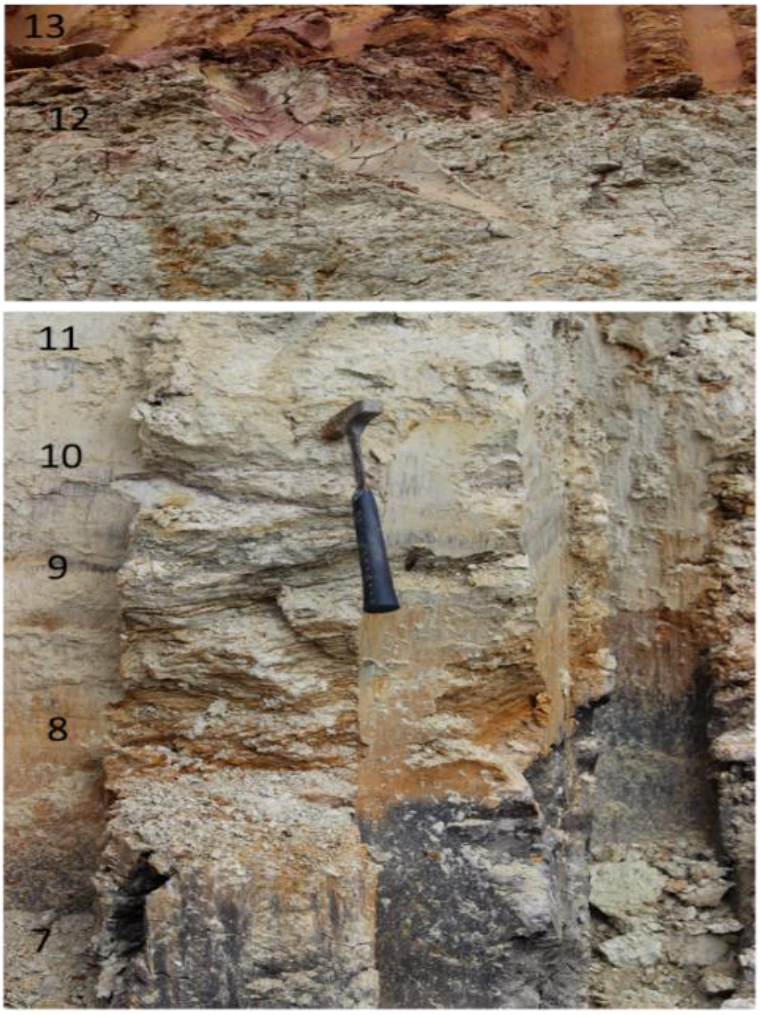

Figure 5.38. Photo of Sump Pit outcrop showing units 7-12. See Figure 5.35 for explanation of units.

Units 13-15 (Figure 5.35) are associated with the trough cross bedded gravel (Gt) facies. Unit 13 is 150 cm alternating light brown/yellow, white, and purple, coarse- to very coarse, sand with horizontal bedding in the lower third of the unit and trough cross-bedding present in the rest

of the unit (Figure 5.39). Unit 14 is a 35 cm thick by 350 cm long gravel lens that pinches out and reappears laterally (Figure 5.39). Unit 15 is an 80 cm thick massive, yellow to light brown, fine sand (Figure 5.39).

Unit 16 (Figure 5.35) is a 20 cm, white, massive, medium sand that is likely the laterally extensive white 'marker bed' (unit 9 and facies Sm1 from stratigraphic sections at the Ponds location, see Figure 5.10) seen throughout the exposures in the quarry. This unit is capped by a yellow and red, horizontally bedded fine- to medium-grained sand likely equivalent to units 10 and 11 at the Ponds location (Figure 5.10) and is also visible throughout most exposures in the field area (Figure 5.39).

Figure 5.39. Photo of Sump Pit outcrop showing units 13-16.

Units located above Unit 16 were not reachable (Figure 5.39) therefore no close observations or samples were collected. However, based on the local stratigraphy, it is likely these are stratigraphically similar to units 10 and 11 at the Ponds location (see Figure 5.10), and associated with facies St+h throughout the field area.

5.5.2 Facies Architecture

The facies architecture at the Sump Pit location (Figure 5.40) provides valuable stratigraphic information not visible at the Ponds and Lignite Pit locations because at the Sump Pit mining operators dug below the lignite deposit and revealed gravel- to cobble-sized clasts underlying the lignite.

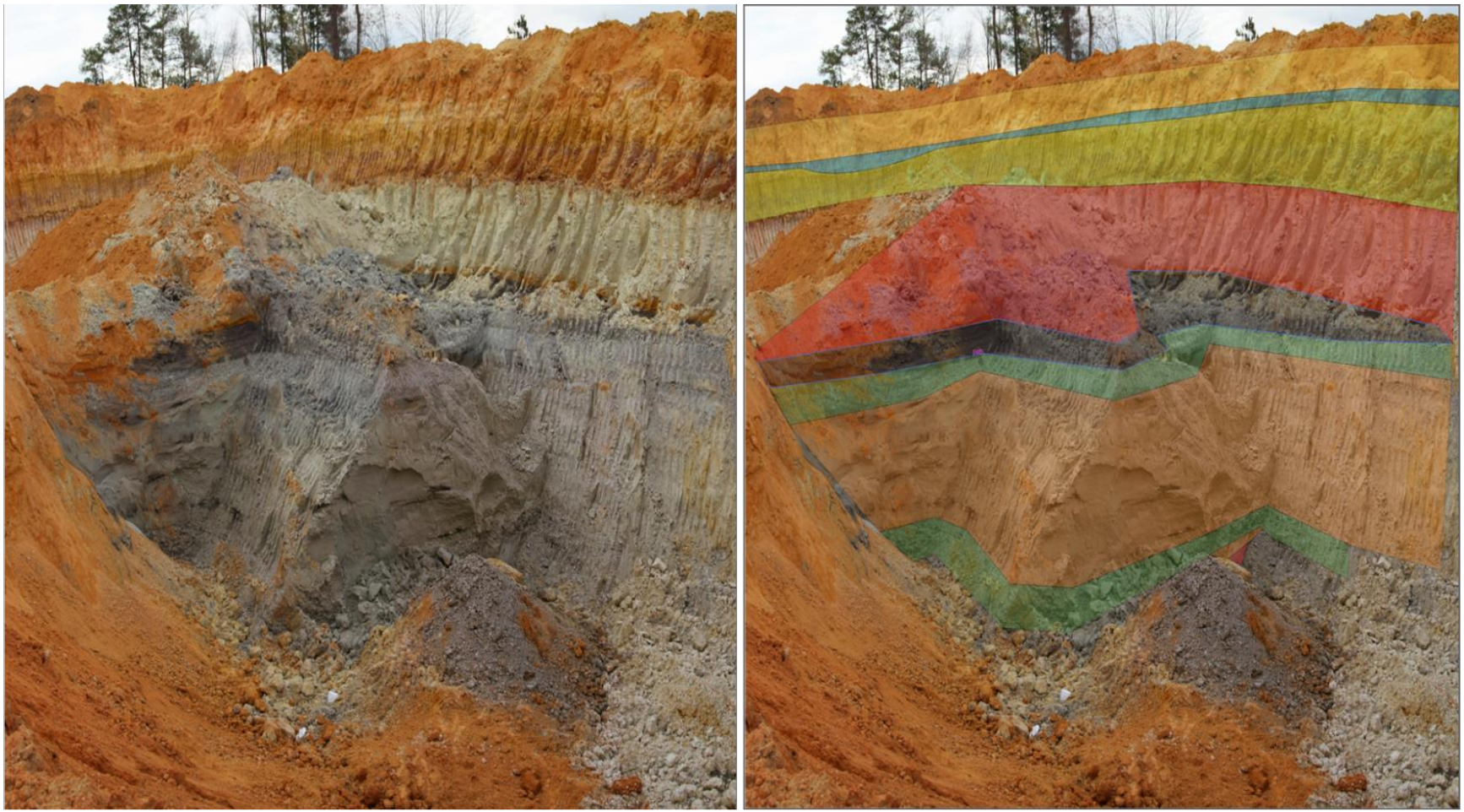

Figure 5.40. Uninterpreted (left) and interpreted (right) panoramas of the outcrop located at the 'Sump Pit' location showing facies Fl (red), Sm3 (orange), Gm (green), Sto (tan), Fo (black), Gt (lime green), Sm1 (blue) and St+h (yellow). Note how gravely deposits are present underneath facies Fo.

5.5.3 Organic Digestion and Grainsize Data

Similar to the Lignite Pit location, organic material in the Sump Pit location needed to be removed before an accurate measurement of the grain size distribution could be obtained for organic-rich samples. Table 5.4 shows that the lignite unit (facies Fo) in the Sump Pit location contained 45% organic material. This proportion of organic to nonorganic material is consistent with the proportions measured in the lignite at the Lignite Pit location (Table 5.4). The grainsize distribution graphs and statistics are in Appendix C. The grainsize data calculated for these units describes the less than 2 mm fraction (phi size -1). Therefore, for facies Gm and Gt, the particles that constitute the matrix (particles finer than -1 phi) of the sample were measured.

Sample	Mass (g) before digestion	Mass (g) after digestion	% Organic
HQ-SP-7	0.78	0.35	45.09

Table 5.4. Results of organic digestion for organic rich sample taken from the Sump Pit location.

5.6 Location at Sump Pit 2 - Overview

The Sump Pit 2 location is adjacent to, and southeast of, the Sump Pit (Figure 5.9). In this location the quarry wall was actively being mined making the quarry walls unstable. The material removed from the outcrop prevented stable footing therefore the outcrop was viewed remotely to create a sedimentological log (Figure 5.41). A soil profile was also created remotely and samples were collected by use of a ladder. Considering the nature of the outcrop wall and floor, sampling was done cautiously and each hand specimen was examined away from the quarry wall for soil descriptions. Sampling was done by starting at the top of the profile and taking 20 cm bulk samples from 0 to 60 centimeters, 40 cm bulk samples from 60 to 340 centimeters and 30 cm bulk samples from 340 to 660 centimeters. Since the stratigraphy at this location was similar to other outcrops in the field area, identification and correlation of sedimentary units, as well as soil units at Sump Pit 2, could easily be made.

5.6.1 Sedimentological Log at Sump Pit 2

The outcrop here is about 6.6 meters in height and a sedimentologic log was recorded remotely (Figure 5.41). The stratigraphy is similar to that at the Lignite Pit and Sump Pit locations where facies Gt is overlain by facies Sm1 (white marker bed).

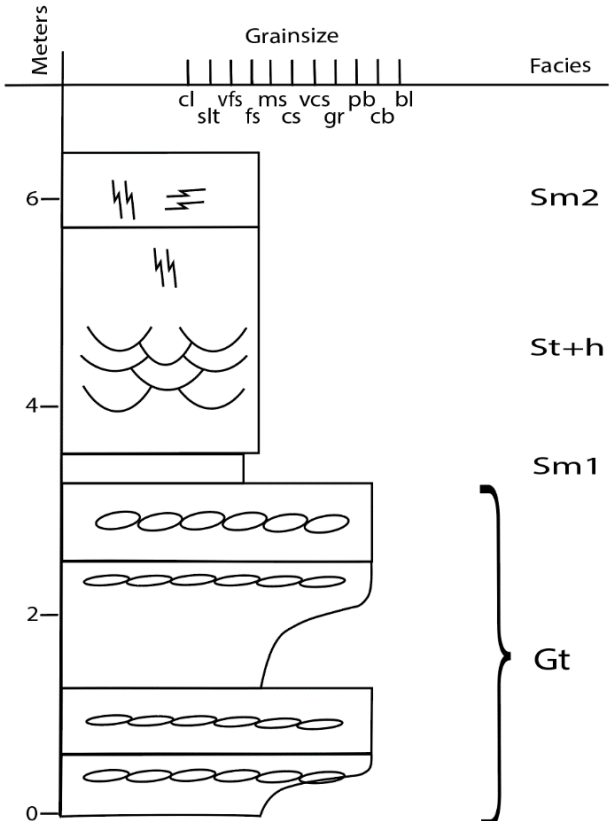

Figure 5.41. Sedimentological log for outcrop at Sump Pit 2 location.

5.6.2 Soil Profile Data from Sump Pit 2

One buried soil (HQB-4) and one modern soil (HQB-1) were present in the outcrop (Figure 5.42). Based on local stratigraphy, these soils are likely equivalent to HQA-5 and HQA-2, respectively, as seen in the Pond 1 location. The degree of mottling and oxidation in HQB-1 appears more abundant than at HQA-1 and exhibits slightly darker red coloration (2.5 YR 4/6, 2.5 YR 5/6). Soil field descriptions are listed in Appendix H. Iron extraction analyses were done for these samples as were done for soil profile HQA. The results of iron extraction are listed in Appendix I.

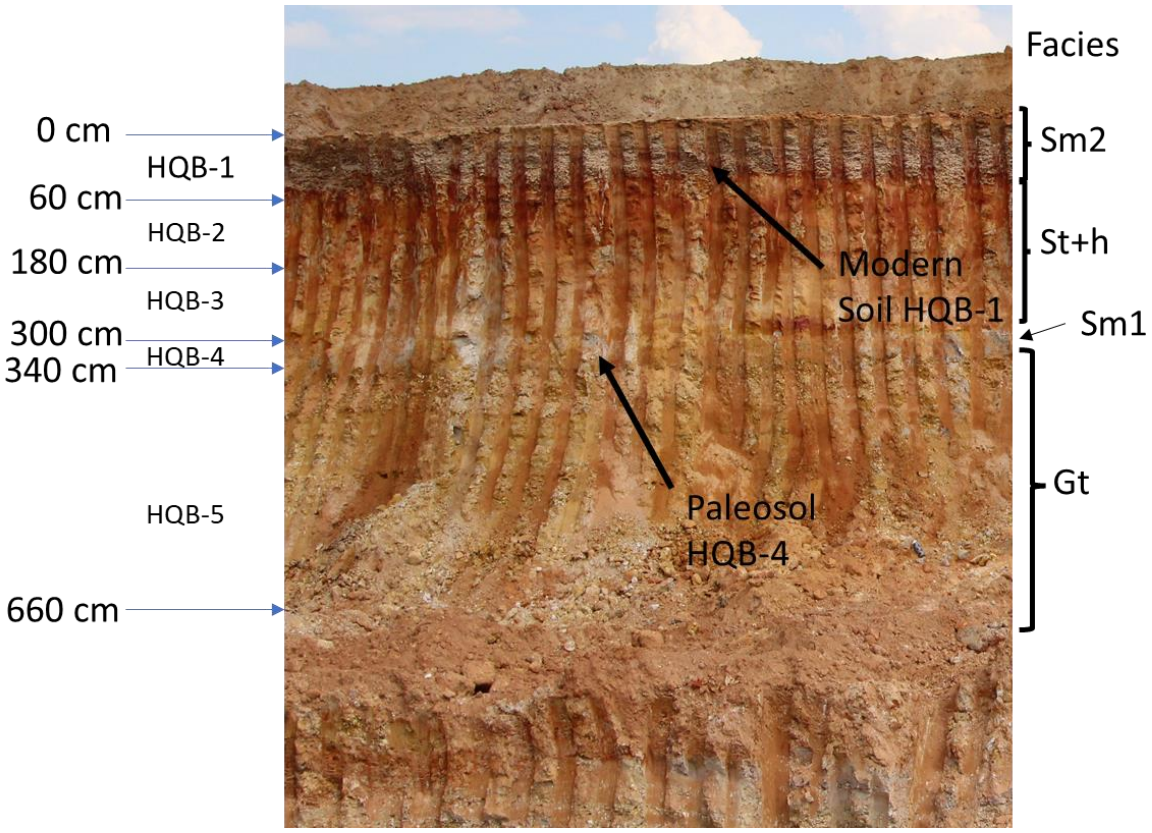

Figure 5.42. Photo of outcrop at Sump Pit 2 showing paleosol HQB-4 and the modern soil HQB-1. See Figure 5.34 for explanation of sedimentary units.

Appendix I contains the results of extractable iron weight percentages for Fe_h and Fe_d and the iron activity ratio were calculated for all samples taken from the soil profile at Sump Pit 2. All three samples from the modern soil with reticulate mottling, HQB-1, have high values of Fe_d (Figure 5.43). The paleosol, sample HQB-4, has the lowest value for Fe_d in the entire profile (Figure 5.36). Directly under HQB-4 there is an increase in the weight percent of Fed in sample HQB-5-1.

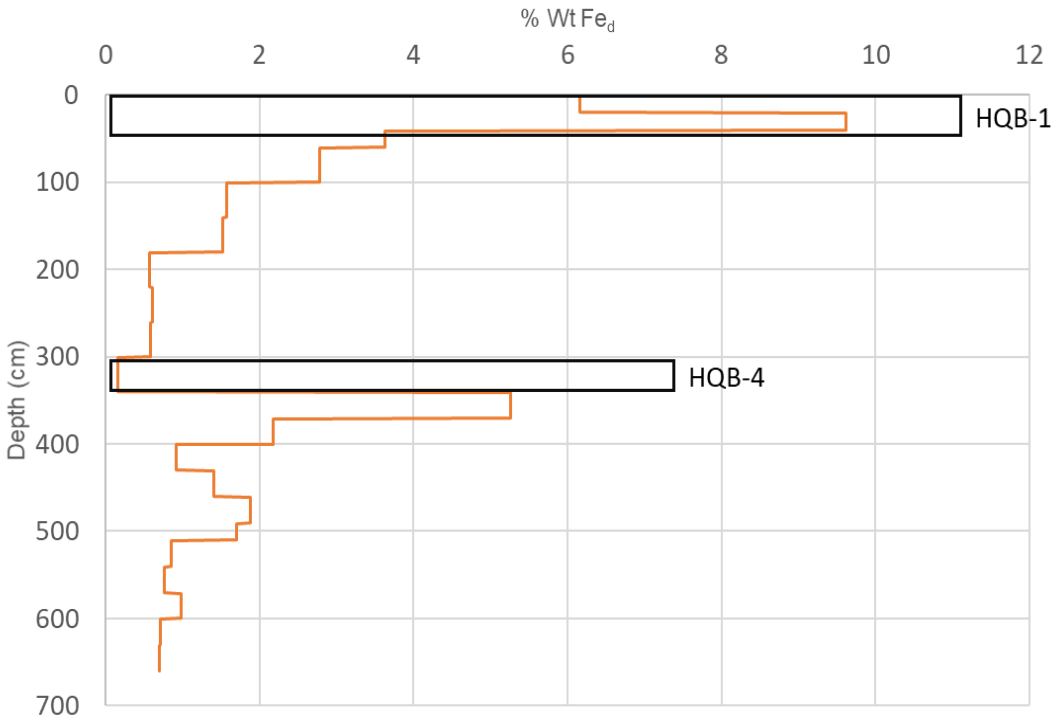

Figure 5.43. Depth profile of Fe_d for soil profile at Sump Pit 2. Boxes outline soils identified in the field.

5.7 HQ-G Samples Grain Size Analysis

The HQ-G samples were collected to obtain grain size data for 8 samples (see Figure 5.44 for HQ-G grain size sample locations) focusing primarily on the massive to crudely bedded gravely (Gm) facies (sample locations 1-5) and secondarily on the trough cross bedded gravel (Gt) facies (sample locations 6 and 7). Lastly, one sample was collected from the laminated sand, silts, and clays (Fl) facies (sample location 8). Facies Fl at this location did have some gravelly material interbedded within the unit with clasts up to 1.6 cm.

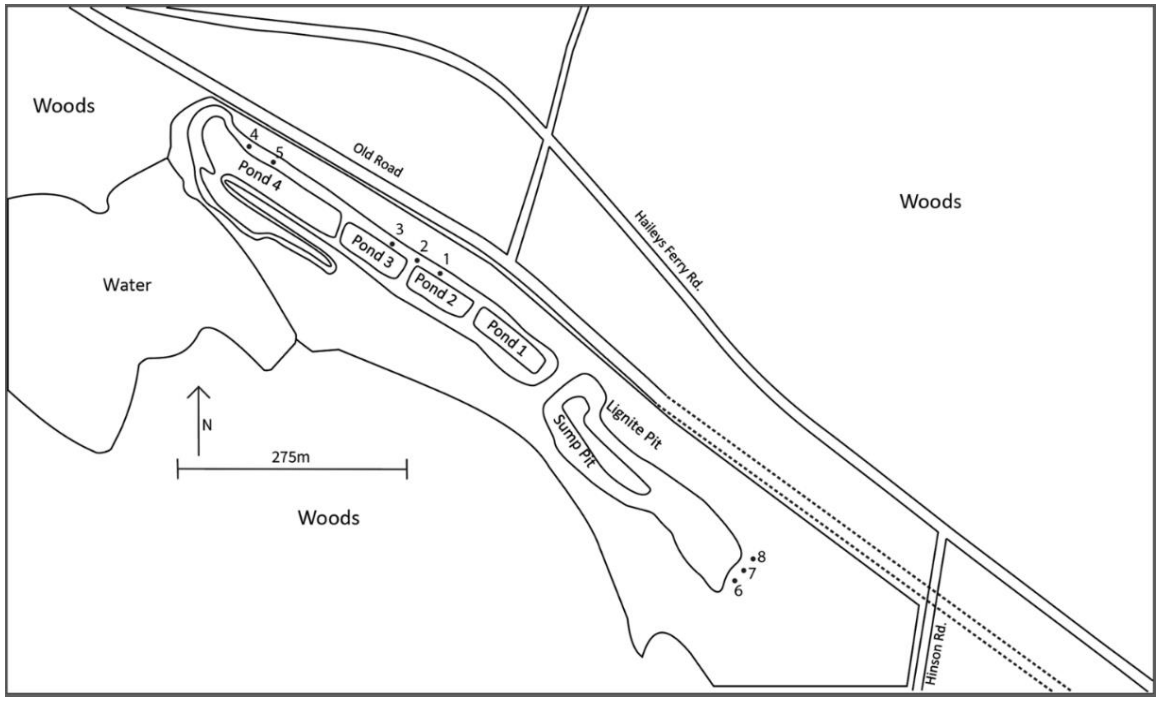

Figure 5.44. Map of field area indicating locations of imbrication sites 1-8 used for grain size analysis samples HQ-G.

At each of these locations, grain size analyses were performed as outlined in the methods section. For sieve sizes coarser than -1 phi (coarser than coarse sand) bulk samples were analyzed in the field. For particles finer than -1 phi, samples were transported to the lab and measured using the laser diffraction system. These two data sets were then combined to create cumulative weight percent curves (Figure 5.45). Table 5.5 shows grain size distribution results in the form of graphic mean grainsize, inclusive graphic standard deviation (sorting), inclusive skewness, and kurtosis. An explanation of the results of these calculations can be seen in Appendix F.

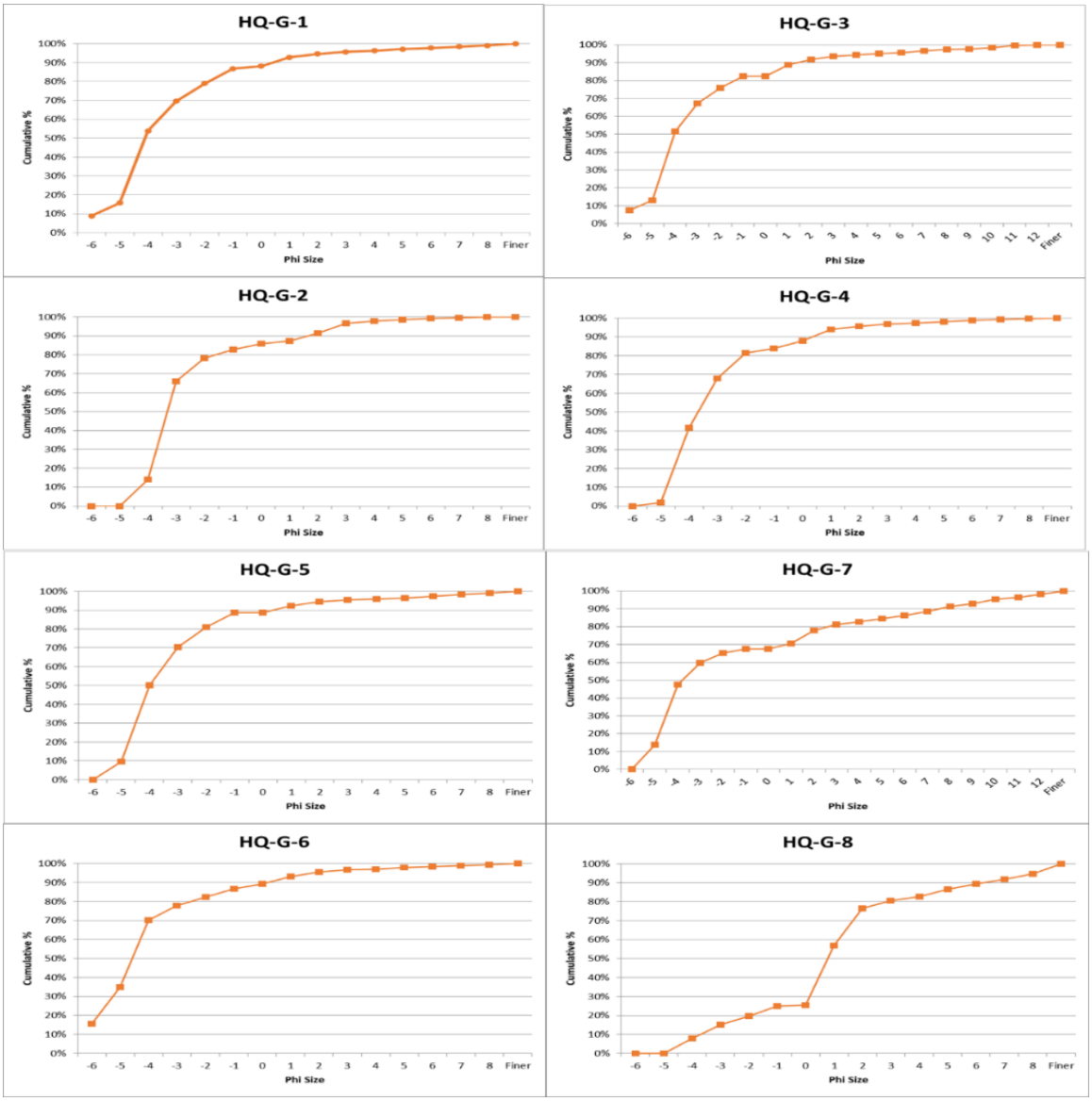

Figure 5.45. Cumulative weight percent graphs for the 8 HQ-G samples.

Sample	Graphic Mean Grainsize	Inclusive Graphic Standard Deviation (sorting)	Inclusive Graphic Skewness	Kurtosis (peakedness)
HQ-G-1	-3.77	2.21	0.49	1.21
HQ-G-2	-3.47	2.88	0.72	2.35
HQ-G-3	-3.17	3.02	0.57	1.75
HQ-G-4	-2.90	2.31	0.60	1.64
HQ-G-5	-3.67	1.97	0.44	1.32
HQ-G-6	-4.20	2.40	0.58	1.60
HQ-G-7	-1.40	4.92	0.71	0.92
HQ-G-8	1.27	4.23	0.19	1.37

Table 5.5. Results of grain size analysis for the HQ-G samples

5.8 Facies Architecture of Other Remotely Viewed Outcrops

Figures 5.47 and 5.48 are remotely viewed photo panoramas of outcrops exposed around the field area at different times due to mining operations (see Figure 5.46 for location map). These temporary outcrops exhibit a facies architecture similar to what is seen elsewhere in the field area.

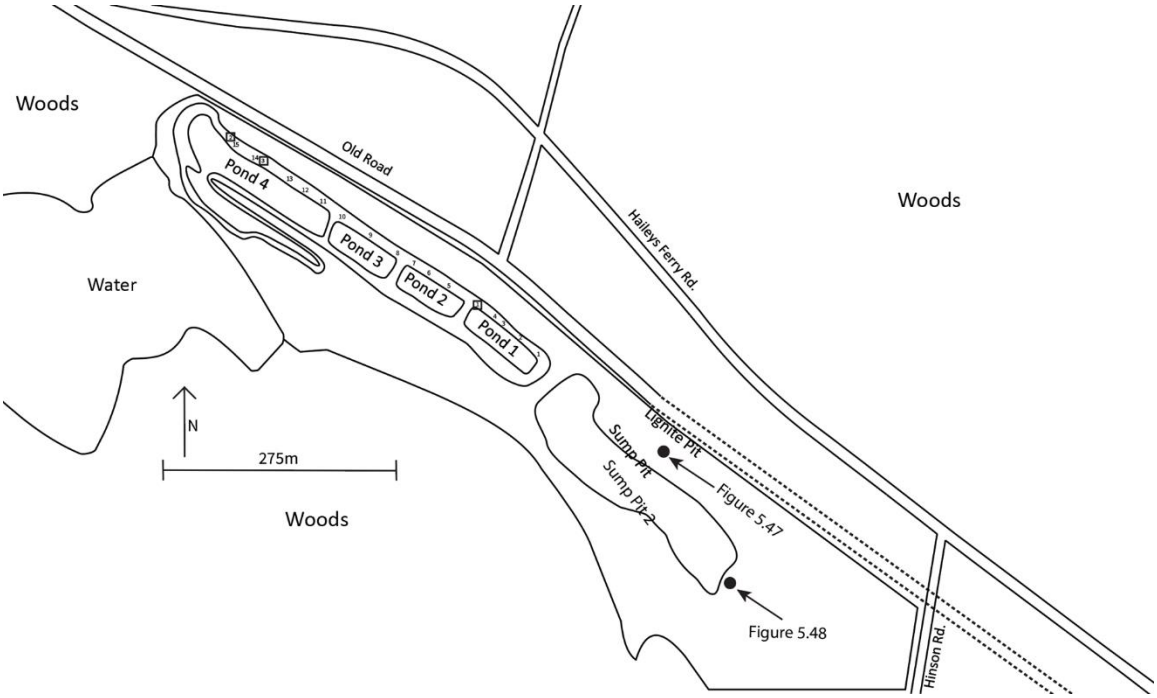

Figure 5.46. Map of field area showing approximate locations of temporary outcrops seen in Figure 5.47 and Figure 5.48.

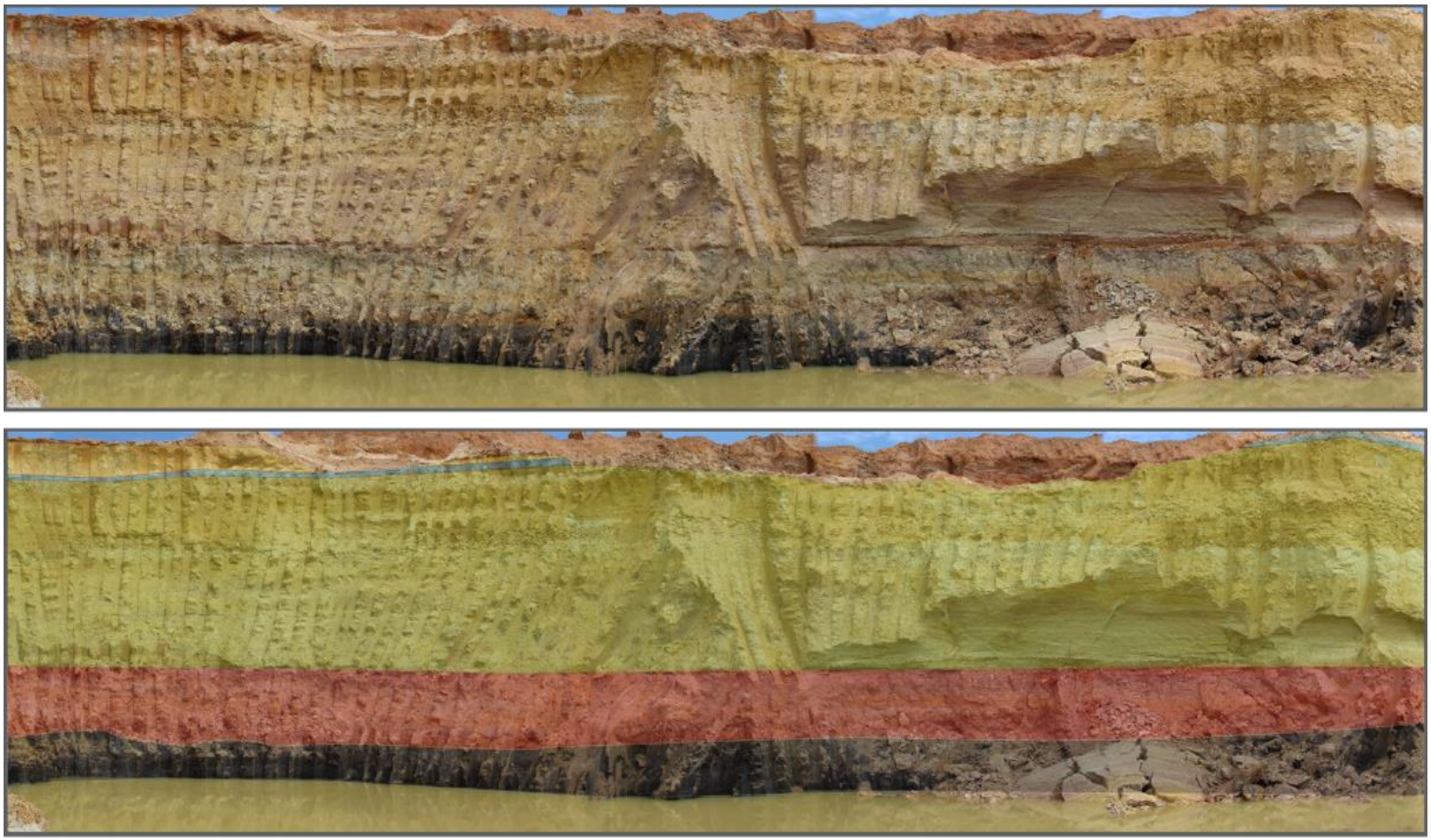

Figure 5.47. Uninterpreted (top) and interpreted (bottom) panoramas of outcrop located near the backside of the ‘Lignite Pit’ location. Facies Fo (black) is located at the base of the outcrop and is partially covered by water. Facies Fl (red) overlies facies Fo. Facies Gt caps most of the outcrop however a thin layer of facies Sm1 (blue) and St+h (yellow) is visible in the upper left of the panorama which were removed from mining operations.

Figure 5.48. Uninterpreted (left) and interpreted (right) panoramas of outcrop located near the locations where samples HQ-G-6, 7 and 8 were taken (Figure 5.37). Starting at the base, facies Fl (red) is overlain by facies Gt (green). The widespread ‘marker bed’ facies Sm1 (blue) and St+h (yellow) overlie facies Gt (green). Portions of facies St+h (yellow) have been removed by the mining operations.

CHAPTER 6: INTERPRETATION

6.1 Facies Associations and Depositional Models

Previous work on the Lilesville gravels describe a scenario that occurred in three stages consisting of (1) an initial high energy fluvial system capable of producing a basal erosion (strath) surface and transporting and depositing pebble to cobble size clasts, (2) the transition to a lower energy fluvial system where stream power transported and deposited mostly sandy material (Cooley, 1970; McLean, 2013) and the active channel eventually abandoned the strath terrace system; and (3) an aeolian system transporting moderately-sorted fine- to medium-sand in dune scale bedforms. Evidence of this three stage facies association model is also present at multiple locations in the BV Hedrick Gravel and Sand quarry based on the lithofacies described.

Stage one (Figure 6.1) of the deposition of the Lilesville gravels began with erosion of a strath surface. That surface was then covered by facies association 1 (FA1). The massive to crudely bedded gravel facies (Gm), trough cross bedded gravel facies (Gt), laminated sands, silts, and clays facies (Fl), trough cross bedded sand with organic fragments (Sto), and ripple cross laminated sand (Sr) all comprise facies association 1 (FA1). FA1 is interpreted as the product of a high energy fluvial system. The stream had enough competence to transport large amounts of clasts up to 11 centimeters in length. The Hjultstrom Velocity Curve (Hjultstrom, 1939) indicates a flow velocity of 110 cm/s to 390 cm/s would be capable of transporting clasts in that size range. The single largest clast recorded in the field area was 32 centimeters in length indicating that a maximum stream velocity of 180 cm/s to 580 cm/s would have been required to transport that size clast. The finer clasts of FA1 were then deposited as stream power diminished forming gravel bars as sheets of gravels stacked onto to one another with little to no sign of bedding. As stream power diminished further, the gravels dropped out of transport creating a clast-supported framework deposit. The space between clasts was then filled in with finer material that progressively dropped out of transport as the stream power diminished further. These gravely bars

aggraded upwards and downstream parallel to flow, forming lozenge shaped deposits, that decreased in grainsize in both directions as stream power fluctuated (Miall, 1977). Between periods of increased and decreased stream flow, fine material was deposited on top of, and around, the gravel bars. The finer facies in FA1, such as Fl, are interpreted to be evidence of this reduction in stream power during deposition of FA1. Figures 5.13 to 5.18 show this relationship between low and high stages of stream velocity where facies Fl is interbedded with facies Gm. At times like this, facies Fl could have been deposited on bar surfaces as well as on the flanks of the bars. Facies Sto is interpreted as having been deposited as fill in the channels that were diverted around the longitudinal bars. Facies Sto contains plant fragments as well as gravel clasts filling the troughs of cross bedding indicating a source of 1) plant fragments and 2) clasts coarser than sandy material.

At the Sump Pit location (Figures 5.36 to 5.40), the organic rich silt and clay facies (Fo, Unit 7 of Figure 5.35), or lignite, is interpreted to have been deposited in a low flow area possibly in a cutoff channel or crevasse splay where fine material could be deposited out of suspended load during flooding. Vegetation became established and created an organic rich deposit. At a time of higher stream power, flooding would occur which would remove plant material from facies Fo and incorporate those plant fragments into facies Sto (Units 4 and 5 of Figure 5.35). On top of facies Fo at the Lignite Pit are facies Fl and facies Sr (Units 2-3 of Figure 5.25). This signals a migration of the channel that would eventually cover and preserve facies Fo (Unit 1-2 of Figure 5.25).

Facies Sr (unit 4 at Lignite Pit, see Figure 5.25 for sedimentological log) is interpreted as part of a crevasse splay deposit associated with river floods, similar to facies Fo, where there is an abundance of sediment and thus net accumulation occurred and created climbing ripples.

The trough cross-bedded gravel facies (Gt, Units 13-15 of Figure 5.35) is interpreted as either lateral accretion deposits on point bars or lateral bars associated with migrating channels in the paleo Pee Dee River during the FA1 stage. Lateral bars could have developed on the sides of

channels in quieter water which could be interpreted as the origin of the coarsening upward sequence seen at the Lignite Pit location which begins with facies Fo (Units 1 and 2 of Figure 5.25). Trough cross-bedded gravel bar deposits are analogous to point bars in meandering rivers and this process was called upon by Collinson, 1970, when describing the sedimentology of the Tana River. Facies Gt (Units 5-9 of Figure 5.25 and Units 13-15 of Figure 5.35) formed as channel fills due to stream water stage increasing within a channel and avulsions occurring and depositing sediment in fining upward packages. As this happened repeatedly, the channel migrated progressively across the landscape. A channel form (see Figure 5.7) is present in the outcrop and indicates a southward flowing channel migrating eastward across the landscape, cutting through facies Gt. The width (W) of the channel is estimated to be ~20 meters and has a depth (H) estimated to be ~2 meters. If we assume the velocity of the channel was from 110 cm/s to 390 cm/s an approximation of the discharge (D) of this channel can be calculated using the equation (D=V*H*W) and it would be between 4400 cm^3/s to 15600 cm^3/s, or 44 f^3/s to 156 f^3/s.

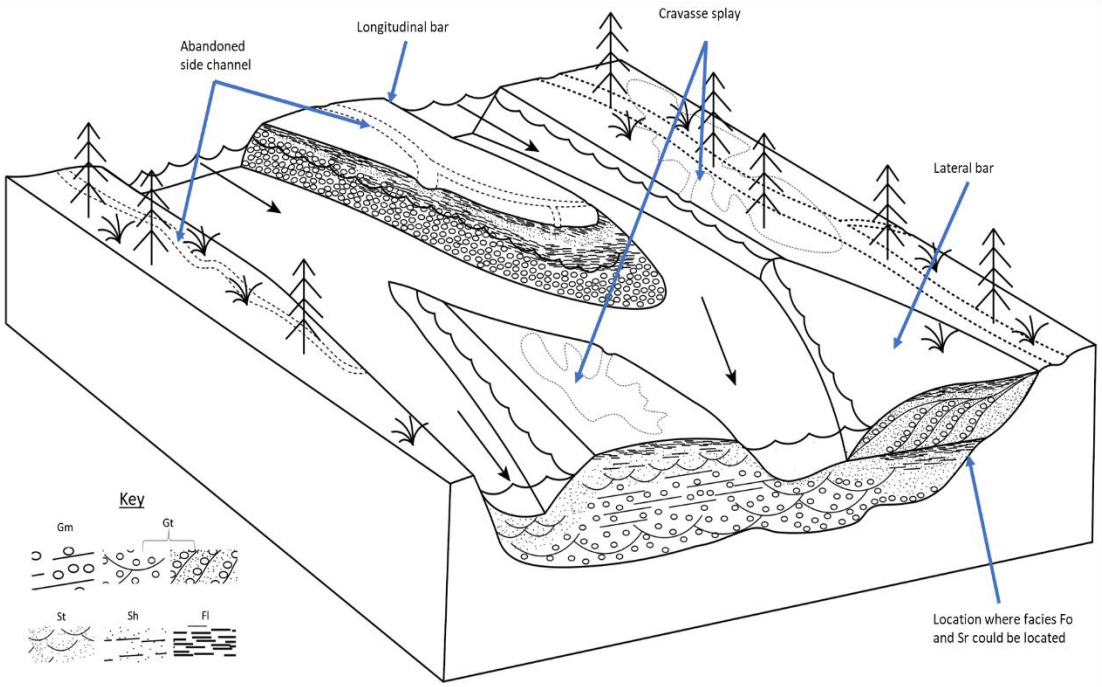

Figure 6.1. Depositional model for facies association FA1. This stage of the fluvial system is interpreted as a braided stream with high enough stream power to transport gravel to cobble size clasts. Black arrow indicate stream flow. Modified from Galloway and Hobday (1983).

The massive fine sand facies (Sm1, Unit 16 of Figure 5.28) likely records a long interval of slow deposition and intense weathering after the FA1 stage river avulsed away from this location. The source of the fine sand could have been flooding events from the distal FA1 channel. Prolonged weathering could then have bleached this 'marker bed' to its distinctive white color. Facies Sm1 has a mean grainsize of 160 microns (fine sand) however, according to the grain size analysis of the unit, 50% of the sample is less than 67 micrometers (fine sand to silt boundary) making a major component of the unit clays and silts. A channel form (Figure 5.7) can be seen cutting into facies Gt indicating one of two things: 1) the return of a channel from the ancestral Pee Dee River, or 2) the migration of another smaller channel cutting through Gt within the same trunk channel. Regardless, FA1 is capped by Sm1 throughout the entire field area.

Stage two (see Figure 6.2) consists of facies association 2 (FA2) and begins at the distinctive erosional contact at the top of Sm1 and base of St+h. Sandy facies St and Sh are interpreted as sedimentary structures from both upper and lower flow regimes. These deposits indicate a less powerful fluvial system not able to transport clasts larger than 2 millimeters (coarser than coarse sand). According to the Hjulstrom Velocity Curve, the required stream velocity to transport grains up to 2 millimeters is from 10 cm/s to 50 cm/s. The FA2 stream channel represents a marked reduction in the stream power compared to FA1. The presence of sandy trough cross-bedding and horizontal bedding indicates a stream that fluctuated in stream power and water level height through time (Miall, 1977). The variation in stream power could be due to seasonal changes in discharge due to variation in precipitation. However, FA2 never reached the stream capacity of FA1 based on the absence of gravel- to cobble-sized material. Eventually FA2 deposition halted, possibly due to the ancestral Pee Dee River shifting positions across the landscape once more. Once FA2 was abandoned a transition to an environment dominated by aeolian deposition occurred, as recorded by Facies Association 3 (FA3) (see Figure 6.3).

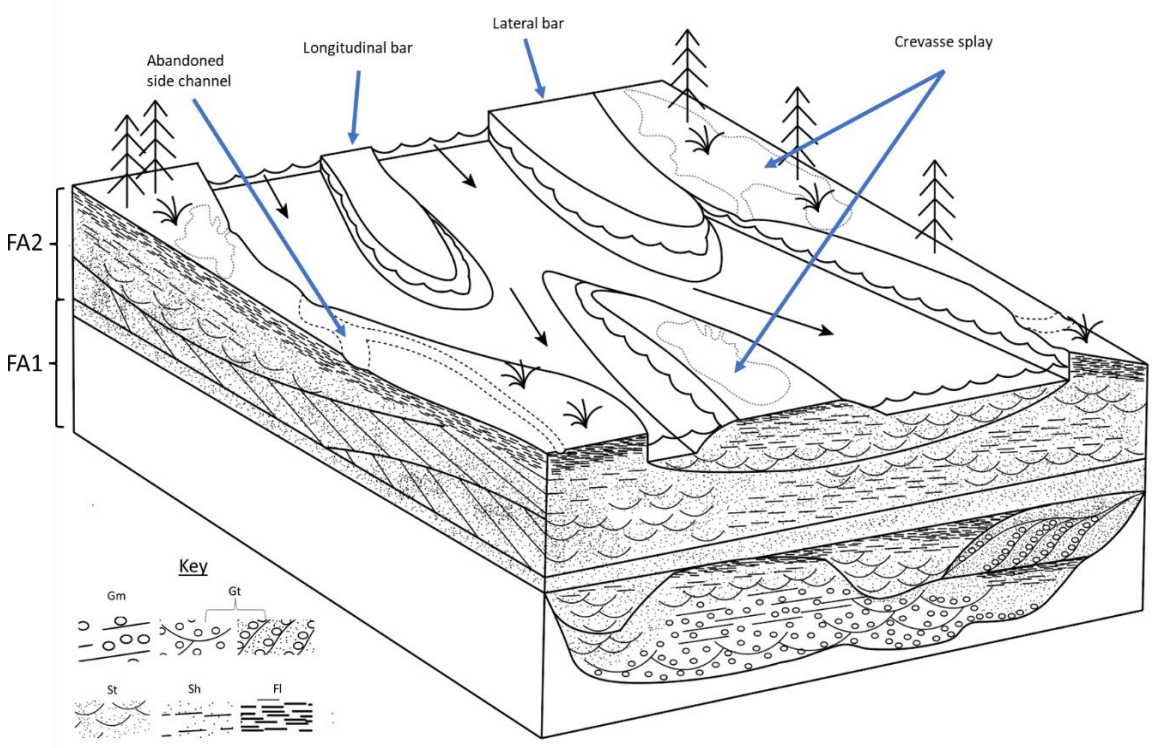

Figure 6.2. Depositional model for facies association during stage 2 (FA2). This stage of the fluvial system is interpreted as a sand dominated braided fluvial system with lower stream power than in stage 1 (FA1). Black arrows indicate stream flow. Modified from Galloway and Hobday (1983).

Stage three (Figure 6.3) consists of Facies Association 3 (FA3) and begins at the abrupt and flat to locally undulating erosional top surface of FA 2 (top of facies St+h, Unit 17 of Figure 5.35). FA3 consists of a variation of the massive sand facies (Sm2, Units 12-14 of Figure 5.10, and top unit of Figure 5.25). These sediments are interpreted as aeolian derived deposits of fine to medium grained, moderate to well sorted sands that have undergone pedogenesis and contain distinct clay and iron rich soil horizons. The late Miocene to Pliocene Pinehurst Formation is recorded in the regional stratigraphy of southeastern United States (Nystrom et al., 1991; Daniels et al., 1978) and facies Sm2 is interpreted to be part of this formation.

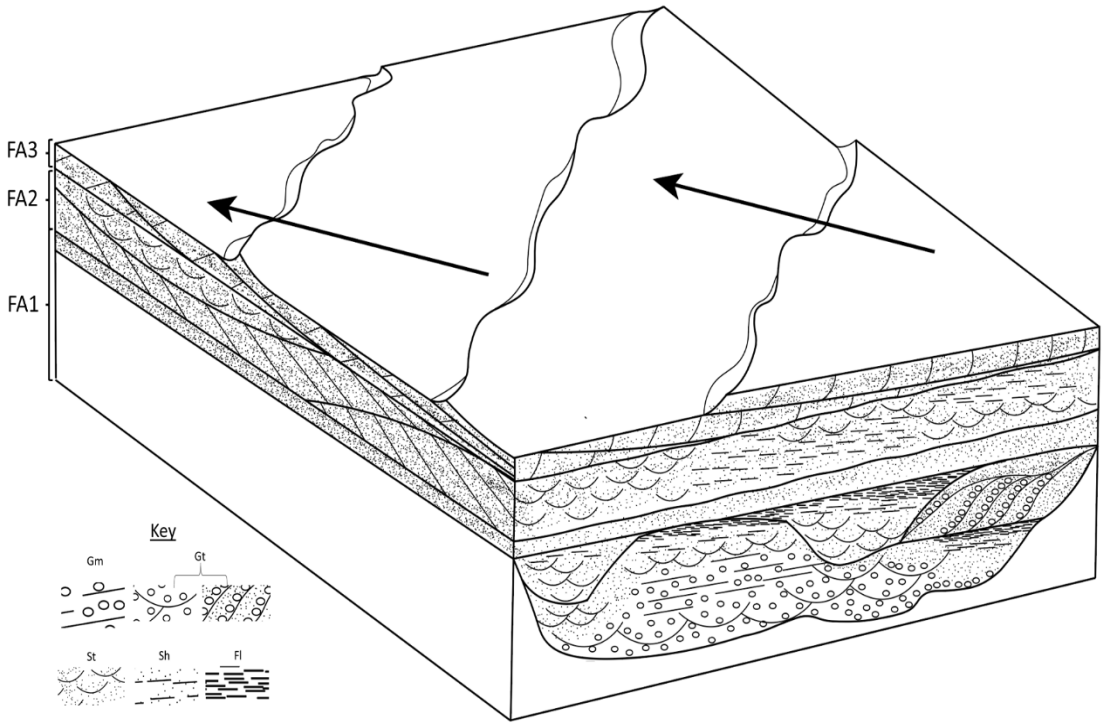

Figure 6.3. Depositional model for facies association FA3 during stage 3. This stage is interpreted as aeolian dominated depositional environment. Black arrows indicate wind direction. Modified from Galloway and Hobday (1983).

6.2 Paleocurrents

The direction of flow for the ancestral Pee Dee River when the Lilesville gravels were deposited was in a southeasterly direction based on the orientations of imbricated clasts measured at the Ponds location in FA1. All measured clasts at imbrication site 2 had similar dip directions oriented to the northwest and average dips of 28.7° (Figure 5.19). Likewise, site 3 had all measured clasts dipping in the same direction but oriented dipping more to the west/northwest with an average dip magnitude of 28° (Figure 5.19). Whereas most of the measured clasts at imbrication site 1 dip to the northwest, a few clasts dip towards the southeast. The average dip magnitude for imbrication site 1 was also less with an average of 22.6°. The variation in dip orientation and magnitude at each of the imbrication sites can be explained by Figure 6.4 B. If all clasts in a gravel bar were initially deposited with generally the same dip direction, parallel to stream flow (Figure 6.4 A), once stream power diminished these imbricated clasts would remain

in place until stream power increased and had enough force to remobilize some of the clasts and transport them across the gravel bar. These remobilized clasts could end up being deposited on other surfaces of the bar, such as the lee side, with dip orientations and magnitudes that are not parallel with stream flow (Figure 6.4 B; Johansson, 1965, as cited in Tucker, 1988).

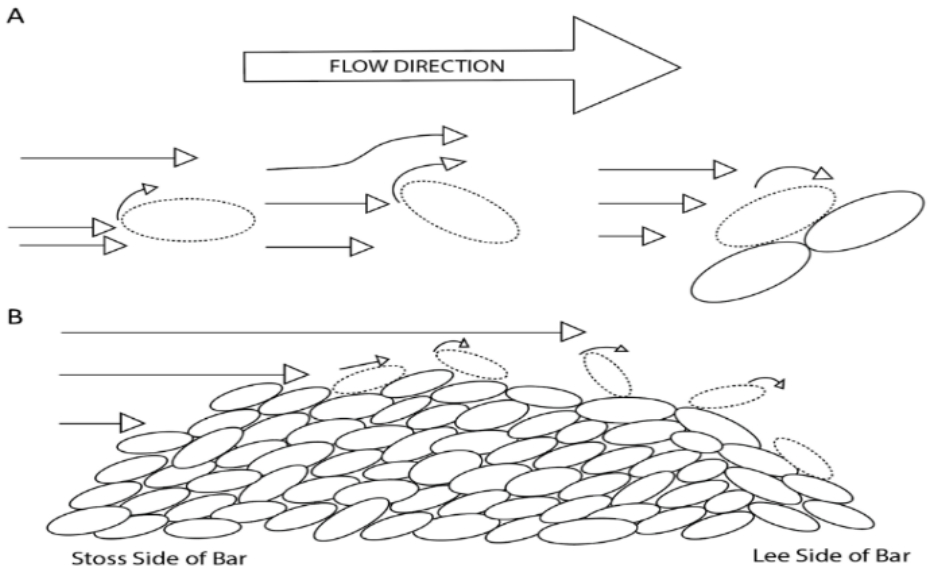

Figure 6.4. A – Diagram showing how imbrication occurs due to stream flow direction. B – Diagram of how clasts can be oriented dipping in directions opposite or at different angles than stream flow direction.

6.3 Provenance

Based on analysis of the bulk samples HQ-P1-1, HQ-P1-2 and HQ-P1-3, the gravely facies that comprise the Lilesville gravels consist of quartzite clasts (92%), vein quartz clasts (8%), and trace amounts of heavy minerals including zircon, kyanite, rutile, tourmaline, sillimanite and monazite. All of these heavy minerals could have been produced either by metamorphism or during crystallization of igneous rock. Considering the complex geologic history of the eastern margin of North America, where multiple series of mountain building events have accreted varying terranes creating the Appalachian Mountains, there are numerous potential geologic source rocks from which the Pee Dee River could receive sediment. The headwaters of the Pee Dee River and its tributaries are located in the Blue Ridge Belt and

continue southeast, cutting across the Sauratown Mountains Anticlinorium, Inner Piedmont Belt, Milton Belt, Charlotte Belt, Carolina Slate Belt, and the Wadesboro Basin (Figure 1.1). McLean (2013) suggested the quartzite (CZq, yellow) that crops out in Stokes County, NC could be the source of quartzite clasts, kyanite and sillimanite which seems like a logical source for these minerals. Vein quartz could be derived from the many intrusive igneous bodies and associated quartz veins, such as from granitic rock (PPg, pink), that occur in the Pee Dee River watershed. Granitic rock could also provide the trace amounts of zircon, tourmaline, rutile and monazite found in the Lilesville gravels.

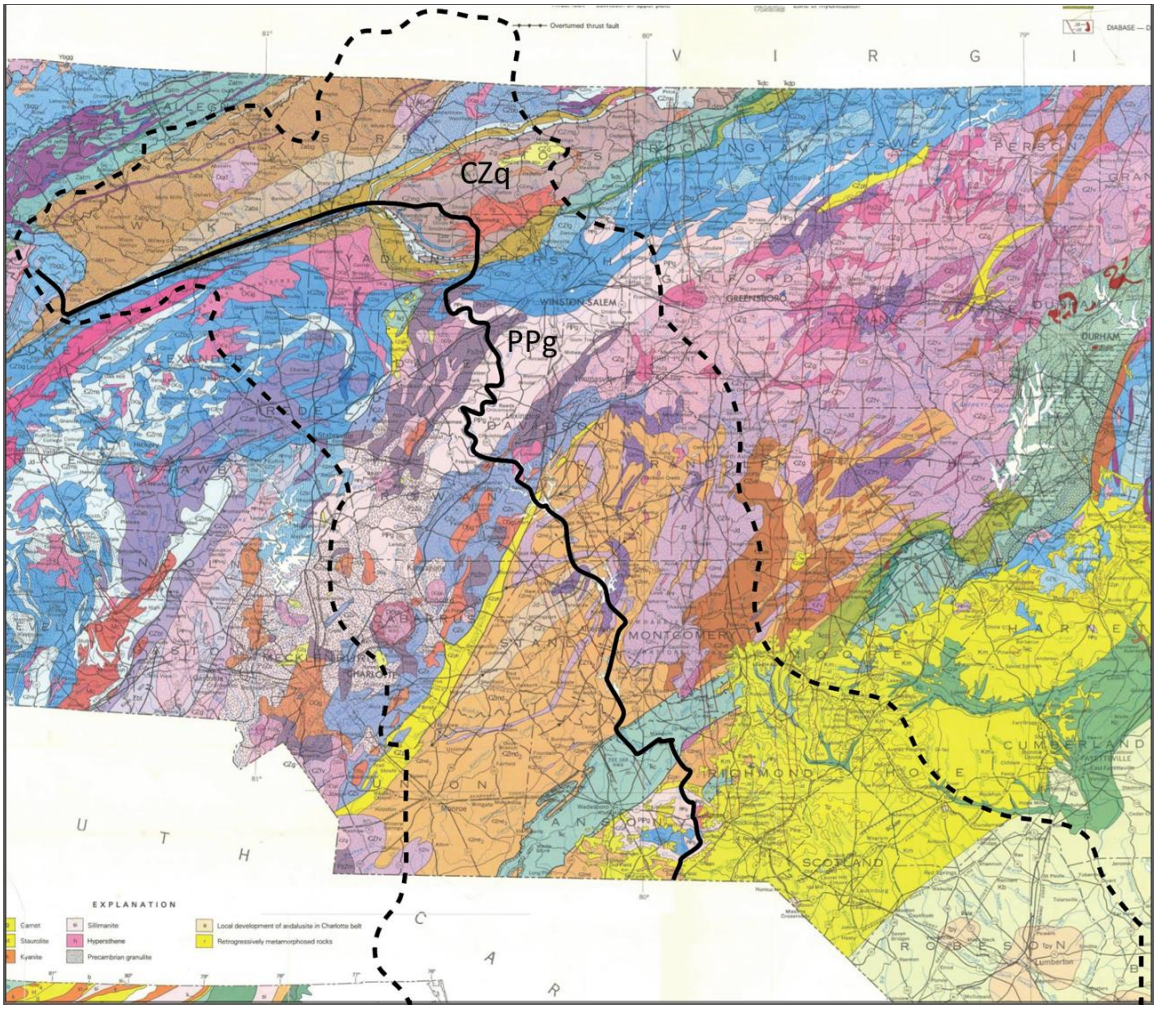

Figure 6.5. Geologic map of North Carolina with the Pee Dee River traced in black. The Pee Dee River watershed is indicated by the dashed black line. CZq (Quartzite) (yellow) is a possible source of quartzite clasts while PPg (Pennsylvanian to Permian Granitic Rock) (pink) is a possible source for vein quartz. (Modified from Brown et al. 1985. Geologic Map of North Carolina, Raleigh: NC Geologic Survey).

6.4 Soil Characteristics

An important soil characteristic observed in the field area is the mottling at the base of facies Sm2 in FA2 which is present throughout the field area. Soil analysis provides information into understanding how this distinct mottling was produced. At the Ponds location, three distinct soil horizons were differentiated on the basis of translocated clays that increase with depth in the unit as well as an increase in the intensity of weathering of iron (HQA-2, refer to Figure 5.20). The evidence for the translocation of clays is recorded by both the change of color and consistence of the horizons. With increasing clay content, the colors of the horizons change from a tan color (10 YR 6/8) in the E horizon to a brown color (7.5 YR 5/6) in the B horizon. The lower horizon has intense reticulate mottling in many outcrops around the field area and appears to be unconformably perched on top of the underlying unit (Figures 6.6 and 6.7).

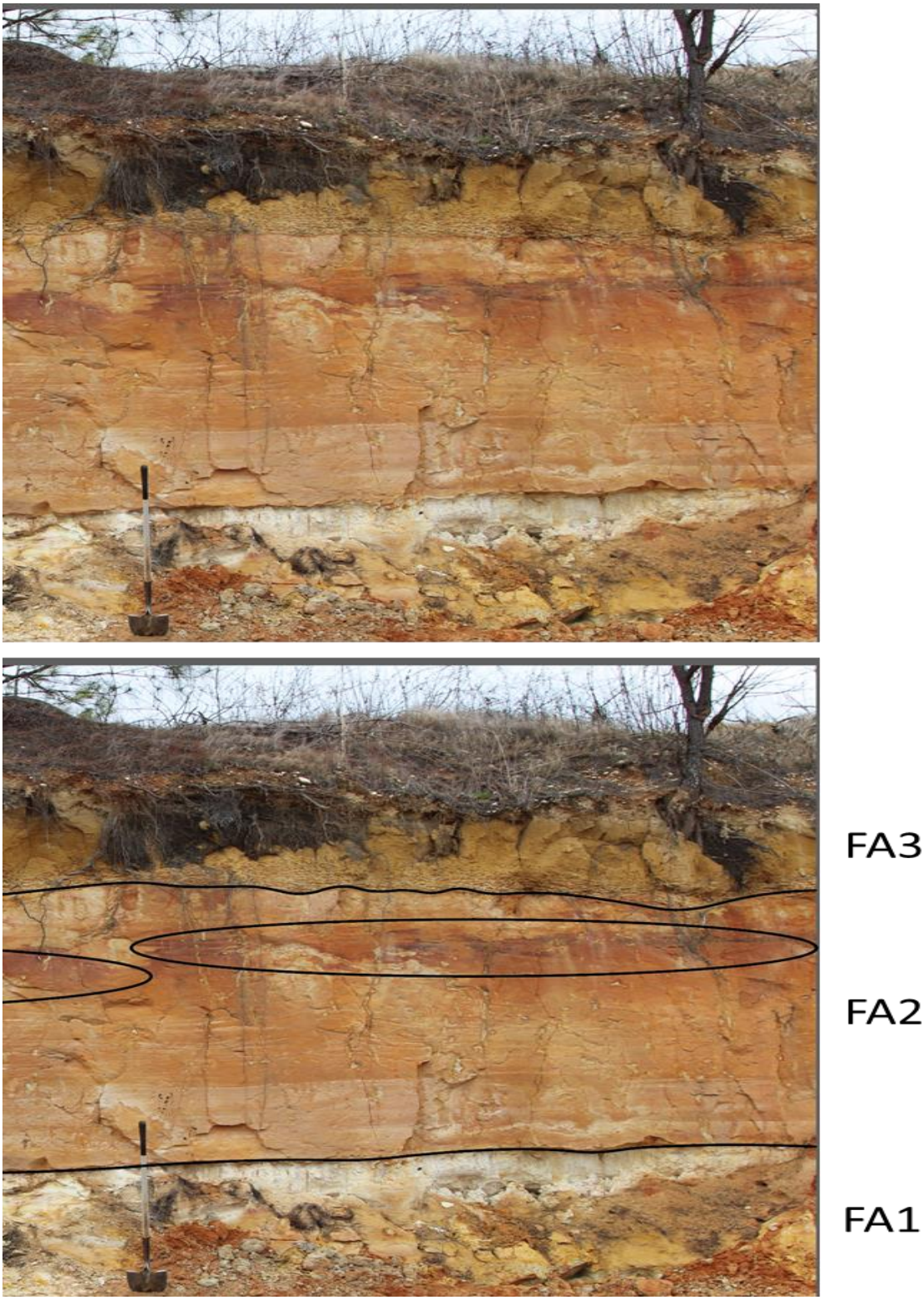

Figure 6.6. Uninterpreted (top) and interpreted (bottom) photos of outcrop at the Ponds location between Pond 1 and 2. The interpreted photo shows the upper wavy boundary between the mottled unit and the much harder underlying unit (FA1 and FA2, respectively). The lower boundary is between FA1 and FA2. Circles indicate positions of concentrated iron, a characteristic of a fragipan.

The heavily mottled horizon, HQB-1, at the Sump Pit 2 location (Figure 5.35), was described as a mottled B horizon in the field but after laboratory analysis it is interpreted as a plinthite because it meets proposed requirements which include its low iron activity ratio (.08), high percentage of dithionite extractable iron (9.62%) and having a thickness greater than 15 centimeters (Kelley et al., 2018).

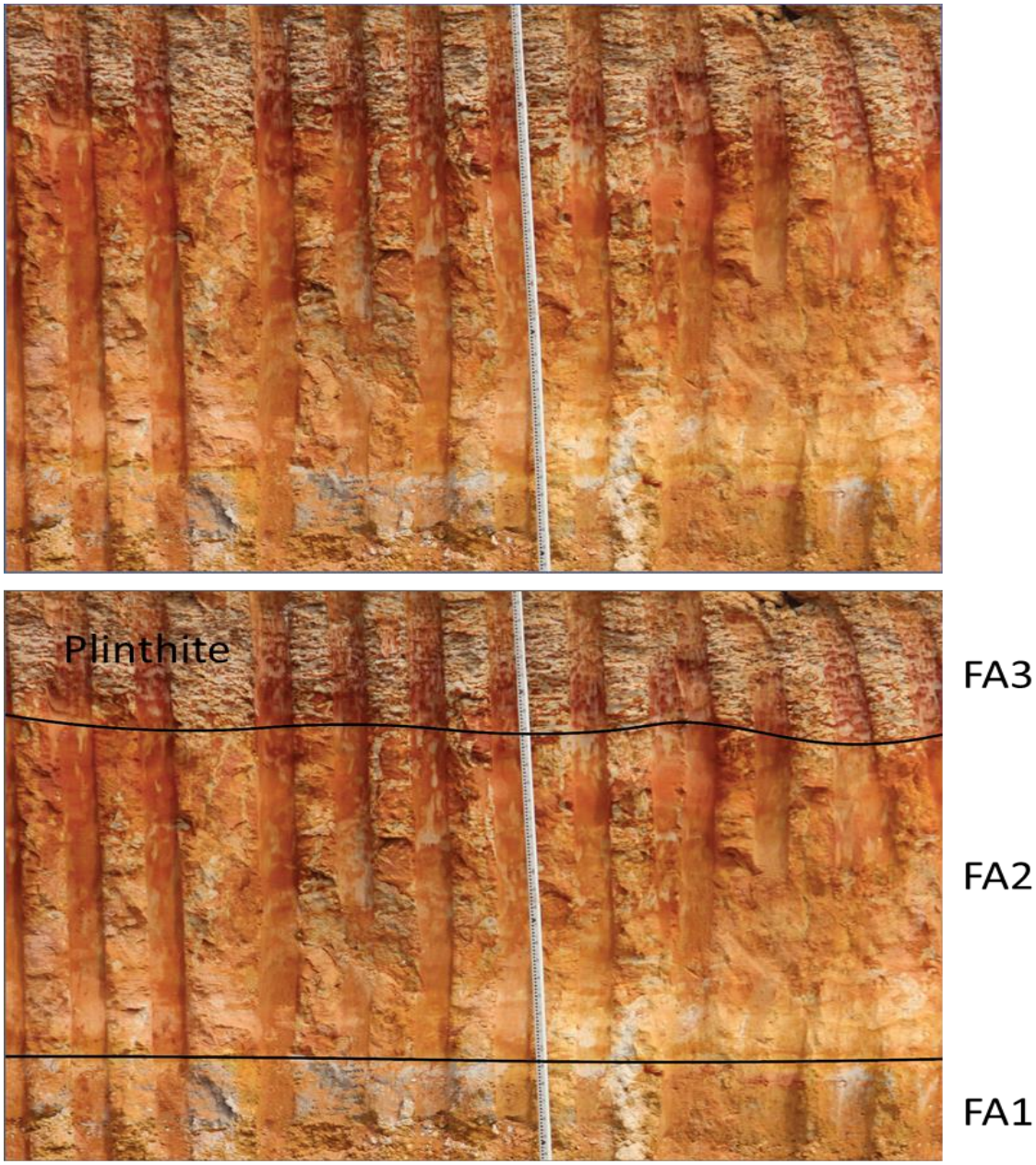

Figure 6.7. Uninterpreted (top) and interpreted (bottom) zoomed in photos of outcrop at Sump Pit 2. The upper black line indicates the boundary between facies associations FA3 and FA2. The bottom black line indicates the boundary between facies associations FA2 and FA1. Note the white marker bed at the top of FA1. Here the outcrop was recently exposed, so the boundaries are not as distinct as in the Ponds location.

The unit directly underlying the plinthite was described as a BC horizon and combined with other field observations this horizon exhibits fragipan characteristics (Figure 6.6 and 6.8). Fragipans, sometimes called hardpans, develop after iron is concentrated via shallow ground water migration and eventual drying and cementation that hinders the flow of water and root penetration (Swezey et al., 2016). This could explain the intense reticulate mottling that occurs at the base of facies Sm2, where the underlying fragipan prevented water from draining between episodes of increased moisture or saturation. The distinctive wavy contact between these two units seen in some outcrops throughout the field area indicates an unconformity, a change in depositional environments and a period during which long term erosion took place between FA2 and FA3 (Nystrom et at., 1991) (Figure 6.6).

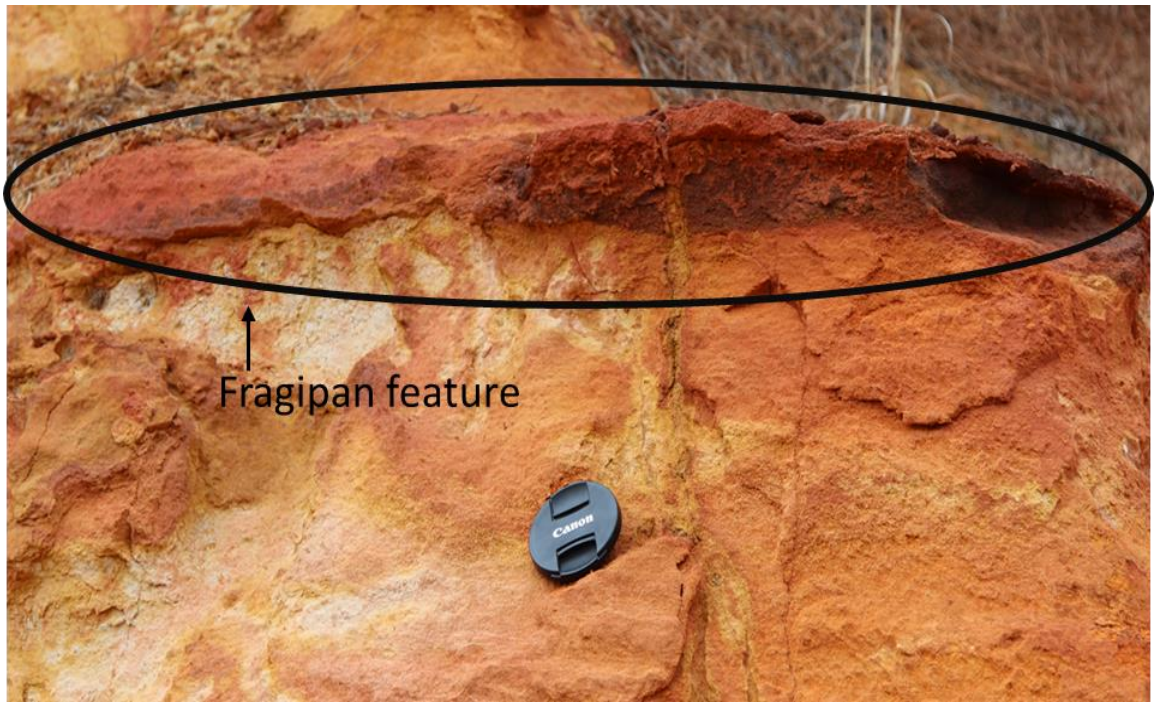

Figure 6.8. Photo in highwall between Pond 1 and Pond 2 of an example of a fragipan. Encircled is a layer within the unit that is harder and cemented to the point it is more resistant to weathering.

The depletion/enrichment curve supports the interpretation of soil formation in the identified soil horizons where elements can migrate and be eluviated and illuviated throughout a soil profile (Figure 5.24). Specifically, in HQA-2 and HQA-9 iron increases with depth. Another interpretation that can be made from the depletion/enrichment curve relates to provenance. The

approach to create this curve assumes the same parent material existed throughout the entire profile, which might not be the case considering the depositional environment was a Neogene fluvial complex deposited by a river that flowed across several geologic provinces (McLean 2013; Figure 6.5). The buried soil HQA-5 (the laterally extensive white 'marker bed', facies Sm1 at the top of FA1) is interpreted as overbank or crevasse splay deposits from the distal FA1 river channel. Sm1 was deeply weathered prior to the return of the FA2 stream channel which then deposited facies St+h. The depletion/enrichment curve shows a distinct change in elemental percentages where iron, aluminum, and silica are enriched and titanium becomes depleted. It is interpreted that initially the ancestral Pee Dee River was a high energy system capable of transporting cobble sized clasts and then it transitioned to a lower energy system transporting mostly sand sized material. This change in fluvial facies associations corresponds with the variation in elemental compositions on the depletion/enrichment curve (Figure 6.9). Once the river incised and transitioned from a fluvial setting (FA2) to an aeolian setting (FA3), we also see a change in elemental composition (Figure 6.9)

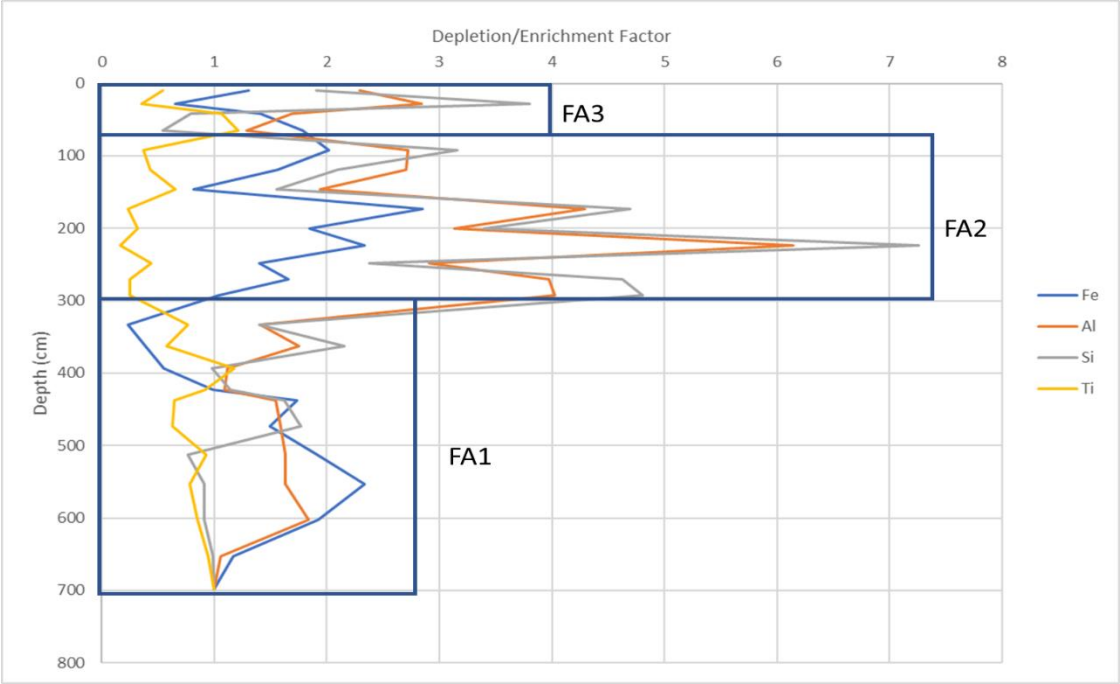

Figure 6.9. Depletion/enrichment factors for elements iron (Fe), aluminum (Al) and silicon (Si). The titanium curve represents the titanium ratio, not the depletion/enrichment factor (because titanium is immobile). Black boxes outline soil horizons.

6.5 Age Estimation

As previously discussed, the age of the Lilesville gravels can be estimated by using the method developed by Mills (2000) where an age of a terrace can be derived from its height above the modern river channel. This method was used by McLean (2013) and in this study indicating that the Lilesville gravels at the Hedrick Sand and Gravel Quarry, located 100 meters above the modern Pee Dee River, are about 10 million years old (late Miocene).

The assemblage of pollen species contained in the lignite indicate an environment dominated by a variety of hardwoods and pines indicating a warm and humid temperate climate much like the conditions that prevail in the southeastern U.S. today. The presence of aquatic plants such as cypress, water lily, and freshwater algae indicates a saturated environment. The absence of grasses could indicate a lack of open space due to dense trees and shrubs. This setting could be interpreted as an environment with a high water table leaving the landscape saturated for long periods of time and increasing the likelihood for surface water to persist. The age of the Lilesville Lignite pollen can be estimated by comparing the pollen assemblage from the Lilesville lignite to pollen assemblages from other Neogene aged lignite deposits throughout the eastern portion of North America (Figure 1.4). The method used by Pazzaglia et al. (1996) to determine the age of the Bryn Mawr Formation used the proportion of QC, FPAT and ANAP (Figure 6.10). Pollen analysis indicates an age for the ‘Lilesville Lignite’ as late Miocene (Figure 6.10).

Preliminary observations of phytoliths and plant macrofossil provide no evidence to contradict the age estimations from the 2 previously discussed modes of age dating the Lilesville Lignite (Hyland, 2021, personal communication). Therefore, a Neogene age is supported, and it is likely ‘later Miocene’ based on this evidence (Hyland, 2021, personal communication).

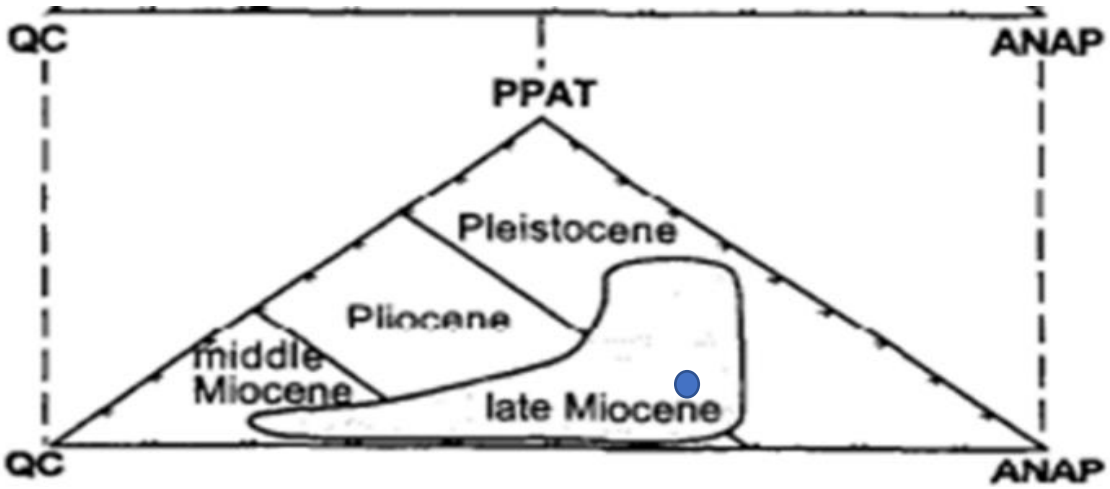

Figure 6.10. Ternary diagram of age relationships between proportions of pollen types. QC= % Quercus+Carya, PPAT= % Pinus+Picea+Abies+Tsuga and ANAP= % woody angiosperms (less Quercus and Carya) and non-arboreal pollen. For the Lilesville Lignite QC=28.9%, PPAT= 17.2% and ANAP= 54% and plotted as a blue circle. (Modified from Pazzaglia et al., 1997).

The presence of plinthite seen at the base of FA3 adds to our understanding the age of the Lilesville gravels. The plinthite horizon developed in facies Sm2 which is interpreted as aeolian deposited sands. Similarly described aeolian deposits are recorded throughout southeastern North America resting on top of Middendorf (Cretaceaous) and other upland gravels of Pliocene-Miocene age. The aeolian deposits are generally interpreted as late Miocene to early Pliocene in age (Nystrom et al., 1991). This helps to constrain the upper age of the Lilesville Gravels as late Miocene to early Pliocene.

6.6 Controls for the Deposition of the Lilesville gravels

The Lilesville gravels are similar to other upland gravel deposits including the Bryn Mawr, Brandywine, and Cohansey formations. Thus, the provenance of these deposits is likely closely related. It is likely that epeirogenic uplift of the Appalachian Mountain region is the source of the sediment to produce the Lilesville gravels and other upland gravel deposits. The pulse of greater amounts of clastic material into the clastic wedge developing outward into the Atlantic Ocean during the Miocene is evidence of increased topography in the Appalachian Mountains.

Climate change occurred in the Miocene and may have played some role in the deposition of the Lilesville gravels as well. The transition to a humid and subtropical climate in the early and middle Miocene could have caused increased weathering and erosion rates.

The combination of increased slope from tectonic uplift and increased weathering and erosion of sediments due to climate change may have created the conditions for the ancestral Pee Dee River to transport much coarser-grained material than is currently being transported.

Some studies suggest external forces such as tectonism and climatic fluctuations are not required for creating high relief in the Appalachian Mountains (Prince et al., 2011, Johnson, 2020). Rather, transient incision of stream systems leading to stream capture events can assimilate higher elevation relict upland landscapes creating disequilibrium in a tectonically passive setting (Prince et al., 2011). Further dissection of the relict upland plateaus of the Blue Ridge is driven by the change in base level and the resulting adjustment of the captured upland fluvial system. This rapid capturing of upland plateaus enlarges the reach in the headwaters of the fluvial system, therefore increasing the amount of erodible material that can be transported by the newly configured drainage basin. The sudden pulse of sediment that is seen in the late Miocene could be evidence of a process such as this.

There is not enough evidence that a base level fall due to a low stand in sea level had any effect on increasing sediment supply or increasing particle size of the sediments being transported by the paleo Pee Dee River. A drop in base level due to a regression of ocean levels would instead affect where sediment was deposited. Therefore, fluctuating sea levels likely did not cause increased relief and mobilization of coarser grained sediment from the source area.

CHAPTER 7: CONCLUSIONS

The origin of enigmatic upland gravels along interfluves in the eastern margin of North America has been a subject of study for many years. This study indicates that the Lilesville gravels were deposited in a southeasterly flowing braided stream system occupying a strath terrace created by the ancestral Pee Dee River. The purpose of this study was twofold: 1) to describe the sedimentology and stratigraphy of the Lilesville gravels at the BV Hedrick Gravel and Sand quarry, and 2) to explore the roles that tectonics, climate change, sea level fluctuation, or some combination of the three, played in the deposition of these enigmatic upland gravel deposits.

The Lilesville gravels comprise three facies types: a gravely facies association, a sandy facies association, and a fine facies association. The gravely facies association includes massive to poorly bedded gravels (Gm) and trough cross bedded gravels (Gt). The sandy facies association includes trough cross bedded sands (St), horizontally laminated sands (Sh), massive sands (Sm) and ripple cross laminated sands (Sr). The fine facies association includes laminated sand, silt and clay (Fl) and organic-rich silt and clay (Fo), or lignite. Architectural elements observed and documented throughout the field area included imbricated clasts, gravel bars, channel fills, lateral accretion surfaces, crevasse splays, overbank fines, and cross-laminated ripples.

The strath surface that the Lilesville gravels rests on is at an elevation of 100 meters above the modern Pee Dee River channel. This indicates a late Miocene age of formation about 10 Mya for the Lilesville gravels. The pollen and plant macro-fossil analysis also suggests a Neogene age for the ‘Lilesville Lignite’ and interbedded gravels, further indicating that the Lilesville gravels were deposited in the late Miocene. The warm and humid climate made it possible for cypress (18.2%), pine (17.1), oak (15.4), hickory/pecan (13.5%) to proliferate. This distribution of pollen indicates that the ‘Lilesville Lignite’ was deposited in a climate very similar

to the climates of modern-day Georgia, South Carolina and North Carolina, the most similar analog of climate being today's Georgia coast.

The Lilesville gravels were deposited likely due to increased relief in the headwaters of the ancestral Pee Dee River system during the late Miocene. Eroded sediments derived from crystalline bedrock were transported by the ancestral Pee Dee River and deposited on a strath terrace in the Lilesville area in a braided fluvial setting (FA1). The 'Lilesville Lignite' was deposited during this time, likely in a cut off channel that received inflow only during periods of high discharge. The ability of the river to transport coarse grained material diminished through time, resulting in a finer grained second stage deposit (FA2). Later incision by the stream channel cut into the underlying bedrock creating a second unpaired strath terrace 82 meters above the current Pee Dee River channel with an estimated age of about 8 million years (McLean, 2013). As the original terrace tread was abandoned the deposits were reworked by aeolian processes and deposition of the aeolian sands (FA3) took place. The down-cutting by the Pee Dee River caused an inversion of the topography where plinthite could form at the base of the aeolian sand deposit in a hot, humid, densely vegetated, and poorly drained environment in the late Miocene to Pliocene.

This study indicates that it is likely a combination of tectonic activity in the form of epeirogenic rejuvenation of the Appalachian Mountains and climatic fluctuations that produced the conditions that influenced the deposition of the Lilesville gravels. This may also be the case for other upland gravel deposits that occur in the Fall Zone of eastern North America.

REFERENCES

Ahnert, F. 1970. Functional relationships between denudation, relief, and uplift in large, mid-latitude drainage basins. American Journal of Science, v. 268, no. 3, p. 243–263.

Baumgartner, K., 2014. Neogene Climate Change in Eastern North America: A Quantitative Reconstruction. Electronic Thesis and Dissertation, Paper

Birkeland, P. 1999. Soils and Geomorphology, 3rd edition. Oxford: Oxford University Press.

Brown, P. M. et al. 1985. Geologic Map of North Carolina. North Carolina Geological Survey General Geologic Map, scale 1:500,000.

Callahan, J. E., and Craig, J. R. 1990. The potential for heavy minerals in the Lilesville, North Carolina sand and gravel deposits. Proceedings of the 24th Forum on the Geology of Industrial Minerals, v. 24, p. 39–44.

Cleaves, E., 1989. Appalachian Piedmont Landscapes from the Permian to the Holocene. In: T.W. Gardner and W.D. Sevon (Editors). Geomorphology, v. 2, p. 159-179.

Cobb, C. 1903. Origin of the sandhill topography of North Carolina. Science, v. 17, p. 226–227.

Coe, A. 2010. Geologic field techniques, Hoboken, NJ: Wiley-Blackwell

Collinson, J.D, 1970. Bed forms of the Tana River, Norway. Georg. Ann., v. 52A, p. 31-55.

Conley, J. F. 1962, Geology and mineral resources of Moore County, North Carolina. Bulletin 76 North Carolina Department of Conservation and Development, 40 p.

Cooke, C. W. 1936. Geology of the Coastal Plain of South Carolina. U.S. Geological Survey Bulletin, 867, 196 p.

Cooley, Jr., T. W. 1970. Post Cretaceous Stratigraphy of the Sandhills Region, North and South Carolina [Doctoral]: UNC Chapel Hill, 127 p.

Daniels, R. B., Gamble, E. E., and Wheeler, W. H. 1978. Age of soil landscapes in North Carolina. Soil Science Society of America Journal, v. 42, p. 98-105.

Delvaux, B. and Brahy, V. 2001. Mineral soils conditioned by a wet (sub)tropical climate. Available online at http://www. fao.org/docrep/003/y1899e/y1899e08a.htm#P67 11036 (verified on January 17, 2014).

Diemer, J. A., Rich, F. J., Yankech, M., McLean, R. C., Bobyarchick, A. R., and Eppes, M. C. 20 17. Pollen evidence for the age of the Lilesville gravels: A Neogene strath terrace deposit from the Fall Zone of North Carolina, GSA Abstracts with Programs, v. 49, no. 3, Richmond, VA.

Dormaar, J. F. and Lutwick, L. E. 1983. Extractable Fe and Al as an indicator for buried soil horizons. Catena, v. 10, p. 167-173.

Emmons, E. 1852. Report of Professor Emmons on his Geological Survey of North Carolina. Raleigh: State Printer, 104 p.

Eze, P. N., Udeigwe, T. K., Meadows, M. E. 2014. Plinthite and its associated evolutionary forms in soils and landscapes: a review. Pedosphere, v. 24, no. 2, p. 153–166.

Eppes, C. E., Bierma, R., Vinson, D., and Pazzaglia, F. 2008. A soil chronosequence study of the Reno valley, Italy: Insights into the relative role of climate versus anthropogenic forcing on hillslope processes during the mid-Holocene. Geoderma, v. 147, i 3-4, p. 97-107.

Fauzi, A. I. and Stoops, G. 2004. Reconstruction of a toposequence on volcanic material in the Honje Mountains, Ujung Kulon Peninsula, West Java. Catena, v. 56, p. 45–66.

Gallen, S. F., and Wegmann, K. W. 2015. Exploring the origins of modern topographic relief in the southern Appalachians: An excursion through the transient landscape of the Cullasaja River basin, North Carolina. In: Holmes, A. E., (ed.), Diverse Excursions in the Southeast: Paleozoic to Present. Geological Society of America Field Guide 39, pp. 145–167, doi:10.1130/2015.0039(05).

Gallen, S. F., Wegmann, K. W., and Bohnenstiehl, D. R. 2013. Miocene rejuvenation of topographic relief in the southern Appalachians. GSA Today v. 23, no.2, p. 4–10, doi: 10.1130/GSATG163A.1.

Gallen, S. F., Wegmann, K. W., Frankel, K. L., Hughes, S., Lewis, R. Q., Lyons, N., Paris, P., Ross, K., Bauer, J. B., and Witt, A. C. 2011. Hillslope response to knickpoint migration in the Southern Appalachians: Implications for the evolution of post-orogenic landscapes. Earth Surface Processes and Landforms 36 (9): 1254–1267, doi: 10.1002/esp.2150.

Galloway, W.E., Hobday, D.K., 1983. Terrigenous Clastic Depositional Systems. New York: Springer-Verlag, 422 p.

Hack, J. T. 1955. Geology of the Brandywine area and origin of the upland of southern Maryland. U. S. Geological Survey Professional Paper 267–A.

Hack, J. T. 1982. Physiographic divisions and differential uplift in the Piedmont and Blue Ridge. U. S. Geological Survey Professional Paper 1265.

Hjulstrom, F., 1939. Transportation of detritus by moving water. AAPG Special Volumes, SP 10: Recent Marine Sediments, p.5-31.

Johansson, C. F., 1965. Structural Studies of Sedimentary Deposits. Geologiska Foreningen I Stockholm forhandlingar, 87 (1): 3-61.

Johnson, B, 2020. Stream capture and geomorphic evolution of the Linville Gorge in the southern Appalachians, USA. Geomorphology, v. 368, p. 107360

Kelley, J. A., Ogg, C. M., Wilson, M. A.Rationale for a plinthic Horizon in Soil Taxonomy. University of Florida, Office of Conferences and Institutes. Available from http://conference. ifas. ufl. edu/ss/pdf/KelleyJ. pdf (Accessed 18 August 2018).

Kerr, W. C. 1875. Report of the Geological Survey of North Carolina, Volume 1. Raleigh: State Printer, 150 p.

Lawrence, K., Coxall, H., Sosdian, S., Steinhrsedottir, M., 2021. Navigating Miocene Ocean Temperatures for Insights into the Future. Eos, 102 p.

Layzell, A. L., Eppes, M. C., Lewis, R. Q., 2012. A soil chronosequence study on terraces of the Catawba River near Charlotte, NC: Insights into the long-term evolution of a major Atlantic Piedmont drainage basin. Southeastern Geology, v. 49, no.1, p. 13-24.

Leeder, M. R. 2011. Sedimentology and Sedimentary Basins: From Turbulence to Tectonics. Oxford: John Wiley.

Leigh, D., Srivastava, P., Brook, G., 2004. Late Pleistocene braided rivers of the Atlantic Coastal Plain, USA. Quaternary Science Reviews, v. 23, p. 65-84.

Lindhom, R. C., 1987. A practical approach to sedimentology. Allen and Unwin, 276 p.

Maddy, D., D. Bridgland & R. Westaway, 2001. Uplift-driven incision and climate-controlled river terrace development in the Thames Valley, UK. Quaternary International, v. 79, p. 22-36.

Mahaney, William C. and Fabey, B. D. 1988. Extractable Fe and Al in late Pleistocene and Holocene paleosols on Niwot Ridge, Colorado Front Range. Catena, v, 15, p. 17-26.

Mahaney, W. C., Fabey, B. D. 1985. Notes on the use of extractable iron and clay minerals for determining soil age. Geografisk Tidsskrift, v, 85, p. 14-19.

Miall, A., 1977. A review of the braided-river depositional environment. Earth-Science Reviews, v. 13, no, 1, p. 1-62.

Miall, A., 1985. Architectural-element analysis: A new method of facies analysis applied to fluvial deposits. Earth-Science Reviews: v. 22 no. 4, pp 261-308.

Markewicz, F.J., Padillo, D.G. and Johnson, M.E., 1958. Titanium Sands of Southern New Jersey. N.J. Geol. Surv. Booklet, 16 p.

McCartan, Lucy et al., 1990. Late Tertiary floral assemblage from upland gravel deposits of the southern Maryland Coastal Plain: Geology, v, 18, p. 311-314.

McKeague, J.A., and Day, J.H., 1966, Dithionite and oxalate extractable Fe and Al as aids in differentiating various classes of soils: Canadian Journal of Soil Science, v. 46, p. 13-22.

Mehra, O.P., Jackson, M.L., 1960, Iron oxide removal from soils and clays by a dithionite citrate systems buffered with sodium bicarbonate: Clays and Clay Minerals, v. 7, p. 313-317.

Mills, H. H. 2000. Apparent increasing rates of stream incision in the eastern United States during the late Cenozoic. Geology, v, 28, p. 955–957.

Mirzai M., Mataji E., Nora, M., Gorji, K., 2017, Grain Size Distribution, Facies and Architecture Elements Analysis of the Fluvial Sediment in Dez and Karkheh Rivers, Khuzestan, Iran. Electronic Journal of Geotechnical Engineering, v. 22.15, p. 5715-5732.

Nystrom, P. G., Willoughby, R. H., and Price, L. K. 1991. Cretaceous and Tertiary stratigraphy of the Upper Coastal Plain, South Carolina. In: The Geology of the Carolinas edited by J. Wright Horton Jr., and Victor A. Zullo. Knoxville: The University of Tennessee Press.

Owens, J. P. 1989. Geology of the Cape Fear region, Florence 1° x 2° quadrangle and northern half of the Georgetown 1° x 2° quadrangle, North Carolina and South Carolina. USGS Miscellaneous Investigations Series, Map I–1948–A.

Owens, J. P., and Minard, J. P. 1924. Upper Cenozoic sediments of the Lower Delaware Valley and the northern Delmarva Peninsula, New Jersey, Pennsylvania, Delaware, and Maryland. U. S. Geological Survey Professional Paper, 1067–D.

Patchineelam, S.M., Kjerve, B., and Gardner, L.R., 1999. A preliminary sediment budget for the Winyah Bay estuary, South Carolina, USA. Marine Geology, v. 162, p. 133-144.

Pazzaglia, F. J. 1993. Stratigraphy, petrography, and correlation of late Cenozoic middle Atlantic Coastal Plain deposits: Implications for late-stage passive-margin geologic evolution. Geological Society of America Bulletin, v. 105, p. 1617–1634.

Pazzaglia, F. J., and Gardner, T. W. 1993. Fluvial terraces of the lower Susquehanna River. Geomorphology, v. 8, p. 83–113.

Pazzaglia, F. J., and Gardner, T. W. 1994. Late Cenozoic flexural deformation of the middle U. S. Atlantic passive margin. Journal of Geophysical Research, v. 99, p. 12,143-12,157.

Pazzaglia, F. J., Brandon, M. T., 1996. Macrogeomorphic evolution of the post-Triassic Appalachian Mountains determined by deconvolution of the offshore basin sedimentary record. Basin Research, v, 8, p. 255–278, doi: 10.1046/j.1365–2117.1996.00274.x.

Pazzaglia, F. J., Robinson, R. A. J., and Traverse, A. 1997. Palynology of the Bryn Mawr Formation (Miocene): insights on the age and genesis of Middle Atlantic margin fluvial deposits. Sedimentary Geology, v. 108, p. 19–44.

Pazzaglia, F. J., Malenda, H. F., McGavick, M. L., Raup, C., Carter, M. W., Berti, C., Mahan, S., Nelson, M., Rittenour, T. M., Counts, R., Willenbring, J., Germanoski, D., Peters, S. C., and Holt, W. D., 2021. River Terrace Evidence of Tectonic Processes in the Eastern North American Plate Interior, South Anna River, Virginia. Journal of Geology, v. 129, n. 5

Poag, C. W., and Sevon, W. D. 1989. A record of Appalachian denudation in postrift Mesozoic and Cenozoic sedimentary deposits of the U.S. Middle Atlantic continental margin. Geomorphology, v, 2, no, 1–3, p. 119–157.

Prince, P. S., Spotila, J. A., Henika, W. S., 2011. Stream capture as driver of transient landscape evolution in a tectonically quiescent setting. Geology, v. 39, p. 823-826.

Rachele, L. D. 1976. Palynology of the Legler lignite: A deposit in the Tertiary Cohansey Formation of New Jersey, U.S.A. Review of Palaeobotany and Palynology v, 22, p. 225–252.

Reinhardt, J., Prowell, D. C., and Christopher, R. A. 1984. Evidence for Cenozoic tectonism in the southwest Georgia Piedmont. Geological Society of America Bulletin, v. 95, no. 10, p. 1176–1187.

Schlee, J. 1957. Upland gravels of southern Maryland. Geological Society of America Bulletin, v. 68, p. 1371–1410.

Schumm, S.A., 1993. River response to base-level change; implications for sequence stratigraphy: The Journal of Geology, v. 101, no. 2, p 279–294.

Stanford, S. D., Ashley, G. M., Russell, E. W. B., and Brenner, G. J. 2002. Rates and patterns of late Cenozoic denudation in the northernmost Atlantic Coastal Plain and Piedmont. Geological Society of America Bulletin, v. 114, p. 1422–1437.

Swezey, C. S., Fitzwater, B. A., and Whittecar G. R. 2016. Geology and geomorphology of the Carolina Sandhills, Chesterfield County, South Carolina. in Doar, W.R., III, ed., Gold, Structures, and Landforms in Central South Carolina – Field Guides for the 2016 GSA Southeastern Section Meeting, Columbia, South Carolina: Geological Society of America Field Guide, v. 42, p. 9-36.

Taylor, A. and Blum, J. D. 1995. Relation between soil age and silicate weathering rates determined from the chemical evolution of a glacial chronosequence. Geology, v. 23, no. 11, p. 979-982.

Thelin, G.P., and Pike, R.J., 1991. Landforms of the conterminous United States—A digital shaded-relief portrayal: USGS Map 2206, scale 1:3,500,000, 1 sheet.

Tornqvist, T. 1994. Middle and late Holocene avulsion history of the River Rhine (Rhine-Meuse delta, Netherlands). Geology, v. 22, p. 711-714.

Tucker, M. 1988. Techniques in Sedimentology. University of Durham DH1 3LE, Blackwell Scientific Publications

Wegmann, K. W. & F. J. Pazzaglia 2002. Holocene strath terraces, climate change, and active tectonics: The Clearwater River basin, Olympic Peninsula, Washington State. GSA Bulletin v. 114, p. 731-744.

Widmer, K., 1964. The Geology and Geography of New Jersey. Van Nostrand, Princeton, N.J. 193 p.

Yankech, M., Diemer, J. A., Eppes, M. C., and Bobyarchik, A. 2018. Depositional environment and timing of formation of the ‘Lileville Gravels’, Anson County, NC, GSA Abstracts with Programs, v. 50, no. 3, Knoxville, TN.

Zhang, J.-Y., A. Yin, W.-C. Liu, L. Ding & X. Mei Xu 2016. First geomorphological and sedimentological evidence for the combined tetctonic and climate control on Quaternary Yarlung river diversion in the eastern Himalaya. Lithosphere, v. 8, p. 293-316.

APPENDIX A: GRAIN SIZE ANALYSIS OF HQ-P1 SAMPLES (PONDS)

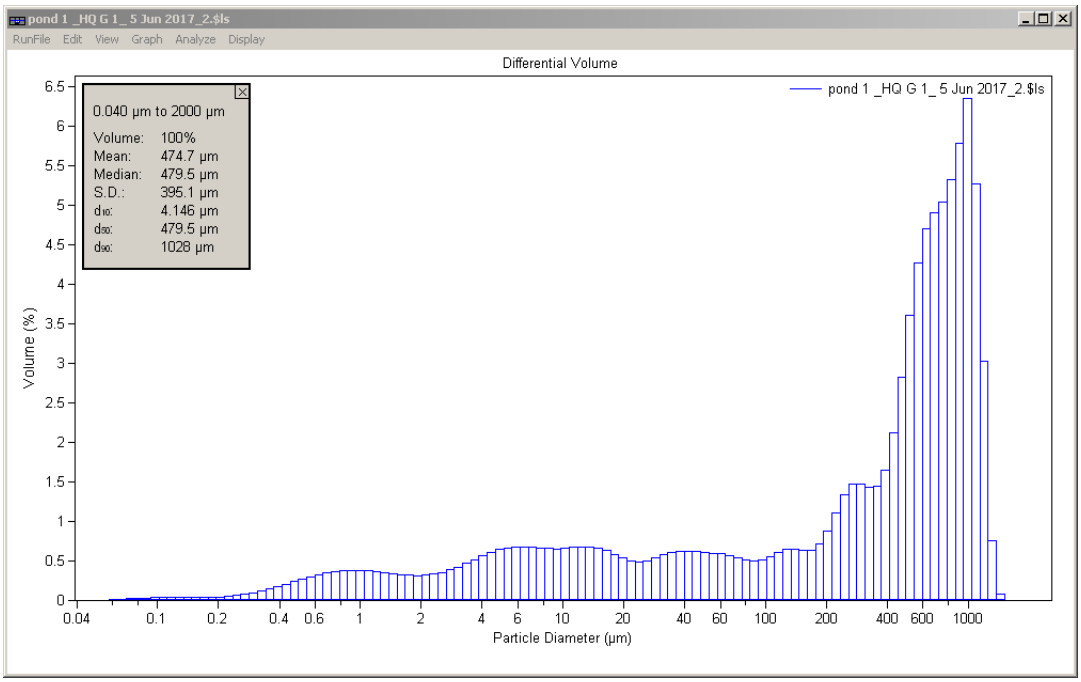

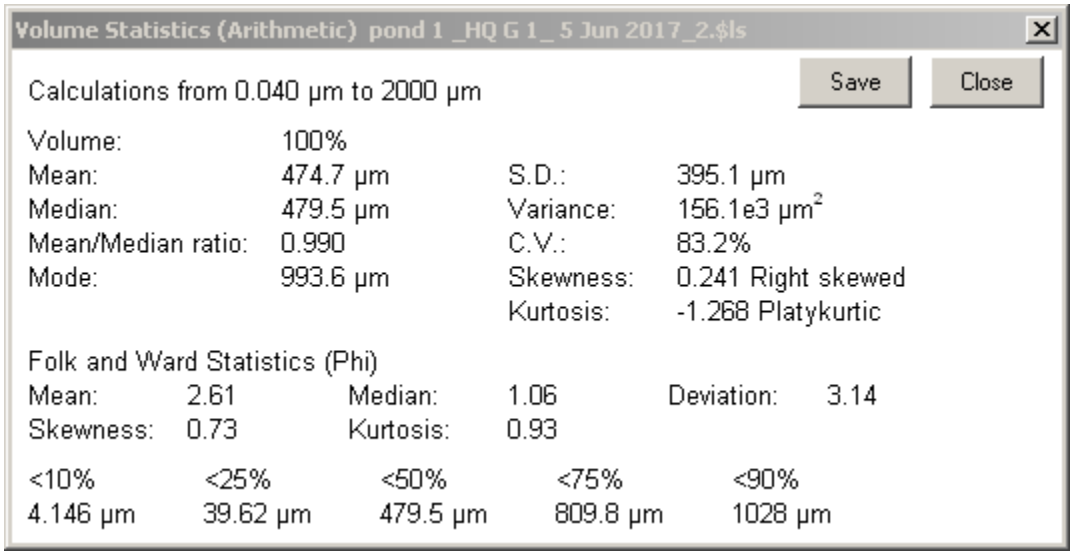

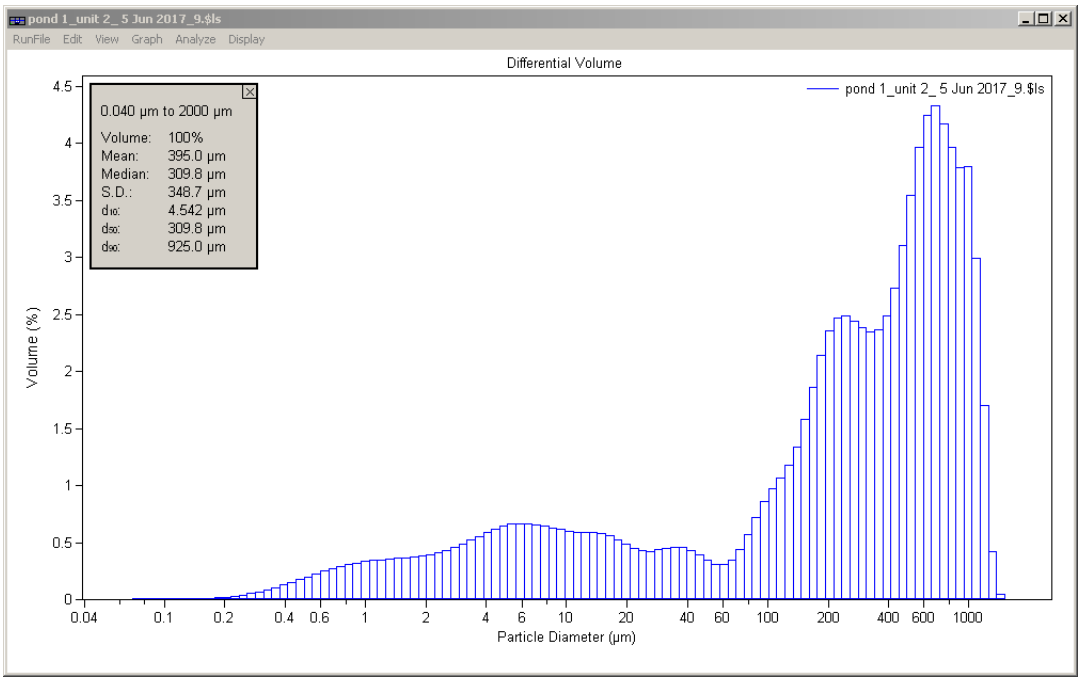

Volume Statistics (Arithmetic) pond 1_unit 2_ 5 Jun 2017_9.$ls

Save Close

Calculations from 0.040 µm to 2000 µm

Volume:	100%		
Mean:	395.0 µm	S.D.:	348.7 µm
Median:	309.8 µm	Variance:	121.6e3 µm^2
Mean/Median ratio:	1.275	C.V.:	88.3%
Mode:	684.2 µm	Skewness:	0.609 Right skewed
		Kurtosis:	-0.725 Platykurtic

Folk and Ward Statistics (Phi)

Mean:	2.85	Median:	1.69	Deviation:	2.96
Skewness:	0.59	Kurtosis:	1.16		

<10%	<25%	<50%	<75%	<90%
4.542 µm	67.68 µm	309.8 µm	656.1 µm	925.0 µm

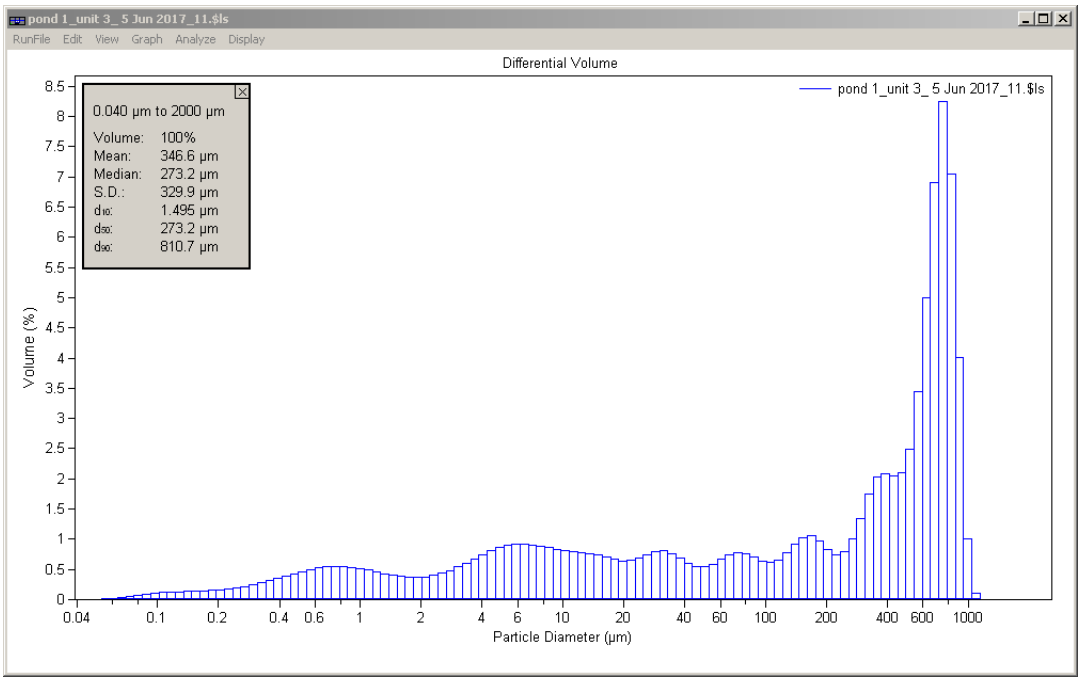

Volume Statistics (Arithmetic) pond 1_unit 3_ 5 Jun 2017_11.$ls

Save Close

Calculations from 0.040 µm to 2000 µm

Volume:	100%		
Mean:	346.6 µm	S.D.:	329.9 µm
Median:	273.2 µm	Variance:	108.8e3 µm^2
Mean/Median ratio:	1.269	C.V.:	95.2%
Mode:	751.1 µm	Skewness:	0.343 Right skewed
		Kurtosis:	-1.463 Platykurtic

Folk and Ward Statistics (Phi)

Mean:	3.36	Median:	1.87	Deviation:	3.44
Skewness:	0.64	Kurtosis:	0.74		

<10%	<25%	<50%	<75%	<90%
1.495 µm	11.87 µm	273.2 µm	674.7 µm	810.7 µm

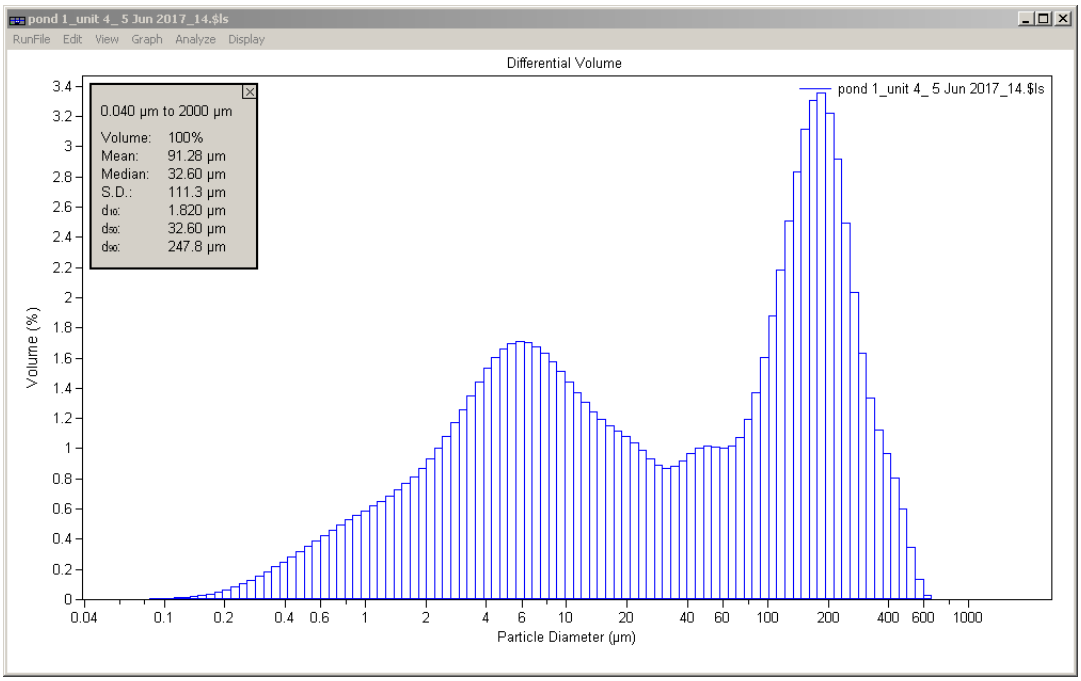

Volume Statistics (Arithmetic) pond 1_unit 4_ 5 Jun 2017_14.$ls

Save Close

Calculations from 0.040 µm to 2000 µm

Volume:	100%		
Mean:	91.28 µm	S.D.:	111.3 µm
Median:	32.60 µm	Variance:	12383 µm^2
Mean/Median ratio:	2.800	C.V.:	122%
Mode:	185.4 µm	Skewness:	1.406 Right skewed
		Kurtosis:	1.646 Leptokurtic

Folk and Ward Statistics (Phi)

Mean:	5.19	Median:	4.94	Deviation:	2.78
Skewness:	0.17	Kurtosis:	0.71		

<10%	<25%	<50%	<75%	<90%
1.820 µm	5.413 µm	32.60 µm	157.9 µm	247.8 µm

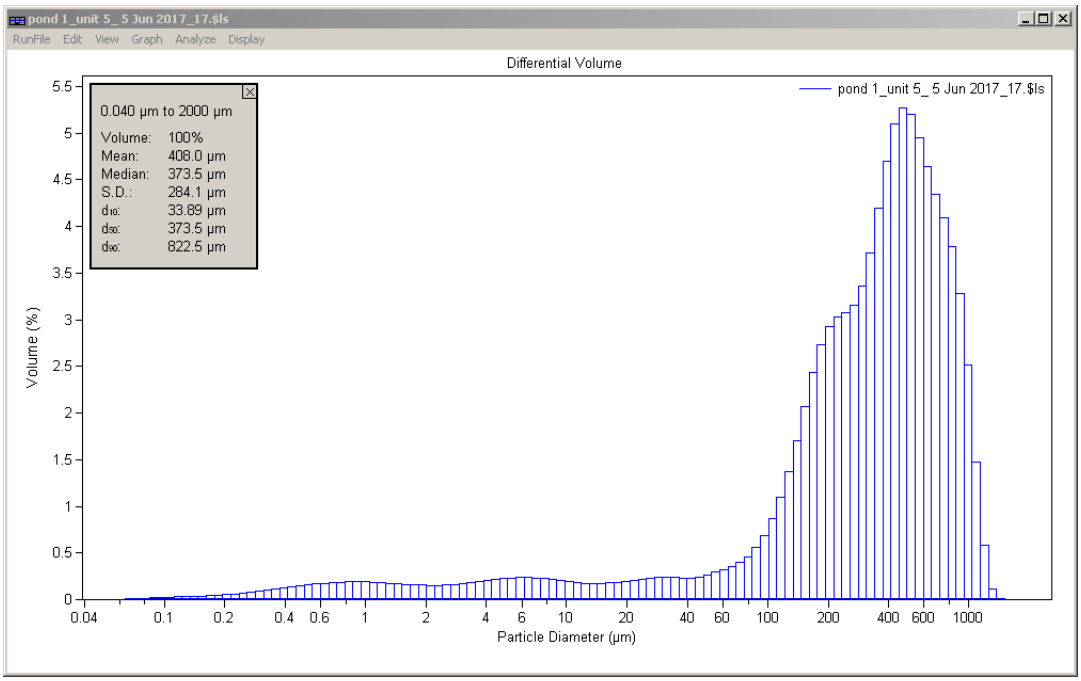

Volume Statistics (Arithmetic) pond 1_unit 5_ 5 Jun 2017_17.$ls

Save Close

Calculations from 0.040 µm to 2000 µm

Volume:	100%		
Mean:	408.0 µm	S.D.:	284.1 µm
Median:	373.5 µm	Variance:	80734 µm^2
Mean/Median ratio:	1.092	C.V.:	69.6%
Mode:	471.1 µm	Skewness:	0.553 Right skewed
		Kurtosis:	-0.357 Platykurtic

Folk and Ward Statistics (Phi)

Mean:	1.66	Median:	1.42	Deviation:	1.85
Skewness:	0.47	Kurtosis:	1.95		

<10%	<25%	<50%	<75%	<90%
33.89 µm	184.7 µm	373.5 µm	593.0 µm	822.5 µm

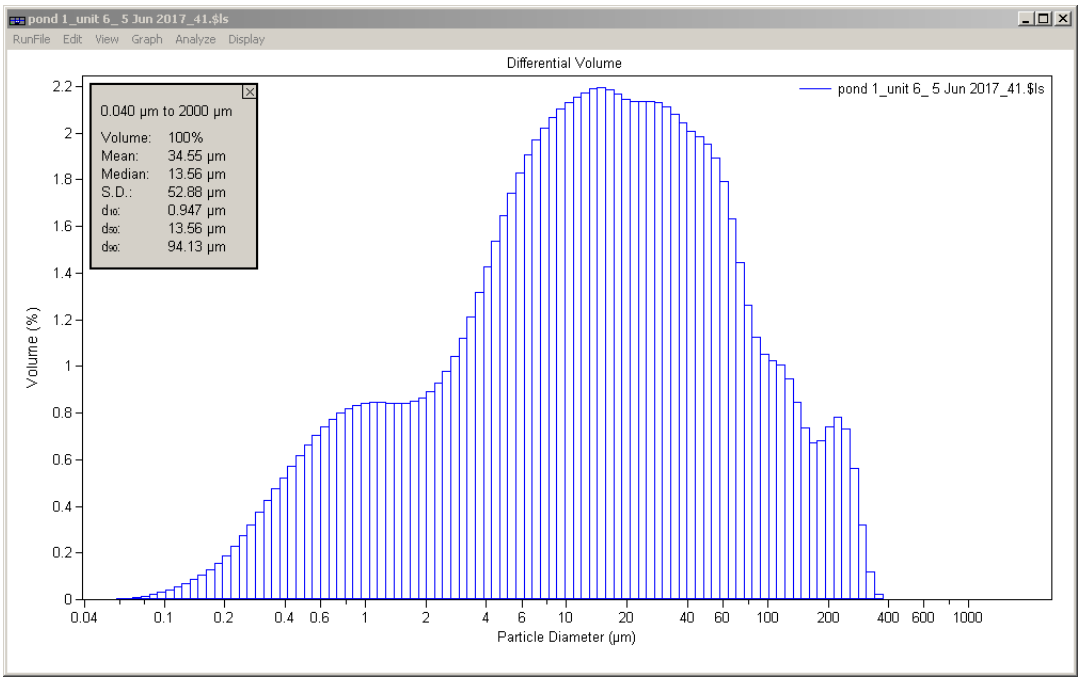

Volume Statistics (Arithmetic) pond 1_unit 6_ 5 Jun 2017_41.$ls

Save Close

Calculations from 0.040 µm to 2000 µm

Volume:	100%		
Mean:	34.55 µm	S.D.:	52.88 µm
Median:	13.56 µm	Variance:	2796 µm^2
Mean/Median ratio:	2.548	C.V.:	153%
Mode:	14.94 µm	Skewness:	2.672 Right skewed
		Kurtosis:	7.714 Leptokurtic

Folk and Ward Statistics (Phi)

Mean:	6.43	Median:	6.20	Deviation:	2.52
Skewness:	0.14	Kurtosis:	1.01		

<10%	<25%	<50%	<75%	<90%
0.947 µm	4.044 µm	13.56 µm	40.41 µm	94.13 µm

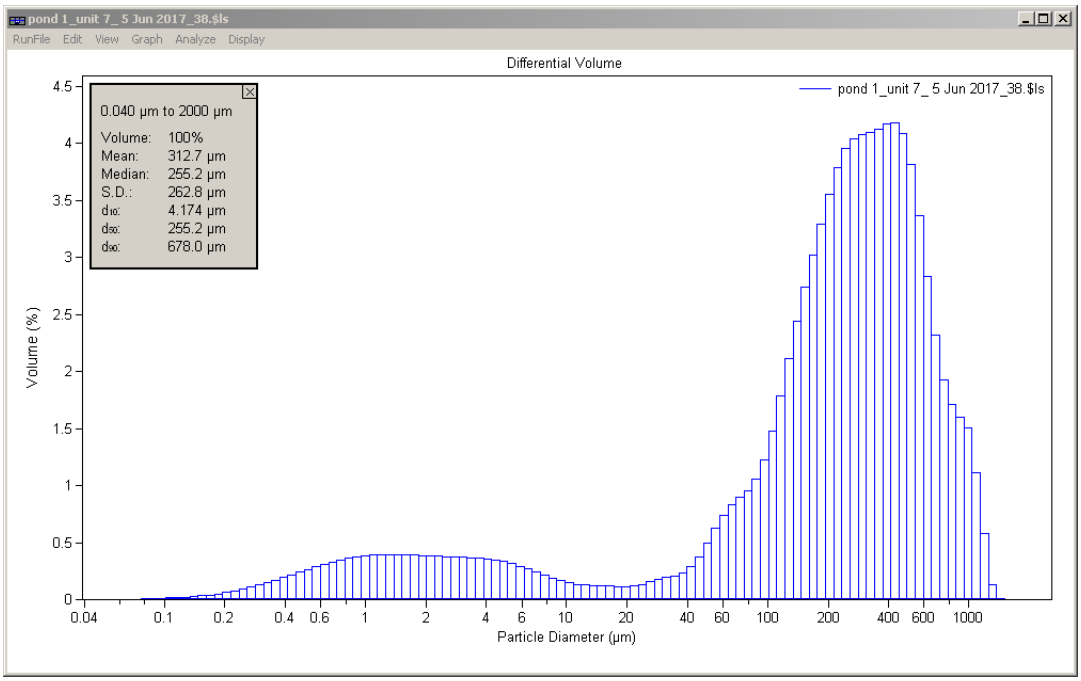

Volume Statistics (Arithmetic) pond 1_unit 7_ 5 Jun 2017_38.$ls

Save Close

Calculations from 0.040 µm to 2000 µm

Volume:	100%		
Mean:	312.7 µm	S.D.:	262.8 µm
Median:	255.2 µm	Variance:	69040 µm^2
Mean/Median ratio:	1.225	C.V.:	84.0%
Mode:	429.2 µm	Skewness:	1.092 Right skewed
		Kurtosis:	0.982 Leptokurtic

Folk and Ward Statistics (Phi)

Mean:	2.34	Median:	1.97	Deviation:	2.27
Skewness:	0.48	Kurtosis:	2.03		

<10%	<25%	<50%	<75%	<90%
4.174 µm	119.4 µm	255.2 µm	449.7 µm	678.0 µm

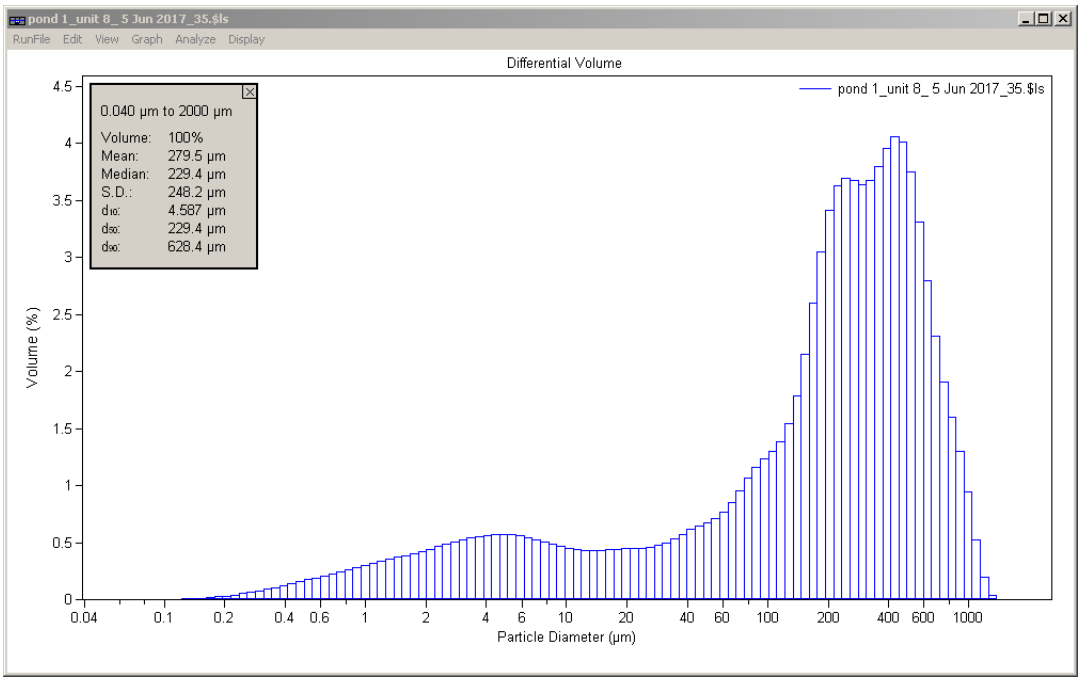

Volume Statistics (Arithmetic) pond 1_unit 8_ 5 Jun 2017_35.$ls

Save Close

Calculations from 0.040 µm to 2000 µm

Volume:	100%		
Mean:	279.5 µm	S.D.:	248.2 µm
Median:	229.4 µm	Variance:	61627 µm^2
Mean/Median ratio:	1.219	C.V.:	88.8%
Mode:	429.2 µm	Skewness:	0.980 Right skewed
		Kurtosis:	0.603 Leptokurtic

Folk and Ward Statistics (Phi)

Mean:	3.07	Median:	2.12	Deviation:	2.63
Skewness:	0.57	Kurtosis:	1.33		

<10%	<25%	<50%	<75%	<90%
4.587 µm	65.70 µm	229.4 µm	426.7 µm	628.4 µm

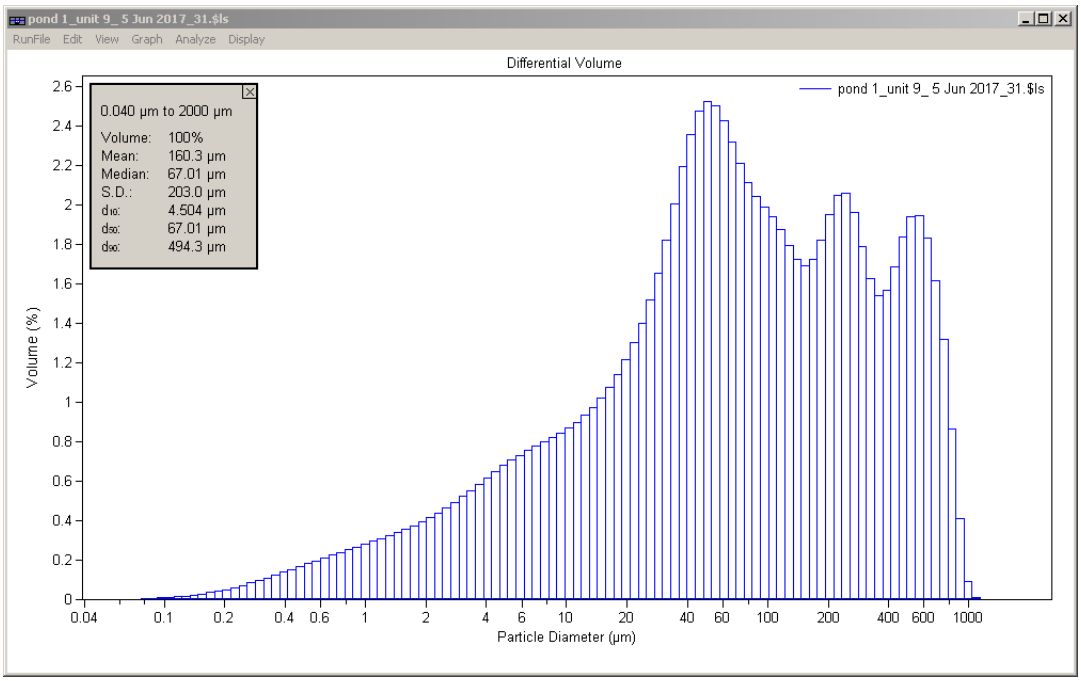

Volume Statistics (Arithmetic) pond 1_unit 9_ 5 Jun 2017_31.$ls

Save Close

Calculations from 0.040 µm to 2000 µm

Volume:	100%		
Mean:	160.3 µm	S.D.:	203.0 µm
Median:	67.01 µm	Variance:	41213 μm^2
Mean/Median ratio:	2.393	C.V.:	127%
Mode:	50.23 µm	Skewness:	1.659 Right skewed
		Kurtosis:	2.017 Leptokurtic

Folk and Ward Statistics (Phi)

Mean:	4.04	Median:	3.90	Deviation:	2.59
Skewness:	0.16	Kurtosis:	1.02		

<10%	<25%	<50%	<75%	<90%
4.504 µm	21.52 µm	67.01 µm	224.8 µm	494.3 µm

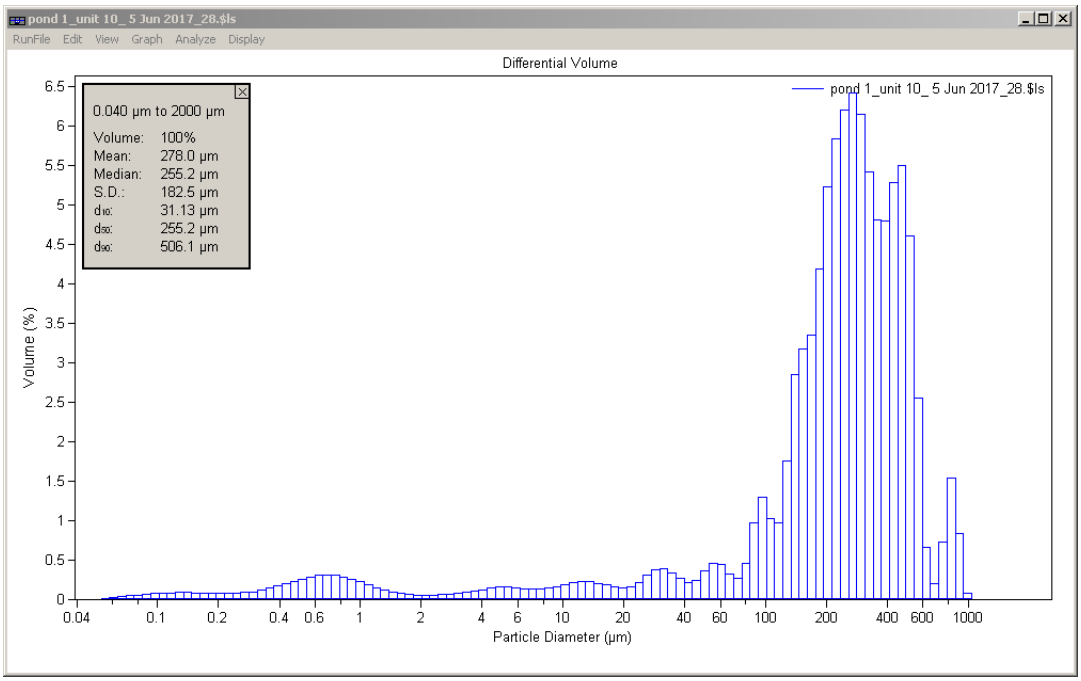

Volume Statistics (Arithmetic) pond 1_unit 10_ 5 Jun 2017_28.$ls

Save Close

Calculations from 0.040 µm to 2000 µm

Volume:	100%		
Mean:	278.0 µm	S.D.:	182.5 µm
Median:	255.2 µm	Variance:	33304 μm^2
Mean/Median ratio:	1.089	C.V.:	65.6%
Mode:	269.2 µm	Skewness:	0.821 Right skewed
		Kurtosis:	1.086 Leptokurtic

Folk and Ward Statistics (Phi)

Mean:	2.13	Median:	1.97	Deviation:	1.84
Skewness:	0.48	Kurtosis:	2.74		

<10%	<25%	<50%	<75%	<90%
31.13 µm	158.2 µm	255.2 µm	386.5 µm	506.1 µm

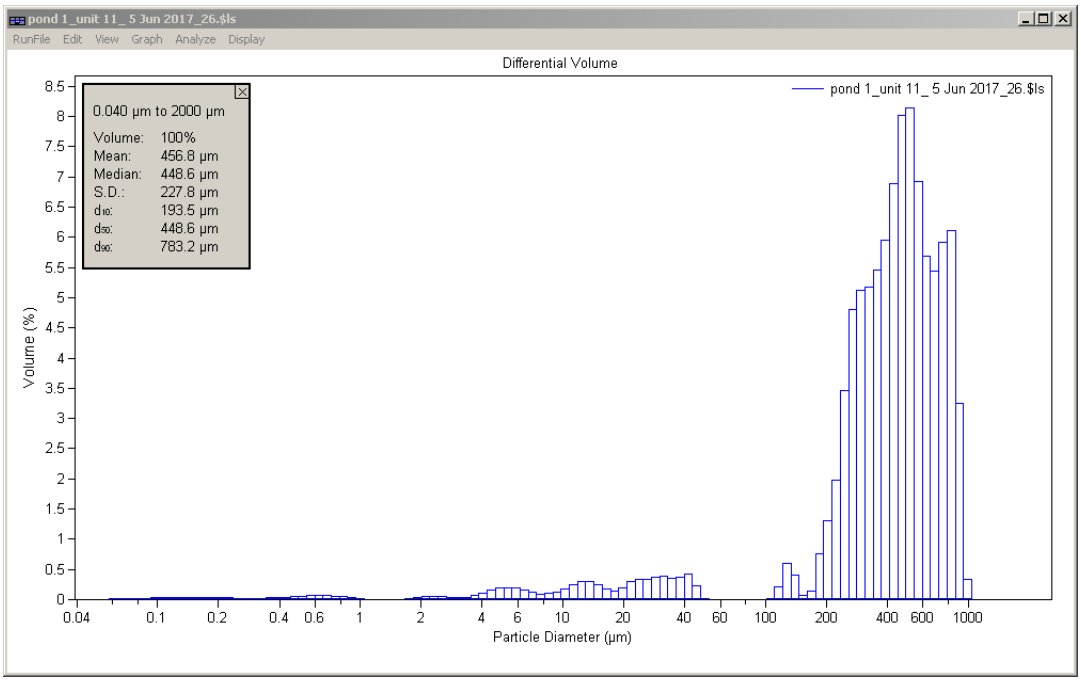

Volume Statistics (Arithmetic) pond 1_unit 11_ 5 Jun 2017_26.$ls

Save Close

Calculations from 0.040 µm to 2000 µm

Volume:	100%		
Mean:	456.8 µm	S.D.:	227.8 µm
Median:	448.6 µm	Variance:	51887 µm^2
Mean/Median ratio:	1.018	C.V.:	49.9%
Mode:	517.2 µm	Skewness:	0.016 Right skewed
		Kurtosis:	-0.479 Platykurtic

Folk and Ward Statistics (Phi)

Mean:	1.21	Median:	1.16	Deviation:	1.17
Skewness:	0.38	Kurtosis:	2.08		

<10%	<25%	<50%	<75%	<90%
193.5 µm	300.4 µm	448.6 µm	612.5 µm	783.2 µm

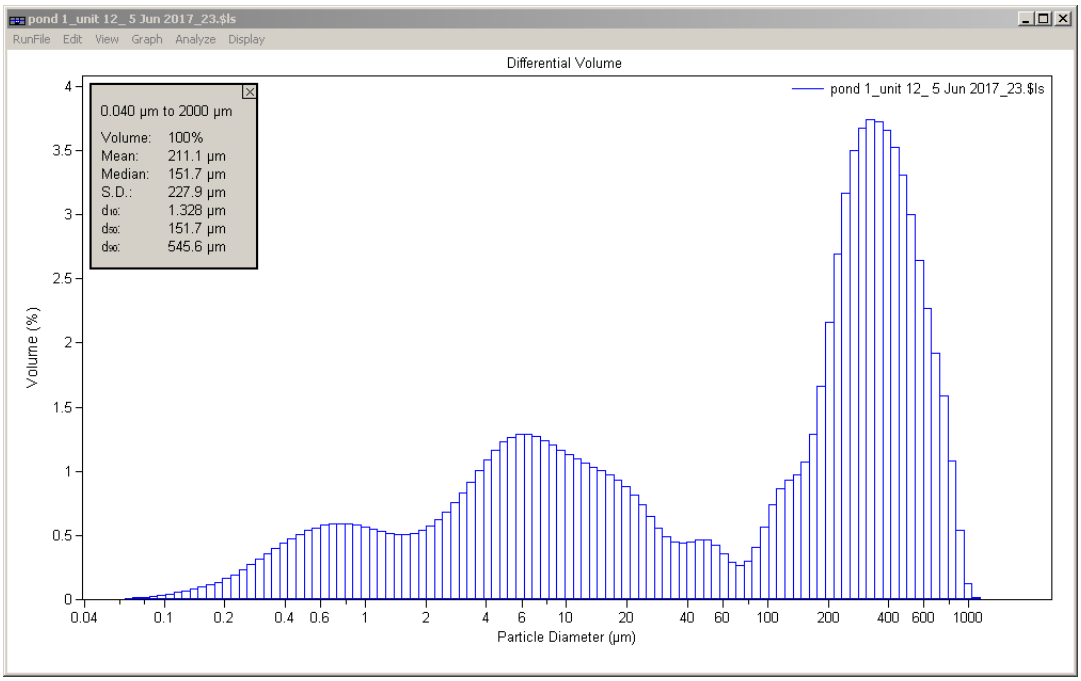

Volume Statistics (Arithmetic) pond 1_unit 12_ 5 Jun 2017_23.$ls

Save Close

Calculations from 0.040 µm to 2000 µm

Volume:	100%		
Mean:	211.1 µm	S.D.:	227.9 µm
Median:	151.7 µm	Variance:	51945 µm^2
Mean/Median ratio:	1.392	C.V.:	108%
Mode:	324.4 µm	Skewness:	0.917 Right skewed
		Kurtosis:	-0.015 Platykurtic

Folk and Ward Statistics (Phi)

Mean:	4.03	Median:	2.72	Deviation:	3.32
Skewness:	0.57	Kurtosis:	0.72		

<10%	<25%	<50%	<75%	<90%
1.328 µm	6.751 µm	151.7 µm	361.4 µm	545.6 µm

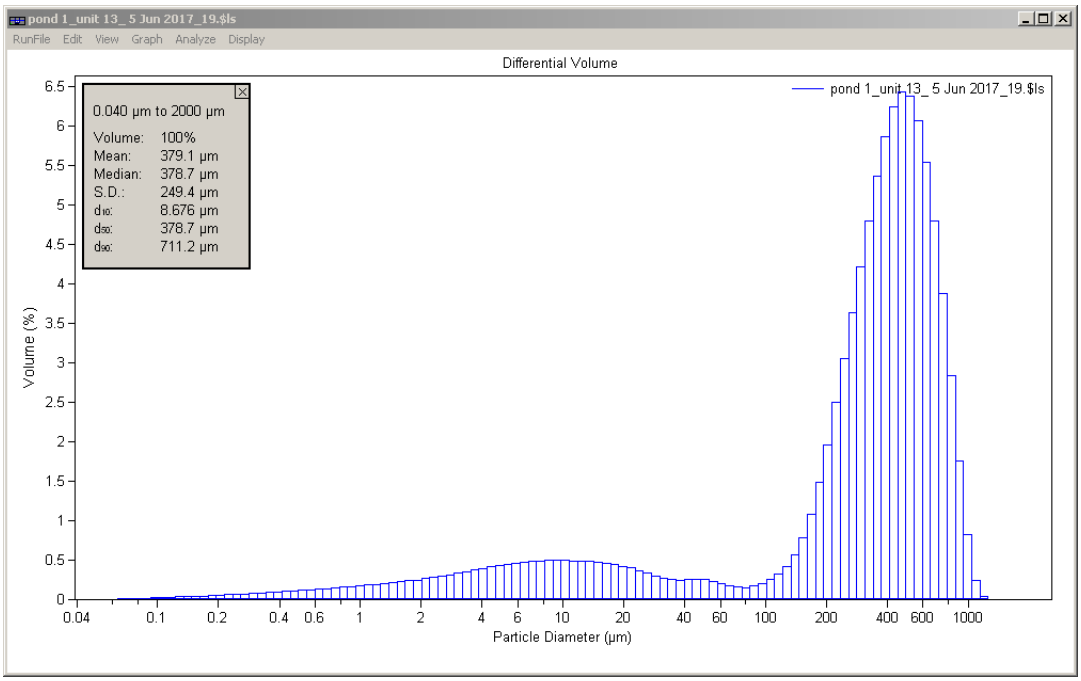

Volume Statistics (Arithmetic) pond 1_unit 13_ 5 Jun 2017_19.$ls

Save Close

Calculations from 0.040 µm to 2000 µm

Volume:	100%		
Mean:	379.1 µm	S.D.:	249.4 µm
Median:	378.7 µm	Variance:	62205 µm^2
Mean/Median ratio:	1.001	C.V.:	65.8%
Mode:	471.1 µm	Skewness:	0.187 Right skewed
		Kurtosis:	-0.569 Platykurtic

Folk and Ward Statistics (Phi)

Mean:	2.34	Median:	1.40	Deviation:	2.31
Skewness:	0.69	Kurtosis:	2.36		

<10%	<25%	<50%	<75%	<90%
8.676 µm	207.8 µm	378.7 µm	550.5 µm	711.2 µm

APPENDIX B: GRAIN SIZE ANALYSIS OF HQ-L SAMPLES (LIGNITE PIT)

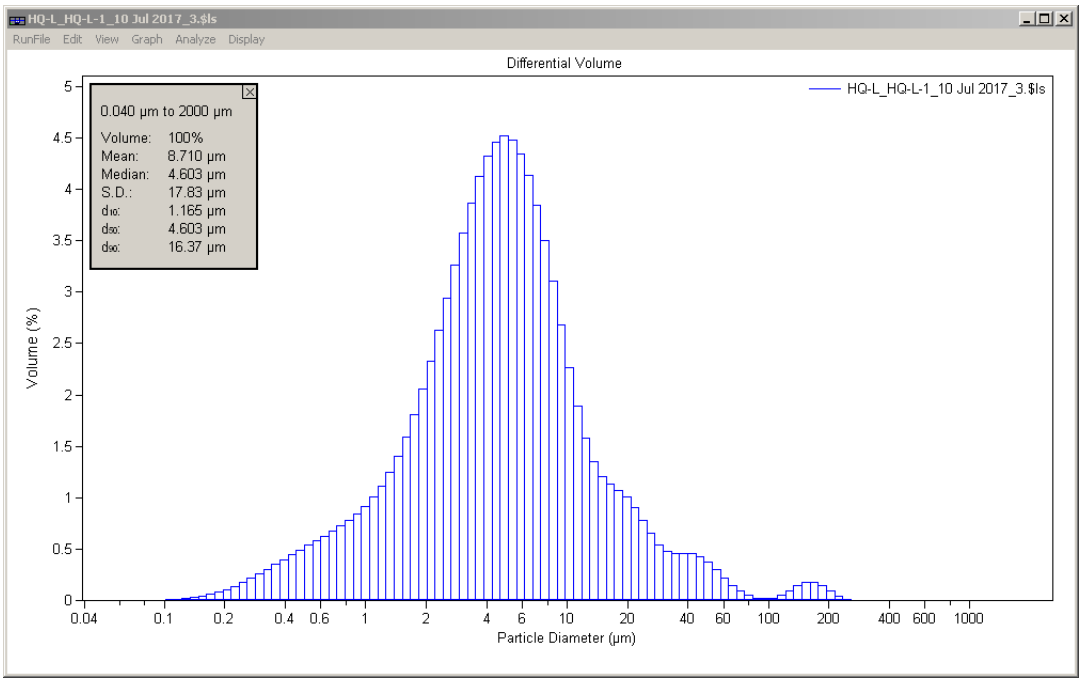

Volume Statistics (Arithmetic) HQ-L_HQ-L-1_10 Jul 2017_3.$ls

Save Close

Calculations from 0.040 µm to 2000 µm

Volume:	100%		
Mean:	8.710 µm	S.D.:	17.83 µm
Median:	4.603 µm	Variance:	317.7 µm^2
Mean/Median ratio:	1.892	C.V.:	205%
Mode:	4.878 µm	Skewness:	7.166 Right skewed
		Kurtosis:	62.64 Leptokurtic

Folk and Ward Statistics (Phi)

Mean:	7.81	Median:	7.76	Deviation:	1.48
Skewness:	0.05	Kurtosis:	1.30		

<10%	<25%	<50%	<75%	<90%
1.165 µm	2.503 µm	4.603 µm	8.068 µm	16.37 µm

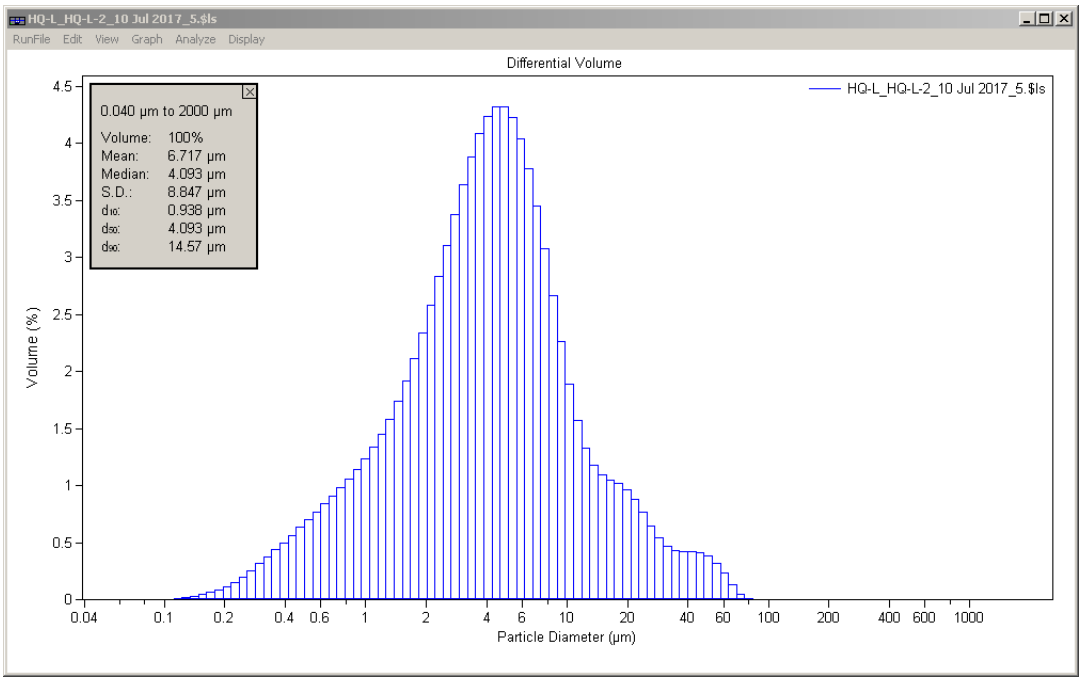
HQ-L_HQ-L-2_10 Jul 2017_5.$ls
RunFile Edit View Graph Analyze Display
Differential Volume
HQ-L_HQ-L-2_10 Jul 2017_5.$ls
0.040 µm to 2000 µm
Volume: 100%
Mean: 6.717 µm
Median: 4.093 µm
S.D.: 8.847 µm
d10: 0.938 µm
d50: 4.093 µm
d90: 14.57 µm
Volume (%)
Particle Diameter (µm)

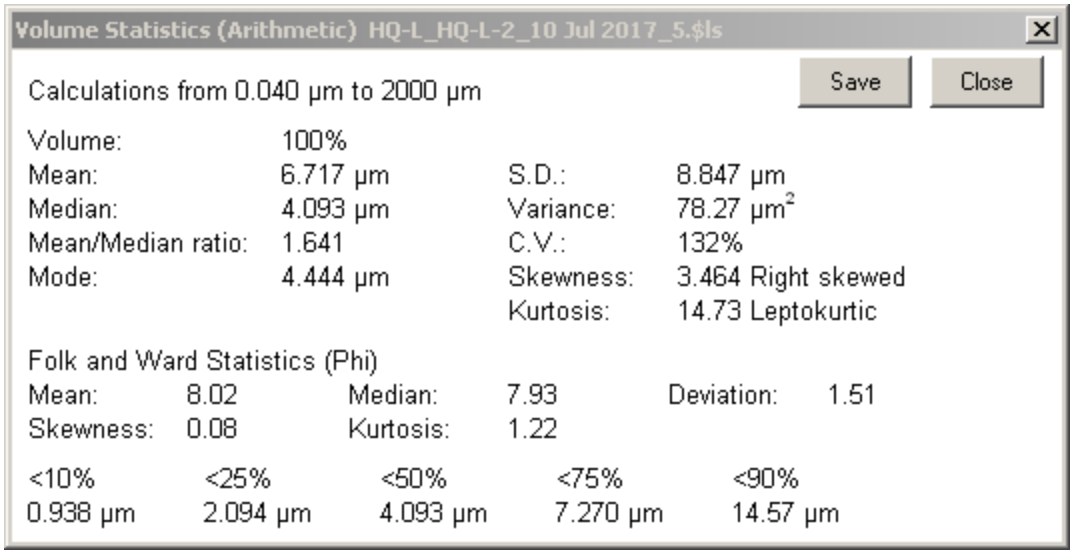
Volume Statistics (Arithmetic) HQ-L_HQ-L-2_10 Jul 2017_5.$ls
Save
Close
Calculations from 0.040 µm to 2000 µm
Volume: 100%
Mean: 6.717 µm
Median: 4.093 µm
Mean/Median ratio: 1.641
Mode: 4.444 µm
S.D.: 8.847 µm
Variance: 78.27 µm2
C.V.: 132%
Skewness: 3.464 Right skewed
Kurtosis: 14.73 Leptokurtic
Folk and Ward Statistics (Phi)
Mean: 8.02
Median: 7.93
Deviation: 1.51
Skewness: 0.08
Kurtosis: 1.22
<10% 0.938 µm
<25% 2.094 µm
<50% 4.093 µm
<75% 7.270 µm
<90% 14.57 µm

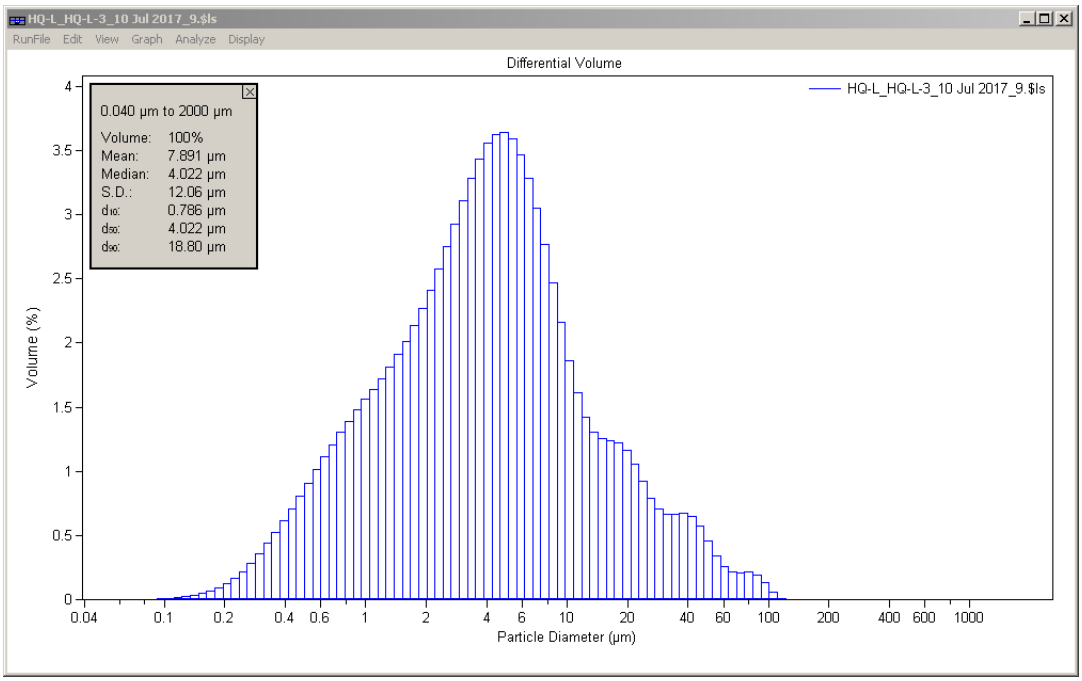

Volume Statistics (Arithmetic) HQ-L_HQ-L-3_10 Jul 2017_9.$ls

Save Close

Calculations from 0.040 µm to 2000 µm

Volume:	100%		
Mean:	7.891 µm	S.D.:	12.06 µm
Median:	4.022 µm	Variance:	145.5 µm^2
Mean/Median ratio:	1.962	C.V.:	153%
Mode:	4.878 µm	Skewness:	3.723 Right skewed
		Kurtosis:	17.59 Leptokurtic

Folk and Ward Statistics (Phi)

Mean:	8.03	Median:	7.96	Deviation:	1.75
Skewness:	0.03	Kurtosis:	1.11		

<10%	<25%	<50%	<75%	<90%
0.786 µm	1.774 µm	4.022 µm	8.019 µm	18.80 µm

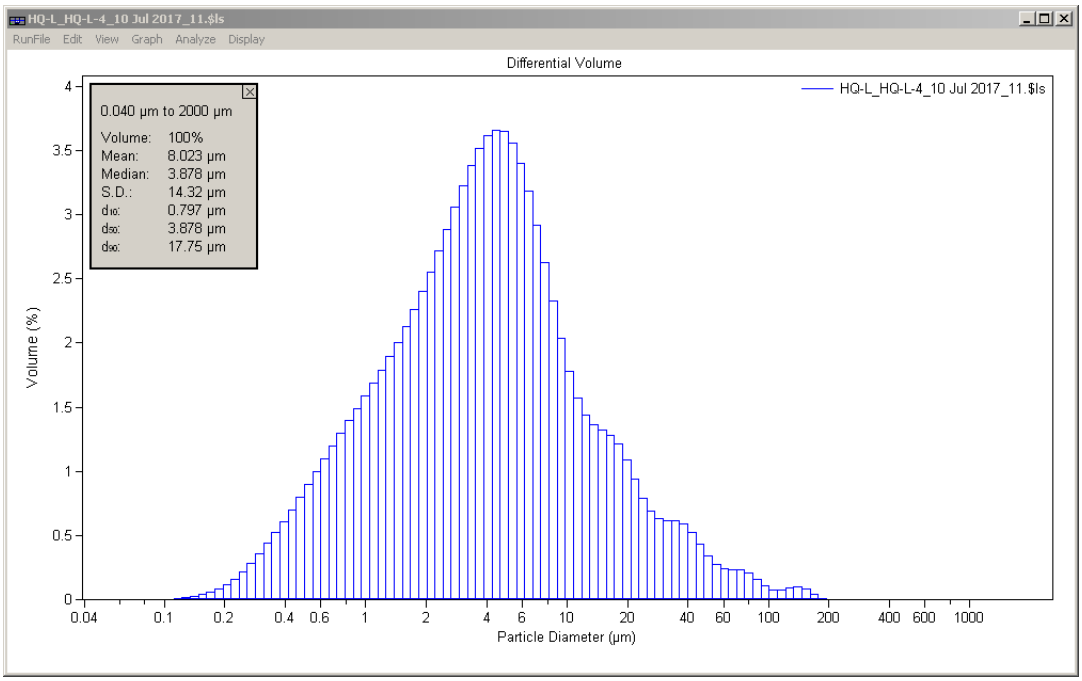

Volume Statistics (Arithmetic) HQ-L_HQ-L-4_10 Jul 2017_11.$ls

Save Close

Calculations from 0.040 µm to 2000 µm

Volume:	100%		
Mean:	8.023 µm	S.D.:	14.32 µm
Median:	3.878 µm	Variance:	205.1 µm^2
Mean/Median ratio:	2.069	C.V.:	178%
Mode:	4.444 µm	Skewness:	5.324 Right skewed
		Kurtosis:	38.74 Leptokurtic

Folk and Ward Statistics (Phi)

Mean:	8.07	Median:	8.01	Deviation:	1.72
Skewness:	0.02	Kurtosis:	1.12		

<10%	<25%	<50%	<75%	<90%
0.797 µm	1.751 µm	3.878 µm	7.741 µm	17.75 µm

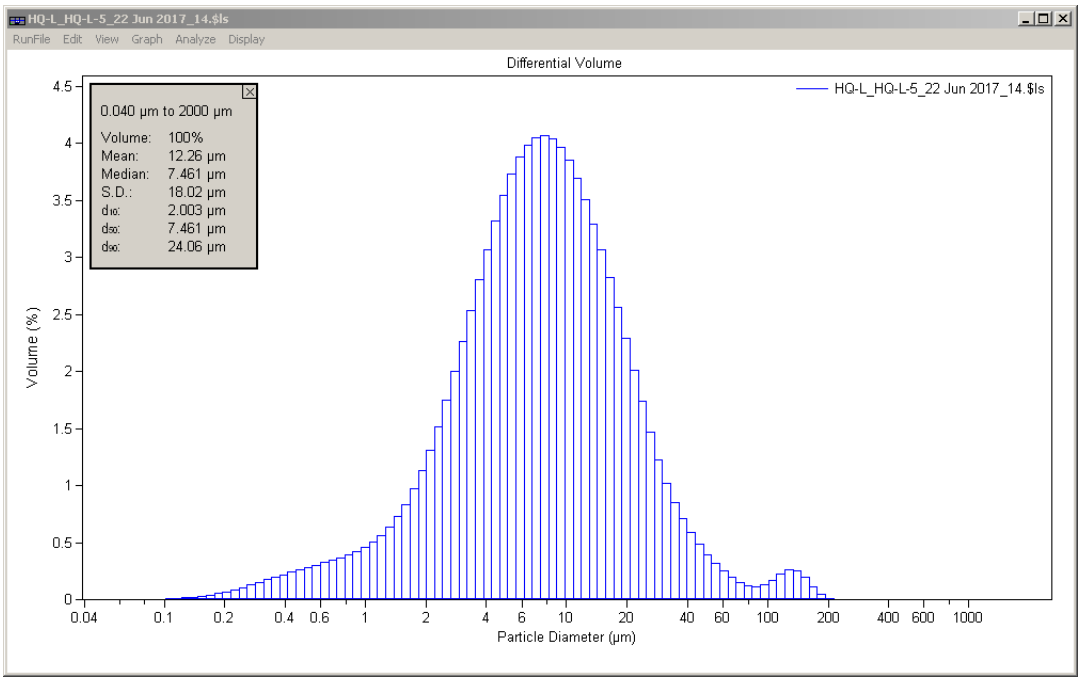

Volume Statistics (Arithmetic) HQ-L_HQ-L-5_22 Jun 2017_14.$ls

Save Close

Calculations from 0.040 µm to 2000 µm

Volume:	100%		
Mean:	12.26 µm	S.D.:	18.02 µm
Median:	7.461 µm	Variance:	324.8 µm^2
Mean/Median ratio:	1.644	C.V.:	147%
Mode:	7.776 µm	Skewness:	5.083 Right skewed
		Kurtosis:	32.87 Leptokurtic

Folk and Ward Statistics (Phi)

Mean:	7.10	Median:	7.07	Deviation:	1.43
Skewness:	0.07	Kurtosis:	1.14		

<10%	<25%	<50%	<75%	<90%
2.003 µm	3.959 µm	7.461 µm	13.79 µm	24.06 µm

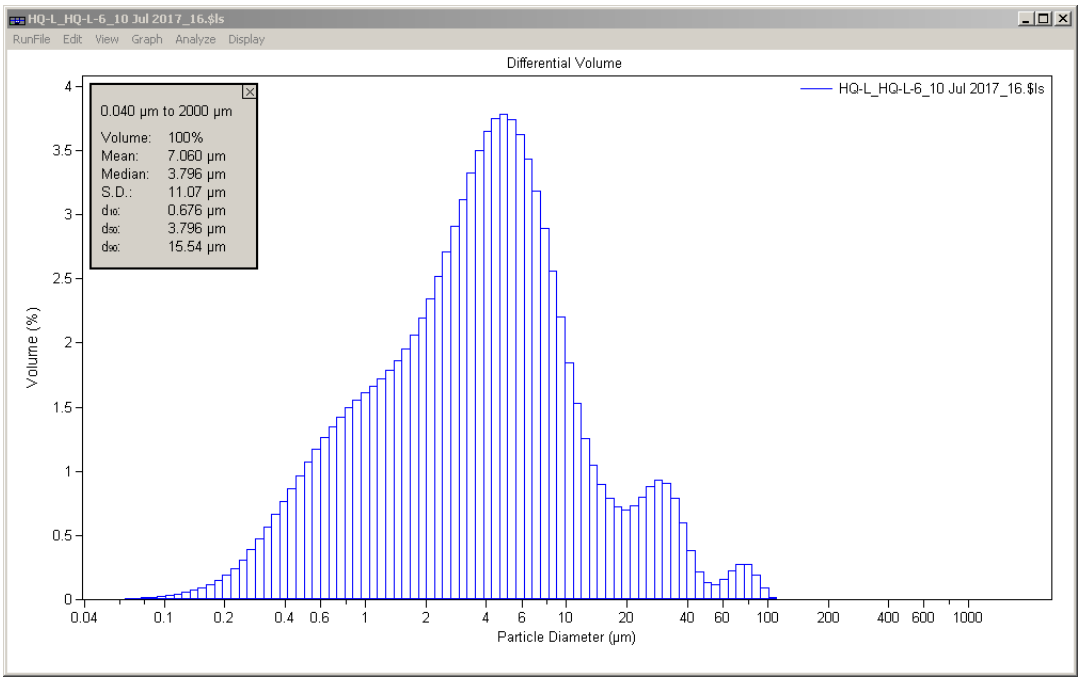

Volume Statistics (Arithmetic) HQ-L_HQ-L-6_10 Jul 2017_16.$ls

Save Close

Calculations from 0.040 µm to 2000 µm

Volume:	100%		
Mean:	7.060 µm	S.D.:	11.07 µm
Median:	3.796 µm	Variance:	122.5 µm^2
Mean/Median ratio:	1.860	C.V.:	157%
Mode:	4.878 µm	Skewness:	4.119 Right skewed
		Kurtosis:	21.65 Leptokurtic

Folk and Ward Statistics (Phi)

Mean:	8.22	Median:	8.04	Deviation:	1.74
Skewness:	0.10	Kurtosis:	1.12		

<10%	<25%	<50%	<75%	<90%
0.676 µm	1.592 µm	3.796 µm	7.248 µm	15.54 µm

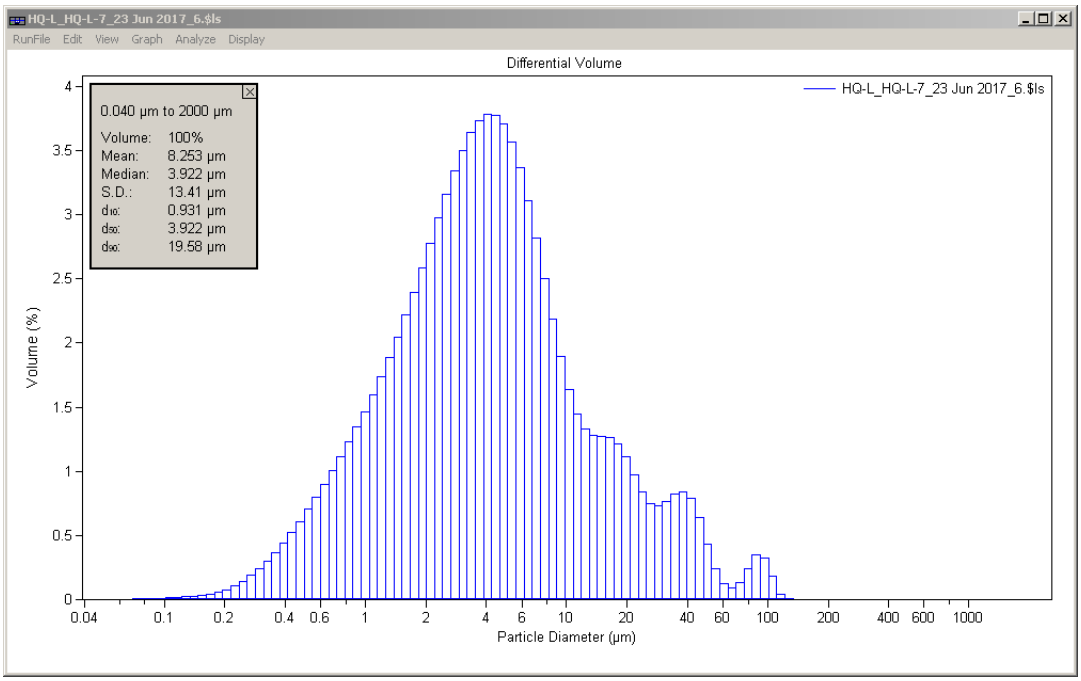

Volume Statistics (Arithmetic) HQ-L_HQ-L-7_23 Jun 2017_6.$ls

Save Close

Calculations from 0.040 µm to 2000 µm

Volume:	100%		
Mean:	8.253 µm	S.D.:	13.41 µm
Median:	3.922 µm	Variance:	179.7 µm^2
Mean/Median ratio:	2.105	C.V.:	162%
Mode:	4.048 µm	Skewness:	4.017 Right skewed
		Kurtosis:	20.08 Leptokurtic

Folk and Ward Statistics (Phi)

Mean:	7.96	Median:	7.99	Deviation:	1.69
Skewness:	-0.05	Kurtosis:	1.17		

<10%	<25%	<50%	<75%	<90%
0.931 µm	1.922 µm	3.922 µm	7.846 µm	19.58 µm

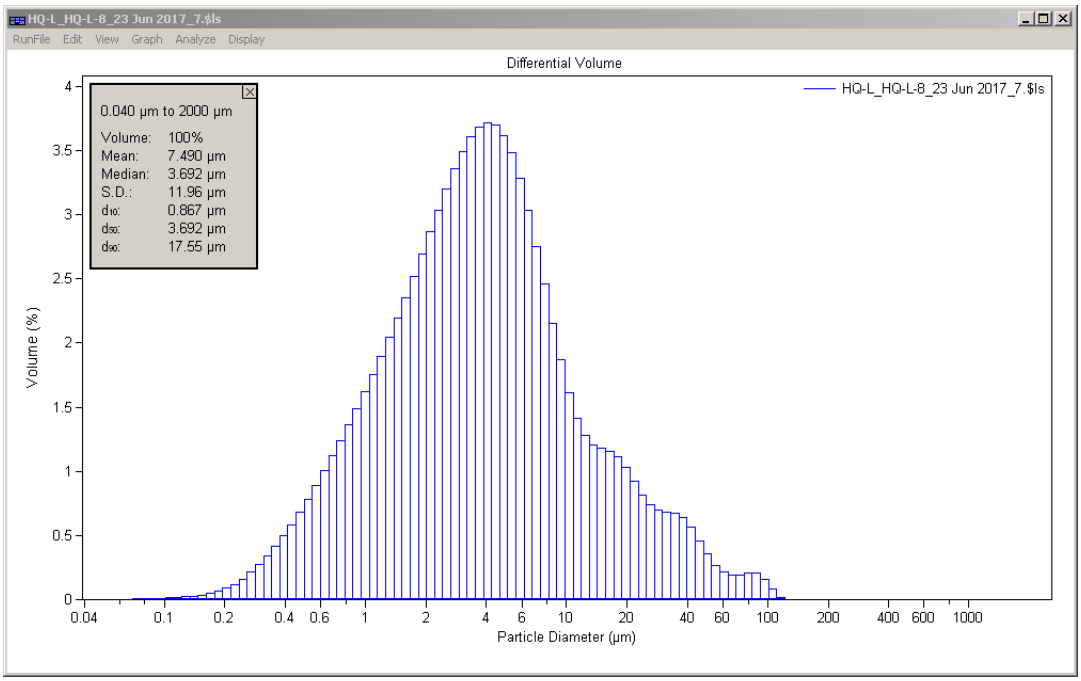
HQ-L_HQ-L-8_23 Jun 2017_7.$ls
RunFile Edit View Graph Analyze Display
Differential Volume
HQ-L_HQ-L-8_23 Jun 2017_7.$ls
0.040 µm to 2000 µm
Volume: 100%
Mean: 7.490 µm
Median: 3.692 µm
S.D.: 11.96 µm
d10: 0.867 µm
d50: 3.692 µm
d90: 17.55 µm
Volume (%)
Particle Diameter (µm)

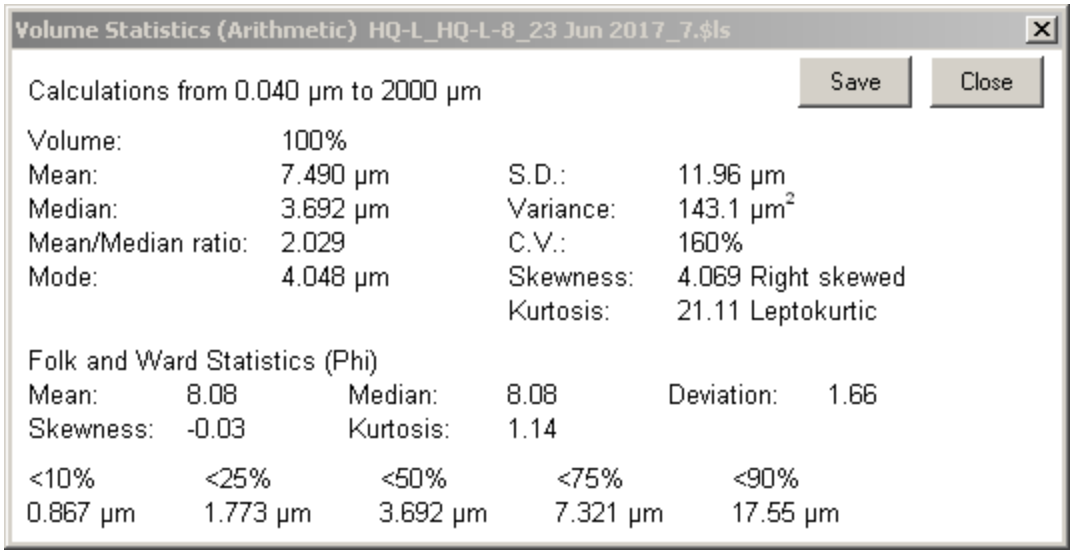
Volume Statistics (Arithmetic) HQ-L_HQ-L-8_23 Jun 2017_7.$ls
Save
Close
Calculations from 0.040 µm to 2000 µm
Volume: 100%
Mean: 7.490 µm
Median: 3.692 µm
Mean/Median ratio: 2.029
Mode: 4.048 µm
S.D.: 11.96 µm
Variance: 143.1 µm²
C.V.: 160%
Skewness: 4.069 Right skewed
Kurtosis: 21.11 Leptokurtic
Folk and Ward Statistics (Phi)
Mean: 8.08
Median: 8.08
Deviation: 1.66
Skewness: -0.03
Kurtosis: 1.14
<10% 0.867 µm
<25% 1.773 µm
<50% 3.692 µm
<75% 7.321 µm
<90% 17.55 µm

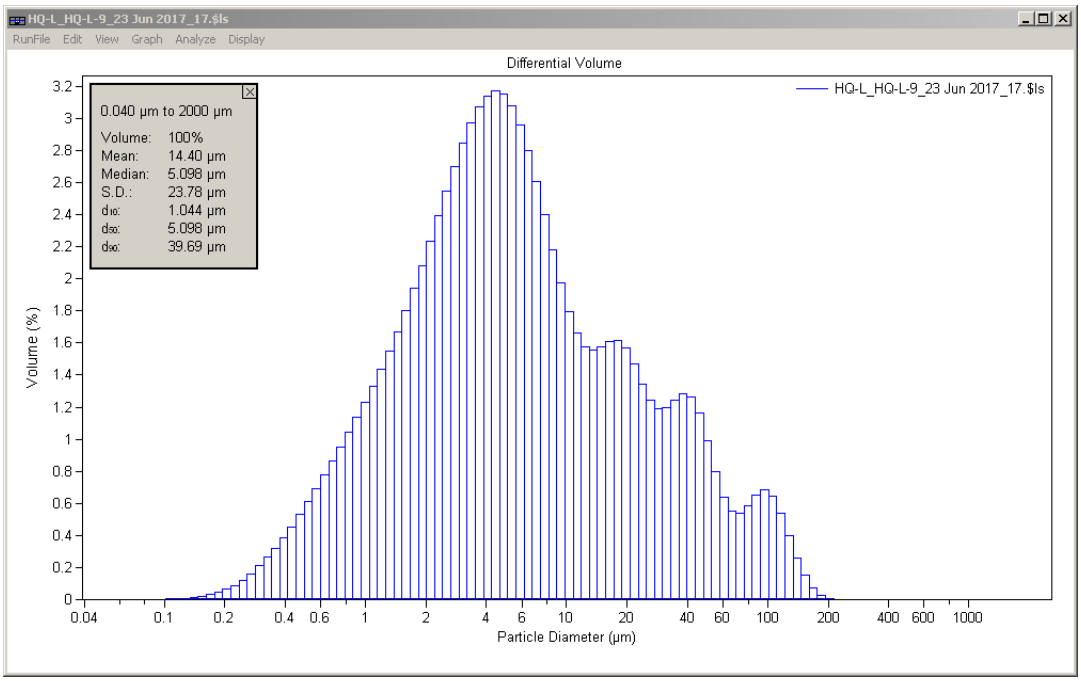

Volume Statistics (Arithmetic) HQ-L_HQ-L-9_23 Jun 2017_17.$ls

Save Close

Calculations from 0.040 µm to 2000 µm

Volume:	100%		
Mean:	14.40 µm	S.D.:	23.78 µm
Median:	5.098 µm	Variance:	565.7 µm^2
Mean/Median ratio:	2.825	C.V.:	165%
Mode:	4.444 µm	Skewness:	3.102 Right skewed
		Kurtosis:	10.93 Leptokurtic

Folk and Ward Statistics (Phi)

Mean:	7.43	Median:	7.62	Deviation:	2.01
Skewness:	-0.12	Kurtosis:	1.01		

<10%	<25%	<50%	<75%	<90%
1.044 µm	2.289 µm	5.098 µm	14.54 µm	39.69 µm

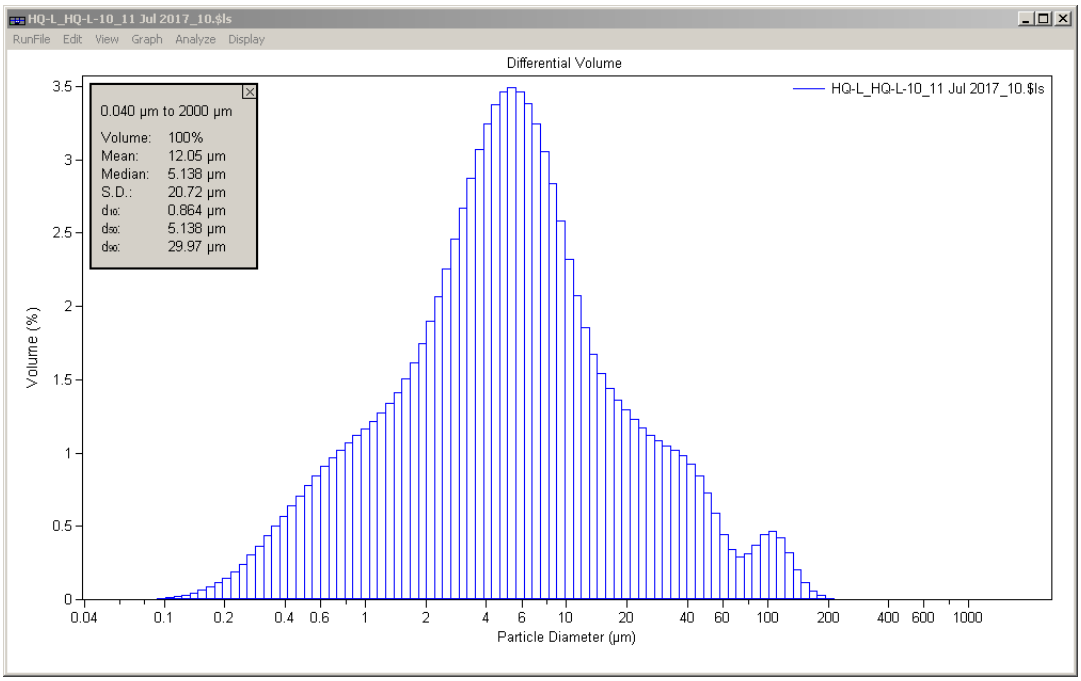

Volume Statistics (Arithmetic) HQ-L_HQ-L-10_11 Jul 2017_10.$ls

Save Close

Calculations from 0.040 µm to 2000 µm

Volume:	100%		
Mean:	12.05 µm	S.D.:	20.72 µm
Median:	5.138 µm	Variance:	429.3 µm^2
Mean/Median ratio:	2.344	C.V.:	172%
Mode:	5.355 µm	Skewness:	3.809 Right skewed
		Kurtosis:	17.35 Leptokurtic

Folk and Ward Statistics (Phi)

Mean:	7.62	Median:	7.60	Deviation:	1.93
Skewness:	0.01	Kurtosis:	1.16		

<10%	<25%	<50%	<75%	<90%
0.864 µm	2.277 µm	5.138 µm	11.19 µm	29.97 µm

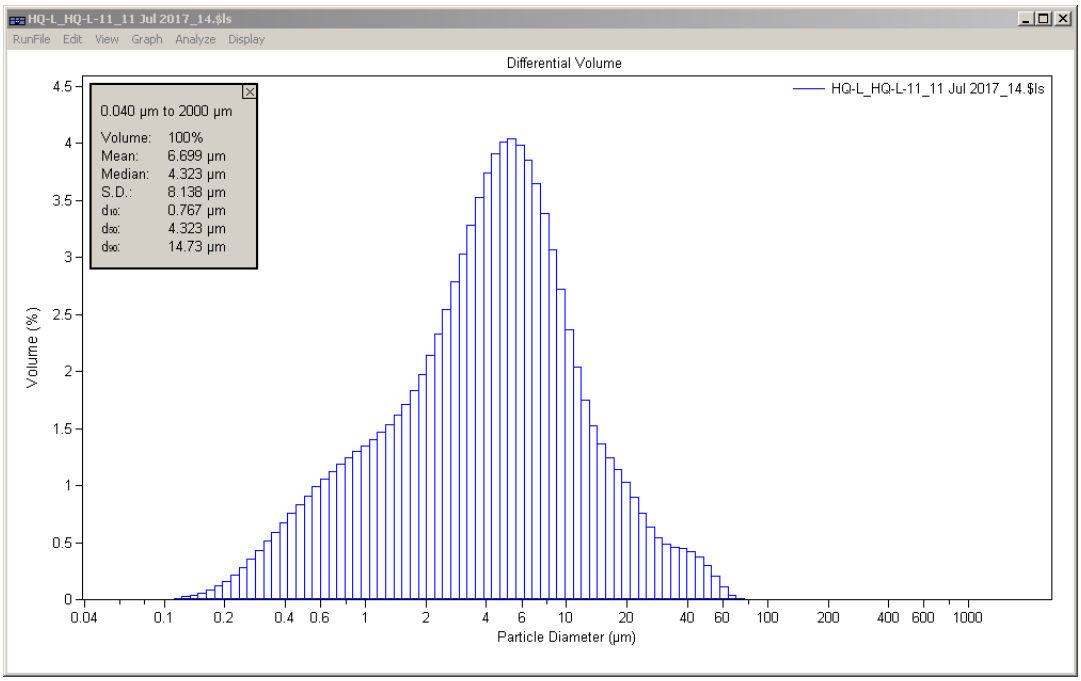

Volume Statistics (Arithmetic) HQ-L_HQ-L-11_11 Jul 2017_14.$ls

Save Close

Calculations from 0.040 µm to 2000 µm

Volume:	100%		
Mean:	6.699 µm	S.D.:	8.138 µm
Median:	4.323 µm	Variance:	66.22 µm^2
Mean/Median ratio:	1.550	C.V.:	121%
Mode:	5.355 µm	Skewness:	3.077 Right skewed
		Kurtosis:	12.12 Leptokurtic

Folk and Ward Statistics (Phi)

Mean:	8.05	Median:	7.85	Deviation:	1.63
Skewness:	0.16	Kurtosis:	1.11		

<10%	<25%	<50%	<75%	<90%
0.767 µm	1.935 µm	4.323 µm	7.919 µm	14.73 µm

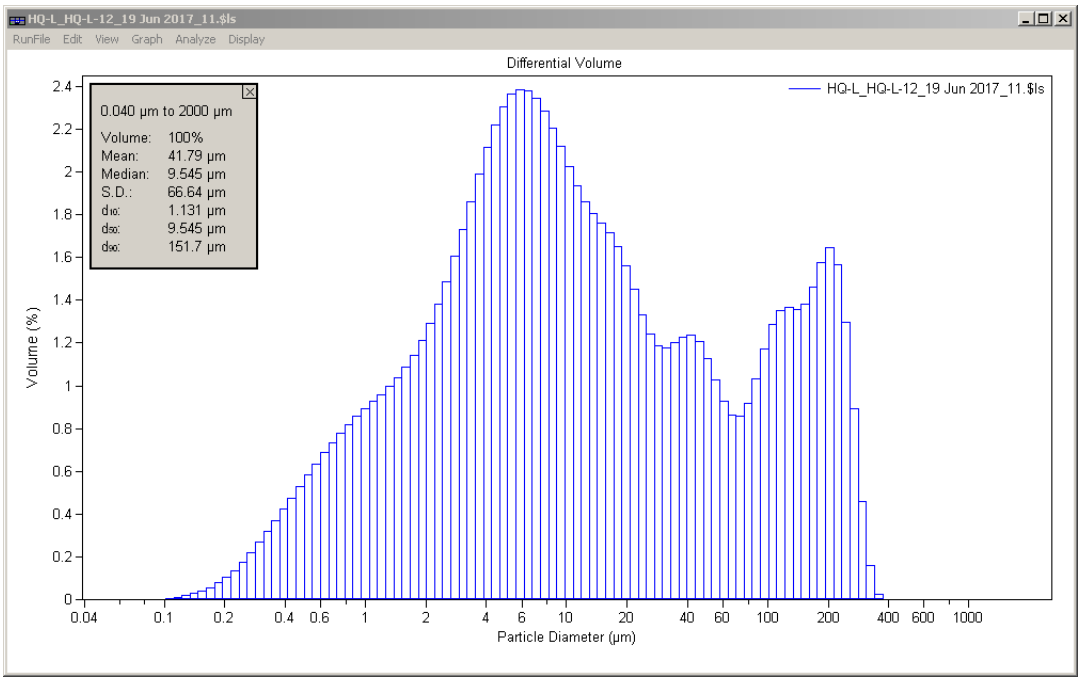

Volume Statistics (Arithmetic) HQ-L_HQ-L-12_19 Jun 2017_11.$ls

Save Close

Calculations from 0.040 µm to 2000 µm

Volume:	100%		
Mean:	41.79 µm	S.D.:	66.64 µm
Median:	9.545 µm	Variance:	4441 µm^2
Mean/Median ratio:	4.378	C.V.:	159%
Mode:	5.878 µm	Skewness:	2.016 Right skewed
		Kurtosis:	3.242 Leptokurtic

Folk and Ward Statistics (Phi)

Mean:	6.35	Median:	6.71	Deviation:	2.69
Skewness:	-0.13	Kurtosis:	0.92		

<10%	<25%	<50%	<75%	<90%
1.131 µm	3.358 µm	9.545 µm	43.56 µm	151.7 µm

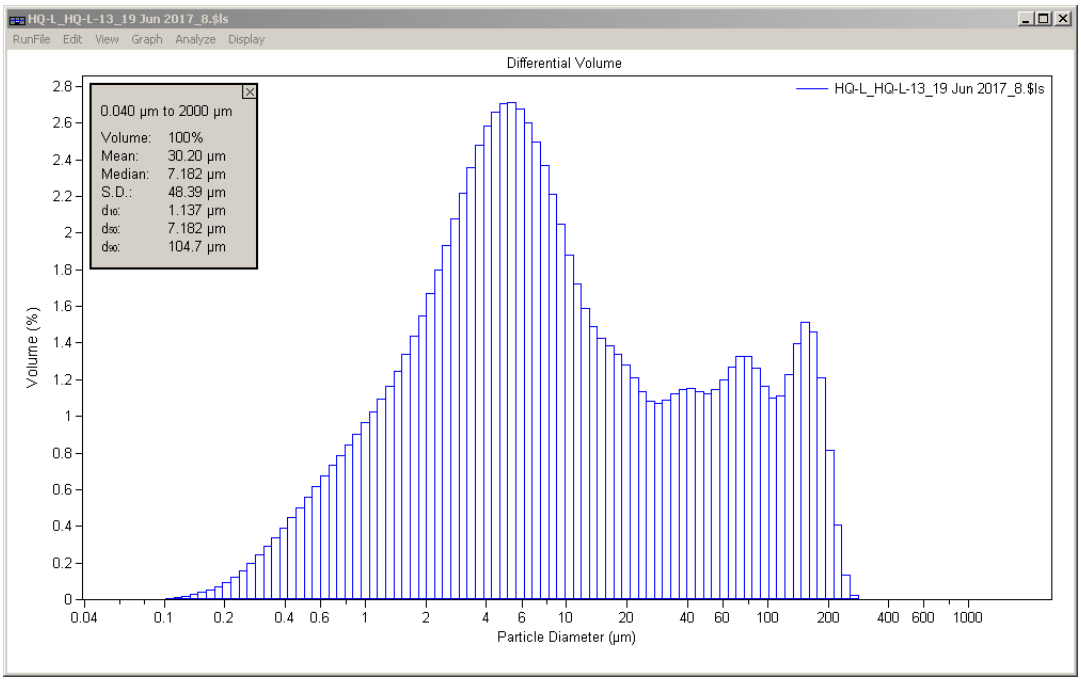
HQ-L_HQ-L-13_19 Jun 2017_8.$ls
RunFile Edit View Graph Analyze Display
Differential Volume
HQ-L_HQ-L-13_19 Jun 2017_8.$ls
0.040 µm to 2000 µm
Volume: 100%
Mean: 30.20 µm
Median: 7.182 µm
S.D.: 48.39 µm
d10: 1.137 µm
d50: 7.182 µm
d90: 104.7 µm
Volume (%)
Particle Diameter (µm)

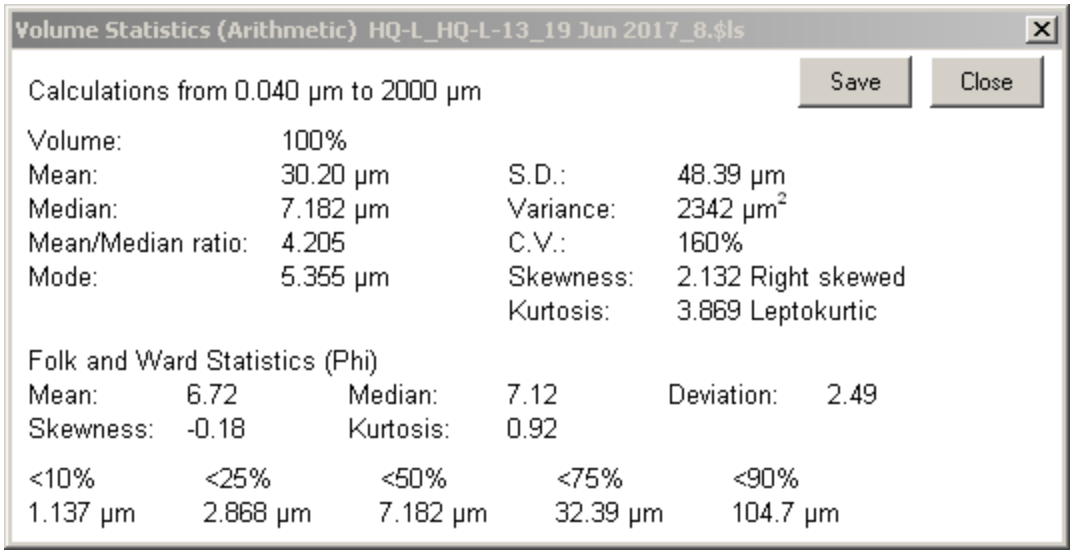
Volume Statistics (Arithmetic) HQ-L_HQ-L-13_19 Jun 2017_8.$ls
Save
Close
Calculations from 0.040 µm to 2000 µm
Volume: 100%
Mean: 30.20 µm
Median: 7.182 µm
Mean/Median ratio: 4.205
Mode: 5.355 µm
S.D.: 48.39 µm
Variance: 2342 µm²
C.V.: 160%
Skewness: 2.132 Right skewed
Kurtosis: 3.869 Leptokurtic
Folk and Ward Statistics (Phi)
Mean: 6.72
Median: 7.12
Deviation: 2.49
Skewness: -0.18
Kurtosis: 0.92
<10% 1.137 µm
<25% 2.868 µm
<50% 7.182 µm
<75% 32.39 µm
<90% 104.7 µm

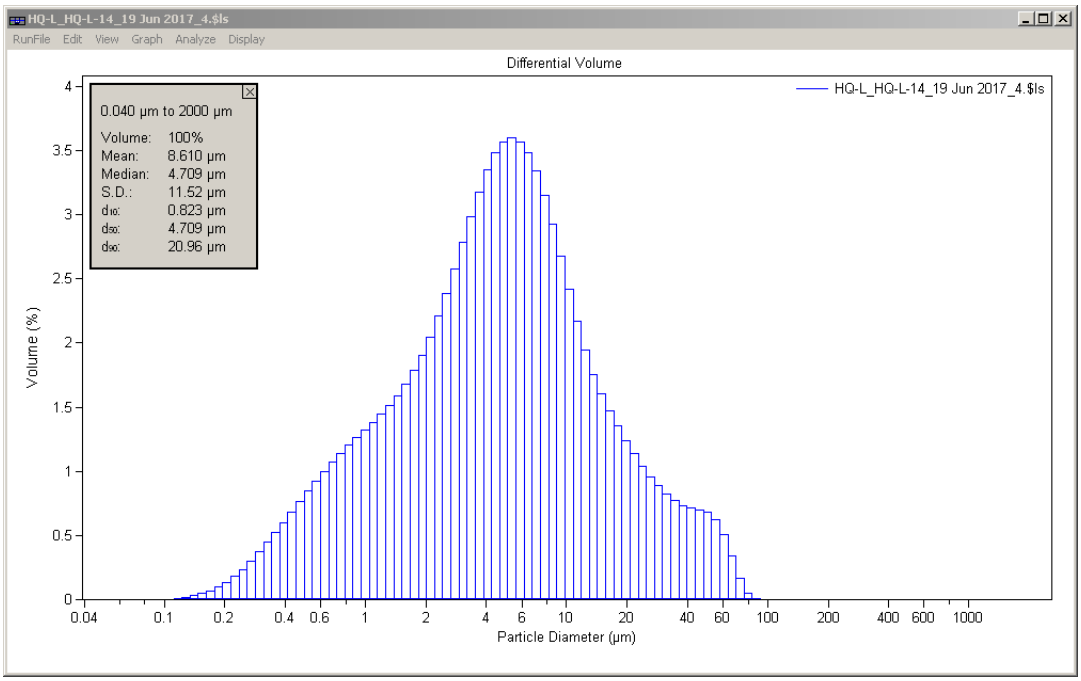

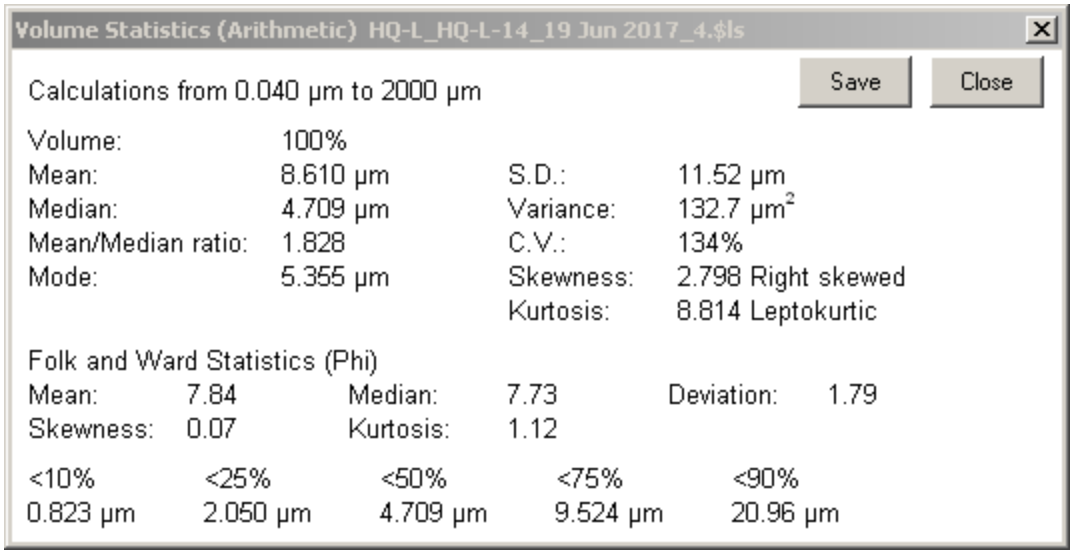

Volume Statistics (Arithmetic) HQ-L_HQ-L-14_19 Jun 2017_4.$ls

Save Close

Calculations from 0.040 µm to 2000 µm

Volume:	100%		
Mean:	8.610 µm	S.D.:	11.52 µm
Median:	4.709 µm	Variance:	132.7 µm^2
Mean/Median ratio:	1.828	C.V.:	134%
Mode:	5.355 µm	Skewness:	2.798 Right skewed
		Kurtosis:	8.814 Leptokurtic

Folk and Ward Statistics (Phi)

Mean:	7.84	Median:	7.73	Deviation:	1.79
Skewness:	0.07	Kurtosis:	1.12		

<10%	<25%	<50%	<75%	<90%
0.823 µm	2.050 µm	4.709 µm	9.524 µm	20.96 µm

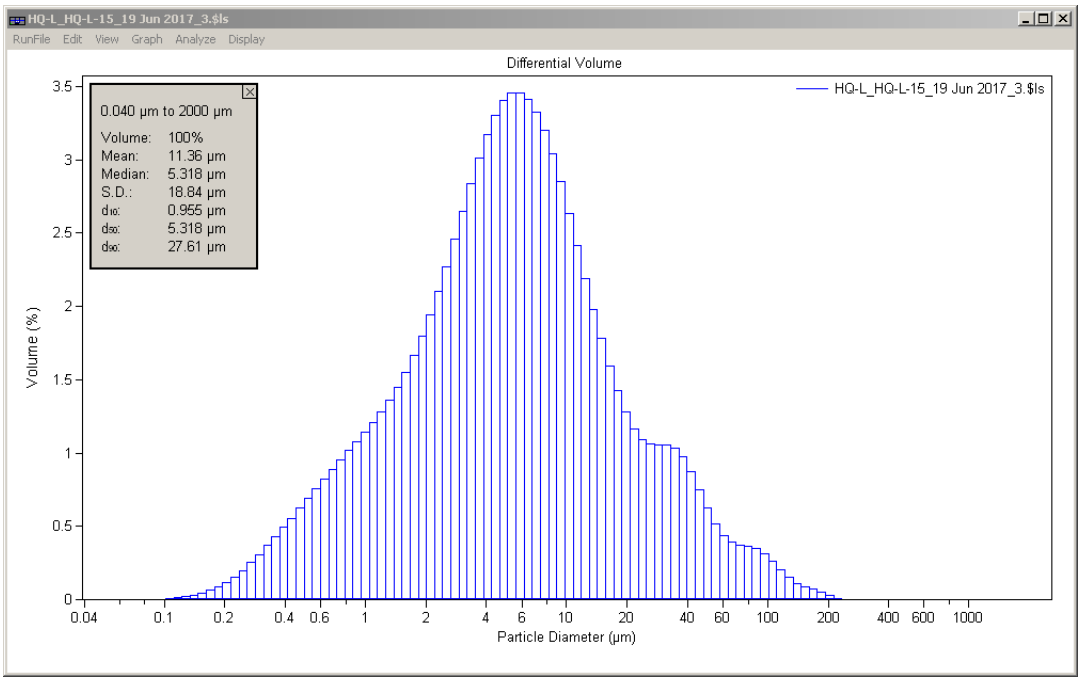

Volume Statistics (Arithmetic) HQ-L_HQ-L-15_19 Jun 2017_3.$ls

Save Close

Calculations from 0.040 µm to 2000 µm

Volume:	100%		
Mean:	11.36 µm	S.D.:	18.84 µm
Median:	5.318 µm	Variance:	354.8 µm^2
Mean/Median ratio:	2.135	C.V.:	166%
Mode:	5.878 µm	Skewness:	4.235 Right skewed
		Kurtosis:	23.97 Leptokurtic

Folk and Ward Statistics (Phi)

Mean:	7.60	Median:	7.55	Deviation:	1.83
Skewness:	0.03	Kurtosis:	1.14		

<10%	<25%	<50%	<75%	<90%
0.955 µm	2.375 µm	5.318 µm	11.24 µm	27.61 µm

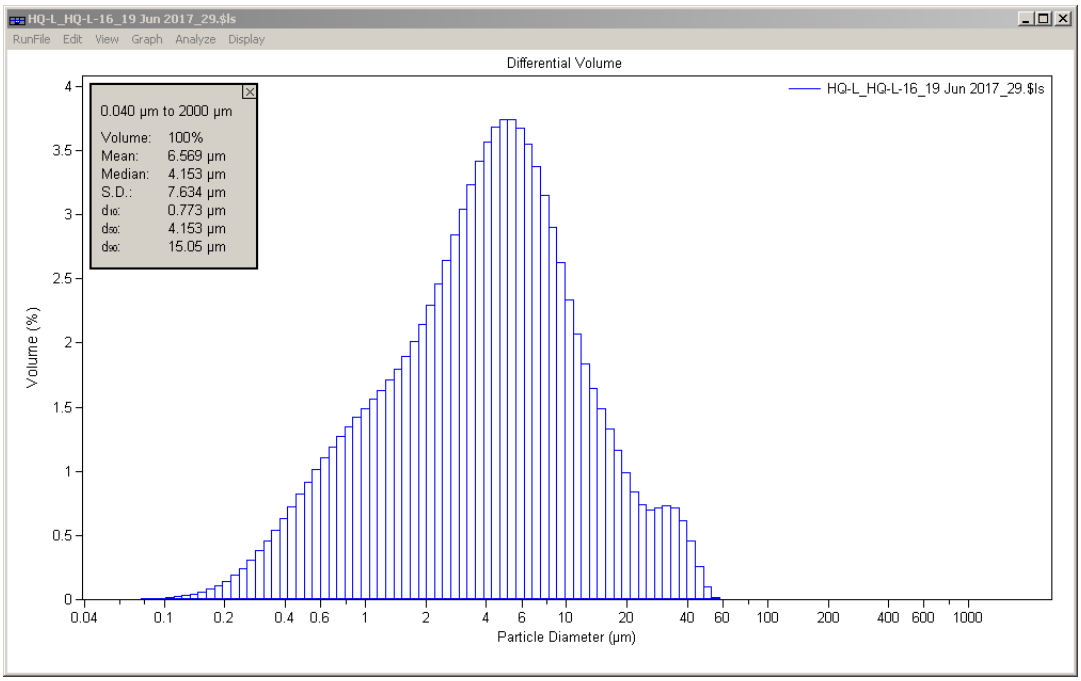

Volume Statistics (Arithmetic) HQ-L_HQ-L-16_19 Jun 2017_29.$ls

Save Close

Calculations from 0.040 µm to 2000 µm

Volume:	100%		
Mean:	6.569 µm	S.D.:	7.634 µm
Median:	4.153 µm	Variance:	58.28 µm^2
Mean/Median ratio:	1.582	C.V.:	116%
Mode:	4.878 µm	Skewness:	2.536 Right skewed
		Kurtosis:	7.520 Leptokurtic

Folk and Ward Statistics (Phi)

Mean:	8.07	Median:	7.91	Deviation:	1.65
Skewness:	0.12	Kurtosis:	1.06		

<10%	<25%	<50%	<75%	<90%
0.773 µm	1.816 µm	4.153 µm	7.977 µm	15.05 µm

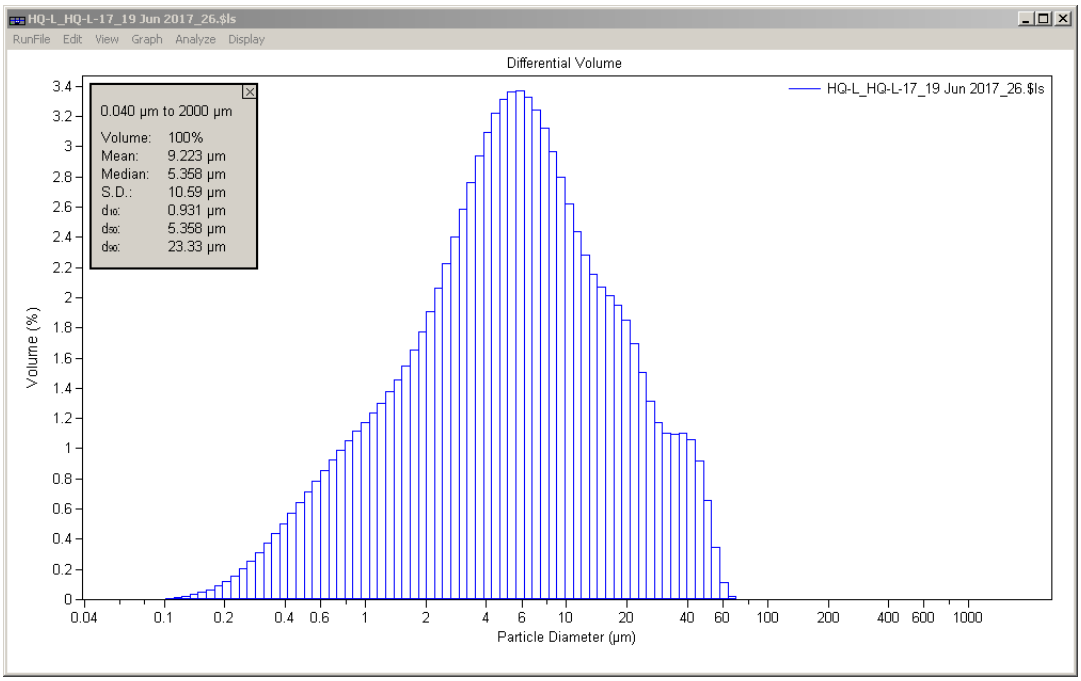
HQ-L_HQ-L-17_19 Jun 2017_26.$ls
RunFile Edit View Graph Analyze Display
Differential Volume
HQ-L_HQ-L-17_19 Jun 2017_26.$ls
0.040 µm to 2000 µm
Volume: 100%
Mean: 9.223 µm
Median: 5.358 µm
S.D.: 10.59 µm
d10: 0.931 µm
d50: 5.358 µm
d90: 23.33 µm
Volume (%)
Particle Diameter (µm)

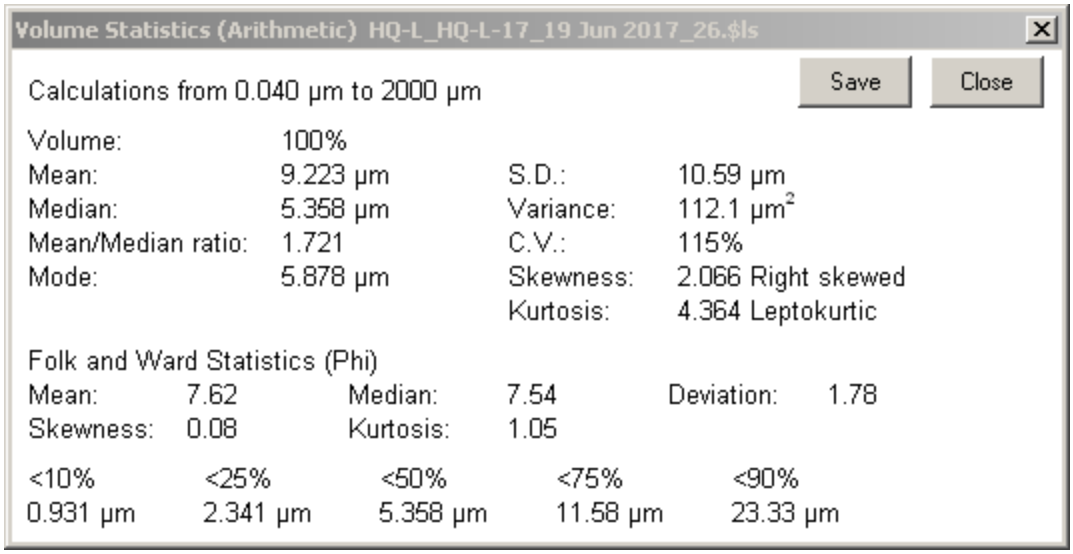
Volume Statistics (Arithmetic) HQ-L_HQ-L-17_19 Jun 2017_26.$ls
Save
Close
Calculations from 0.040 µm to 2000 µm
Volume: 100%
Mean: 9.223 µm
Median: 5.358 µm
Mean/Median ratio: 1.721
Mode: 5.878 µm
S.D.: 10.59 µm
Variance: 112.1 µm²
C.V.: 115%
Skewness: 2.066 Right skewed
Kurtosis: 4.364 Leptokurtic
Folk and Ward Statistics (Phi)
Mean: 7.62
Median: 7.54
Deviation: 1.78
Skewness: 0.08
Kurtosis: 1.05
<10% 0.931 µm
<25% 2.341 µm
<50% 5.358 µm
<75% 11.58 µm
<90% 23.33 µm

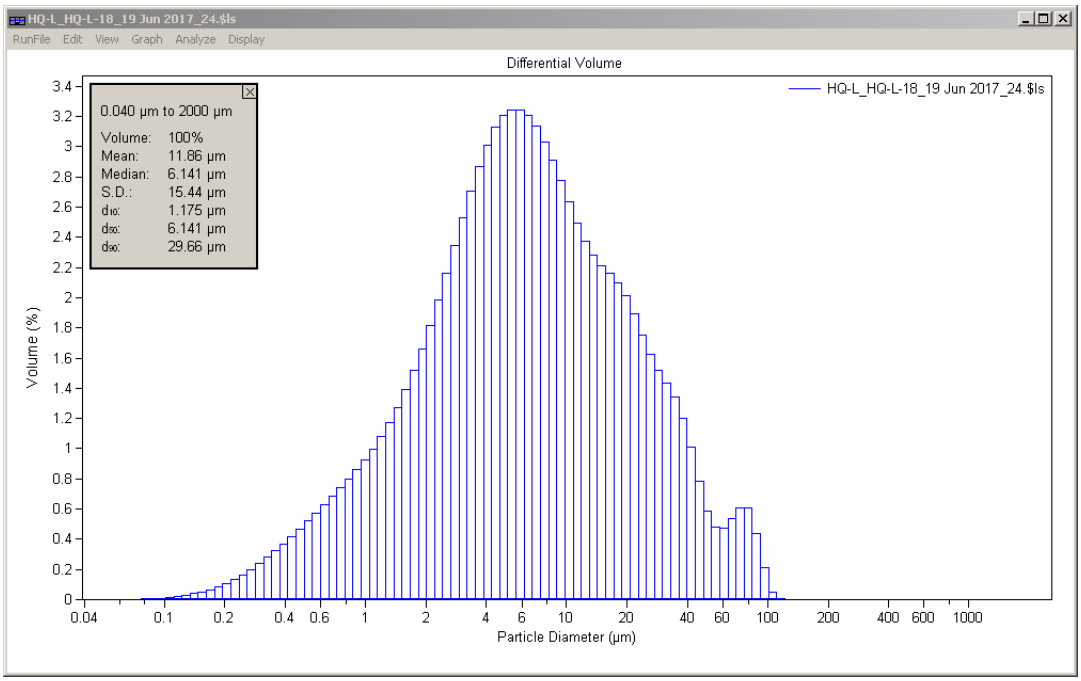

Volume Statistics (Arithmetic) HQ-L_HQ-L-18_19 Jun 2017_24.$ls

Save Close

Calculations from 0.040 µm to 2000 µm

Volume:	100%		
Mean:	11.86 µm	S.D.:	15.44 µm
Median:	6.141 µm	Variance:	238.5 µm^2
Mean/Median ratio:	1.932	C.V.:	130%
Mode:	5.355 µm	Skewness:	2.692 Right skewed
		Kurtosis:	8.461 Leptokurtic

Folk and Ward Statistics (Phi)

Mean:	7.34	Median:	7.35	Deviation:	1.79
Skewness:	0.03	Kurtosis:	1.04		

<10%	<25%	<50%	<75%	<90%
1.175 µm	2.791 µm	6.141 µm	14.29 µm	29.66 µm

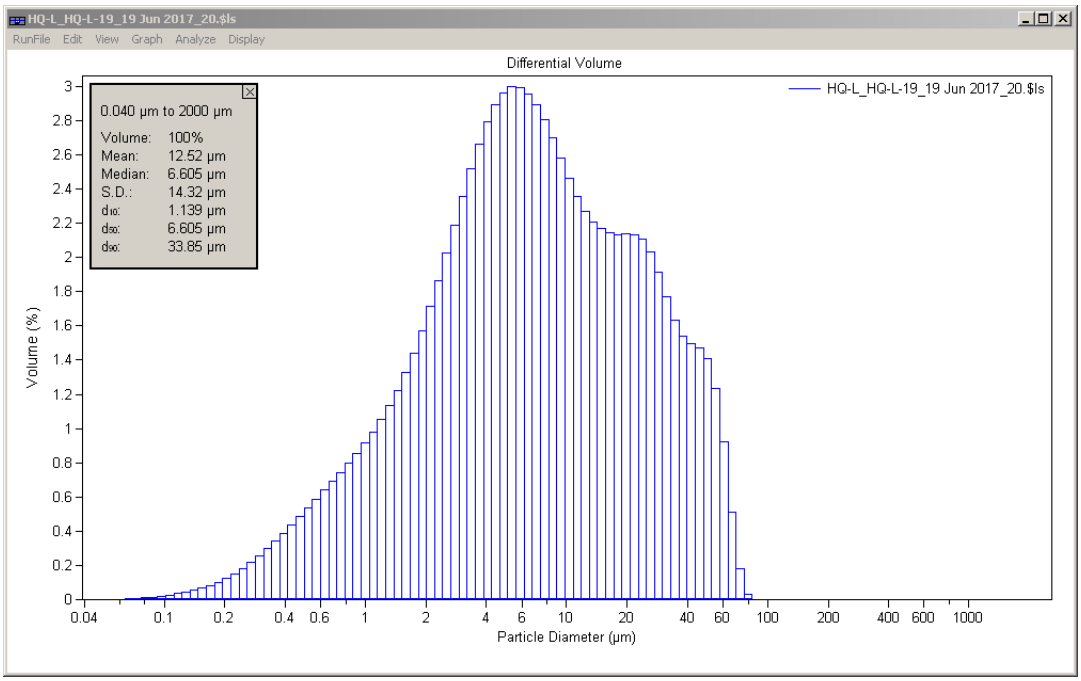
HQ-L_HQ-L-19_19 Jun 2017_20.$ls
RunFile Edit View Graph Analyze Display
Differential Volume
HQ-L_HQ-L-19_19 Jun 2017_20.$ls
0.040 µm to 2000 µm
Volume: 100%
Mean: 12.52 µm
Median: 6.605 µm
S.D.: 14.32 µm
d10: 1.139 µm
d50: 6.605 µm
d90: 33.85 µm
Volume (%)
Particle Diameter (µm)

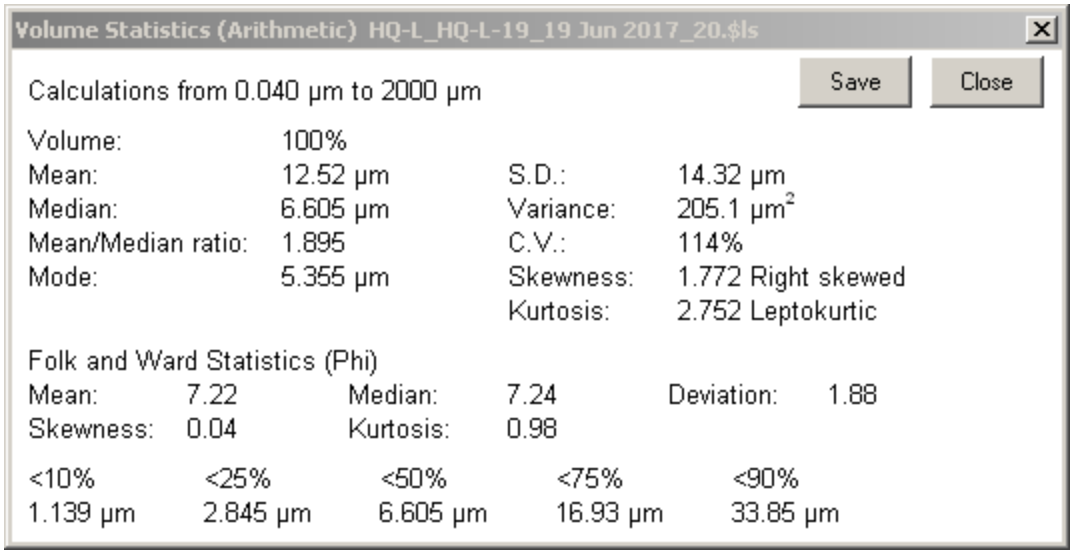
Volume Statistics (Arithmetic) HQ-L_HQ-L-19_19 Jun 2017_20.$ls
Save
Close
Calculations from 0.040 µm to 2000 µm
Volume: 100%
Mean: 12.52 µm
Median: 6.605 µm
Mean/Median ratio: 1.895
Mode: 5.355 µm
S.D.: 14.32 µm
Variance: 205.1 µm2
C.V.: 114%
Skewness: 1.772 Right skewed
Kurtosis: 2.752 Leptokurtic
Folk and Ward Statistics (Phi)
Mean: 7.22
Median: 7.24
Deviation: 1.88
Skewness: 0.04
Kurtosis: 0.98
<10% 1.139 µm
<25% 2.845 µm
<50% 6.605 µm
<75% 16.93 µm
<90% 33.85 µm

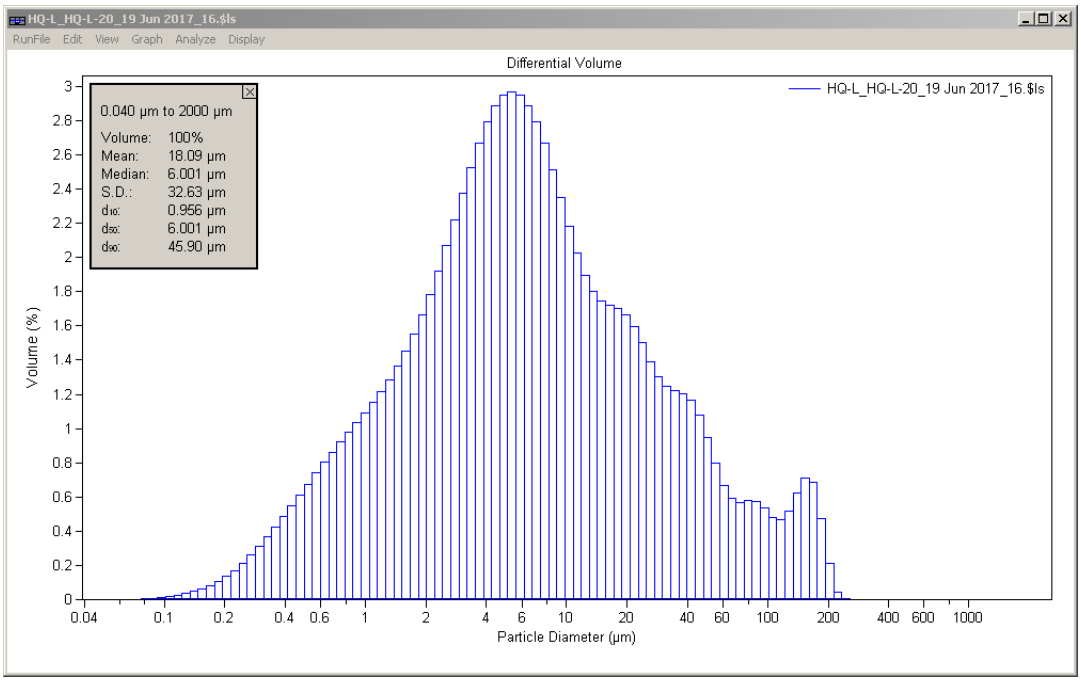

Volume Statistics (Arithmetic) HQ-L_HQ-L-20_19 Jun 2017_16.$ls

Save Close

Calculations from 0.040 µm to 2000 µm

Volume:	100%		
Mean:	18.09 µm	S.D.:	32.63 µm
Median:	6.001 µm	Variance:	1065 µm^2
Mean/Median ratio:	3.014	C.V.:	180%
Mode:	5.355 µm	Skewness:	3.294 Right skewed
		Kurtosis:	11.59 Leptokurtic

Folk and Ward Statistics (Phi)

Mean:	7.29	Median:	7.38	Deviation:	2.17
Skewness:	-0.07	Kurtosis:	1.08		

<10%	<25%	<50%	<75%	<90%
0.956 µm	2.486 µm	6.001 µm	16.79 µm	45.90 µm

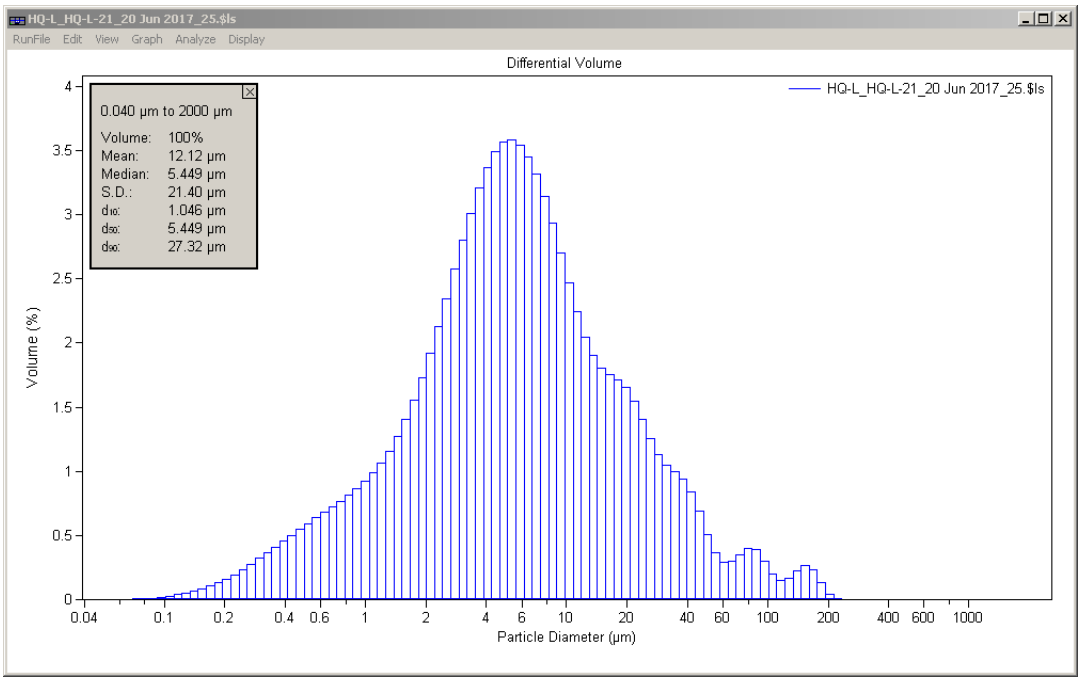

Volume Statistics (Arithmetic) HQ-L_HQ-L-21_20 Jun 2017_25.$ls

Save Close

Calculations from 0.040 µm to 2000 µm

Volume:	100%		
Mean:	12.12 µm	S.D.:	21.40 µm
Median:	5.449 µm	Variance:	457.8 µm^2
Mean/Median ratio:	2.224	C.V.:	177%
Mode:	5.355 µm	Skewness:	4.574 Right skewed
		Kurtosis:	25.99 Leptokurtic

Folk and Ward Statistics (Phi)

Mean:	7.49	Median:	7.52	Deviation:	1.81
Skewness:	0.01	Kurtosis:	1.17		

<10%	<25%	<50%	<75%	<90%
1.046 µm	2.604 µm	5.449 µm	11.86 µm	27.32 µm

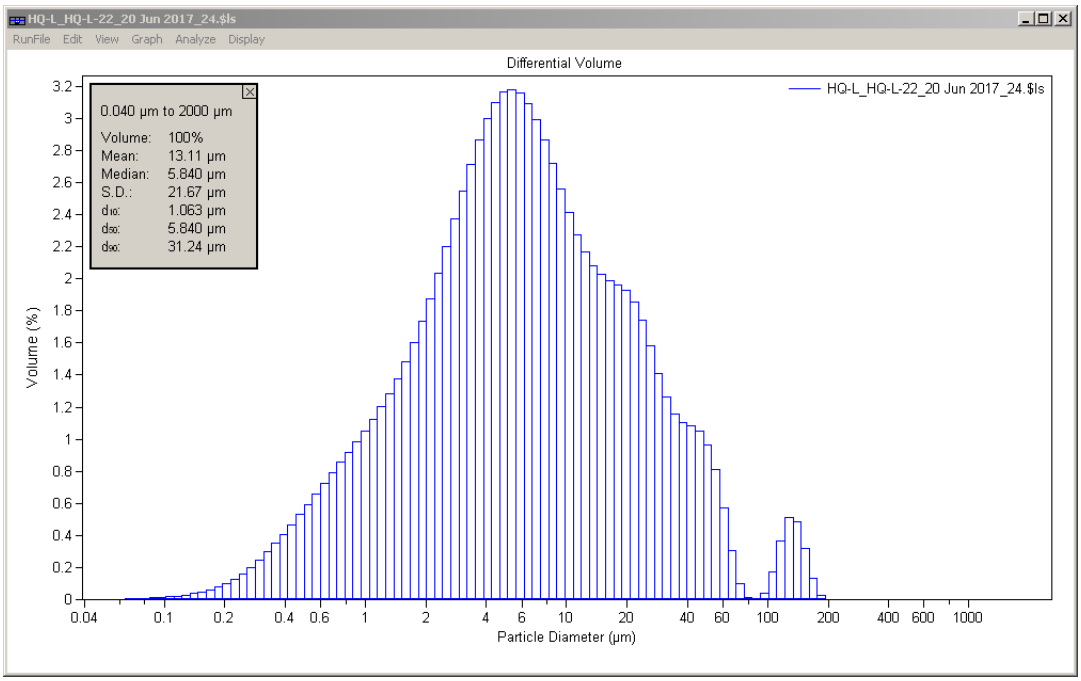
HQ-L_HQ-L-22_20 Jun 2017_24.$ls
RunFile Edit View Graph Analyze Display
Differential Volume
HQ-L_HQ-L-22_20 Jun 2017_24.$ls
0.040 µm to 2000 µm
Volume: 100%
Mean: 13.11 µm
Median: 5.840 µm
S.D.: 21.67 µm
d10: 1.063 µm
d50: 5.840 µm
d90: 31.24 µm
Volume (%)
Particle Diameter (µm)

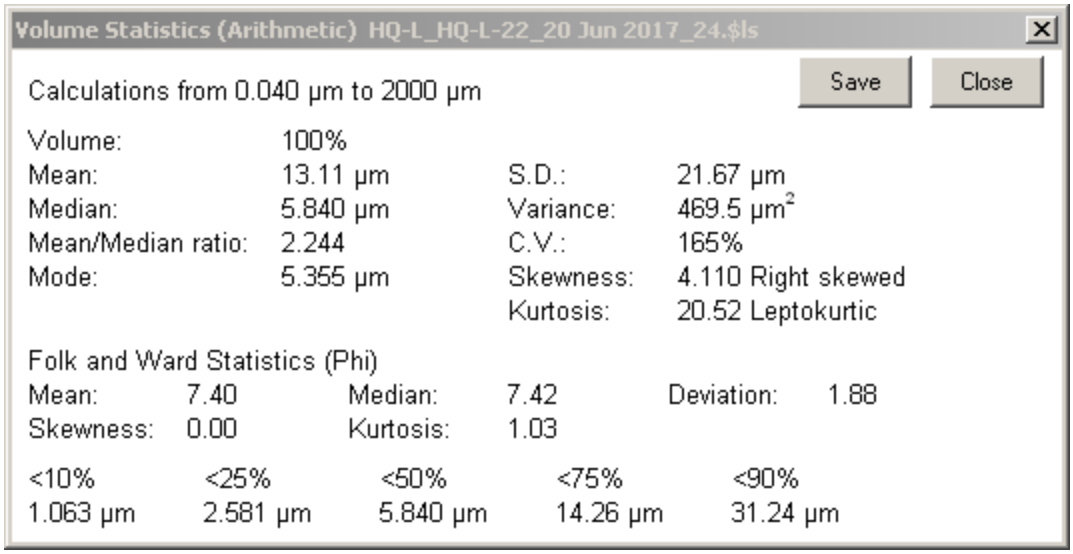
Volume Statistics (Arithmetic) HQ-L_HQ-L-22_20 Jun 2017_24.$ls
Save
Close
Calculations from 0.040 µm to 2000 µm
Volume: 100%
Mean: 13.11 µm
Median: 5.840 µm
Mean/Median ratio: 2.244
Mode: 5.355 µm
S.D.: 21.67 µm
Variance: 469.5 µm2
C.V.: 165%
Skewness: 4.110 Right skewed
Kurtosis: 20.52 Leptokurtic
Folk and Ward Statistics (Phi)
Mean: 7.40
Median: 7.42
Deviation: 1.88
Skewness: 0.00
Kurtosis: 1.03
<10% 1.063 µm
<25% 2.581 µm
<50% 5.840 µm
<75% 14.26 µm
<90% 31.24 µm

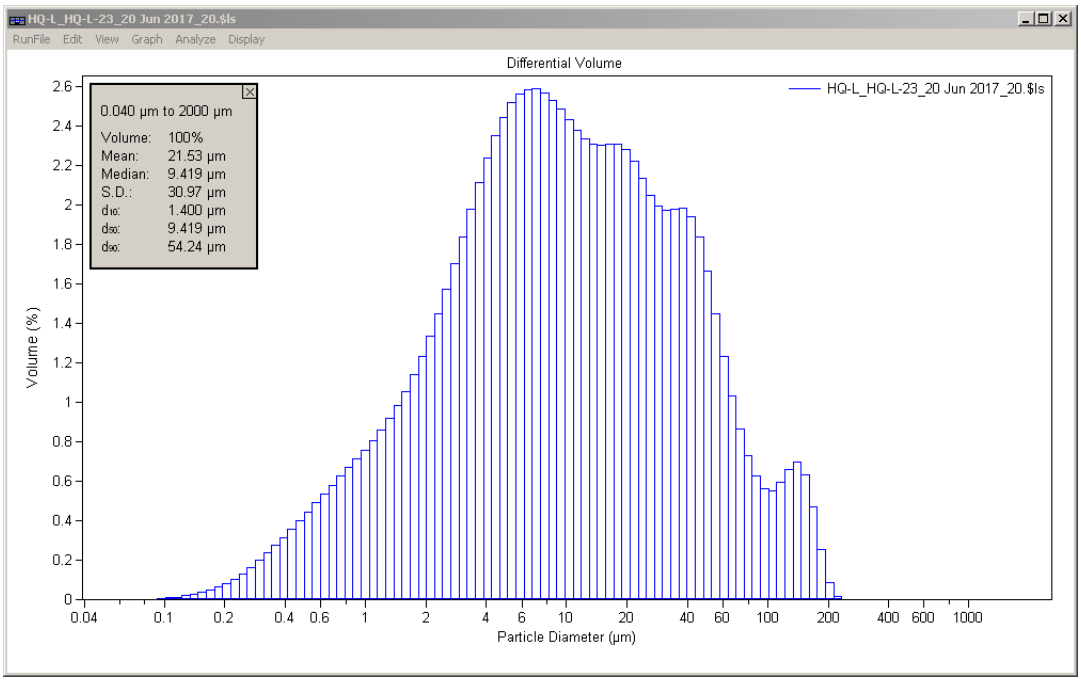
HQ-L_HQ-L-23_20 Jun 2017_20.$ls
RunFile Edit View Graph Analyze Display
Differential Volume
HQ-L_HQ-L-23_20 Jun 2017_20.$ls
0.040 µm to 2000 µm
Volume: 100%
Mean: 21.53 µm
Median: 9.419 µm
S.D.: 30.97 µm
d10: 1.400 µm
d50: 9.419 µm
d90: 54.24 µm
Volume (%)
Particle Diameter (µm)

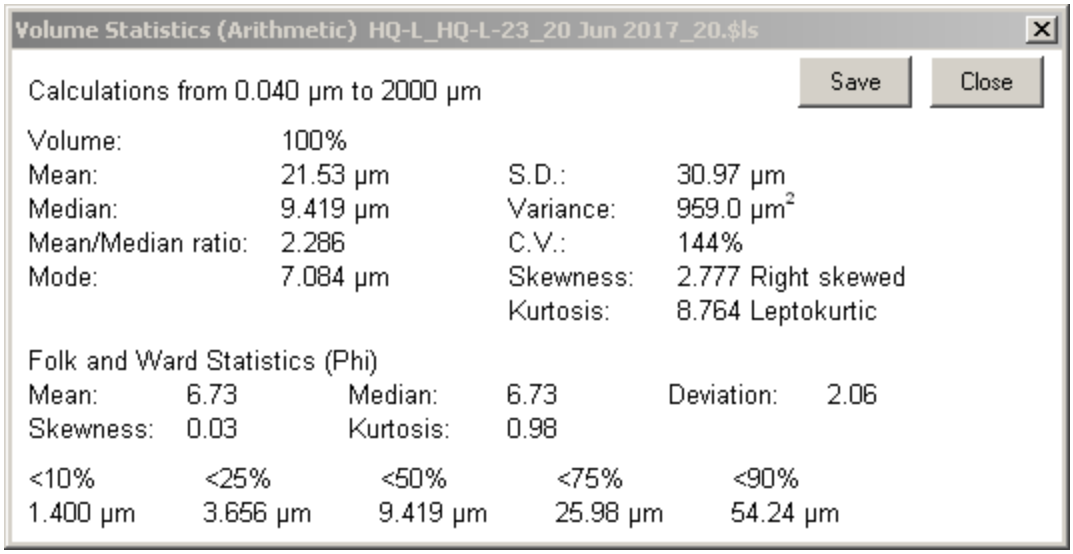
Volume Statistics (Arithmetic) HQ-L_HQ-L-23_20 Jun 2017_20.$ls
Save
Close
Calculations from 0.040 µm to 2000 µm
Volume: 100%
Mean: 21.53 µm
Median: 9.419 µm
Mean/Median ratio: 2.286
Mode: 7.084 µm
S.D.: 30.97 µm
Variance: 959.0 µm2
C.V.: 144%
Skewness: 2.777 Right skewed
Kurtosis: 8.764 Leptokurtic
Folk and Ward Statistics (Phi)
Mean: 6.73
Median: 6.73
Deviation: 2.06
Skewness: 0.03
Kurtosis: 0.98
<10% 1.400 µm
<25% 3.656 µm
<50% 9.419 µm
<75% 25.98 µm
<90% 54.24 µm

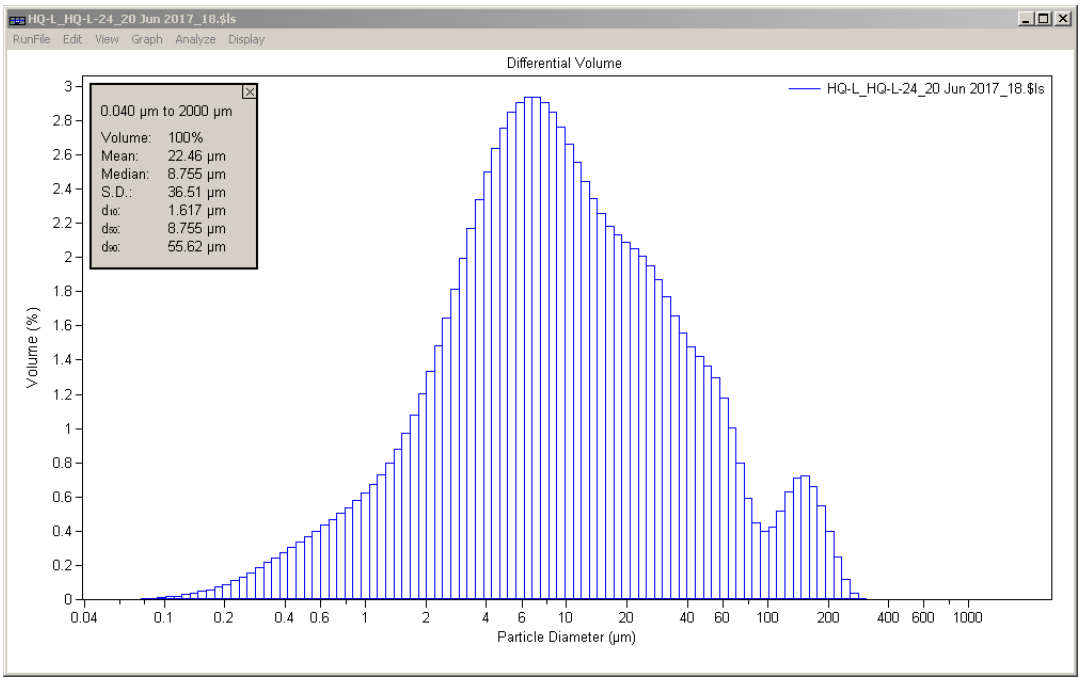

Volume Statistics (Arithmetic) HQ-L_HQ-L-24_20 Jun 2017_18.$ls

Save Close

Calculations from 0.040 µm to 2000 µm

Volume:	100%		
Mean:	22.46 µm	S.D.:	36.51 µm
Median:	8.755 µm	Variance:	1333 µm^2
Mean/Median ratio:	2.566	C.V.:	163%
Mode:	6.453 µm	Skewness:	3.187 Right skewed
		Kurtosis:	11.30 Leptokurtic

Folk and Ward Statistics (Phi)

Mean:	6.74	Median:	6.84	Deviation:	2.02
Skewness:	-0.05	Kurtosis:	1.07		

<10%	<25%	<50%	<75%	<90%
1.617 µm	3.803 µm	8.755 µm	23.67 µm	55.62 µm

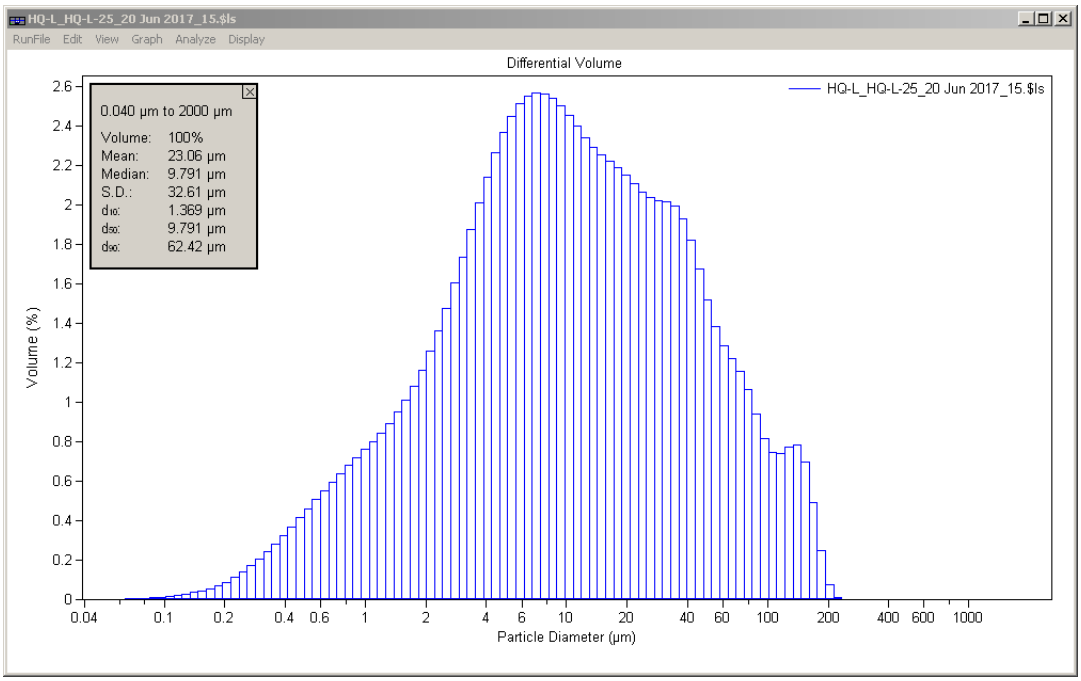

Volume Statistics (Arithmetic) HQ-L_HQ-L-25_20 Jun 2017_15.$ls

Save Close

Calculations from 0.040 µm to 2000 µm

Volume:	100%		
Mean:	23.06 µm	S.D.:	32.61 µm
Median:	9.791 µm	Variance:	1063 µm^2
Mean/Median ratio:	2.355	C.V.:	141%
Mode:	7.084 µm	Skewness:	2.506 Right skewed
		Kurtosis:	6.780 Leptokurtic

Folk and Ward Statistics (Phi)

Mean:	6.67	Median:	6.67	Deviation:	2.12
Skewness:	0.03	Kurtosis:	0.99		

<10%	<25%	<50%	<75%	<90%
1.369 µm	3.754 µm	9.791 µm	27.95 µm	62.42 µm

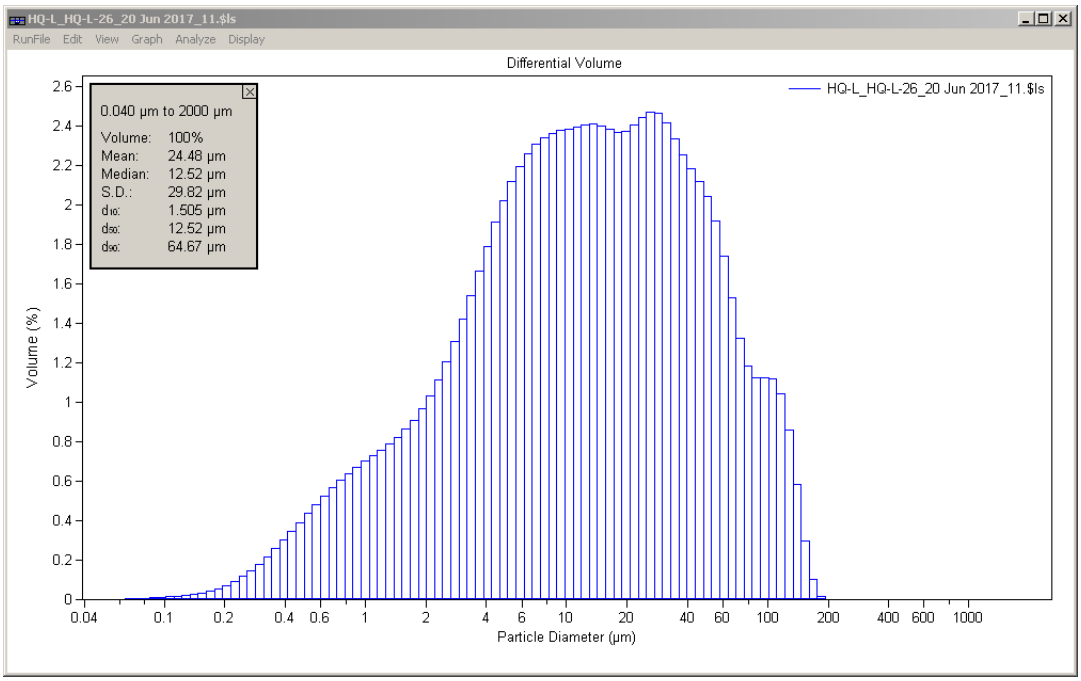

Volume Statistics (Arithmetic) HQ-L_HQ-L-26_20 Jun 2017_11.$ls

Save Close

Calculations from 0.040 µm to 2000 µm

Volume:	100%		
Mean:	24.48 µm	S.D.:	29.82 µm
Median:	12.52 µm	Variance:	889.4 µm^2
Mean/Median ratio:	1.955	C.V.:	122%
Mode:	26.15 µm	Skewness:	1.985 Right skewed
		Kurtosis:	3.986 Leptokurtic

Folk and Ward Statistics (Phi)

Mean:	6.42	Median:	6.32	Deviation:	2.09
Skewness:	0.12	Kurtosis:	0.98		

<10%	<25%	<50%	<75%	<90%
1.505 µm	4.480 µm	12.52 µm	32.89 µm	64.67 µm

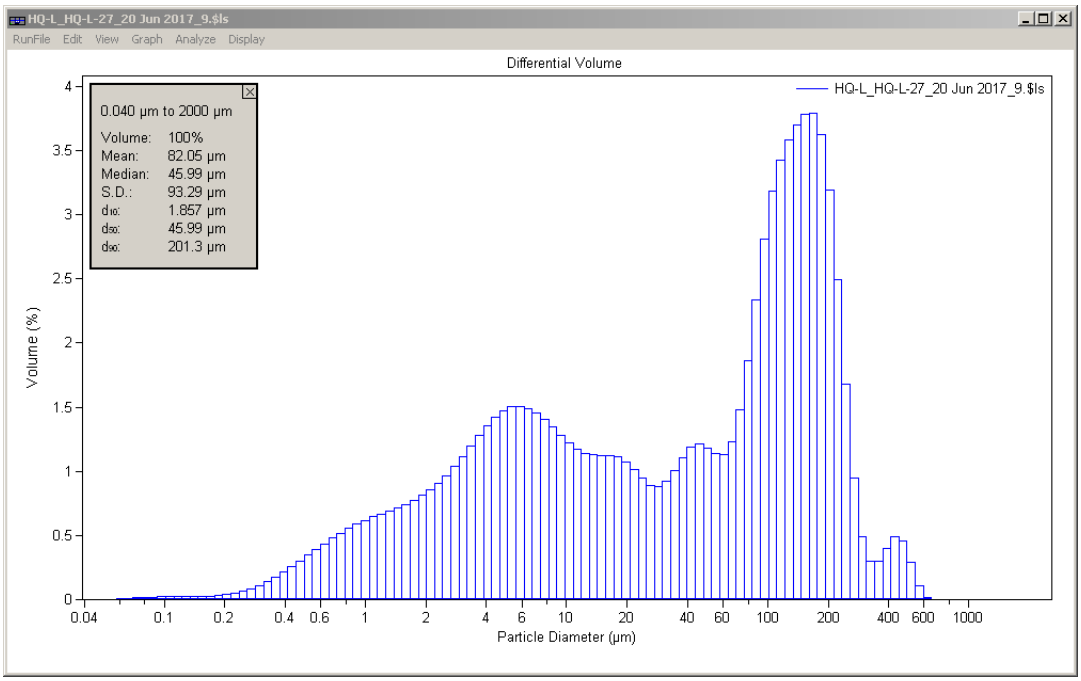

Volume Statistics (Arithmetic) HQ-L_HQ-L-27_20 Jun 2017_9.$ls

Save Close

Calculations from 0.040 µm to 2000 µm

Volume:	100%		
Mean:	82.05 µm	S.D.:	93.29 µm
Median:	45.99 µm	Variance:	8704 µm^2
Mean/Median ratio:	1.784	C.V.:	114%
Mode:	168.9 µm	Skewness:	1.610 Right skewed
		Kurtosis:	3.590 Leptokurtic

Folk and Ward Statistics (Phi)

Mean:	5.07	Median:	4.44	Deviation:	2.63
Skewness:	0.37	Kurtosis:	0.73		

<10%	<25%	<50%	<75%	<90%
1.857 µm	6.047 µm	45.99 µm	137.6 µm	201.3 µm

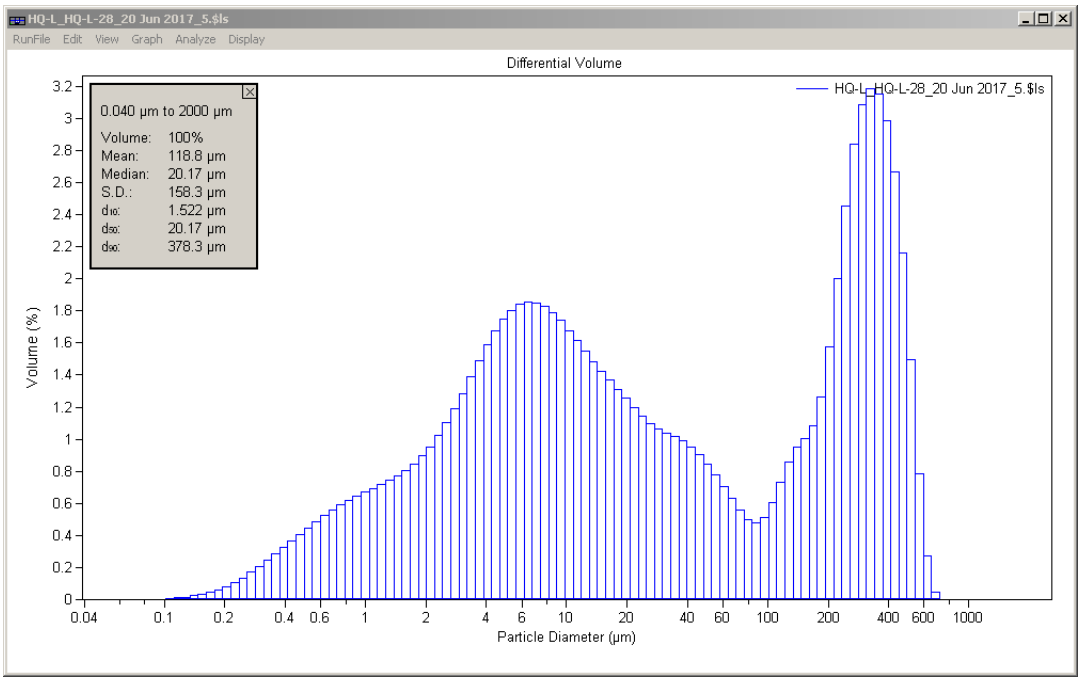
HQ-L_HQ-L-28_20 Jun 2017_5.$ls
RunFile Edit View Graph Analyze Display
Differential Volume
0.040 µm to 2000 µm
Volume: 100%
Mean: 118.8 µm
Median: 20.17 µm
S.D.: 158.3 µm
d10: 1.522 µm
d50: 20.17 µm
d90: 378.3 µm
HQ-L_HQ-L-28_20 Jun 2017_5.$ls
Volume (%)
Particle Diameter (µm)

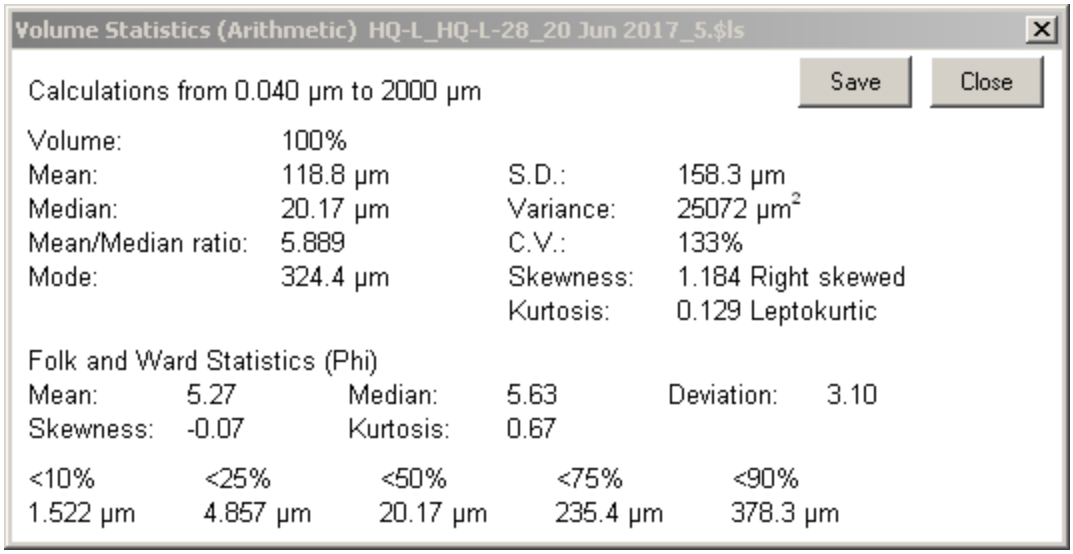
Volume Statistics (Arithmetic) HQ-L_HQ-L-28_20 Jun 2017_5.$ls
Save
Close
Calculations from 0.040 µm to 2000 µm
Volume: 100%
Mean: 118.8 µm
Median: 20.17 µm
Mean/Median ratio: 5.889
Mode: 324.4 µm
S.D.: 158.3 µm
Variance: 25072 µm²
C.V.: 133%
Skewness: 1.184 Right skewed
Kurtosis: 0.129 Leptokurtic
Folk and Ward Statistics (Phi)
Mean: 5.27
Median: 5.63
Deviation: 3.10
Skewness: -0.07
Kurtosis: 0.67
<10% 1.522 µm
<25% 4.857 µm
<50% 20.17 µm
<75% 235.4 µm
<90% 378.3 µm

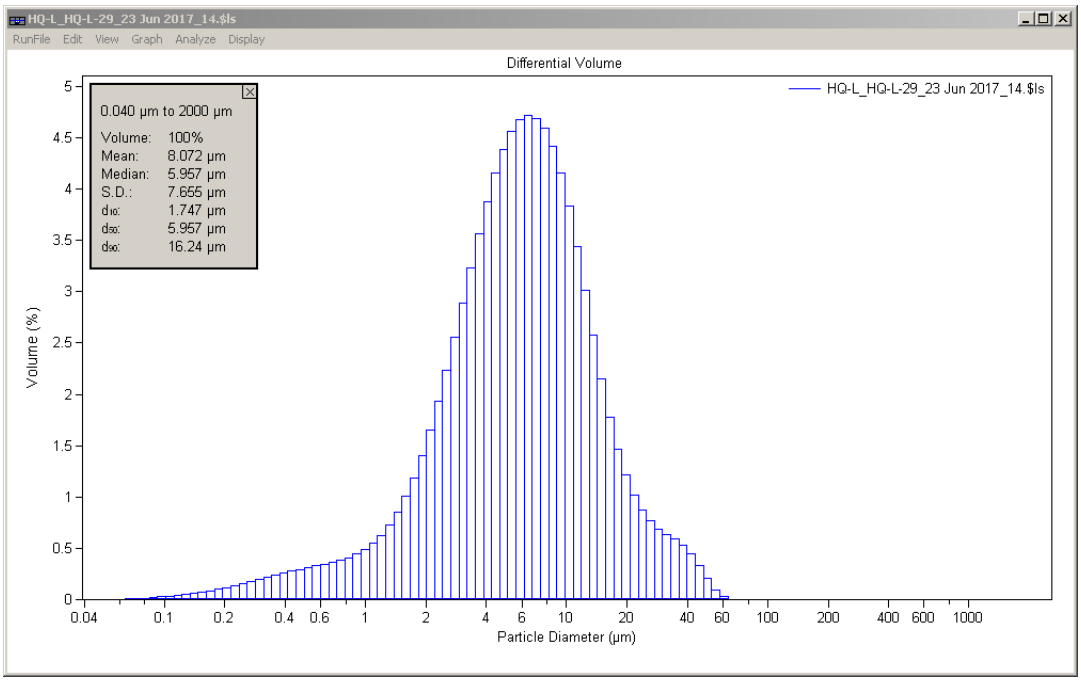

Volume Statistics (Arithmetic) HQ-L_HQ-L-29_23 Jun 2017_14.$ls

Save Close

Calculations from 0.040 µm to 2000 µm

Volume:	100%		
Mean:	8.072 µm	S.D.:	7.655 µm
Median:	5.957 µm	Variance:	58.59 µm^2
Mean/Median ratio:	1.355	C.V.:	94.8%
Mode:	6.453 µm	Skewness:	2.523 Right skewed
		Kurtosis:	8.402 Leptokurtic

Folk and Ward Statistics (Phi)

Mean:	7.45	Median:	7.39	Deviation:	1.30
Skewness:	0.12	Kurtosis:	1.22		

<10%	<25%	<50%	<75%	<90%
1.747 µm	3.373 µm	5.957 µm	9.995 µm	16.24 µm

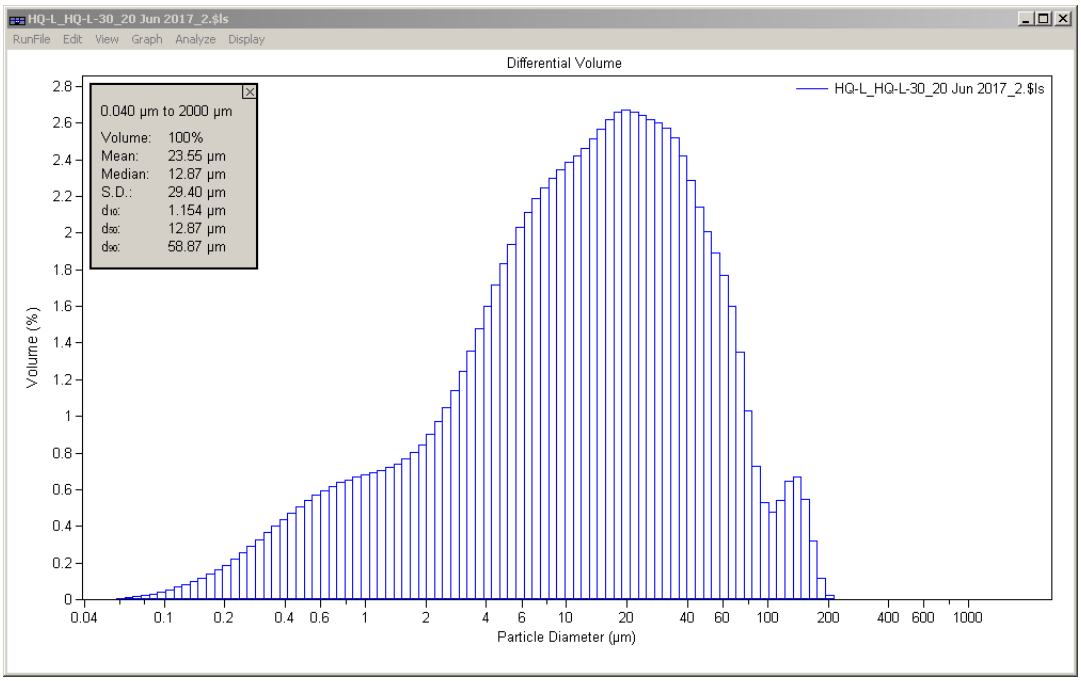

Volume Statistics (Arithmetic) HQ-L_HQ-L-30_20 Jun 2017_2.$ls

Save Close

Calculations from 0.040 µm to 2000 µm

Volume:	100%		
Mean:	23.55 µm	S.D.:	29.40 µm
Median:	12.87 µm	Variance:	864.3 µm^2
Mean/Median ratio:	1.830	C.V.:	125%
Mode:	19.76 µm	Skewness:	2.384 Right skewed
		Kurtosis:	6.805 Leptokurtic

Folk and Ward Statistics (Phi)

Mean:	6.51	Median:	6.28	Deviation:	2.15
Skewness:	0.21	Kurtosis:	1.04		

<10%	<25%	<50%	<75%	<90%
1.154 µm	4.414 µm	12.87 µm	31.43 µm	58.87 µm

APPENDIX C: GRAIN SIZE ANALYSIS OF HQ-SP SAMPLES (SUMP PIT)

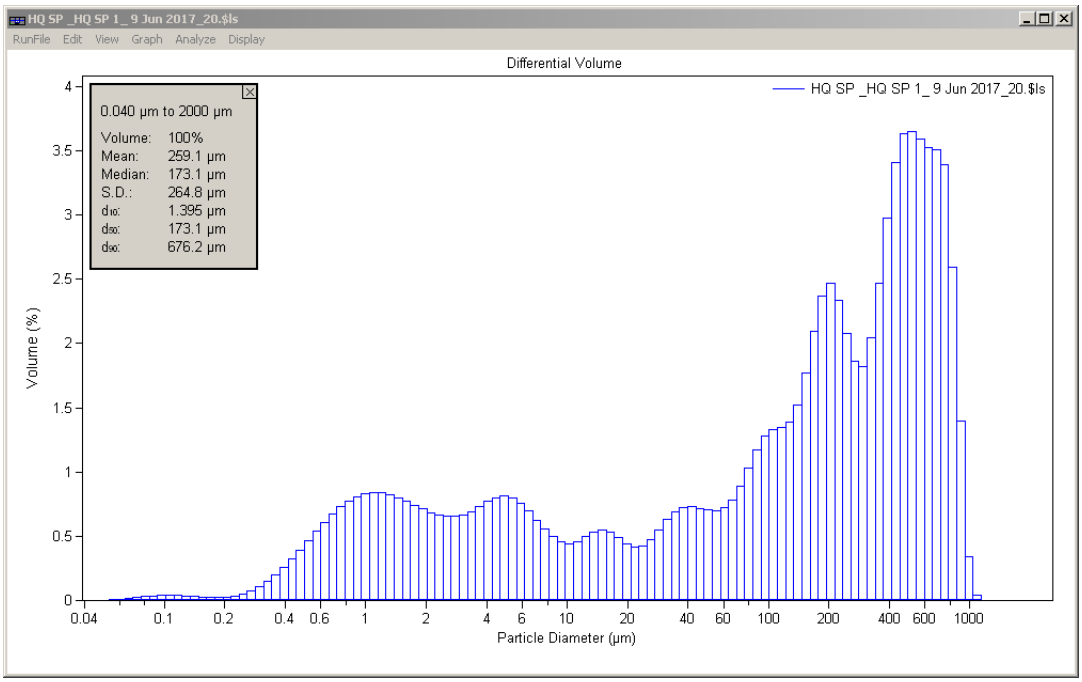

Volume Statistics (Arithmetic) HQ SP _HQ SP 1_ 9 Jun 2017_20.$ls

Save Close

Calculations from 0.040 µm to 2000 µm

Volume:	100%		
Mean:	259.1 µm	S.D.:	264.8 µm
Median:	173.1 µm	Variance:	70105 µm^2
Mean/Median ratio:	1.497	C.V.:	102%
Mode:	517.2 µm	Skewness:	0.797 Right skewed
		Kurtosis:	-0.544 Platykurtic

Folk and Ward Statistics (Phi)

Mean:	3.89	Median:	2.53	Deviation:	3.39
Skewness:	0.55	Kurtosis:	0.76		

<10%	<25%	<50%	<75%	<90%
1.395 µm	10.97 µm	173.1 µm	457.8 µm	676.2 µm

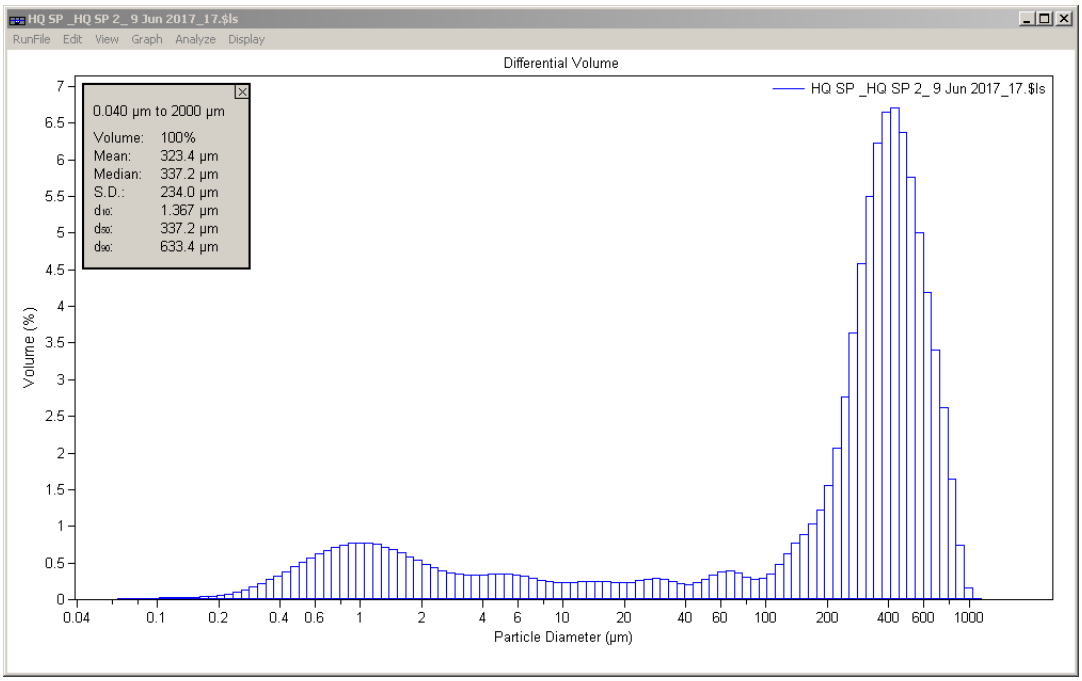

Volume Statistics (Arithmetic) HQ SP _HQ SP 2_ 9 Jun 2017_17.$ls

Save Close

Calculations from 0.040 µm to 2000 µm

Volume:	100%		
Mean:	323.4 µm	S.D.:	234.0 µm
Median:	337.2 µm	Variance:	54740 µm^2
Mean/Median ratio:	0.959	C.V.:	72.3%
Mode:	429.2 µm	Skewness:	0.184 Right skewed
		Kurtosis:	-0.725 Platykurtic

Folk and Ward Statistics (Phi)

Mean:	3.37	Median:	1.57	Deviation:	3.23
Skewness:	0.78	Kurtosis:	1.79		

<10%	<25%	<50%	<75%	<90%
1.367 µm	100.2 µm	337.2 µm	483.6 µm	633.4 µm

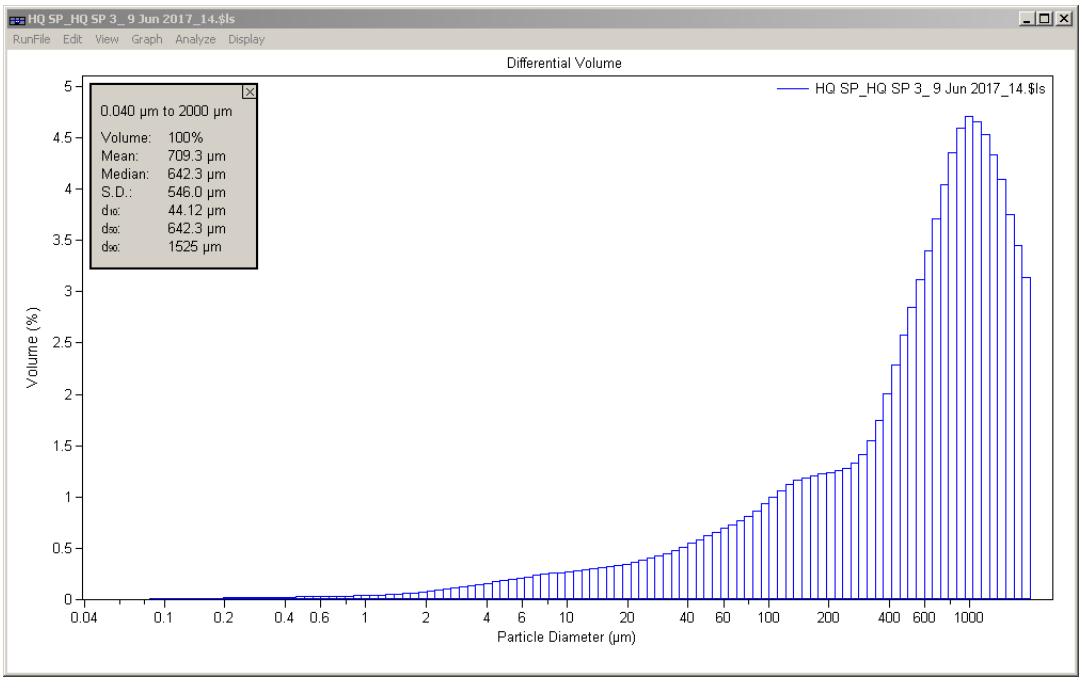

Volume Statistics (Arithmetic) HQ SP_HQ SP 3_ 9 Jun 2017_14.$ls

Save Close

Calculations from 0.040 µm to 2000 µm

Volume:	100%		
Mean:	709.3 µm	S.D.:	546.0 µm
Median:	642.3 µm	Variance:	298.1e3 µm^2
Mean/Median ratio:	1.104	C.V.:	77.0%
Mode:	993.6 µm	Skewness:	0.474 Right skewed
		Kurtosis:	-0.821 Platykurtic

Folk and Ward Statistics (Phi)

Mean:	1.21	Median:	0.64	Deviation:	2.01
Skewness:	0.52	Kurtosis:	1.16		

<10%	<25%	<50%	<75%	<90%
44.12 µm	200.8 µm	642.3 µm	1106 µm	1525 µm

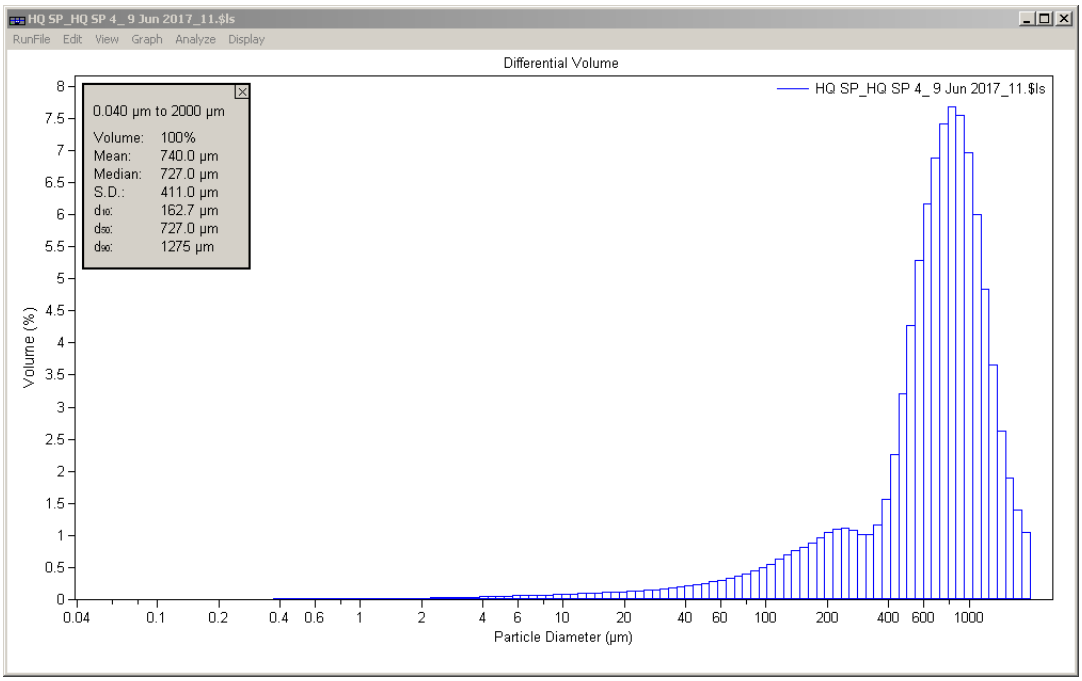
HQ SP_HQ SP 4_ 9 Jun 2017_11.$ls
RunFile Edit View Graph Analyze Display
Differential Volume
HQ SP_HQ SP 4_ 9 Jun 2017_11.$ls
0.040 µm to 2000 µm
Volume: 100%
Mean: 740.0 µm
Median: 727.0 µm
S.D.: 411.0 µm
d10: 162.7 µm
d50: 727.0 µm
d90: 1275 µm
Volume (%)
Particle Diameter (µm)

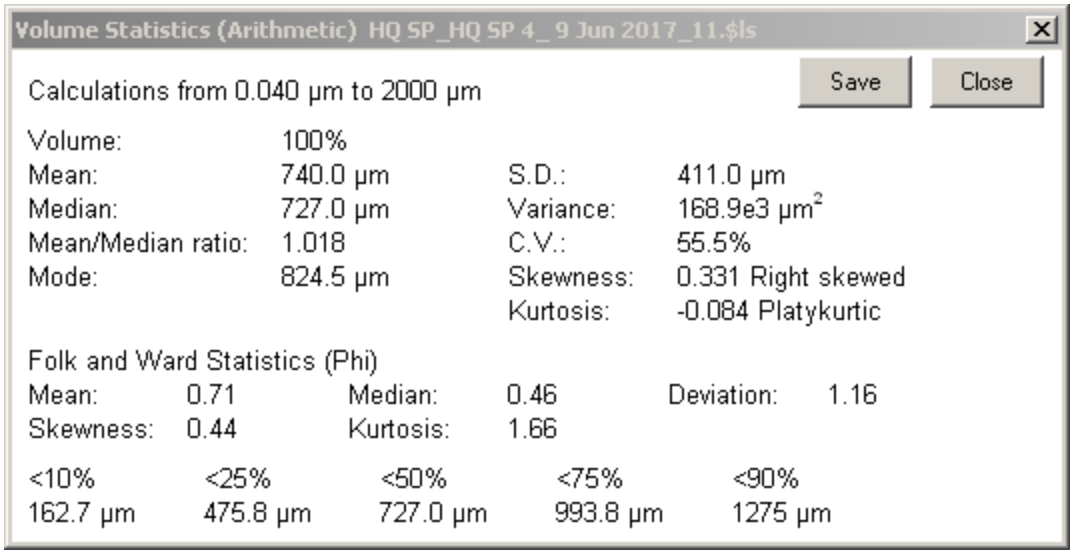
Volume Statistics (Arithmetic) HQ SP_HQ SP 4_ 9 Jun 2017_11.$ls
Save
Close
Calculations from 0.040 µm to 2000 µm
Volume: 100%
Mean: 740.0 µm
Median: 727.0 µm
Mean/Median ratio: 1.018
Mode: 824.5 µm
S.D.: 411.0 µm
Variance: 168.9e3 µm²
C.V.: 55.5%
Skewness: 0.331 Right skewed
Kurtosis: -0.084 Platykurtic
Folk and Ward Statistics (Phi)
Mean: 0.71
Median: 0.46
Deviation: 1.16
Skewness: 0.44
Kurtosis: 1.66
<10% 162.7 µm
<25% 475.8 µm
<50% 727.0 µm
<75% 993.8 µm
<90% 1275 µm

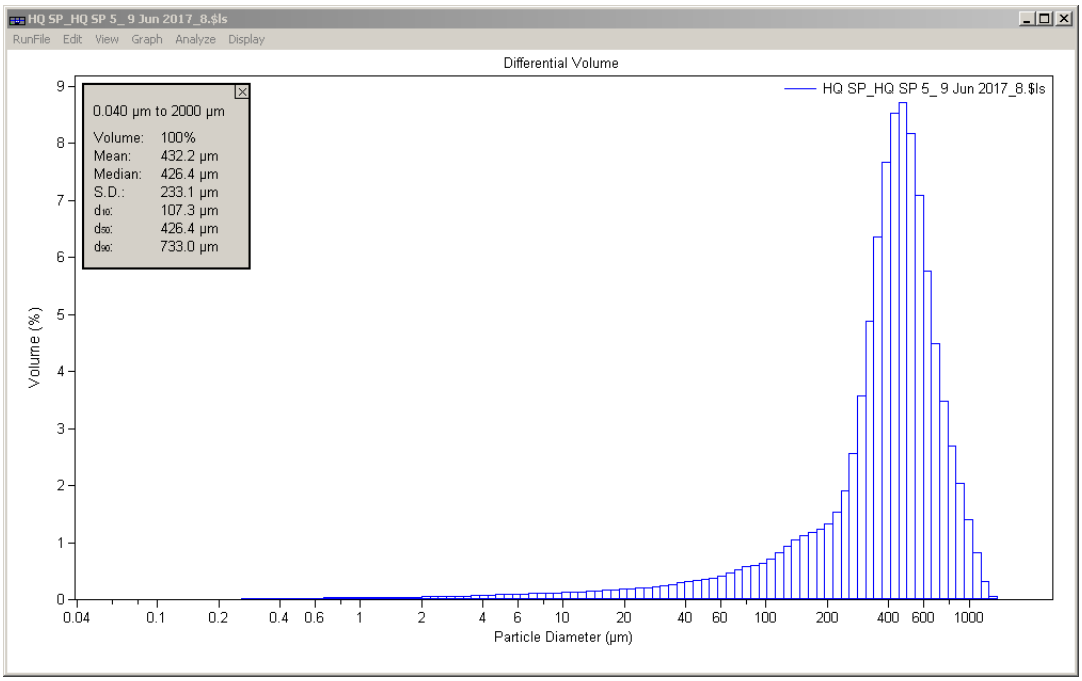

Volume Statistics (Arithmetic) HQ SP_HQ SP 5_ 9 Jun 2017_8.$ls

Save Close

Calculations from 0.040 µm to 2000 µm

Volume:	100%		
Mean:	432.2 µm	S.D.:	233.1 µm
Median:	426.4 µm	Variance:	54340 µm^2
Mean/Median ratio:	1.014	C.V.:	53.9%
Mode:	471.1 µm	Skewness:	0.371 Right skewed
		Kurtosis:	0.240 Leptokurtic

Folk and Ward Statistics (Phi)

Mean:	1.43	Median:	1.23	Deviation:	1.11
Skewness:	0.44	Kurtosis:	1.87		

<10%	<25%	<50%	<75%	<90%
107.3 µm	290.2 µm	426.4 µm	565.4 µm	733.0 µm

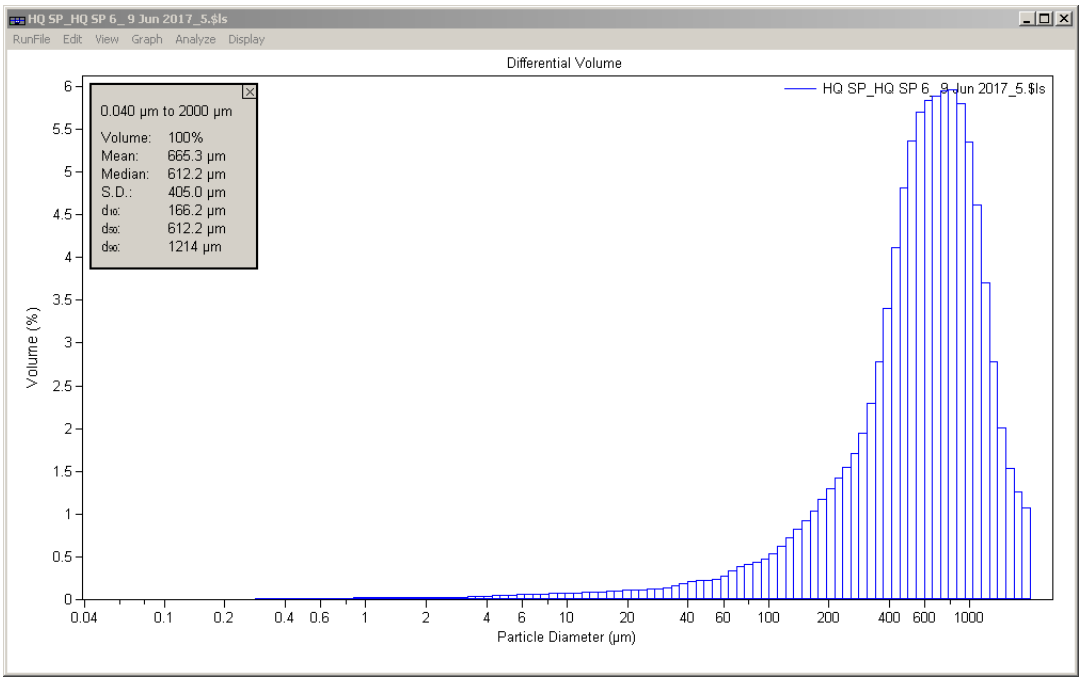

Volume Statistics (Arithmetic) HQ SP_HQ SP 6_ 9 Jun 2017_5.$ls

Save Close

Calculations from 0.040 µm to 2000 µm

Volume:	100%		
Mean:	665.3 µm	S.D.:	405.0 µm
Median:	612.2 µm	Variance:	164.0e3 µm^2
Mean/Median ratio:	1.087	C.V.:	60.9%
Mode:	824.5 µm	Skewness:	0.682 Right skewed
		Kurtosis:	0.253 Leptokurtic

Folk and Ward Statistics (Phi)

Mean:	0.86	Median:	0.71	Deviation:	1.14
Skewness:	0.32	Kurtosis:	1.33		

<10%	<25%	<50%	<75%	<90%
166.2 µm	374.7 µm	612.2 µm	909.1 µm	1214 µm

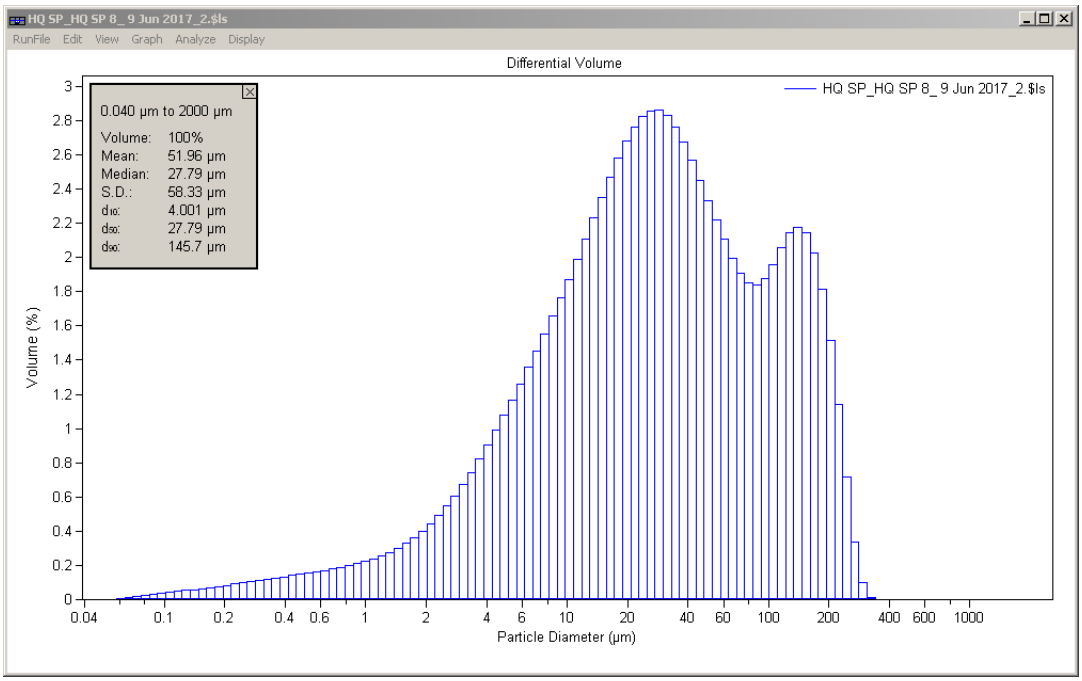

Volume Statistics (Arithmetic) HQ SP_HQ SP 8_ 9 Jun 2017_2.$ls

Save Close

Calculations from 0.040 µm to 2000 µm

Volume:	100%		
Mean:	51.96 µm	S.D.:	58.33 µm
Median:	27.79 µm	Variance:	3403 µm^2
Mean/Median ratio:	1.870	C.V.:	112%
Mode:	28.70 µm	Skewness:	1.567 Right skewed
		Kurtosis:	1.813 Leptokurtic

Folk and Ward Statistics (Phi)

Mean:	5.19	Median:	5.17	Deviation:	2.03
Skewness:	0.10	Kurtosis:	1.00		

<10%	<25%	<50%	<75%	<90%
4.001 µm	10.92 µm	27.79 µm	71.82 µm	145.7 µm

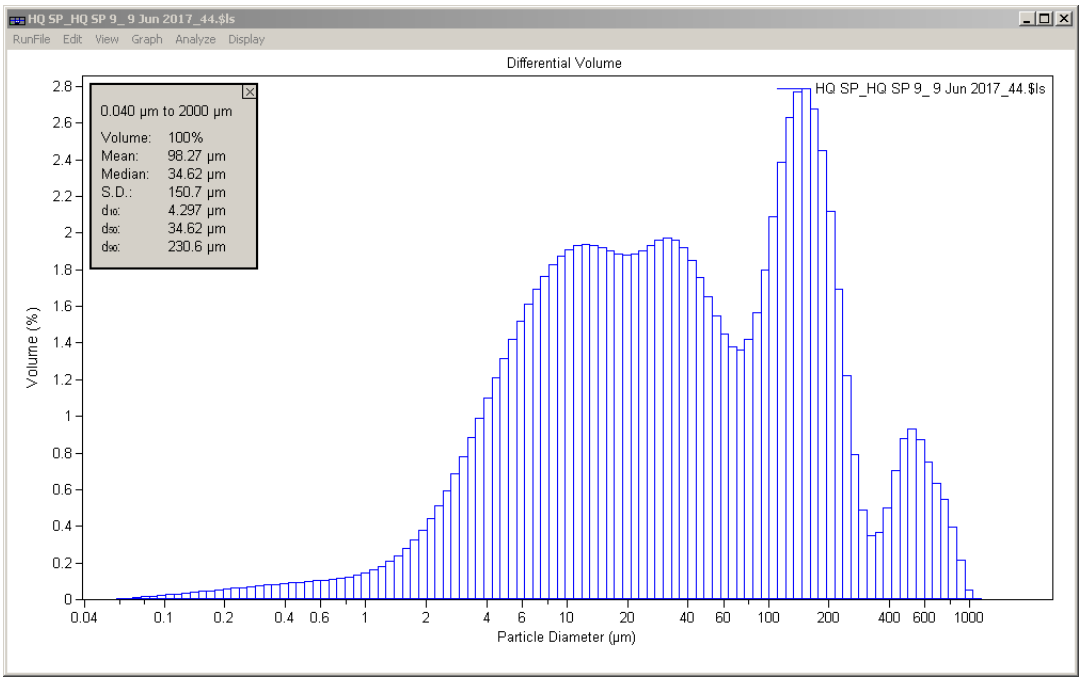
HQ SP_HQ SP 9_ 9 Jun 2017_44.$ls
RunFile Edit View Graph Analyze Display
Differential Volume
HQ SP_HQ SP 9_ 9 Jun 2017_44.$ls
0.040 µm to 2000 µm
Volume: 100%
Mean: 98.27 µm
Median: 34.62 µm
S.D.: 150.7 µm
d10: 4.297 µm
d50: 34.62 µm
d90: 230.6 µm
Volume (%)
Particle Diameter (µm)

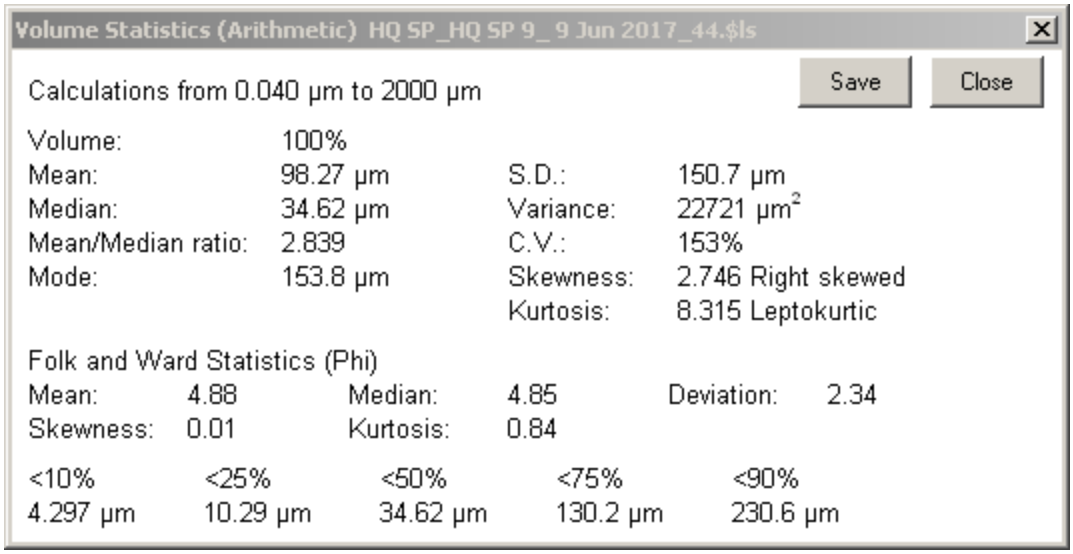
Volume Statistics (Arithmetic) HQ SP_HQ SP 9_ 9 Jun 2017_44.$ls
Save
Close
Calculations from 0.040 µm to 2000 µm
Volume: 100%
Mean: 98.27 µm
Median: 34.62 µm
Mean/Median ratio: 2.839
Mode: 153.8 µm
S.D.: 150.7 µm
Variance: 22721 µm2
C.V.: 153%
Skewness: 2.746 Right skewed
Kurtosis: 8.315 Leptokurtic
Folk and Ward Statistics (Phi)
Mean: 4.88
Median: 4.85
Deviation: 2.34
Skewness: 0.01
Kurtosis: 0.84
<10% 4.297 µm
<25% 10.29 µm
<50% 34.62 µm
<75% 130.2 µm
<90% 230.6 µm

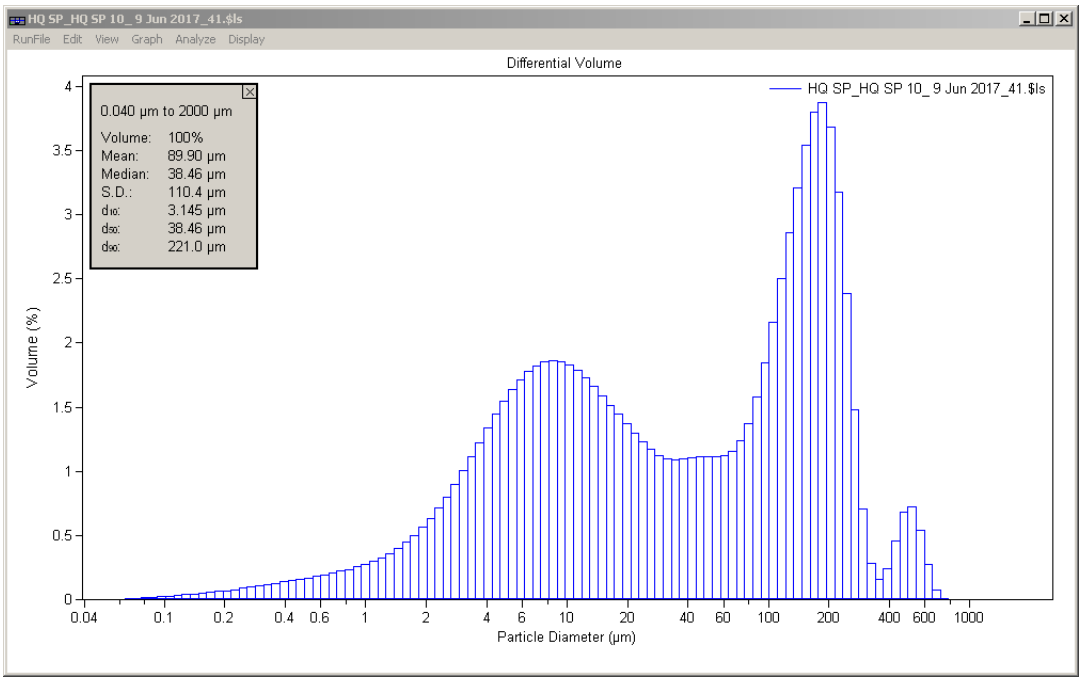

Volume Statistics (Arithmetic) HQ SP_HQ SP 10_ 9 Jun 2017_41.$ls

Save Close

Calculations from 0.040 µm to 2000 µm

Volume:	100%		
Mean:	89.90 µm	S.D.:	110.4 µm
Median:	38.46 µm	Variance:	12195 µm^2
Mean/Median ratio:	2.338	C.V.:	123%
Mode:	185.4 µm	Skewness:	1.942 Right skewed
		Kurtosis:	4.957 Leptokurtic

Folk and Ward Statistics (Phi)

Mean:	4.93	Median:	4.70	Deviation:	2.44
Skewness:	0.18	Kurtosis:	0.71		

<10%	<25%	<50%	<75%	<90%
3.145 µm	7.882 µm	38.46 µm	151.2 µm	221.0 µm

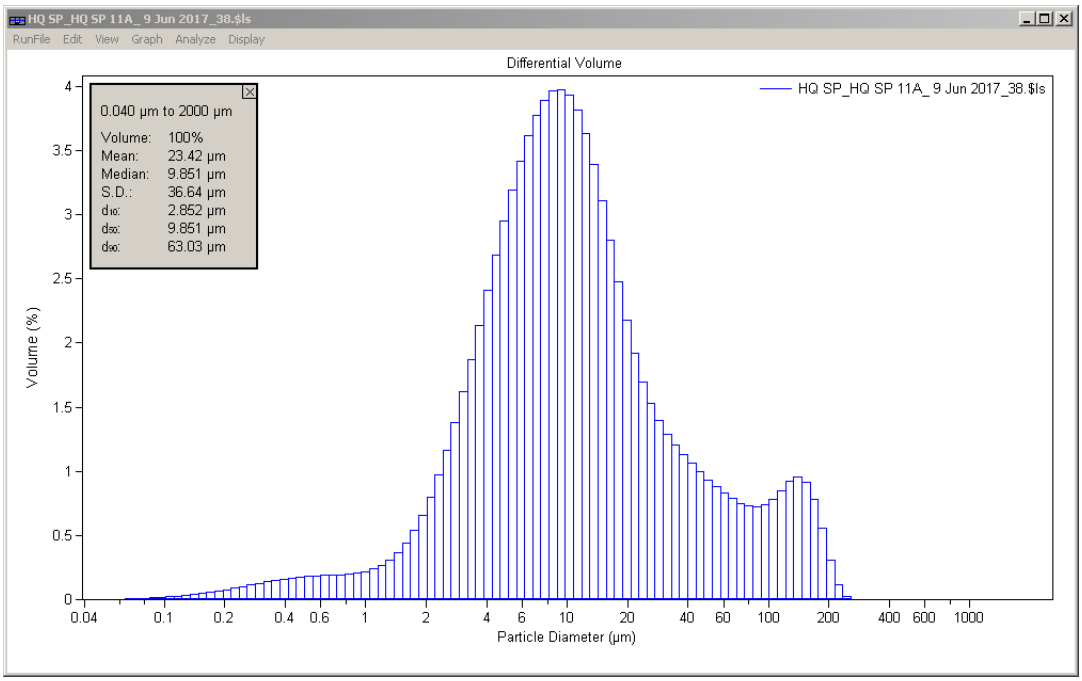

Volume Statistics (Arithmetic) HQ SP_HQ SP 11A_ 9 Jun 2017_38.$ls

Save Close

Calculations from 0.040 µm to 2000 µm

Volume:	100%		
Mean:	23.42 µm	S.D.:	36.64 µm
Median:	9.851 µm	Variance:	1343 μm^2
Mean/Median ratio:	2.378	C.V.:	156%
Mode:	9.371 µm	Skewness:	2.851 Right skewed
		Kurtosis:	8.170 Leptokurtic

Folk and Ward Statistics (Phi)

Mean:	6.50	Median:	6.67	Deviation:	1.72
Skewness:	-0.16	Kurtosis:	1.27		

<10%	<25%	<50%	<75%	<90%
2.852 µm	5.261 µm	9.851 µm	20.53 µm	63.03 µm

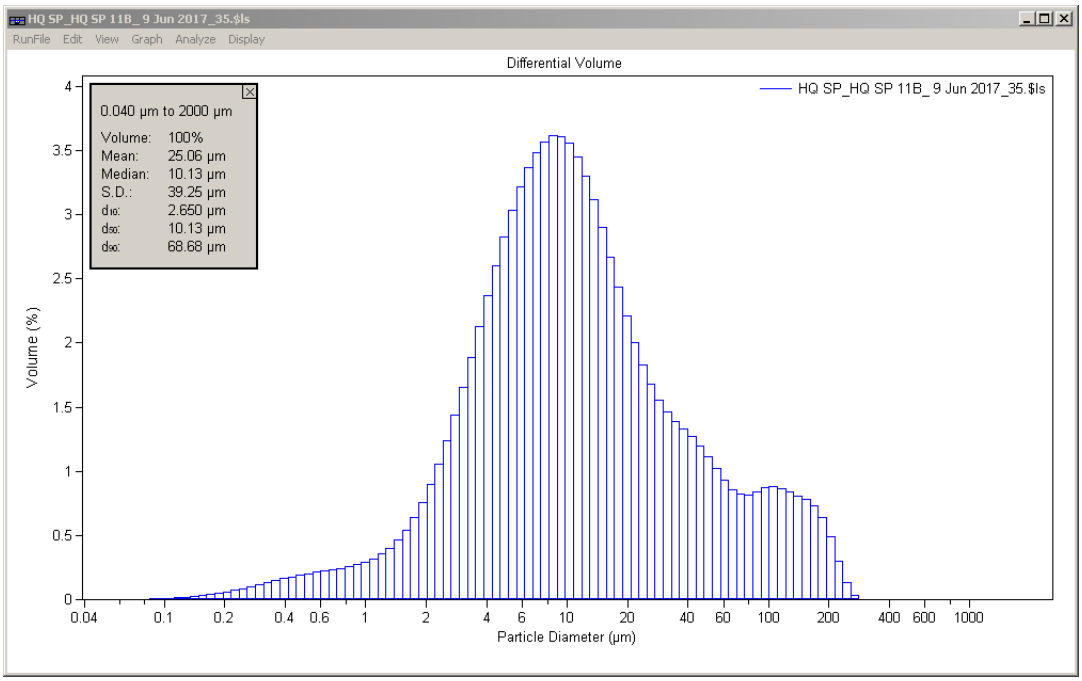

Volume Statistics (Arithmetic) HQ SP_HQ SP 11B_ 9 Jun 2017_35.$ls

Save Close

Calculations from 0.040 µm to 2000 µm

Volume:	100%		
Mean:	25.06 µm	S.D.:	39.25 µm
Median:	10.13 µm	Variance:	1541 µm^2
Mean/Median ratio:	2.474	C.V.:	157%
Mode:	8.537 µm	Skewness:	2.872 Right skewed
		Kurtosis:	8.651 Leptokurtic

Folk and Ward Statistics (Phi)

Mean:	6.45	Median:	6.63	Deviation:	1.82
Skewness:	-0.14	Kurtosis:	1.17		

<10%	<25%	<50%	<75%	<90%
2.650 µm	5.115 µm	10.13 µm	23.34 µm	68.68 µm

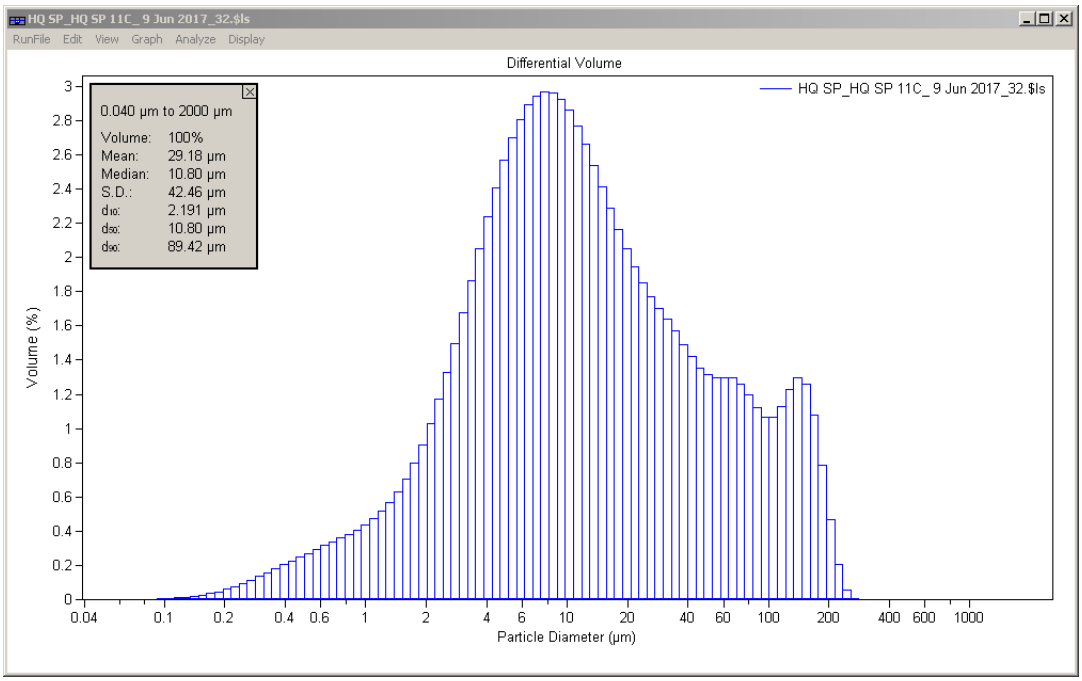

Volume Statistics (Arithmetic) HQ SP_HQ SP 11C_ 9 Jun 2017_32.$ls

Save Close

Calculations from 0.040 µm to 2000 µm

Volume:	100%		
Mean:	29.18 µm	S.D.:	42.46 µm
Median:	10.80 µm	Variance:	1803 µm^2
Mean/Median ratio:	2.702	C.V.:	146%
Mode:	7.776 µm	Skewness:	2.269 Right skewed
		Kurtosis:	4.816 Leptokurtic

Folk and Ward Statistics (Phi)

Mean:	6.31	Median:	6.53	Deviation:	2.07
Skewness:	-0.11	Kurtosis:	1.03		

<10%	<25%	<50%	<75%	<90%
2.191 µm	4.775 µm	10.80 µm	31.68 µm	89.42 µm

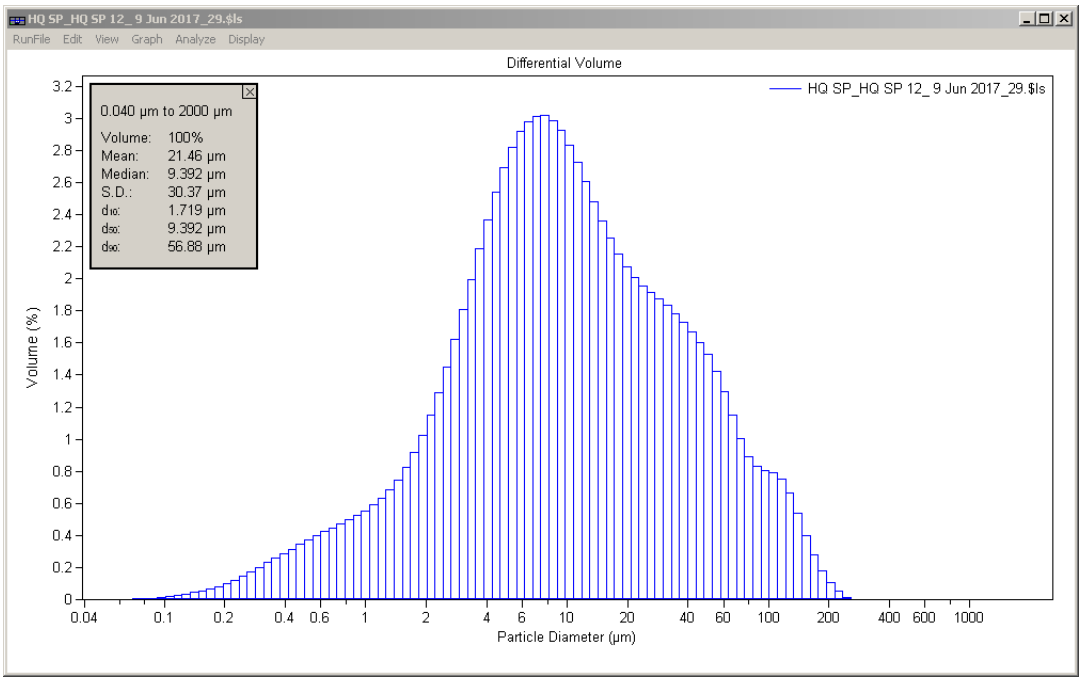

Volume Statistics (Arithmetic) HQ SP_HQ SP 12_ 9 Jun 2017_29.$ls

Save Close

Calculations from 0.040 µm to 2000 µm

Volume:	100%		
Mean:	21.46 µm	S.D.:	30.37 µm
Median:	9.392 µm	Variance:	922.6 µm^2
Mean/Median ratio:	2.285	C.V.:	142%
Mode:	7.776 µm	Skewness:	2.733 Right skewed
		Kurtosis:	8.828 Leptokurtic

Folk and Ward Statistics (Phi)

Mean:	6.63	Median:	6.73	Deviation:	1.98
Skewness:	-0.02	Kurtosis:	1.06		

<10%	<25%	<50%	<75%	<90%
1.719 µm	4.157 µm	9.392 µm	25.10 µm	56.88 µm

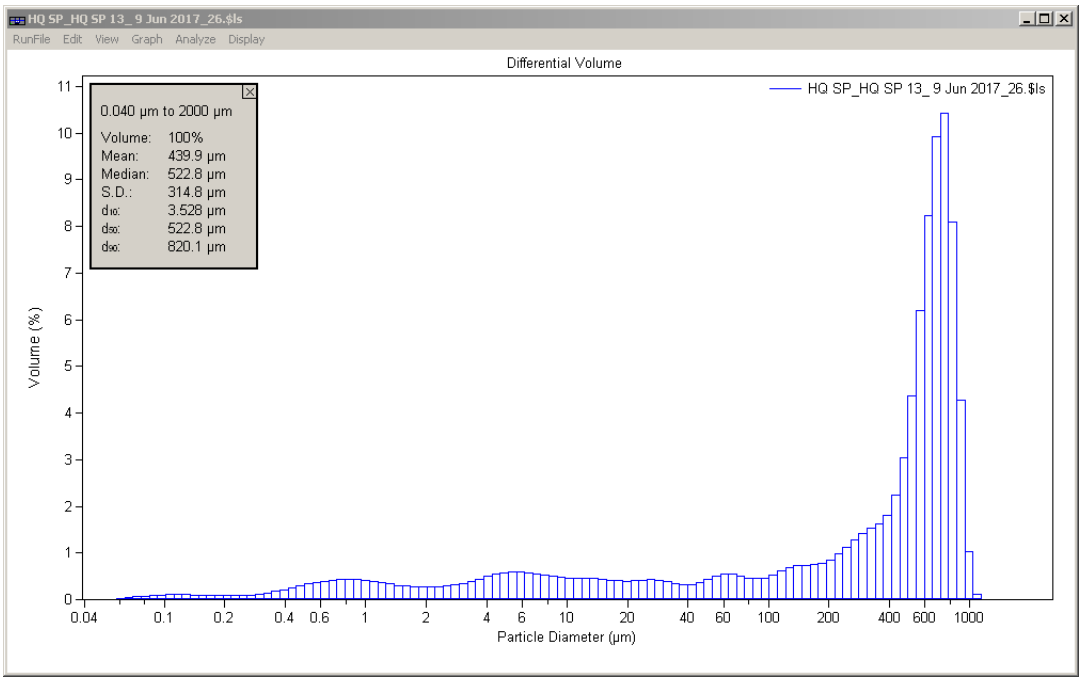

Volume Statistics (Arithmetic) HQ SP_HQ SP 13_ 9 Jun 2017_26.$ls

Save Close

Calculations from 0.040 µm to 2000 µm

Volume:	100%		
Mean:	439.9 µm	S.D.:	314.8 µm
Median:	522.8 µm	Variance:	99071 µm^2
Mean/Median ratio:	0.841	C.V.:	71.6%
Mode:	751.1 µm	Skewness:	-0.183 Left skewed
		Kurtosis:	-1.428 Platykurtic

Folk and Ward Statistics (Phi)

Mean:	2.65	Median:	0.94	Deviation:	3.08
Skewness:	0.84	Kurtosis:	1.25		

<10%	<25%	<50%	<75%	<90%
3.528 µm	72.95 µm	522.8 µm	709.9 µm	820.1 µm

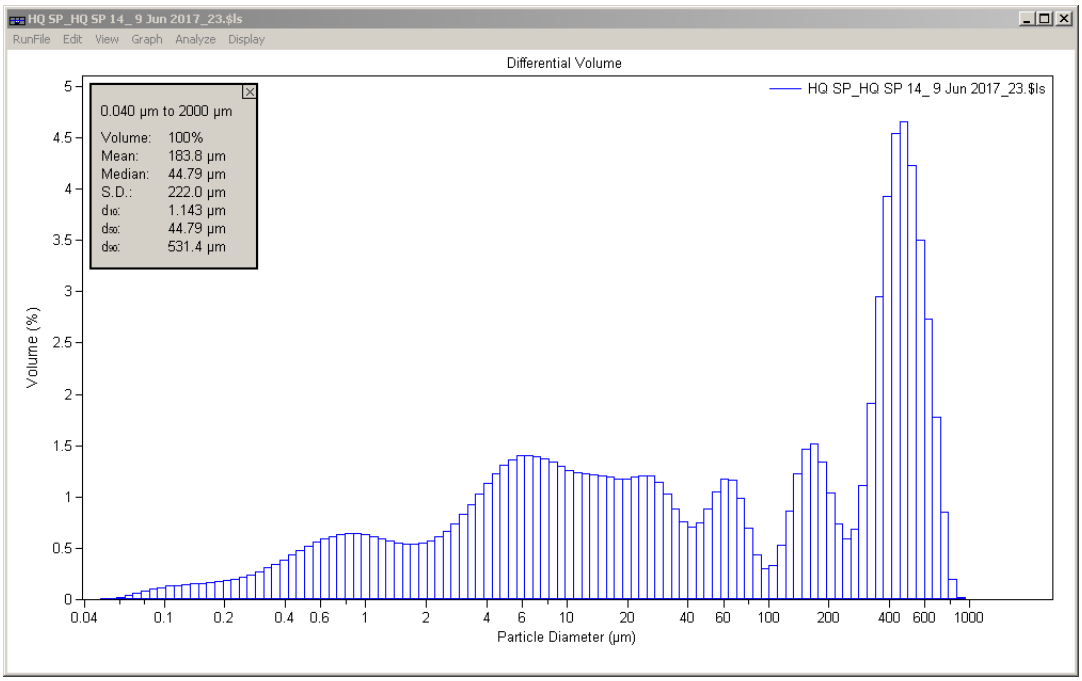

Volume Statistics (Arithmetic) HQ SP_HQ SP 14_ 9 Jun 2017_23.$ls

Save Close

Calculations from 0.040 µm to 2000 µm

Volume:	100%		
Mean:	183.8 µm	S.D.:	222.0 µm
Median:	44.79 µm	Variance:	49290 μm^2
Mean/Median ratio:	4.104	C.V.:	121%
Mode:	471.1 µm	Skewness:	0.896 Right skewed
		Kurtosis:	-0.632 Platykurtic

Folk and Ward Statistics (Phi)

Mean:	4.66	Median:	4.48	Deviation:	3.37
Skewness:	0.17	Kurtosis:	0.69		

<10%	<25%	<50%	<75%	<90%
1.143 µm	6.079 µm	44.79 µm	386.5 µm	531.4 µm

APPENDIX D: GRAIN SIZE ANALYSIS OF HQ-G SAMPLES

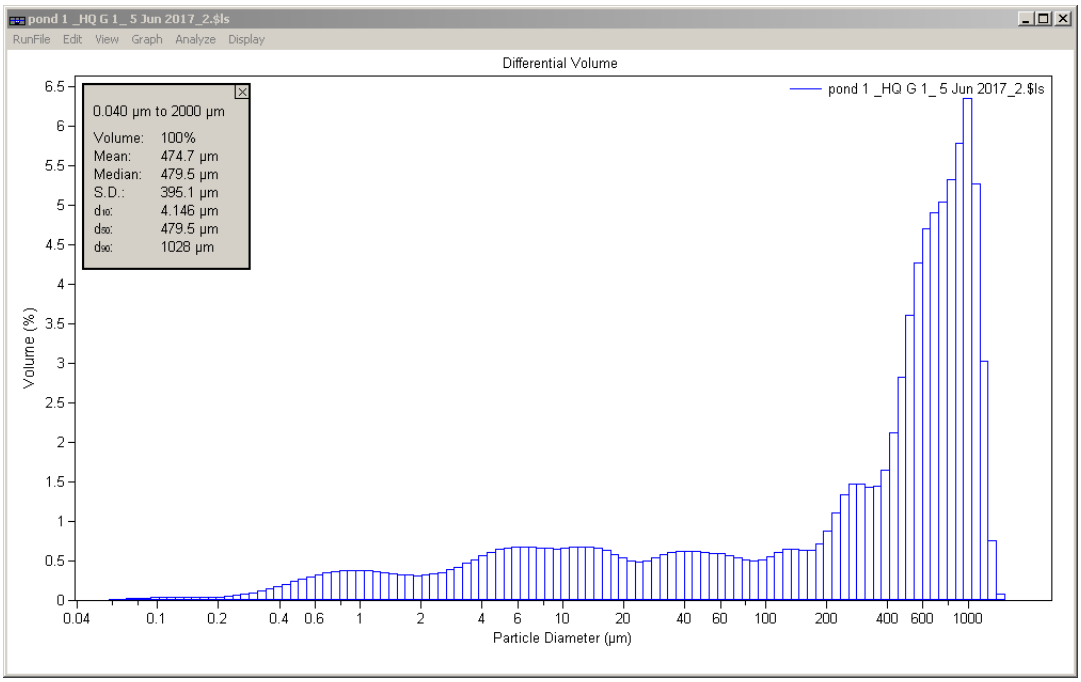

Volume Statistics (Arithmetic) pond 1 _HQ G 1_ 5 Jun 2017_2.$ls

Save Close

Calculations from 0.040 µm to 2000 µm

Volume:	100%		
Mean:	474.7 µm	S.D.:	395.1 µm
Median:	479.5 µm	Variance:	156.1e3 µm^2
Mean/Median ratio:	0.990	C.V.:	83.2%
Mode:	993.6 µm	Skewness:	0.241 Right skewed
		Kurtosis:	-1.268 Platykurtic

Folk and Ward Statistics (Phi)

Mean:	2.61	Median:	1.06	Deviation:	3.14
Skewness:	0.73	Kurtosis:	0.93		

<10%	<25%	<50%	<75%	<90%
4.146 µm	39.62 µm	479.5 µm	809.8 µm	1028 µm

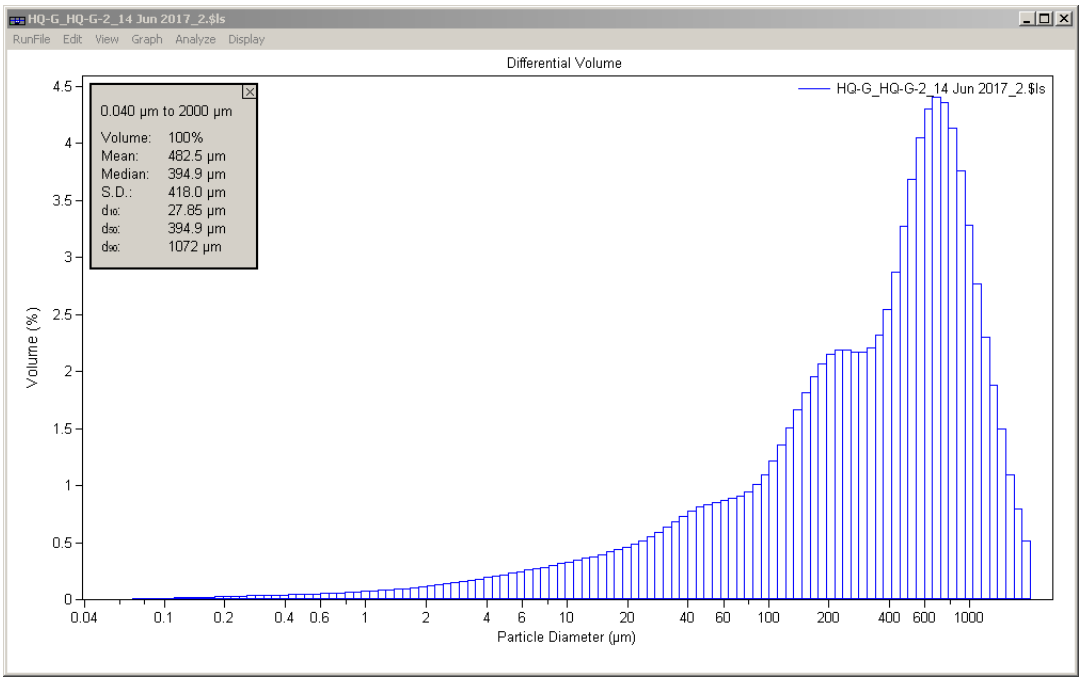

Volume Statistics (Arithmetic) HQ-G_HQ-G-2_14 Jun 2017_2.$ls

Save Close

Calculations from 0.040 µm to 2000 µm

Volume:	100%		
Mean:	482.5 µm	S.D.:	418.0 µm
Median:	394.9 µm	Variance:	174.7e3 µm^2
Mean/Median ratio:	1.222	C.V.:	86.6%
Mode:	684.2 µm	Skewness:	0.944 Right skewed
		Kurtosis:	0.399 Leptokurtic

Folk and Ward Statistics (Phi)

Mean:	1.86	Median:	1.34	Deviation:	2.07
Skewness:	0.45	Kurtosis:	1.16		

<10%	<25%	<50%	<75%	<90%
27.85 µm	129.0 µm	394.9 µm	739.0 µm	1072 µm

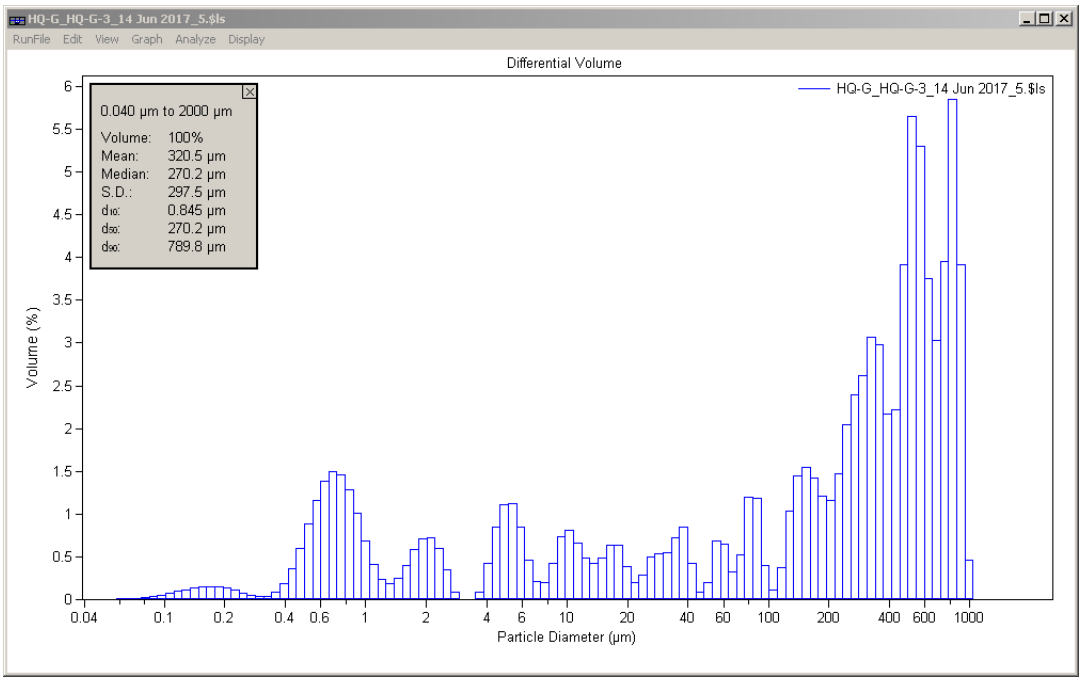

Volume Statistics (Arithmetic) HQ-G_HQ-G-3_14 Jun 2017_5.$ls

Save Close

Calculations from 0.040 µm to 2000 µm

Volume:	100%		
Mean:	320.5 µm	S.D.:	297.5 µm
Median:	270.2 µm	Variance:	88513 µm^2
Mean/Median ratio:	1.186	C.V.:	92.8%
Mode:	824.5 µm	Skewness:	0.489 Right skewed
		Kurtosis:	-1.072 Platykurtic

Folk and Ward Statistics (Phi)

Mean:	3.73	Median:	1.89	Deviation:	3.63
Skewness:	0.68	Kurtosis:	0.79		

<10%	<25%	<50%	<75%	<90%
0.845 µm	12.87 µm	270.2 µm	554.4 µm	789.8 µm

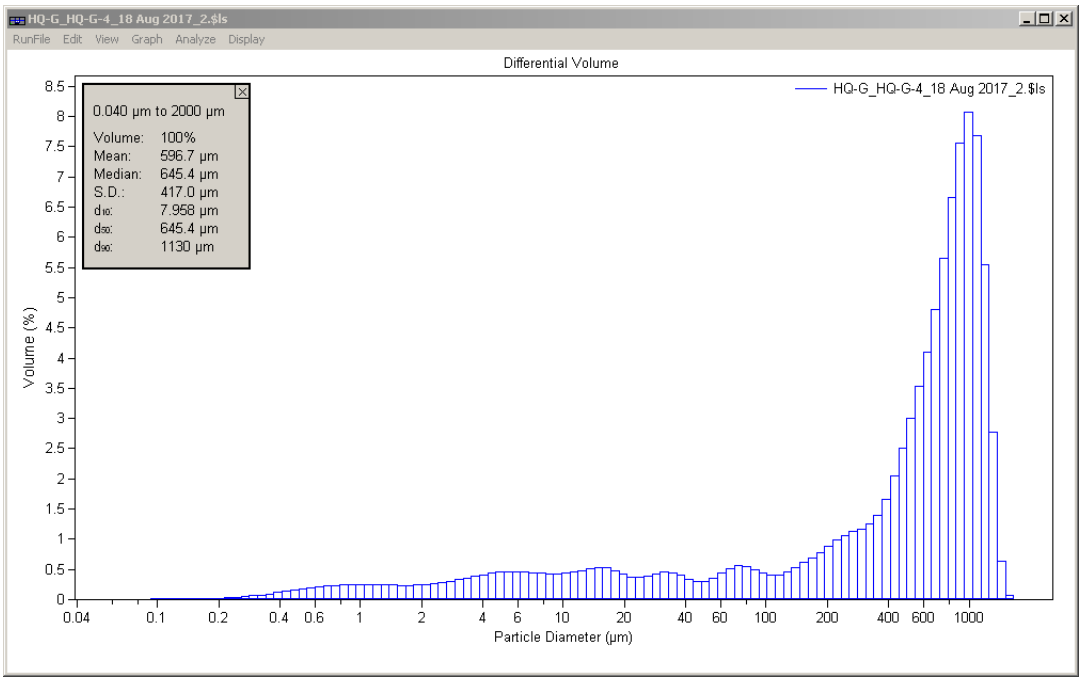

Volume Statistics (Arithmetic) HQ-G_HQ-G-4_18 Aug 2017_2.$ls

Save Close

Calculations from 0.040 µm to 2000 µm

Volume:	100%		
Mean:	596.7 µm	S.D.:	417.0 µm
Median:	645.4 µm	Variance:	173.9e3 µm^2
Mean/Median ratio:	0.925	C.V.:	69.9%
Mode:	993.6 µm	Skewness:	-0.057 Left skewed
		Kurtosis:	-1.253 Platykurtic

Folk and Ward Statistics (Phi)

Mean:	1.91	Median:	0.63	Deviation:	2.66
Skewness:	0.76	Kurtosis:	1.51		

<10%	<25%	<50%	<75%	<90%
7.958 µm	176.1 µm	645.4 µm	946.0 µm	1130 µm

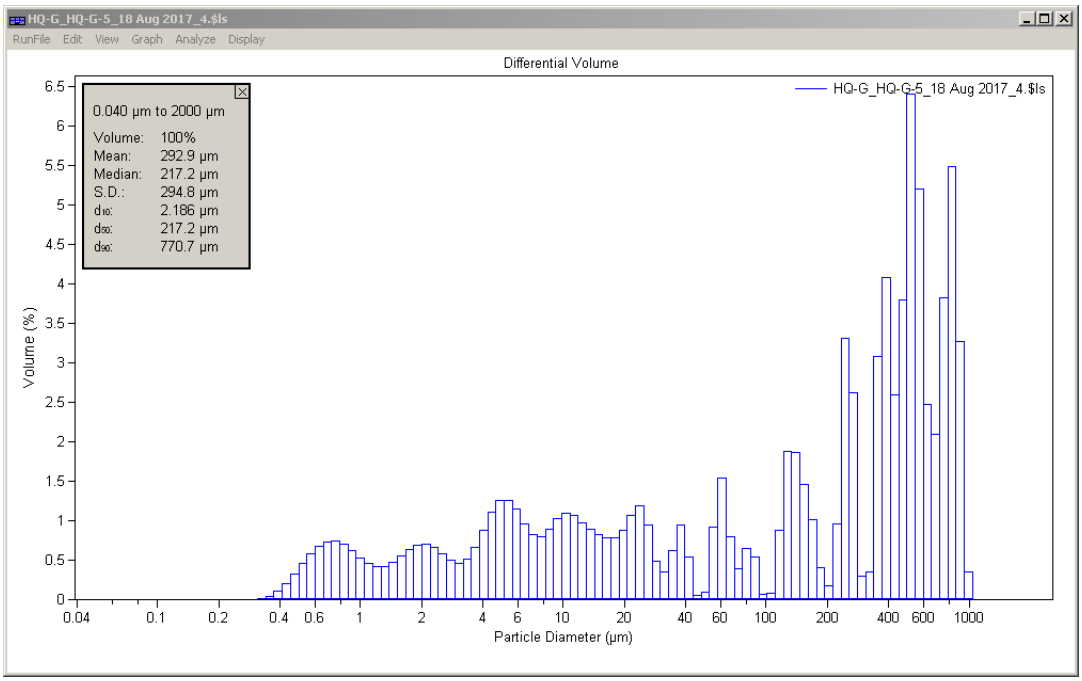

Volume Statistics (Arithmetic) HQ-G_HQ-G-5_18 Aug 2017_4.$ls

Save Close

Calculations from 0.040 µm to 2000 µm

Volume:	100%		
Mean:	292.9 µm	S.D.:	294.8 µm
Median:	217.2 µm	Variance:	86927 µm^2
Mean/Median ratio:	1.349	C.V.:	101%
Mode:	517.2 µm	Skewness:	0.610 Right skewed
		Kurtosis:	-0.965 Platykurtic

Folk and Ward Statistics (Phi)

Mean:	3.52	Median:	2.20	Deviation:	3.24
Skewness:	0.58	Kurtosis:	0.72		

<10%	<25%	<50%	<75%	<90%
2.186 µm	11.10 µm	217.2 µm	524.6 µm	770.7 µm

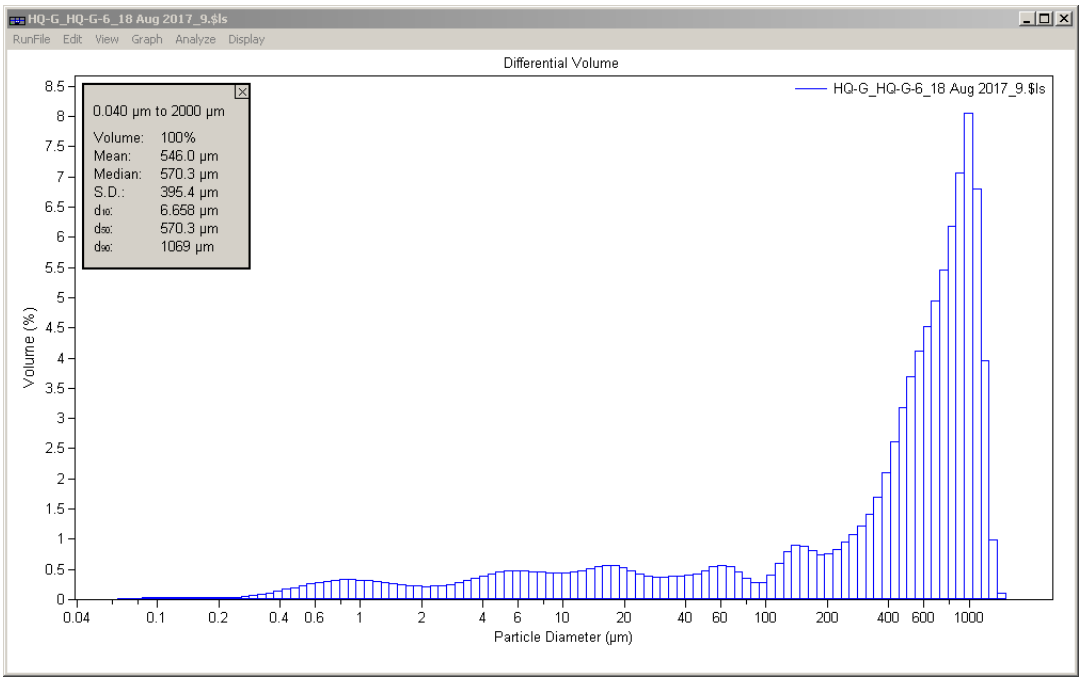
HQ-G_HQ-G-6_18 Aug 2017_9.$ls
RunFile Edit View Graph Analyze Display
Differential Volume
HQ-G_HQ-G-6_18 Aug 2017_9.$ls
0.040 µm to 2000 µm
Volume: 100%
Mean: 546.0 µm
Median: 570.3 µm
S.D.: 395.4 µm
d10: 6.658 µm
d50: 570.3 µm
d90: 1069 µm
Volume (%)
Particle Diameter (µm)

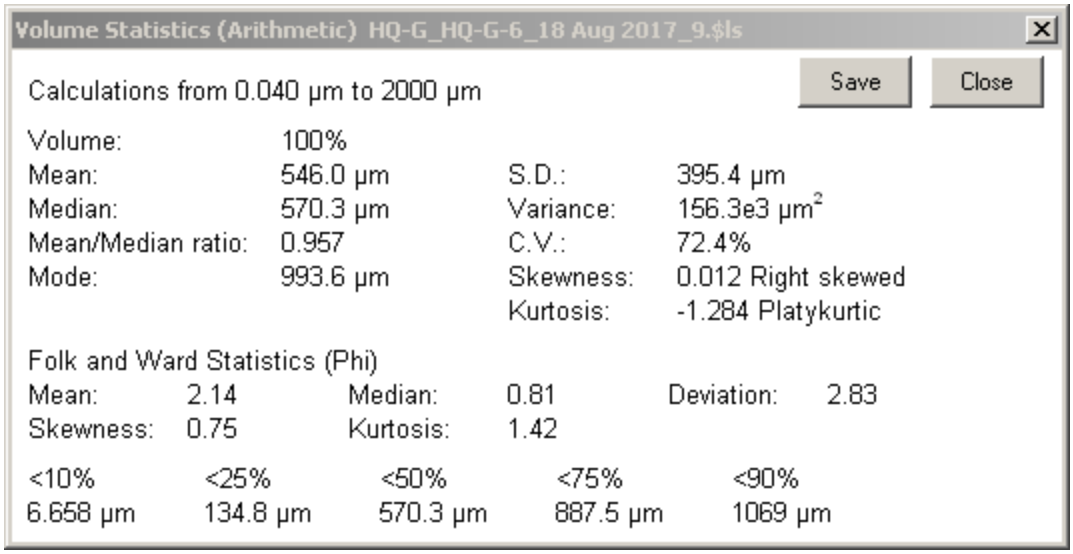
Volume Statistics (Arithmetic) HQ-G_HQ-G-6_18 Aug 2017_9.$ls
Save
Close
Calculations from 0.040 µm to 2000 µm
Volume: 100%
Mean: 546.0 µm
Median: 570.3 µm
Mean/Median ratio: 0.957
Mode: 993.6 µm
S.D.: 395.4 µm
Variance: 156.3e3 µm²
C.V.: 72.4%
Skewness: 0.012 Right skewed
Kurtosis: -1.284 Platykurtic
Folk and Ward Statistics (Phi)
Mean: 2.14
Median: 0.81
Deviation: 2.83
Skewness: 0.75
Kurtosis: 1.42
<10% 6.658 µm
<25% 134.8 µm
<50% 570.3 µm
<75% 887.5 µm
<90% 1069 µm

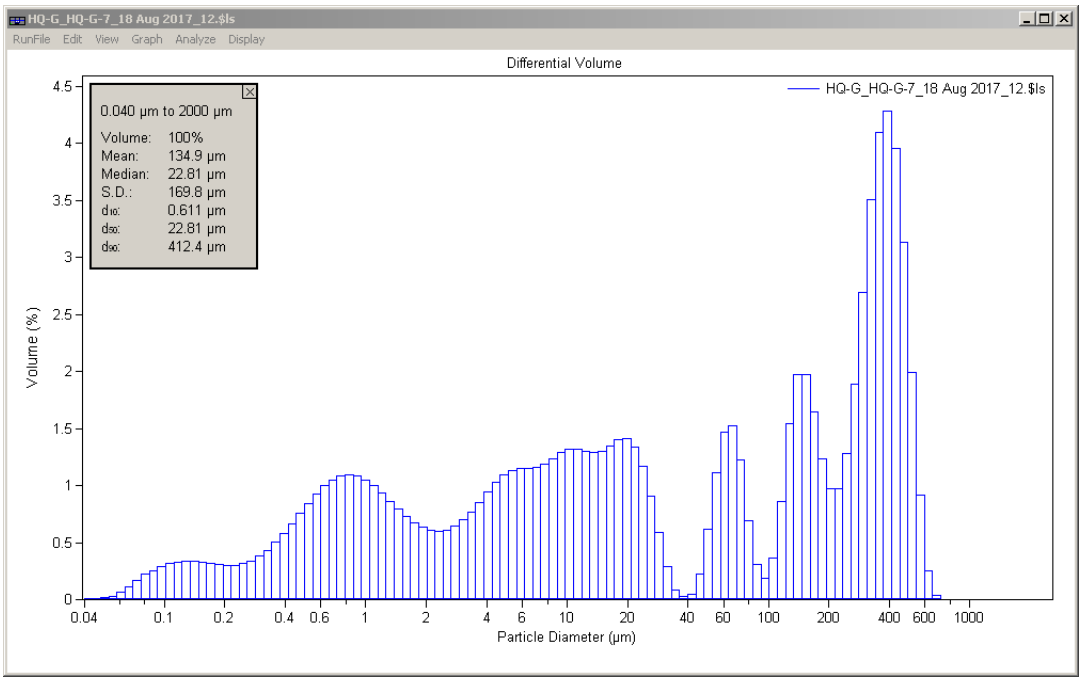

Volume Statistics (Arithmetic) HQ-G_HQ-G-7_18 Aug 2017_12.$ls

Save Close

Calculations from 0.040 µm to 2000 µm

Volume:	100%		
Mean:	134.9 µm	S.D.:	169.8 µm
Median:	22.81 µm	Variance:	28815 µm^2
Mean/Median ratio:	5.913	C.V.:	126%
Mode:	391.0 µm	Skewness:	0.991 Right skewed
		Kurtosis:	-0.446 Platykurtic

Folk and Ward Statistics (Phi)

Mean:	5.61	Median:	5.45	Deviation:	3.72
Skewness:	0.12	Kurtosis:	0.67		

<10%	<25%	<50%	<75%	<90%
0.611 µm	3.241 µm	22.81 µm	280.1 µm	412.4 µm

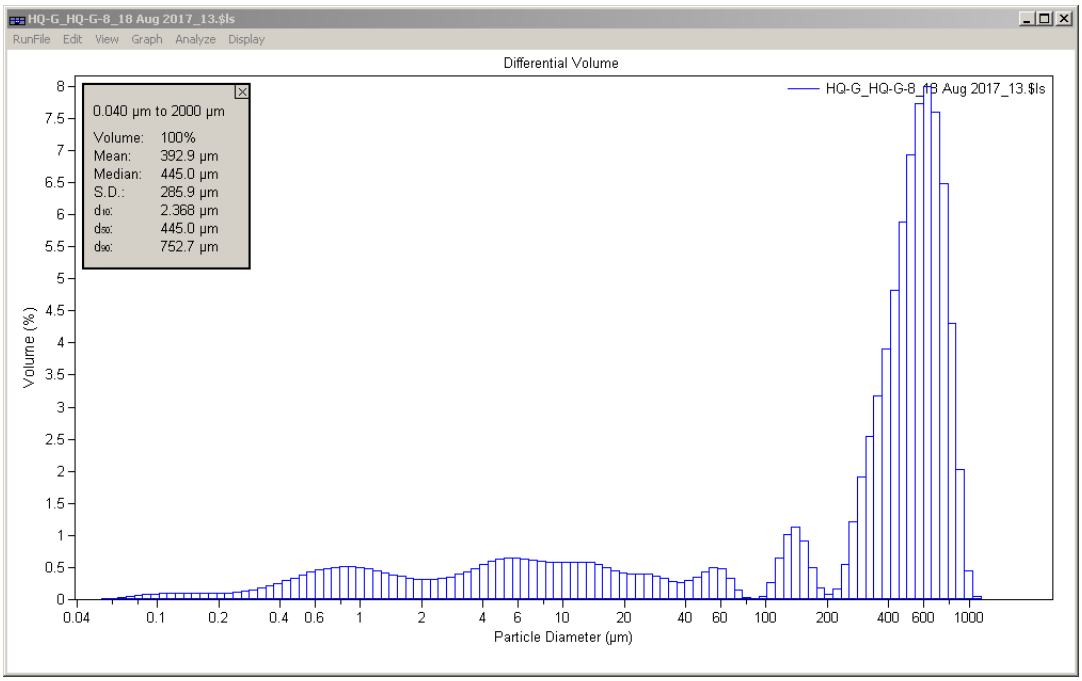
HQ-G_HQ-G-8_18 Aug 2017_13.$ls
RunFile Edit View Graph Analyze Display
Differential Volume
0.040 µm to 2000 µm
Volume: 100%
Mean: 392.9 µm
Median: 445.0 µm
S.D.: 285.9 µm
d10: 2.368 µm
d50: 445.0 µm
d90: 752.7 µm
HQ-G_HQ-G-8_18 Aug 2017_13.$ls
Volume (%)
Particle Diameter (µm)

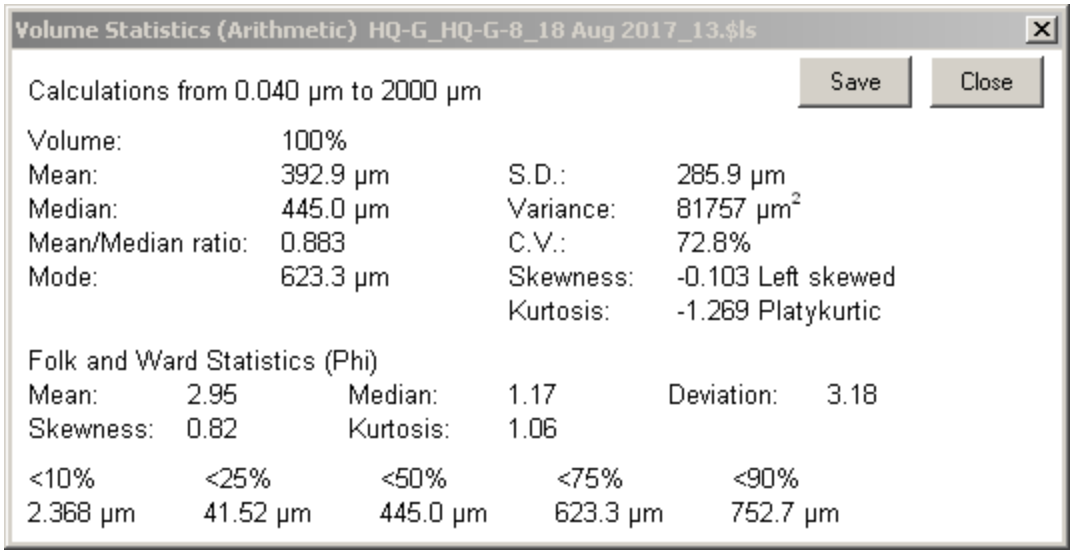
Volume Statistics (Arithmetic) HQ-G_HQ-G-8_18 Aug 2017_13.$ls
Save
Close
Calculations from 0.040 µm to 2000 µm
Volume: 100%
Mean: 392.9 µm
Median: 445.0 µm
Mean/Median ratio: 0.883
Mode: 623.3 µm
S.D.: 285.9 µm
Variance: 81757 µm²
C.V.: 72.8%
Skewness: -0.103 Left skewed
Kurtosis: -1.269 Platykurtic
Folk and Ward Statistics (Phi)
Mean: 2.95
Median: 1.17
Deviation: 3.18
Skewness: 0.82
Kurtosis: 1.06
<10% 2.368 µm
<25% 41.52 µm
<50% 445.0 µm
<75% 623.3 µm
<90% 752.7 µm

APPENDIX E: IMBRICATION DATA FOR SITES 1,2 AND 3

Imbrication Measurements Location 1								
Sample	Composition	A Axis Length (cm)	B Axis Length (cm)	C Axis Length (cm)	Dip Direction relative to A Axis	Dip Direction	Dip Angle	Weathering Rind (mm)
1	Q	10	4	3	N	305	35	1
2	Q	7.5	6	5	N	355	5	1
3	Q	8	2.5	2	N	345	10	1
4	Q	4	3	3	N	250	20	1
5	Q	5.5	4	2	N	265	20	<1
6	V	7	4	2	P	45	36	1
7	Q	8	5	2.5	P	294	12	2
8	Q	5	3.5	1.5	45	300	40	2
9	Q	6	3	2.5	P	273	33	2
10	Q	4.5	3	1.5	P	335	30	1
11	Q	6	4	2.5	P	197	17	2
12	Q	7	4	3	P	45	24	2
13	Q	5	3	1.5	N	0	40	1.5
14	Q	4.5	2.5	1.5	N	260	5	2
15	Q	6	5	2	N	355	13	3
16	Q	5.5	4	2.5	P	330	22	1
17	Q	5.5	5	2	N	360	21	<1
18	Q	5	3.5	1.5	P	340	44	3
19	Q	5.5	4	4	P	345	30	1
20	Q	7	4	2	N	270	47	1
21	Q	7	5	2	P	300	35	0
22	V	5	4	2	45	250	18	0
23	Q	8.5	5.5	3	N	320	35	1
24	Q	6.5	5	2.5	N	275	11	0
25	Q	9	5.5	2.5	P	270	20	1.5
26	Q	8	5.5	2.5	45	280	25	4
27	Q	6	3.5	1.5	P	255	24	0
28	Q	6.5	5	2	P	240	15	1
29	Q	13	7.5	6.5	P	250	40	7
30	V	10	6	5	P	300	19	<1
31	Q	8.5	4.5	2	N	230	9	1
32	V	8.5	4.5	3	N	255	19	<1
33	Q	4	3	1.5	N	140	9	3.5
34	Q	6.5	5	2	N	340	22	2.5
35	Q	9	7	4	N	235	11	2
36	Q	6	5	1.5	N	310	30	1
37	Q	3.5	3	1.5	N	255	9	1.5
38	Q	6	4	2	N	70	25	10
39	Q	8.5	6	2.5	N	220	26	1
40	Q	10	8	5	N	265	20	10
41	Q	6	4	2.5	P	320	12	3.5
42	Q	11	7	3	N	280	9	2

Imbrication Measurements Location 2								
Sample	Composition	A Axis Length (cm)	B Axis Length (cm)	C Axis Length (cm)	Dip Direction relative to A Axis	Dip Direction	Dip Angle	Weathering Rind (mm)
1	Q	6.9	5	3.8	N	315	15	1
2	Q	5.8	4.1	2.6	N	300	35	<1
3	Q	4.7	3	2.2	N	295	15	1
4	V	5.9	5.4	4.1	N	290	15	1
5	Q	6.3	2.7	2	P	320	36	1
6	Q	5.7	4.2	1.8	P	335	33	4
7	V	5.3	4.2	2.6	P	335	36	<1
8	Q	9.4	7.2	5.8	P	300	32	1
9	Q	7.2	4.8	3.8	N	320	25	2
10	Q	6	4.5	2.8	45	330	36	4
11	Q	7	4.4	3.3	45	345	55	<1
12	Q	8.5	5.1	4	P	335	36	<1
13	Q	5.4	5	2.5	N	345	37	2
14	Q	5.7	4.4	2.7	N	320	20	<1
15	Q	3.8	3.5	1.6	P	280	32	1
16	Q	5.8	5.3	2.1	N	350	26	1
17	Q	5.6	4.9	1.6	P	340	42	2
18	Q	4	2.2	1.6	P	330	37	0
19	Q	4.4	3.2	1.8	N	290	20	<1
20	Q	7.7	5.3	2.7	P	340	19	1
21	Q	6.3	3.8	2.3	P	310	29	2
22	Q	6.7	5.3	2.9	45	10	30	1
23	Q	5.2	4	2.5	N	345	29	4
24	Q	5.2	4.4	1.8	N	335	26	2
25	Q	5.1	4.2	2.5	P	315	29	1
26	Q	6.4	2.9	1.9	P	350	27	1
27	Q	4.3	2.9	1.7	45	300	26	3
28	Q	6.9	4	2.3	N	335	37	1
29	V	4.2	3.3	2.4	N	340	5	<1
30	Q	6.8	4.7	3.2	N	335	36	2
31	Q	3.8	2.7	1.2	P	295	22	<1
32	Q	3.9	2.8	1.2	P	290	27	<1
33	Q	5	4.4	2.4	N	10	45	1
34	Q	5.1	3.8	1.5	P	190	25	1
35	Q	4.8	4.6	2.5	N	305	49	1
36	Q	9.3	6.3	5.9	P	305	10	1
37	V	8	5.5	3.4	P	345	19	1
38	Q	4.9	4	2.2	P	10	26	1
39	Q	5.4	4.3	1.9	P	300	15	3
40	Q	5	4.2	1.9	P	0	32	15

Imbrication Measurements Location 3								
Sample	Composition	A Axis Length (cm)	B Axis Length (cm)	C Axis Length (cm)	Dip Direction relative to A Axis	Dip Direction	Dip Angle	Weathering Rind (mm)
1	Q	5.3	4	2.6	N	320	38	1
2	Q	4.5	4.1	2.7	N	310	23	<1
3	Q	4.6	3.4	1.6	N	115	36	1
4	Q	6	4.2	3	P	275	10	1
5	Q	7.2	3.2	2	P	100	44	3
6	Q	8.2	4.4	2.4	P	80	9	<1
7	Q	5.8	3.6	1.4	N	85	50	3
8	Q	6	4.2	1.5	P	85	34	5
9	Q	8.7	4.6	2	P	80	34	18
10	Q	8.6	5.3	3.1	P	145	23	1
11	Q	8.5	5	2.9	P	120	36	2
12	Q	4.9	3.8	1.3	N	110	26	<1
13	Q	3.8	1.9	1.3	P	105	26	2
14	Q	7.2	6.6	4	P	100	40	1
15	Q	6.4	4.1	2.2	N	160	26	<1
16	Q	4.4	3.8	1.7	N	50	52	<1
17	V	6.5	4.9	2.2	P	105	22	1
18	Q	4.5	3.4	2.2	P	75	38	3
19	Q	6.7	5.4	2.7	P	105	10	<1
20	Q	10.9	6.8	4.6	P	110	21	<1
21	Q	6.3	4.7	2.4	N	105	13	2
22	Q	5.4	4.9	2.5	P	340	66	2
23	Q	9	3.8	3	P	315	9	1
24	Q	8.5	5.3	2.4	P	300	36	3
25	Q	6.9	3.4	2.6	P	270	26	1
26	Q	4.8	4.4	1.1	P	280	26	2
27	Q	7.3	5.5	3.5	N	260	23	2
28	Q	4.5	4	1.8	P	350	40	2
29	Q	5.6	3.5	1.6	45	190	47	2
30	Q	7.1	3.8	2.4	P	250	36	1
31	Q	5.6	4	2.2	P	250	25	2
32	V	6.1	3.9	2.5	P	315	24	1
33	Q	6.2	5.6	3.7	P	290	20	2
34	Q	9.9	7	1.8	N	290	11	1
35	Q	10.2	5.3	3.9	P	355	9	3
36	Q	6.4	4.8	2	N	20	36	4
37	Q	7.2	4.8	2	P	280	16	3
38	Q	3.7	3.5	2	N	295	21	<1
39	Q	5.1	3.9	2	P	275	13	<1
40	Q	7.6	5.8	4	P	260	25	2

APPENDIX F: HEAVY MINERAL SEPARATION GRAIN COUNTS

Sample	Opaque	Zircon	Kyanite	Rutile	Tourmaline	Sillimenite	Monzonite	Unknown	Total Counts
HQ-P1-1	194	6	3	4	4				211
HQ-P1-2	337	38	5	8	9	4	4		405
HQ-P1-3	130	9		2	3		3	1	148
HQ-P1-4	180	5		3	1		1		190
HQ-P1-5	210	13	2	8	2		1		236
HQ-P1-6	335	25	12	28	6	6			412
HQ-P1-7	350	6	3	11	5		3		378
HQ-P1-8	189	1	3	12	2	1	2		210
HQ-P1-9	266	13		32	7				318
HQ-P1-10	180	4	3	14	7	3	1	1	213
HQ-P1-11	48	21	8	8	11	2		1	99
HQ-P1-12	235	25	5	23	13	5			306
HQ-P1-13	272	26	8	17	14	2	2		341

APPENDIX G: SOIL FIELD DESCRIPTIONS

Soil Profile HQA

Location														
Pond 1, Site 1			Color (Moist)	Mottle Color (Moist)					Consistance					
Unit	Horizon	Depth (cm)	Matrix	Mottle	Rim	Gravel %	Texture	Structure	Wet	Moist	Clay Films	Boundary	Roots	Pores
HQA-2-1	E	10-28	10 YR 6/8			<5	LS	1 m sbk	po	vfr		a s	2c, 2m, 3f, 2vf	2vf
HQA-2-2	B	28-42	7.5 YR 5/6			<5	SCL	1 m sbk	s p	fr	1 d cobr	c s	1c, 2m, 1f, 1vf	1f, 2vf
HQA-2-3	B2mot	42-65	2.5 YR 5/8	10 YR 6/8		<5	SCL	1 m pl	ss ps	fr, fi (glay)	2 d cobr	a w		2fn, 2vf
HQA-3-1	BC	65-92	10 YR 7/8	10 YR 7/3	2.5 YR 5/8	0	LS	2 m sbk	ss po	fr		g s		1f, 2vf
HQA-3-2	Cox	92-119	7.5 YR 5/8	10 YR 6/8	10 R 6/8	0	LS	1 m sbk	ss po	fr		g s		1f, 2vf
HQA-3-3	Cox2	119-146	10 R 5/8	10 YR 6/8		<5	LS	1 m sbk	ss po	fr		g s		1f, 2vf
HQA-3-4	Cox3	146-173	5 YR 6/6	10 YR 6/8		0	LS	1 m sbk	ss po	fr		g s		1f, 2vf
HQA-3-5	Cox4	173-200	5 YR 5/6	10 YR 6/8		<5	LS	1 m sbk	ss po	fr		c w		1f, 2vf
HQA-4-1	Cox	200-224	5 YR 6/8			0	LS	1 m sbk	ss	fr		g s		
HQA-4-2	Cox2	224-248	5 YR 5/6	10 YR 7/6	5 YR 6/8	0	LS	1 m sbk	ss	fr		g s		
HQA-4-3	Cox3	248-270	5 YR 5/8			0	LS	1 m sbk	ss	fr		g s		
HQA-4-4	Cox4	270-293	5 YR 6/8			0	LS	1 m sbk	ss	fr		a w		
HQA-5-1	Bgc	293-333	10 YR 8/4			<5	SCL	1 m abk	ss ps	fr, fi (glay)	1 f cobr	a s		1f, 2vf
HQA-6-1	Ab	333-363	10 YR 7/6			<2	SCL	1 m abk	ss ps	fr		c s		1f, 2vf
HQA-6-2	B	363-393	2.5 YR 7/6			tr	SCL	1 m sbk	s p	fr		c w		1f, 2vf
HQA-6-3	Bbt	393-423	2.5 Y 6/6			<5	SCL	1 m sbk	s p	fr		c w		1f, 2vf
HQA-7-1	Ab	423-438	2.5 Y 3/3			0	CL	2 c abk	vs p	fi	2 d cobr	a s		1vf
HQA-8-1	BC	438-473	10 YR 5/3			10	L	1 c abk	ss ps	fr		g s		1f, 2vf
HQA-9-1	Bb	473-513	10 R 4/1	10 YR 8/1, 10 R 4/1, 7.5 YR 6/5		tr	SC	2 m abk	vs p	fi	3 p pf	a s		
HQA-9-2	Btb	513-553	10 R 4/1	10 R 4/1, 10 YR 8/1, 7.5 YR 6/8, 10 R 4/8		0	SC	2 m abk	s p	fi	3 p pf	c s		
HQA-9-3	Coxb	553-603	10 R 4/2	10 YR 8/1, 10 R 4/1, 7.5 YR 3/6, 10 R 8/8		0	SC	2 m abk	s p	fr	3 p pf	a s		
HQA-10-1	Ab	603-643	2.5 YR 4/4			50	L	sg f	ss ps	lo		c s		1c, 2m, 3f, 3vf
HQA-10-2	ABb	643-698	10 R 5/6			>75	L	sg f	ss ps	lo		c s		1c, 2m, 3f, 3vf

Soil Profile HQB

Location														
Sump Pit 2			Color (Moist)	Mottle Color (Moist)					Consistance					
Unit	Horizon	Depth (cm)	Matrix	Mottle	Rim	Gravel %	Texture	Structure	Wet	Moist	Clay Films	Boundary	Roots	Pores
HQB-1-1	Bmot	0-20	2.5 YR 4/6	10 YR 8/3	10 YR 7/3	<5	SCL	1 m pl	ss ps	fr, fi (glay)	2 d cobr			1f 1vf
HQB-1-2	Bmot	20-40	2.5 YR 4/6	10 YR 8/3	10 YR 7/3	<5	SCL	1 m pl	ss ps	fr, fi (glay)	2 d cobr			1f 1vf
HQB-1-3	Bmot	40-60	2.5 YR 5/6	10 YR 8/2	10 YR 7/3	<5	SCL	1 m pl	ss ps	fr, fi (glay)	2 d cobr	a s		1f 1vf
HQB-2-1	BC	60-100	5 YR 5/8	10 YR 8/4	10 YR 6/6	0	SL	2 m sbk	ss po	fr				1f 1vf
HQB-2-2	BC	100-140	5 YR 5/8	10 YR 8/4	10 YR 6/6	0	SL	1 m sbk	ss po	fr				1f 1vf
HQB-2-3	BC	140-180	5 YR 5/6	10 YR 8/4	10 YR 7/6	0	SL	1 m sbk	ss po	fr				1f 1vf
HQB-3-1	Cox	180-220	5 YR 5/6			0	SL	1 m sbk	ss po	fr				1f 1vf
HQB-3-2	Cox	220-260	10 YR 7/7			0	SL	1 m sbk	ss po	fr				1f 1vf
HQB-3-3	Cox	260-300	10 YR 7/7			0	SL	1 m sbk	ss po	fr		a s		1f 1vf
HQB-4-1	Bgc	300-340	10 YR 8/3			<10	SCL	1 m abk	ss ps	fr	1 F cobr	a s		1f 1vf
HQB-5-1	Cox	340-370	7.5 YR 5/6			25	L	1 m sbk	ss po	fr				1c, 2m, 3f, 3vf
HQB-5-2	Cox	370-400	7.5 YR 5/6			20	L	1 m sbk	ss po	fr				1c, 2m, 3f, 3vf
HQB-5-3	Cox	400-430	7.5 YR 6/6			50	L	1 m sbk	ss po	fr				1c, 2m, 3f, 3vf
HQB-5-4	Cox	430-460	7.5 YR 6/8			40	L	1 m abk	ss po	fr				1c, 2m, 2f, 3vf
HQB-5-5	Cox	460-490	7.5 YR 6/6			40	L	1 m sbk	ss po	fr				1c, 2m, 3f, 3vf
HQB-5-6	Cox	490-510	10 YR 6/4			20	L	1 m sbk	ss po	fr				1c, 1m, 2f, 3vf
HQB-5-7	Cox	510-540	10 YR 5/6			30	L	1 m sbk	ss po	fr				1c, 2m, 3f, 3vf
HQB-5-8	Cox	540-570	7.5 YR 5/6			30	L	1 m sbk	ss po	fr				1c, 2m, 2f, 3vf
HQB-5-9	Cox	570-600	10 YR 6/6			25	L	1 m abk	ss po	fr				1c, 2m, 3f, 3vf
HQB-5-10	Cox	600-630	7.5 YR 6/6			15	L	1 m sbk	ss po	fr				1c, 1m, 2f, 3vf
HQB-5-11	Cox	630-660	7.5 YR 6/6			40	L	1 m sbk	ss po	fr				1c, 1m, 2f, 3vf

APPENDIX H: EXTRACTABLE IRON ANALYSIS

Soil Profile HQA

Unit	Depth (cm)	%wt FeD	%wt FeH	FeH/FeD
HQA-1-1	0-10	1.41	1.14	0.81
HQA-2-1	10-28	0.63	1.93	3.07
HQA-2-2	28-42	2.60	1.16	0.45
HQA-2-3	42-65	4.89	1.54	0.32
HQA-3-1	65-92	1.39	2.37	1.71
HQA-3-2	92-119	1.67	1.14	0.69
HQA-3-3	119-146	1.16	1.03	0.89
HQA-3-4	146-173	1.58	1.31	0.83
HQA-3-5	173-200	1.06	1.37	1.29
HQA-4-1	200-224	0.85	1.22	1.44
HQA-4-2	224-248	1.29	0.83	0.64
HQA-4-3	248-270	1.01	1.38	1.36
HQA-4-4	270-293	0.73	1.09	1.49
HQA-5-1	293-333	0.61	0.99	1.61
HQA-6-1	333-363	0.59	1.33	2.26
HQA-6-2	363-393	1.05	0.93	0.88
HQA-6-3	393-423	1.79	1.83	1.03
HQA-7-1	423-438	2.25	1.63	0.73
HQA-8-1	438-473	1.53	1.57	1.03
HQA-9-1	473-513	3.42	1.19	0.35
HQA-9-2	513-553	3.58	1.04	0.29
HQA-9-3	553-603	2.45	0.95	0.39
HQA-10-1	603-643	1.36	1.38	1.02
HQA-10-2	643-698	1.33	1.43	1.08

Soil Profile HQB

Unit	depth (cm)	%wt Fed	%wt FeH	FeH/FeD
HQB-1-1	0-20	6.16	1.24	0.20
HQB-1-2	20-40	9.62	0.76	0.08
HQB-1-3	40-60	3.63	0.80	0.22
HQB-2-1	60-100	2.78	1.59	0.57
HQB-2-2	100-140	1.58	1.32	0.83
HQB-2-3	140-180	1.52	1.15	0.76
HQB-3-1	180-220	0.58	0.91	1.59
HQB-3-2	220-260	0.61	0.88	1.45
HQB-3-3	260-300	0.58	1.34	2.31
HQB-4-1	300-340	0.16	0.51	3.20
HQB-5-1	340-370	5.26	1.09	0.21
HQB-5-2	370-400	2.18	0.80	0.36
HQB-5-3	400-430	0.92	0.77	0.83
HQB-5-4	430-460	1.41	0.71	0.51
HQB-5-5	460-490	1.88	0.94	0.50
HQB-5-6	490-510	1.70	1.00	0.59
HQB-5-7	510-540	0.86	1.10	1.28
HQB-5-8	540-570	0.76	2.40	3.14
HQB-5-9	570-600	0.98	0.91	0.93
HQB-5-10	600-630	0.72	0.68	0.94
HQB-5-11	630-660	0.70	1.03	1.49

APPENDIX I: XRF ANALYSIS DATA FOR SOIL PROFILE HQA

ID	Ti intensity	% TI	Fe intensity	minus background	% Fe	Al intensity	minus background	% Al	Ca intensity	% Ca	Si intensity	% Si		titanium ratio	Fe ratio	Al ratio	Si ratio	Fe depletion factor	Al depletion factor	Si depletion factor
HQ.1-1	82155	0.41244	1164755	1146850	2.16435	18770	1569	5.6933	8493	-0.09377	343049	38.92543		0.541367832	0.706798076	1.239020675	1.030986462	1.305578267	2.28868544	1.904410276
HQ.2-1	64106	0.268048	679520	661615	0.708645	11876	0	4.595	7791	-0.10079	509071	50.54697		0.351839212	0.231417711	1	1.338796817	0.657737122	2.842207366	3.805138175
HQ.2-2	131798	0.809584	1971694	1953789	4.585167	22448	5247	8.2679	7996	-0.09874	242120	31.8604		1.062658168	1.497348956	1.799325354	0.843860712	1.409059847	1.693230625	0.794103633
HQ.2-3	145622	0.920176	2643586	2625681	6.600843	20855	3654	7.1528	7246	-0.10624	141761	24.83527		1.207820983	2.155595505	1.556648531	0.657791761	1.784697845	1.288807326	0.544610311
HQ.3-1	65640	0.28032	1200961	1183056	2.272968	13349	0	4.595	6809	-0.11061	413514	43.85798		0.367947412	0.742268768	1	1.161630935	2.017322976	2.71777968	3.157056951
HQ.3-2	71974	0.330992	1136068	1118163	2.078289	18335	1134	5.3888	5444	-0.12426	276885	34.29395		0.434459367	0.67869368	1.172752992	0.908316188	1.562156858	2.69933872	2.090681561
HQ.3-3	93168	0.500544	991522	973617	1.644651	19020	1819	5.8683	5582	-0.12288	337332	38.52524		0.657012947	0.537083264	1.277105555	1.020386953	0.817462222	1.943805757	1.553069778
HQ.3-4	52803	0.177624	1120670	1102765	2.032095	14975	0	4.595	5777	-0.12093	376710	41.2817		0.233144887	0.663608398	1	1.093395085	2.846286148	4.289105076	4.689688409
HQ.3-5	60976	0.243008	1044569	1026664	1.803792	15644	0	4.595	5610	-0.1226	370957	40.87899		0.318971763	0.589053933	1	1.08272883	1.846724382	3.135073742	3.394434725
HQ.4-1	46102	0.124016	831883	813978	1.165734	16176	0	4.595	5613	-0.12257	424260	44.6102		0.162783127	0.380686372	1	1.181554379	2.33861075	6.14314282	7.258457302
HQ.4-2	72350	0.334	1068304	1050399	1.874997	19000	1799	5.8543	6456	-0.11414	349317	39.36419		0.438407661	0.612305899	1.274058766	1.042607545	1.396658755	2.906105143	2.37816908
HQ.4-3	54554	0.191632	868372	850467	1.275201	16124	0	4.595	5959	-0.11911	414304	43.91328		0.251535739	0.416434317	1	1.163095622	1.655567187	3.975578192	4.623977588
HQ.4-4	54275	0.1894	707756	689851	0.793353	16618	0	4.595	6303	-0.11567	431514	45.11798		0.248606021	0.259080266	1	1.195003539	1.042131904	4.022428722	4.806816557
HQ.5-1	103728	0.585024	625805	607900	0.5475	17727	526	4.9632			366557	40.57099		0.767901209	0.178793608	1.080130577	1.074571083	0.232834128	1.406600959	1.399361103
HQ.6-1	85097	0.435976	669571	651666	0.678798	16196	0	4.595	6705	-0.11165	452389	46.57923		0.572261133	0.221670765	1	1.233706488	0.387359462	1.747453988	2.155845324
HQ.6-2	142631	0.896248	1107583	1089678	1.992834	19268	2067	6.0419			407769	43.45583		1.176413143	0.650787182	1.314885745	1.150979512	0.553196116	1.11770746	0.978380359
HQ.6-3	117788	0.697504	1367590	1349685	2.772855	14078	0	4.595			349396	39.36972		0.915542208	0.905513701	1	1.042754013	0.983046374	1.092248933	1.138946959
HQ.7-1	92219	0.492952	1589141	1571236	3.437508	14078	0	4.595	5613	-0.12257	351995	39.55165		0.647047705	1.122565223	1	1.047572646	1.734903337	1.545481102	1.619003777
HQ.8-1	90504	0.479232	1400091	1382186	2.870358	14411	0	4.595			386356	41.95692		0.629038863	0.937354638	1	1.111279092	1.49013788	1.589726896	1.766630263
HQ.9-1	118656	0.704448	2251199	2233294	5.423682	20551	3350	6.94			167874	26.66318		0.924656887	1.771177491	1.510337323	0.706206139	1.915496997	1.633402989	0.763749396
HQ.9-2	105449	0.598792	2318543	2300638	5.625714	19061	1860	5.897			171666	26.92862		0.785973055	1.837153802	1.283351469	0.713236634	2.337425933	1.632818658	0.907456852
HQ.9-3	111606	0.648048	2109277	2091372	4.997916	20905	3704	7.1878			203906	29.18542		0.850626372	1.632137784	1.564265506	0.773010675	1.918748158	1.838957218	0.908754655
HQ.10-1	120524	0.719392	1569211	1551306	3.377718	16980	0	4.595			290669	35.25883		0.944272348	1.103039981	1	0.933872186	1.168137543	1.059016503	0.988986057
HQ.10-2 (pm)	125831	0.761848	1464035	1446130	3.06219	16728	0	4.595			326336	37.75552			1	1	1	1	1	1
HQ.3-4 check	51914	0.170512	1100227	1082322	1.970766	14777	0	4.595	5289	-0.12581	377975	41.37025		0.223813674	0.643580575	1	1.095740437	2.875519457	4.468002252	4.895770742
HQ.4-1 check	54486	0.191088	970567	952662	1.581786	18093	892	5.2194	6810	-0.1106	480896	48.57472		0.250821686	0.516553839	1.135886834	1.286559422	2.059446481	4.528662775	5.12937873
HQ.5-1 check	122527	0.735416	749178	731273	0.917619	19751	2550	6.38			412880	43.8136		0.965305415	0.299661027	1.388465724	1.160455478	0.310431312	1.438369351	1.202164061

APPENDIX J: DOCUMENTED PLANT MACRO AND MICRO FOSSILS

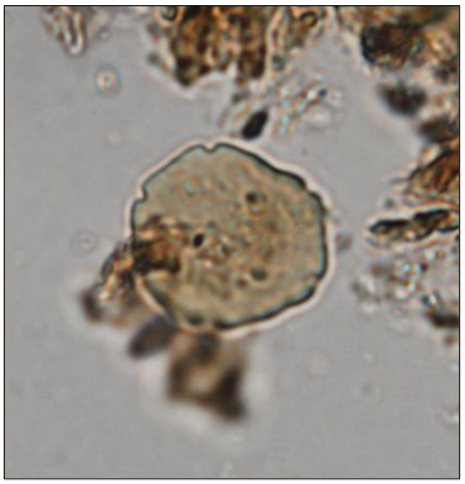

Pterocarya (winged hickory), 40 µ across

Carya (hickory), 50 µ across

Ulmus (elm), 32.5 µ across

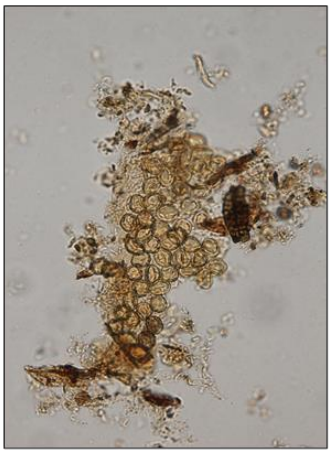

Tricolporopollenites macula (an extinct form genus), each grain 20 µ long

Nuphar (yellow waterlily), 52.5 µ long

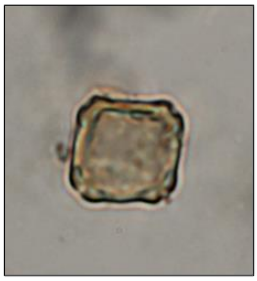

Alnus (alder), 25 µ across

Castanea (chestnut), 20 µ long

Photomicrographs of pollen from the lignite unit.

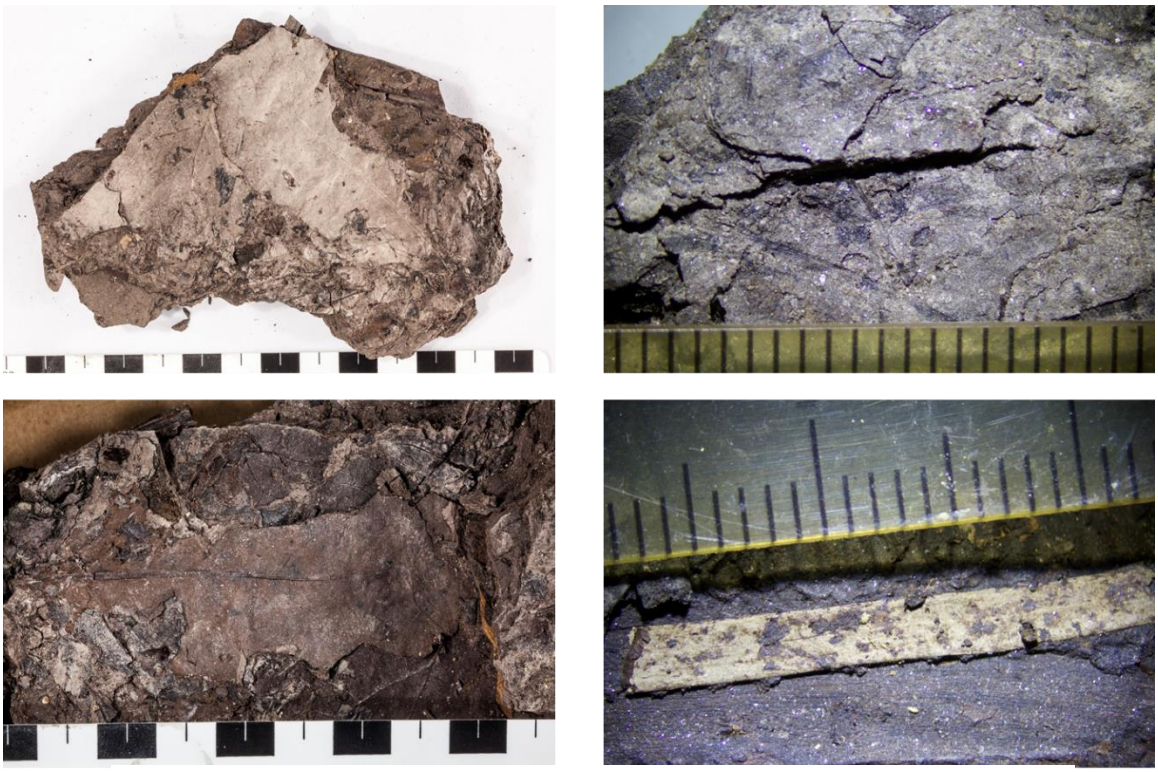

Leaf fragments from the lignite unit. Scales in cm on left and mm on right.

Seed pods from the lignite unit in upper row and surface textures on woody fragments in lower row. Scale in mm.

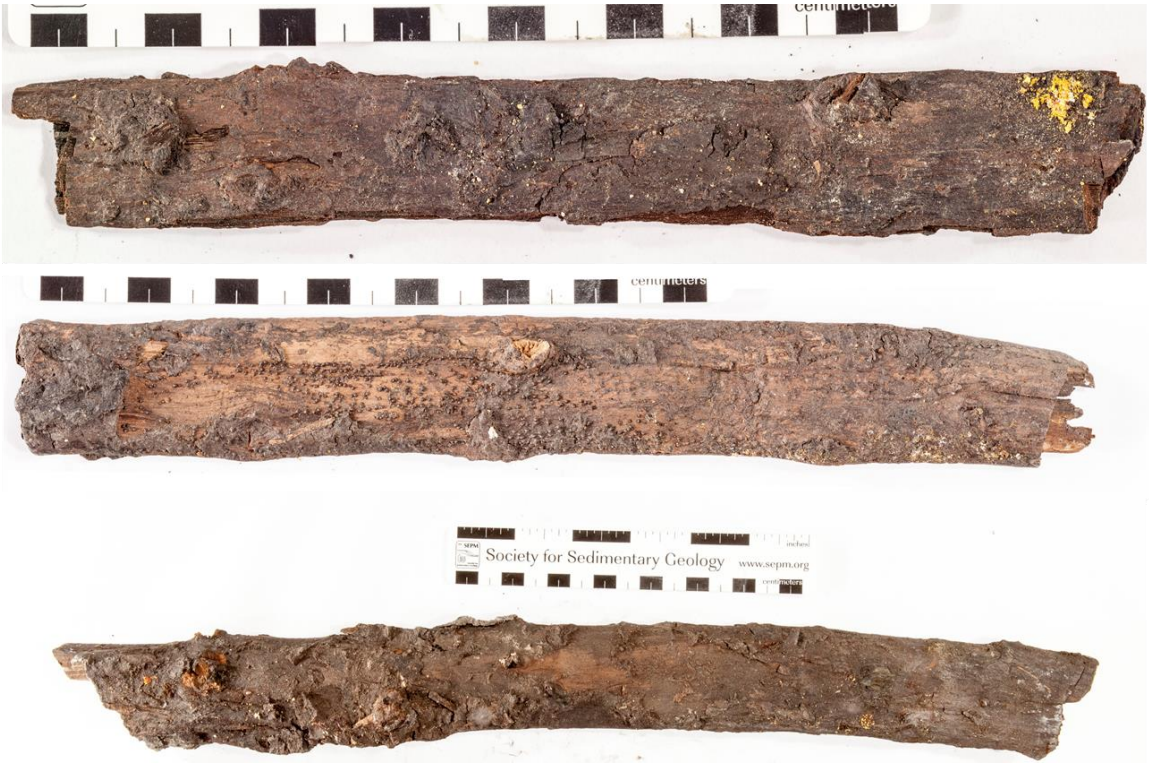

Woody material from the lignite. Scale is in cm.

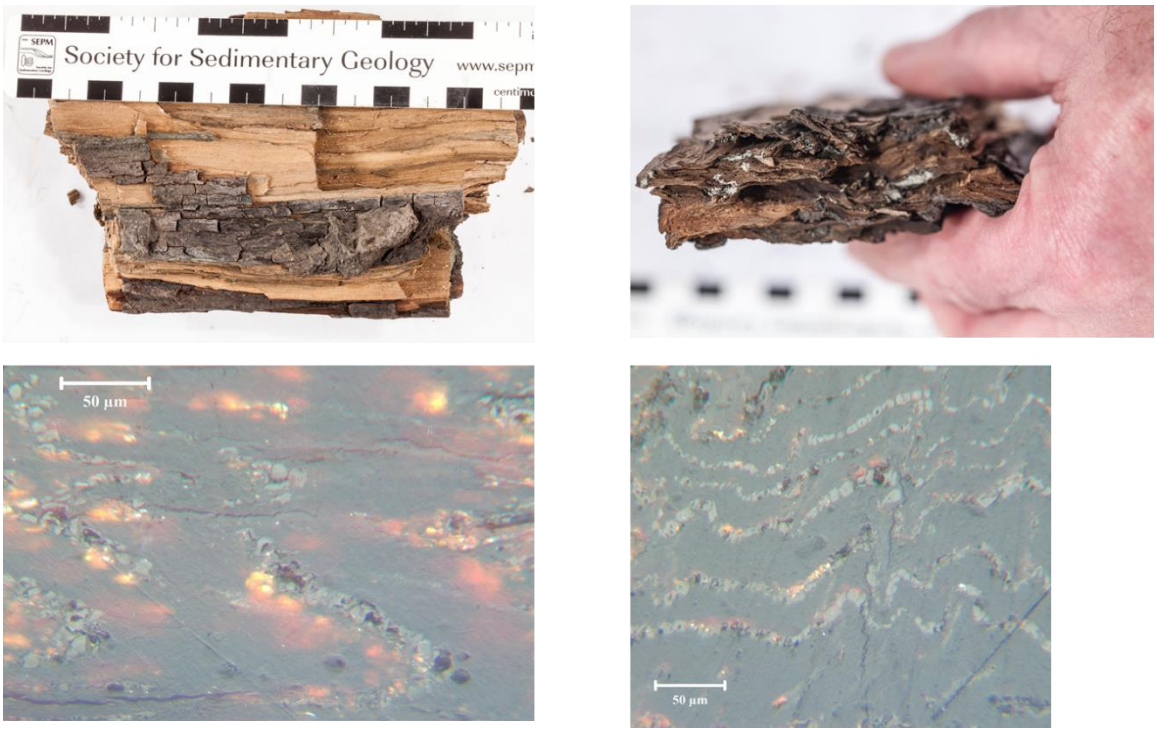

Well preserved woody material in upper left. End view of wood fragment in upper right. Lower two photos are incident light microscopy prepared by Jim Hower with radial views on the left and cross-sectional view on the right, suggesting vascular structure with growth rings.